Development of Novel and Sustainable Refractories for the Glass Industries

Masimba Phillip Toperesu

Submitted in accordance with the requirements for the degree of

Doctor of Philosophy

The University of Leeds

School of Chemical and Process Engineering

December 2018

The candidate confirms that the work submitted is his/her own, except where work which has formed part of jointly-authored publications has been included. The contribution of the candidate and the other authors to this work has been explicitly indicated below. The candidate confirms that appropriate credit has been given within the thesis where reference has been made to the work of others.

The following publications have been a result of this research and formed part of the following chapters to the Thesis

Chapter 5:

> *Hot Corrosion Behaviour of Sintered AZS Refractories in Special (Type 1, Class A) Glass Melt with Increasing Soda Content. Ceramics International Journal, In-press.*
>
> *Masimba Phillip Toperesu (90% of the contribution); Wetsookile Kusepile , Girish Kale, Jafar Daji and David Parkinson (10%).*

Chapter 6:

> *Development and Evolution of a Promising $Zr_{1-x}Sn_xO_2$ reinforced Mullite and Alumina Slip Cast Refractory. Effect of SnO_2. Journal of European Ceramics Society. In-press.*
>
> *Phillip Toperesu (90% contribution); Girish Kale, Jafar Daji and David Parkinson (10% contribution).*

The following publication was also a result of part of this research. Only the part of the methodology for dynamic corrosion was included in section of Methods and Methodology chapter in this thesis.

Dynamic and Static Corrosion of alpha-Alumina Bonded Refractory in Contact with Molten soda-lime-silica (SLS) Glass. Zihua Wang, Phillip M. Toperesu, Tlamelo Maotsela, Girish M. Kale, Jafar Daji, David Parkinson, Ceramics International, Volume 45, Issue 1, (2019).

This copy has been supplied on the understanding that it is copyright material and that no quotation from the thesis may be published without proper acknowledgement.

© 2018

The University of Leeds

Masimba Phillip Toperesu

Acknowledgements

This research has been carried out by a team which has included Dr Girish Kale, Dr Jafar Daji and David Parkinson. My own contributions, fully and explicitly indicated in the thesis, have been in the research, development, synthesising and characterisation of refractory compositions at PSR-Ltd and the University of Leeds.

I would like to thank the following for their unwavering support throughout this research. Dr Girish Kale, who has been my supervisor and for his guidance at each step of my journey. Dr Jafar Daji, my industrial supervision for his guidance at Parkinson Spencer refractories and throughout the research. Lastly, I would like to thank Mr David Parkinson for allowing me to study and research at his company and the support he gave throughout the research.

A heartfelt dedication of this Thesis to;

To my dearest wife, **Zanele**; and son, **Tatenda**;

Much love and thank you for your understanding
& support throughout my research, especially
through the difficult periods.

Mum and **Dad**;

Thank you for your unconditional
Love, support and belief in me.

Abstract

This research investigated the development and synthesis of modified and novel refractory materials and compositions of the $Al_2O_3 – ZrO_2 – SiO_2$ (AZS) systems that offer promising sustainable qualities; both from the manufacturing and service end of their application in the glass industries. In the glass industry the key challenges of production costs and glass quality are greatly affected by the performance of refractories. Therefore there is a demand for refractories that enhance furnace life and increase productivity whilst achieving fewer glass defects and downtime.

Three dense AZS refractory composites, AZS-01, AZS-T1 and AZS-T2, that contain very low apparent porosities of 13%; 7% and 6% respectively were developed and synthesized by slip cast methods through reaction sintering of alumina and zircon raw materials, which met these criteria.

The AZS-01 refractory is a high zirconia refractory composition, designed with a tailored matrix microstructure consisting of interlocked zirconia grains in a mullite-zircon matrix. The material was developed utilising the evaluation of compositional phase fields of ternary and binary phase diagrams and thermodynamic consideration of the phases. A hybrid of empirical particle packing models and a computational modelling approach that utilised scanned and digitised particle shapes as voxels in a 3D digital packing environment were also utilised to optimise the packing fractions of the refractory formulations.

AZS-T1 and AZS-T2 are SnO_2 doped variants of the AZS-01 and AZS refractories, respectively, studied in this thesis. The AZS-01, AZS-T1 and AZS-T2 refractories developed in this research, offered improved physical, thermo-

mechanical and chemical properties when compared to the standard refractories, PSR-315 and PSR-333; widely used in the forehearth glass industry.

PSR-315 and PSR-333, used in this research as reference refractory compositions, are well known international standard refractories widely used as forehearth and feeder glass furnace applications. Therefore, they are a benchmark to which other compositions that are used in similar forehearth and feeder application are compared to. With that being so; the developed compositions in this research, AZS-01, AZS-T1 and AZS-T2, presented enhanced thermos-mechanical properties than the benchmark refractories.

They were also shown to perform better and offer improved corrosion resistant properties than the standard PSR-315 and PSR-333 in both borosilicate and soda lime silicate glass melts. The improved thermo-mechanical and corrosion resistant properties of the AZS-01, AZS-T1 and AZS-T2 provides them with long service life properties than the standard benchmark refractories, PSR-315 and PSR-333.

Therefore, this research has successfully addressed the research objectives of developing and synthesising sustainable refractories for the glass industry. Results from the research have also shown successfully the effect SnO_2 as a sintering aid in reaction sintering of Alumina-zircon starting mixtures above 1550 °C.

Of the compositions, AZS-T1 and AZS-T2 were developed by using SnO_2 as a sintering agent which brought novelty to the research. Three types of mullite crystals, MI; MII and MIII, based on their morphology and aspect ratios; were evolved across the matrix microstructure. The microstructures of the reaction sintered refractory samples were characterized by Scanning Electron Microscopy (SEM) and Energy Dispersive X-ray Spectroscopy (EDX). Volatisation of SnO_2

was mitigated by the formation of a $Zr_{1-x}Sn_xO_2$ solid solution and a pro-eutectic transient Al_2O_3-SnO_2-ZrO_2 and SnO_2-SiO2 amorphous phase.

Liquid phase sintering from the presence of a SnO_2-SiO_2 amorphous phase from the dissociated zircon grains and transient pro-eutectic Al_2O_3-SnO_2-ZrO_2 amorphous phase is believed to have enhanced densification.

SEM microstructural analysis revealed coalescence and grain growth of the matrix alumina grains and the presence of an acicular tertiary MIII mullite which acts as a reinforcement and bridging network of matrix to aggregate grains. An increase in the thermo-mechanical properties of the refractories was attributed to the secondary MII and tertiary, interlocked, acicular MIII mullite crystals. This addressed the research gap where the use of SnO2 was reported to have had negligible effect on the mullitisation of the alumina-zircon composites and the thermo-mechanical properties of the sintered bodies.

The chemical compatibility of the tin oxide doped compositions, AZS-T1 and AZS-T2, in this research against Soda lime Silica and borosilicate glasses, demonstrated the potential of the refractories replacing Chrome based refractories which are not sustainable environmentally.

This research will contribute immensely towards industry and knowledge through increased furnace service life, a sustainable production of commercial and special glasses.

Chapter 1 looks at the background to the research, the scope and the research question to the Thesis.

Chapter 2 is an extensive literature survey related to the topic and research area of interest. It draws on gaps in research that this research area will cover and contribute towards.

Chapter 3 and 4 are is the experimental design and methodology sections which describe the methodologies implemented in developing, synthesising and characterising the novel composition.

Chapter 5 to 7 show and discuss the results obtained from the work conducted.

Chapter 8 and 9 presents the thesis conclusions and highlights future work of the research.

Contents

List of Tables

List of Figures

Abbreviation

PSR:	Parkinson Spencer Refractories Ltd, Halifax
PSR-315	Standard PSR-Ltd Refractory widely used in the glass industries.
PSR-333	Standard PSR-Ltd Refractory widely used in the glass industries
AZS:	Refractory compositions from the Al_2O_3-ZrO_2-SiO_2 system
AZS-01	New developed refractory composition of the Al_2O_3-ZrO_2-SiO_2 system
AZS-T1	Tin oxide doped AZS-01 refractory composition of interest in this study.
AZS-T2	Tin oxide doped AZS-02 refractory composition of interest in this study.
TSR:	Thermal Shock Resistance
ASTM	American Standards of Testing and Materials
Tm	Melting Temperature
T_g	Glass Transition Temperature
J:	Rate of Dissolution of refractories
δ:	Effective boundary layer thickness
D:	Diffusion coefficient
k:	Mass transfer coefficient
Cs, Cb:	Saturation concentrations ($g.cm^{-3}$) of refractory at interface/bulk melt,
PSD:	Particle size distribution of the refractory formulation
SLS	Soda Lime Silicate glass
BSG	Borosilicate glass

1 General Background

1.1 Refractories

The term refractories or refractory materials is generally referred to a subgroup of ceramics, specifically, the non-technical ceramics, and are chiefly made up of inorganic and non-metallic compounds with high melting and Tammann temperatures [1]. The Tammann temperature represents the temperature at which the atoms or molecules of the solid has acquired sufficient energy to allow for their bulk mobility and reactivity, in processes such as sintering, to become appreciable [1]. The Tammann temperature is about ¾ of the absolute melting temperature of a crystalline compound. Above this temperature range, diffusion-controlled processes become more dominant in a material for mechanisms such as vacancy diffusion and plastic flow, including some corrosion processes that are rate limited by diffusion in the host material [1]. As such, refractory materials find common applications in high temperature processes as furnace or process unit liners [2].

According to the ASTM C71 definition, refractory materials are resistant to high thermal (> 1000°C); chemical and mechanical loads at the point of application in the exposure to various industrial thermochemical processes that they are applied in [2].

Therefore, refractory linings serve a twofold purpose. One, of insulation and protection of both the process unit vessels and steel support structures, and the other, of maintenance of the endo and or exothermic thermochemical processes (be it glass production or iron & steel making) through the control of heat loss

from the process [1,3,4]. Control of the heat loss helps to maintain an economic and feasible process. As such, refractories play a significant role as technology enablers in their application as furnace and process unit liners in the metallurgical, chemical and petroleum, energy and glass Industries [1,3,4].

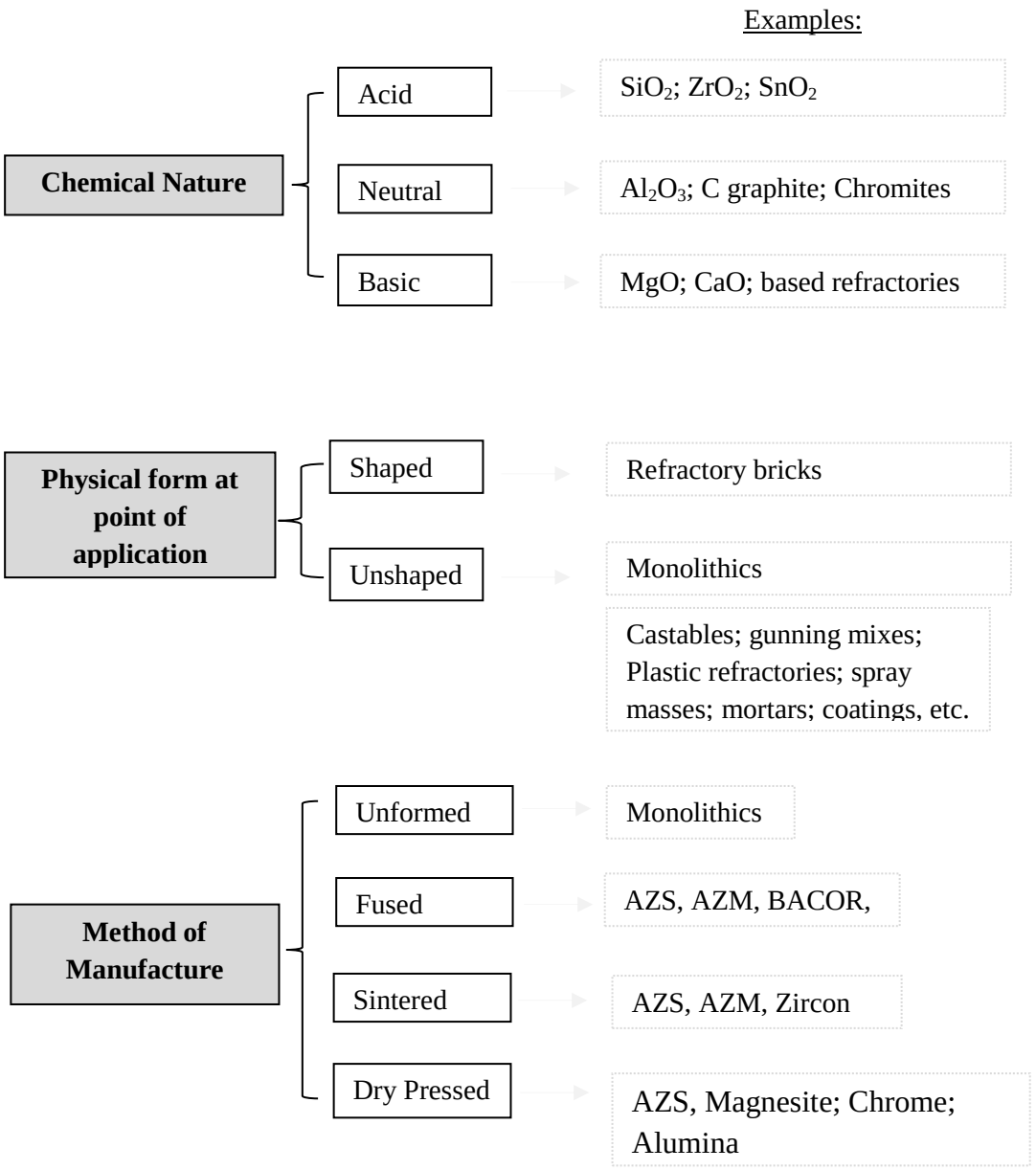

Figure 1-1: Classification of refractories.

Refractories are classified according to their chemical composition; method of manufacture; and or shape at the point of application [1, 2]. This classification is highlighted in figure 1.1. Refractories classified as acidic include SiO_2, ZrO_2 and Cr_2O_3 based refractories and are readily attacked by alkalis and basic slags [1, 3]. Refractories are chosen according to the conditions they face during their application in service. Therefore, acid refractories find most application in areas where the slag and local atmosphere conditions are acidic such as in the flat and container glass furnaces [4-6]. Other areas where acid refractories find application are Coke ovens and acid steel furnaces [4]. This wide variety in the area of application of refractories is also used as a basis of classification; where the nomenclature for refractories under this classification can be; e.g., (i) coke ovens refractories; (ii) steel refractories; (iii) glass furnace refractories.

For glass production such as in the container glass furnaces where the furnace is characterised by two sections, the melting chamber and the working end conditioning/forehearth and forming section, there exist a diversity in the operating conditions of the melting chamber and forehearth sections. Figure 1-2 shows a picture of an End-port Container glass Furnace and its schematic diagram showing the different sections of the furnace. The diagram highlights the process conditions that prevail from the melting chamber to the working end. This means that different parts of the furnace demand different refractory grades for different areas of application. On an industrial scale for the container glass production, refractories from the $Al_2O_3 – ZrO_2 – SiO_2$ (AZS) system, either fused cast and or reaction/direct sintered, are employed in the glass furnaces [5-6]. Fused cast AZS refractories, BACOR, with zirconia contents of 31 – 41wt%, are superior and widely used for glass contact applications in the glass furnace tank Melter zones

(temperature range of 1400 °C - 1550 °C) because of their low porosity (< 2 %) as compared to the sintered refractories.

The sintered AZS refractories, which, by nature of their synthesis, are characterised by a microstructure with a higher level of porosity (> 15%) compared to the fused cast (< 3%), find application in the Channel, forehearth and Feeder section of the container glass furnaces (temperature range 1400 °C – 1100 °C) because of their inherent excellent thermal shock properties,

Also, each production shop has requirements of refractories which need special shapes as well as technical specifications necessary for meeting the process requirements for the shop. Hence, the refractories are often named after these shop names and for the container glass furnace, refractories may be classified as Melter refractories; conditioning channel blocks; forehearth and feeder expendable refractories.

Due to their nature at the point application, refractories may also be classified as either shaped (bricks) or unshaped (monolithic – e.g., gunning mixes, castables). Refractories may be made into bricks as furnace channels and walls or into complex shapes for the glass industry such as the feeder expendable products (e.g., feeder tubes, spouts, stirrers and orifice rings), as shown in figure 1-2 (b); or they may be used as loosely charged grains such as the monolithic [1,3]. Feeder expendables' is the name given to refractory parts used in the gob forming process. They are 'expendable' because they are changed frequently during the life of the furnace depending upon the requirements of the forming operation.

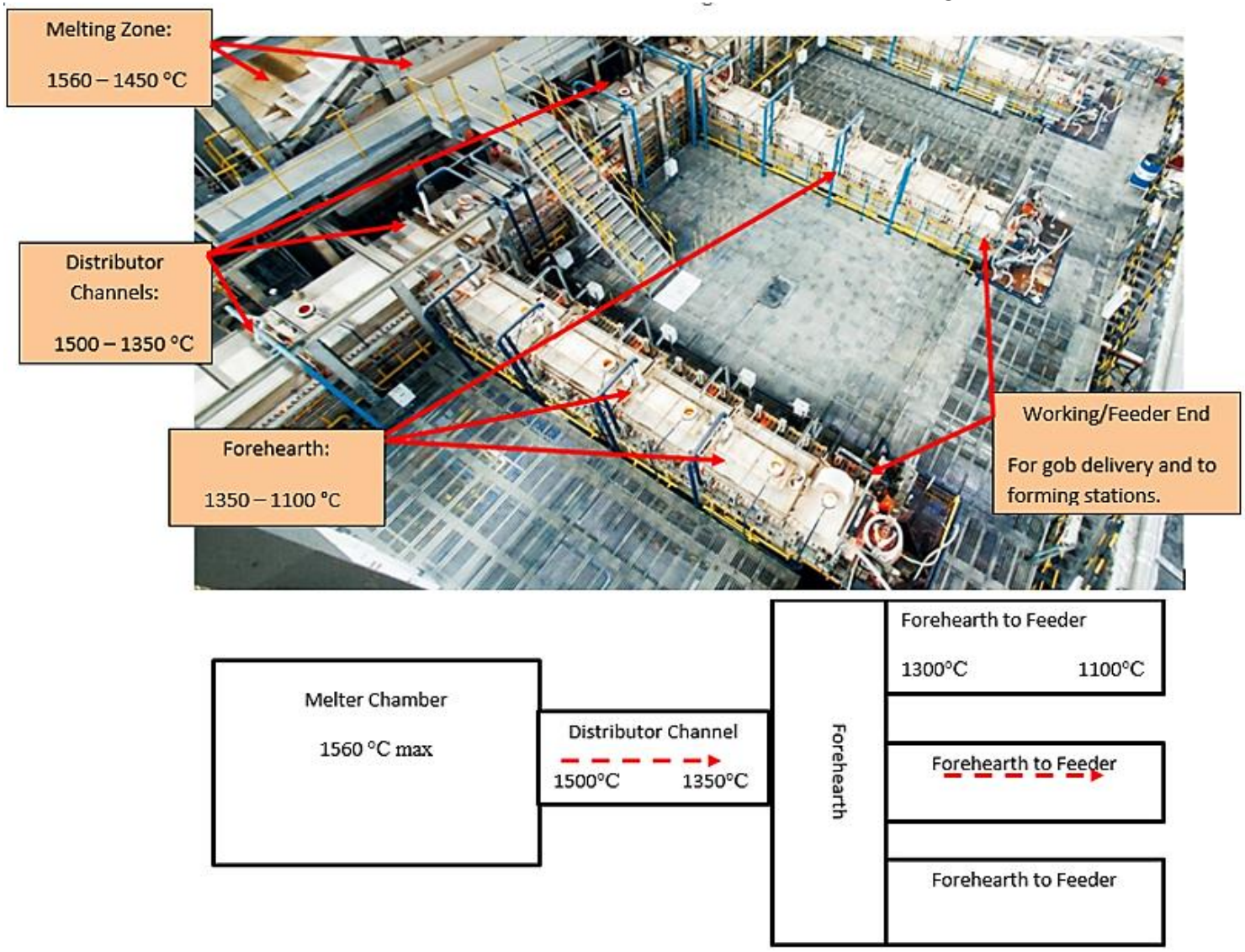

Figure 1-2: Picture of an industrial container glass furnace showing the set-up and sections of the respective sections of the section. The schematic diagram of the glass furnace highlights the temperature process conditions in each section of the furnace [1, 14].

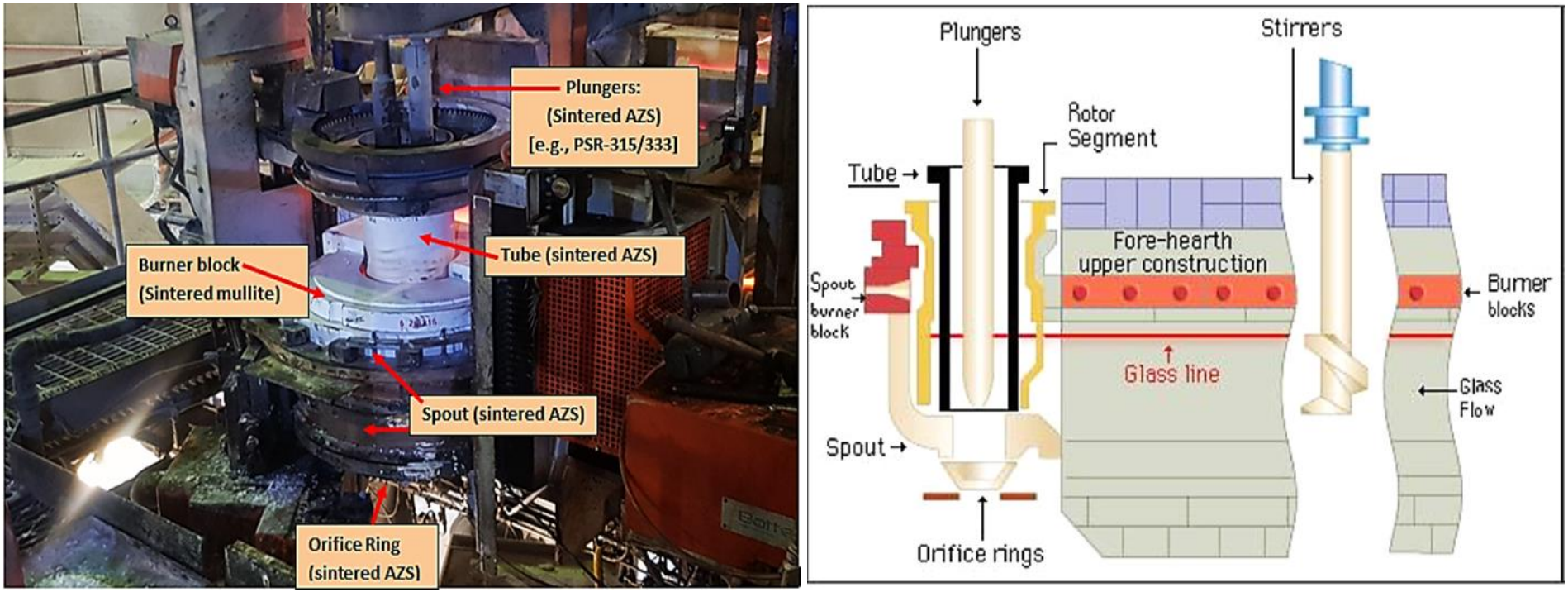

Figure 1-3: Working Feeder glass end: (a) Figure 1.3a shows the set-up of the feeder expendable products at the working end of the glass furnace where forming of the glass is conducted to make container glass bottles. (b) Figure 1-3b is the schematic of the working which details the set-up of the spout, tube plungers and orifice rings as part of the feeder glass system utilised in glass forming for the production of container glass bottles [14].

Examples of feeder expendable products used in the glass industry are shown in figure 1-2 below.

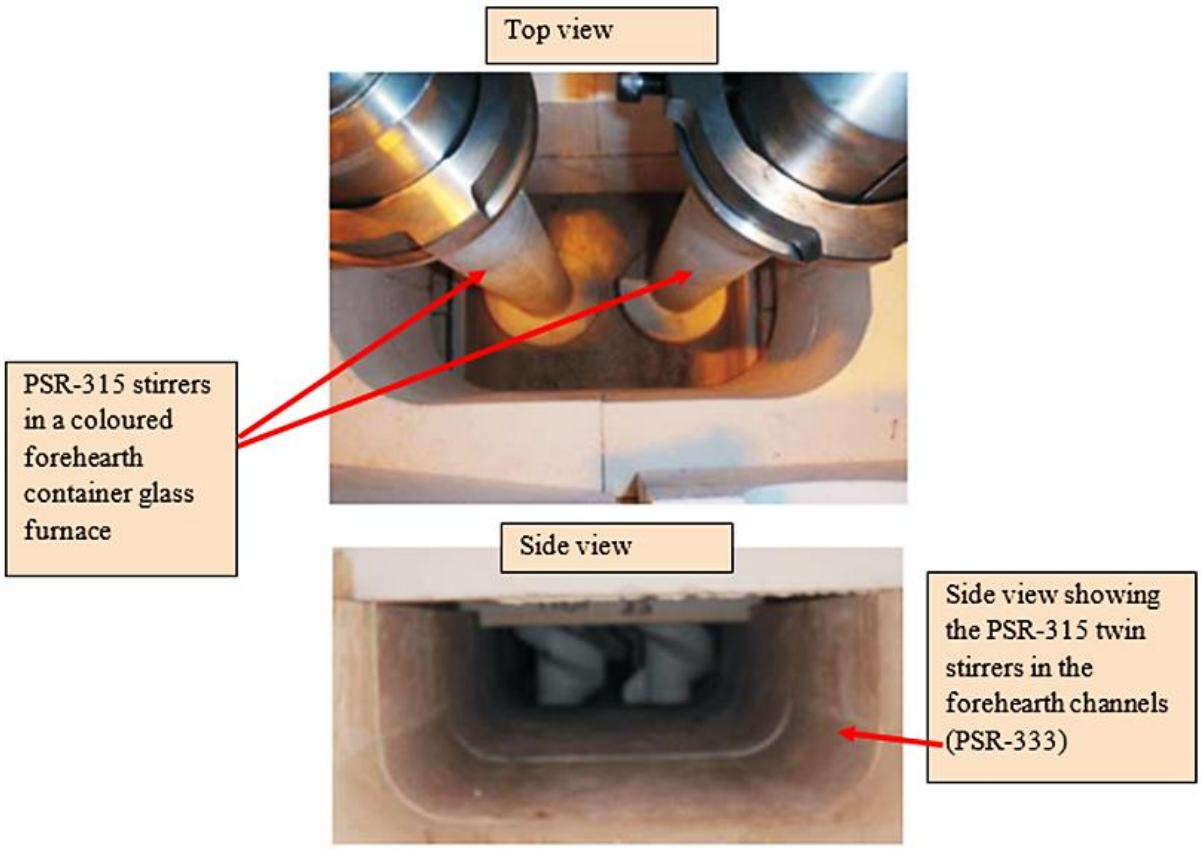

Figure 1-4: Top and side view of Twin stirrers in a coloured glass forehearth glass furnace. Stirrers are examples of forehearth and feeder expendable refractory products that find use in the glass industry [14].

It is known that corrosion and erosion of refractories greatly affects the service life of glass melting and production which often leads to increased costs from low quality end products and shutdowns [1-3]. Literature analysis indicate that high service temperatures, glass composition (Alkali and alkaline earth content) and quality of the refractory material, all determine the extent of corrosion and service life of refractory linings [5,6]. The service temperatures are limited by the quality of the refractories employed, i.e., any possible low eutectic forming phases and the increased solubility of individual refractory oxides within the glass melt at high

temperatures. This in turn limits the end product durability and choice of possible glass compositions [3].

The quality of glass contact refractories is determined to a large extent by the physical properties (apparent porosity and bulk density) and chemical properties (solubility in glass melt, formation of amorphous phase assemblages and low melting eutectic phases) of the refractory. The texture of the refractory, from porosity effects, is dependent largely on the processing of the refractory material, and thus effects the wettability and hence mass transfer reactions between the refractories and the glass melt. Most studies reported that slag corrosion rates of refractory increase linearly with percentages of apparent porosity in the range 12 – 16 %; and even greater at higher apparent porosities (> 20%) [7,8]. Studies by Manfredo and McNally 3, (2002), showed that the order of solubility in silicate glass melts as Al_2O_3>ZrO_2>SnO_2>Cr_2O_3 [9].

The fused cast refractories are however characterised by an inhomogeneous microstructure of interconnected corundum-Baddeleyite (α-Al_2O_3-ZrO_2) particles and interstitial glassy phase [4-6,10,11].

However, fusion cast methods do not represent an economical means of producing refractories due to the high melting temperatures of the oxide constituents [6]. Baddeleyite-Corundum (ZrO_2- α-Al_2O_3) based refractories; also known as Bacor; with un-stabilised ZrO_2 contents > 41wt% are difficult to produce and result in micro cracks, loosening of the structure and increased porosity [2,7]. This is attributed to the allotropic transformation of ZrO_2 from monoclinic (5.72g cm^{-3}) to cubic (5.31g cm^{-3}) [10]. Hence, production of high zirconia refractories is done with the use of the stabilised form of zirconia, either fully or partially stabilised by CaO, Y_2O_3 and MgO

additions or through the or reaction sintering of zircon. This is discussed further in the literature review section.

1.2 Glass and Glass Production

The word glass is taken from the Latin term *glaesum*, which means a lustrous and transparent material. Many of the applications of glasses utilise these properties such as windows, automobile wind screens in flat glass products and beverages and pharmaceuticals in container glass products [12]. Glasses may be organic or inorganic, and those of commercial interest are mainly inorganic produced through the melting of oxide constituents with silica (Quartz - SiO_2) as the principal inorganic oxide [12,13]. For this research, interest and focus will be on inorganic silica-based container glasses, specifically the soda lime silica and borosilicate glasses as they represent the main market for container glass production for the refractory manufactures such as Parkinson Spencer Refractories (PSR-Ltd), Halifax who are part of the major sponsor of this Industrial CASE research project.

Table 2.3 shows the typical glass composition limits of some of the batches of commercial interest [13].

Table 1-1: Typical glass compositions (wt. %) of commercial interest. Acquired from [1; 7; 13-17]

Glass type	SiO_2	Na_2O	K_2O	CaO	MgO	PbO	Al_2O_3	B_2O_3	Other
Container	72-75	13-15	0-0.5	10-12	0.1	-	1.6_{max}	-	0.3
Flat	70-72	12-14	0-0.8	8.1	3.8	-	1.4	-	0.4
Borosilicate	80.1	4.5	0.3	0.1	-	-	2.6	4-15	0.2
Lead crystal	54.0	0.2	12.2	-	-	31.2	0.1	0.5	0.4

Glass production is done in either discontinuously in pot/crucible furnaces for mainly optical glasses; small blown and pressed tableware hand-made glass; or continuously in “Tank Furnaces” for the container glasses, flat glass, fibre wool and other speciality glass and glass-ceramics production [12,13]. Container Glass Tank furnaces are characterised by two sections, the melting chamber and the working end conditioning/forehearth chambers [14]. These sections are separated by a submerged throat in the bridge wall. Figure 1-2 shows a schematic of a container glass tank furnace highlighting the various zones of the furnace.

Glass production in the “Tank furnaces” proceeds in steps of “Batch Preparation” and “Batch Melting” in the melting chamber; “Refining” (Fining, homogenizing and Conditioning) in the distributor and forehearths at the working end section before leaving as a gob at the forming machines. The refining phase of the glass is done in the distributor and forehearth channel zones of the furnace, commencing after melting to control the viscosity, surface tension, density differences of glass melt and bubbles as well as the chemical stability of the glass by addition of fining agents and homogenization of the melt [12-14].

Glass production has evolved over the last half century mainly as a result of improvements in the enabling technology of refractory materials [1,12]. The very potent flux nature of alkali oxides has been exploited in glass production to reduce the viscosity and melting temperatures of silicate glasses. The fluxing action however is detrimental to the refractory materials in service at high temperatures (> 1000 °C) where chemical interactions with refractory constituent parts and phases may result in low melting liquids and hence increased corrosion of the refractories [5,6,12]. Over this period, the industry has seen increasing operating temperature and

an increased throughput of molten glass due to higher melting rates as result of the advent of oxy-fuel fired furnaces from air fired ones [11,12].

The temperature range in the glass melting chamber varies with composition and, for silicate glasses, is between 1400°C – 1550°C [14]. The superior corrosion resistant fused cast AZS refractories are employed as furnace melting tank linings. As shown earlier, in figure 1-2, refractories for the distributor, forehearth and feeder applications form the final link between the melting and the forming processes of glass production. The temperatures from the distributor to the forming station ranges from 1400°C – 1100°C depending on the glass composition [12-14]. This means that the viscosity of the glass from the melting tank to the forming machines spans a range of 10 Pa·s to 10^3 Pa·s [12,13]. While the process conditions of the Distributor, Forehearth and Forming sections are significantly lower than that of the Melter zones, the properties of the refractories applied in these sections have immense influence on the success or failure of the entire forming operation [1,5,12-14]. They must be able to resist the corrosion from molten glass at the same time as being able to withstand the thermal shock of immersion in molten glass [1,2,5,12-14].

During the service life of refractories in glass production, chemical loads play a significant part in the lifetime and efficiency of glass melting furnaces due to corrosion of the refractories [5,6]. Mechanical loads also attribute to failure mechanism of refractories, while the thermal loads and subsequent increased fluidity of the glass melts affects the corrosion rates of the refractories. The concentrations of the alkali hydroxides, in oxy-fuel fired furnaces, produced as a product of the reaction between combustion generated water vapour with alkali and alkaline-earth oxides in the glass melt is of a factor four times higher than in air-fired furnaces [5] and leads to increased corrosion rates on the refractory [5,14].

The limitations on the current refractory materials exerted by these chemical mechanical and thermal loads affects the service life of the glass furnace and glass product quality. Continuous glass furnaces have an expected service life of about 10 years which is normally limited by the corrosion of the refractories [14]. The corrosion of glass melting furnace refractories is an expected albeit expensive occurrence for glass manufacturers with the cost of about £8M ($10M) being spread over the shut-down period and tearing of worn refractories, reconstruction and subsequent loss in production downtimes involved [1].

The main material property requirements demanded of are excellent thermal shock resistance, glass corrosion resistance with little and uniform erosion especially at the glass flux-line, and the elimination of the potential to stoning, seeding and colouring of the glass [14,15,16]. Colouring of glass is done by addition of small quantities, < 0.5 wt.%, of metal oxides which absorb and transmit certain wavelengths of light in the visible spectrum. Table 2.4 list some of the oxides that are used as colorants in SLS and BSG glasses and this demonstrates the limitations on Al_2O_3, SiO_2 SnO_2 and ZrO_2 being only metal oxides applied as raw materials for glass contact refractories.

Table 1-2: List of oxide used as colorants in glasses. Taken from [1, 13-15]

Oxide colourants (Application and colour**)**	
Cobalt oxide: Co_2O_3.CoO (Strong blue)	**Potassium dichromate** ($K_2Cr_2O_7$)
Iron Oxides: FeO, Fe_2O_3, Fe_3O_4 (flint, green bottles)	**Selenium**: (Decolorizing agent for coloured glass)
Chromite: FeO.Cr_2O_3 (Green bottles)	**Nickel oxide (**grey-brown/green/ blue depending on glass matrix.)
Pyrite- Iron sulphide: (Colorant in amber glass)	**Vanadium (**green or brown)

1.3 Parkinson Spencer Refractories (PSR) Ltd.

Parkinson Spencer Refractories (PSR) Ltd is one of the oldest and still leading manufacturers and suppliers of forehearth and distributor refractory products and glass conditioning systems both to the UK and worldwide glass industries. The business was established in 1800 as a partnership between the Parkinson family and the Spencer family [14]. In 1970, the company was awarded the Emhart Glass licence for the manufacture of feeder expendable refractories to Emhart design spec. The current gob forming process is dominated by the patented technology of Bucher Emhart Glass [14]. Licenced Refractory products such as PSR-315 and PSR-333 have become the global benchmark of forehearth and Feeder expendable products in container glass production [14]. As a licensee of Emhart Glass they are one of the world's leading suppliers of feeder expendable refractories. PSR-Ltd, are also specialists in refractories and glass conditioning equipment [14].

The main demand placed on renowned refractory manufacturers such as PSR. Ltd-Halifax, by the glass industry are that the refractory materials for forehearth and feeder applications meet the technical needs of the furnaces at lower costs and longer service life while providing quality glass output that is free from defects such as blisters, stone and cords [12,14,15]. The current service life of PSR-315 expendable glass Feeder products such tubes, plungers and Orifice rings in flint soda-lime silicate glass is about 2-6 months; while for the Forehearth channel blocks as in PSR-333, it is circa 10 years; depending on the service conditions [14].

This has necessitated the need to explore for new refractory compositions or materials that may meet the demand of longer-service life expendable products from glass producers by PSR-Ltd. This requires the use of a dense refractory with a low apparent porosity macrostructure that has oxide constituents with low solubility

within the glass melts. The high porosity of slip-cast sintered refractories provides them with good thermal shock properties but offers zones of the refractory surface with an increased surface area to volume ratio (SA/V) to the molten glass for an increased dissolution rates and corrosion attacks [6-9]. Most studies have found and reported that slag corrosion rates of refractory increase linearly with percentages of apparent porosity in the range 12 – 16 %; but higher at higher apparent porosities (> 20%) [7,8].

This research was enabled by the support and sponsorship of Parkinson Spencer Refractories-(PSR-Ltd)-Halifax. The company's main raw materials are alumina, mullite and zircon for their standard AZS refractories, such as PSR-315, a licenced 'Buchar Emhart Glass' refractory. A research area of interest which forms the main part of this research is to develop both new and or improved zircon/zirconia containing dense refractories that can offer improved corrosion and erosion resistant properties and thus provide an increased service life to the glass industries. This will be achieved by producing Alumina-Mullite-Zirconia refractories with a low apparent porosity macrostructure, (which are comparable to fused cast refractories) as well as having oxide constituents/phases with low solubility within the glass melts and at the interface.

The bulk of the work which included (batch/refractory composition preparation, particle size distribution analysis, slip casting, sintering and material property testing) was conducted under industrial commercial processes at PSR-Ltd Halifax; while much of the characterisation work (SEM, XRD, XRF analysis) as well as the Particle packing modelling was done at the University of Leeds.

2 Literature Review

2.1 Glass

A glass is defined by the ASTM and DIN [12] as a solid whose structure lacks long range atomic order and upon heating past its glass transition temperature T_g softens to becomes a viscoelastic melt and into a liquid above its melting point T_m. The glass transition T_g is characterised by a continuity of volume and rapid change in a material's physical properties such as specific heat, thermal expansion, from a supercooled liquid state. Figure 2-1 shows a schematic first-order thermodynamic properties plot for glass-forming substances as a function of temperature.

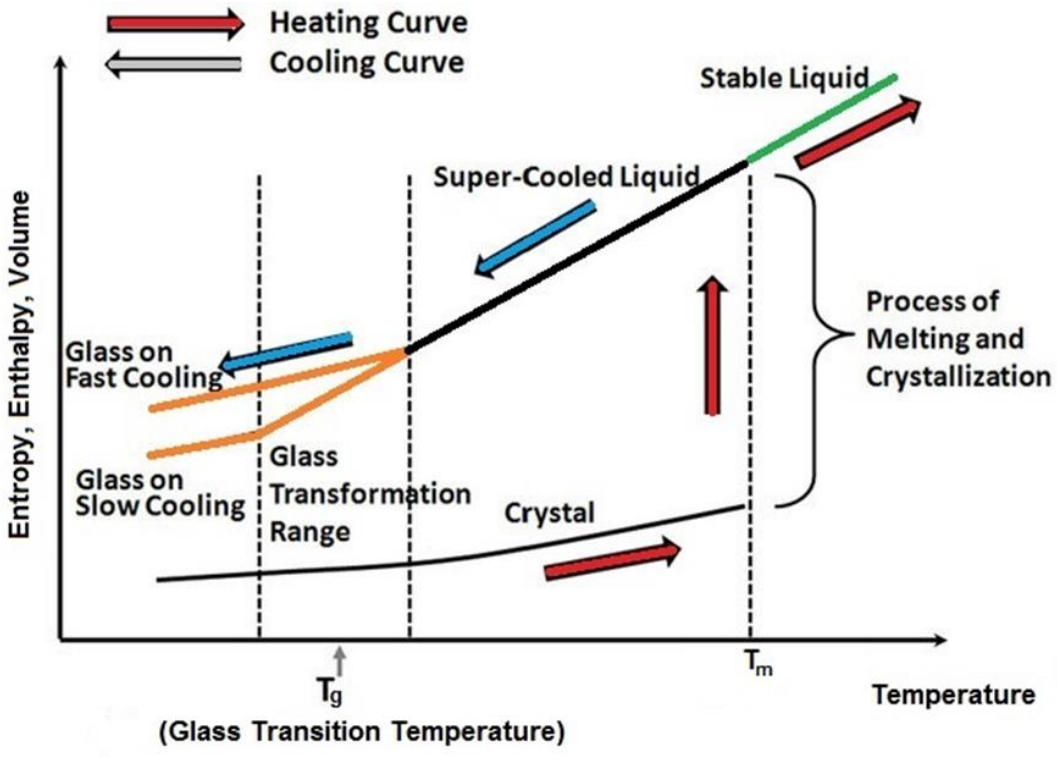

Figure 2-1: First-order thermodynamic properties of enthalpy, entropy, and volume as a function of temperature highlighting four distinct states: liquid (L), supercooled liquid (SCL), glass (G), and crystal (C). Tm = melting point or liquidus temperature, T_g = glass transition temperature.

The glass forming viscoelastic melt is considered a super-cooled liquid when quenched below T_m *to* T_g, and from the classical nucleation and growth theory, the nucleation and growth of a crystal nuclei within the super-cooled melt is thermodynamically favourable [12]. However, surface free energies and increasing melt viscosities (with decreasing temperature towards the T_g*)* provide thermodynamic and kinetic barriers respectively, beyond which it forms a glass (grey area in figure 2-1). As such, most traditional glasses are formed by rapid quenching from the melt at some temperature above their crystallisation temperature and avoiding crystallisation, down past the T_g to a solid glass; i.e., when $T > T_m$ to $T < T_g$ [12,13].

Rapid quenching will lead to a higher T_g and less dense glass than slow quenching [17]. Therefore, glasses (G) exist below the glass transition temperature, T_g. They are thermodynamically unstable and spontaneously relax toward the supercooled liquid state at any nonzero temperature (grey arrow in Fig.2-1). The glass transition takes place at Tg, the temperature where the experimental or observation time, t_{obs}, is similar to the average structural relaxation time of the SCL, τ_R. On the heating path, a glass changes to a SCL at Tg. At any positive temperature, above or below Tg, for sufficiently long times ($t_{obs} \gg \tau_R$), any SCL or glass relaxes and then eventually crystallizes (arrows in Fig. 2-1).

2.1.1 Commercial glasses (Soda Lime Silicate glasses)

Silica sand is the main glass forming constituent of all commercial glasses but melting it on its own requires high temperatures (>1710°C) for fusion due to its close linked Si-O-Si network structure which results in high T_g and viscosity at the fusion temperature $\eta(T_m)$ of 10^7 P. Alkali (Na_2O) and alkali earth (CaO; MgO) glass modifiers are added to

the silica glass forming network in the form of soda ash (Na_2CO_3); lime ($CaCO_3$) and dolomite ($MgCO_3$). The Na_2O aids in increasing the relative fractions of non-bridging oxygen atoms within the silicate glass network [12,13]. Addition of the alkali ions reduces the cross-link density and the oxygen density network structure as shown in figure 2-2 and this results in a decreasing Tg and melt viscosity and hence melting temperatures of the silicate glasses.

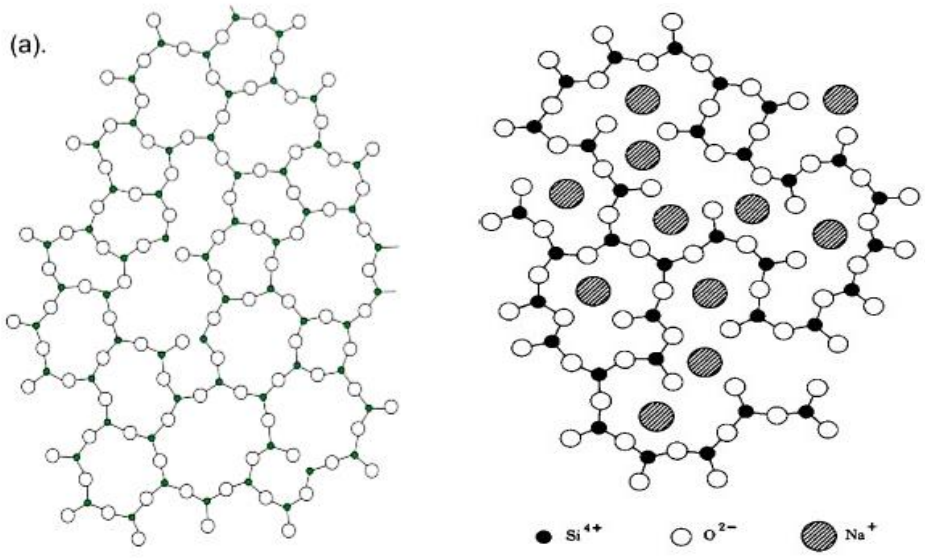

Figure 2-2: Schematic 2D representation of the structure of crystalline silica and as an amorphous glass. (a) Crystalline Silica (SiO_2) showing crosslinked Si-O-Si network in the structure which results in high bond energies; T_g and melting temperatures (b) Random network of alkali silicates. [13].

The alkali earth (R^{2+} ions) from CaO and MgO are located between two non-bridge oxygen ions, promoting structural ordering of the network, stability to the glass and reduces its solubility in water [13]. Addition of R^{2+} ions also has the effect of increasing the glass transition temperature (Tg); while the dilatometric softening point () is decreased on addition of CaO, SrO, and BaO [14]

The soda-lime silicate glasses are the most common commercial glasses and their compositions in container and flat glass applications is somewhat similar, as shown in table 5.2, with the exception of an increased MgO concentrations for the flat glass [15–18]. The presence of alkali cations (R^+ and R^{2+} ions) within the silicate glass network increases the thermal expansion coefficient of the glass due to the decreased cross-linked density and resulting open network.

Common features of all oxide glasses are their ease of mobility of cations within the open glass structure but since the R^{2+} are bound tightly within the framework, their mobility is less than that of the R^+ ions. The activation energy for diffusion increases with increasing silicon-oxygen network density in the glass and increasing size of the diffusing ion. According to Ray [12], the diffusion coefficient in soda lime silicate glasses of calcium ions is 100 times smaller than that of sodium ions in the same glass at the same temperatures. This means that sodium ions have more effect on the corrosion of refractories in soda lime silicate glasses than alkaline earth ions [12,17]. This is agreement with our observation on the studies of static corrosion of refractories in this research which are highlighted in chapter 7 of the thesis.

2.1.2 Borosilicate glasses.

Pyrex-type Borosilicate glasses contain up to ~15 mol % B_2O_3, those with B_2O_3 > 12 mol % have very low thermal expansion coefficient (4.0 – 4.8 x 10^{-6} m/(m K) [18,19]. As highlighted earlier, few systematic studies have been recorded on the solubility of zirconia in glasses or mixtures close to the composition of glasses and enamels. King and Andrews, [20] conducted and reported experimental studies on the solubility of zirconia in borosilicate glasses with various amounts of alkali (Na_2O) and the effects

other various oxides (Al_2O_3; ZnO; MgO; BaO; CaO; B_2O_3) had on the solubility of zirconia in these glasses. Their findings established that the amount of zirconia dissolved in glasses containing Na_2O, Al_2O_3, B_2O_3, and SiO_2; or Na_2O, ZnO, B_2O_3, and SiO_2 depends mainly on the sodium oxide content up to about 30wt. %. Beyond this soda content, complete devitrification of the glasses occurs with reduced zirconia solubility [18]. Fig 2-3 shows the solubility data of zirconia in soda borosilicate glasses without any other oxide additions.

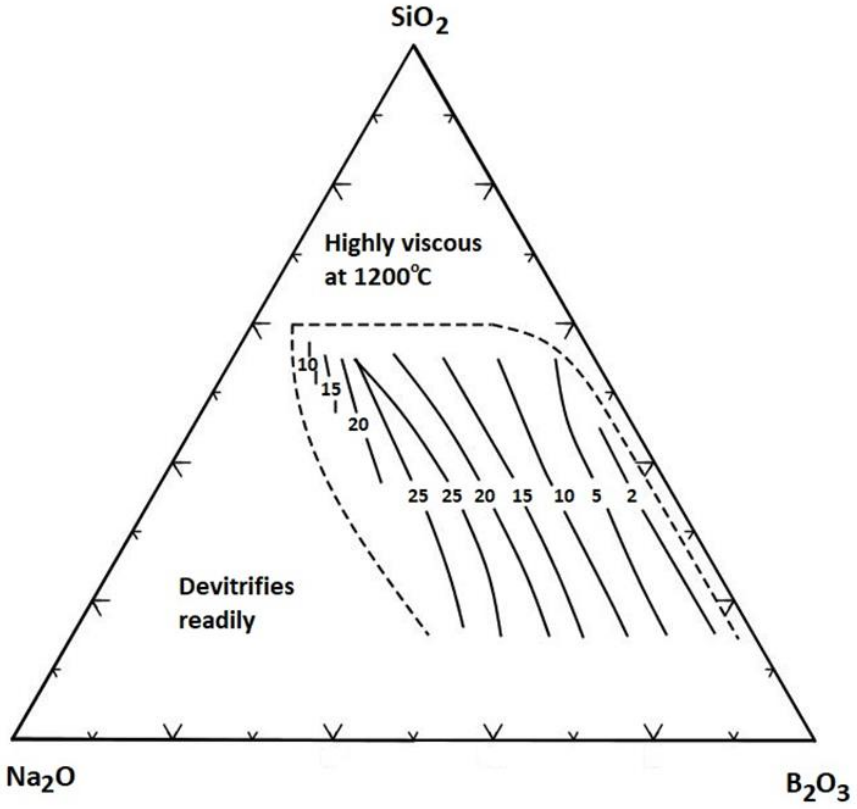

Figure 2-3: Ternary phase diagram of the Na_2O-B_2O_3-SiO_2 glass composition system. Glass compositions by wt%, $Na_2O + B_2O_3 + SiO_2$= 100% and the system highlights the parts of ZrO_2 (wt %) soluble > 900°C in the glasses. Adapted from [23] and digitised using the AcerS-NIST PED editor

While about 2 wt% ZrO_2 is always soluble in frit [18], King and Andrews reported that Al_2O_3; ZnO and MgO decreased the solubility of zirconia in the glass. A summary of their findings is as follows;

- *Alkali and alkaline earths*:
  - Solubility of ZrO_2 up to 16 wt% when Al_2O_3 content was < 6 wt.%.
- *Al_2O_3, ZnO* and *MgO*
  - All decreased the solubility of ZrO_2 with Al_2O_3 having the most effect. Absence of Al_2O_3 and *ZnO_2* increased solubility of ZrO_2 to ~ 17 wt.%. About > 20 wt.% was required to keep solubility of ZrO_2 to ~ 2 wt% in the absence of ZnO and MgO.
- B_2O_3:
  - Flux; and with a constant ratio of SiO_2:B_2O_3; the solubility of ZrO_2 increases, as a generally rule from the solubility curves; proportionally to the Na_2O content up to about 30% of Na_2O.
  - Variations in the ratio of boric oxide to silica cause relatively small changes in solubility, except for glasses high in Al_2O_3 (> 20 wt. %)

2.2 Refractories Materials used in glass tank furnaces

The sintered refractories are produced from a green packed powder compact of a broad particle size distribution of premixed dry particulate formulation systems. These consist of aggregates (> 100 µm); matrix components (< 100µm) and binders. Table 2.1 list some of the aggregate and matrix material used that make up the mix formulation in refractory castable systems and their functions [4-5].

Various techniques or processes, such as compaction and slip casting are utilised in pre-consolidating the mix formulation into a green ceramic before sintering or firing. The resultant structure consists of the aggregate material bound by the fine matrix.

Table 2-1: Aggregate and matrix material commonly used in aluminosilicate refractories. Taken from [5]

Aggregates	**Chemical composition**		**Maximum Service Temperature**
	Al_2O_3	**SiO_2**	
Tabular Alumina	99	0	1870
Mullite	55 – 78	> 22	1760
Andalusite		38 – 40	1760
Matrix	**Function**		
Calcined	α-Al_2O_3	Chemistry /mineralogy adjustments/ bond modification/ development	
Reactive	α-Al_2O_3	Slip/cast Flow/ rheology control/ bond modification/ development	
Quartz	SiO_2	Shrinkage control	
Fume	SiO_2	Flow, rheology control/ bond modification/ development/ mullite formation	
Zircon	$ZrSiO_4$	Reduce metal/slag/alkali attack	
Nano-additives	Various	Optimize packing and thermo- mechanical properties/ bond modification/ development	
Clay (Ball, fire)	Various	Filler / flow/ rheology control	
Zircon	$ZrSiO_4$	Reduce metal/slag/alkali attack	

2.2.1 Alumina

Alumina is one of the most important ceramic materials widely used due to its properties which include high melting temperature, 2054 °C; chemical

stability/inertness; electrical resistivity both as a pure material, a ceramic/refractory component and glass component [5]. Alumina exist in eight polymorphs, seven metastable (κ, γ, δ, θ, η, χ and ρ) and a thermally stable α-Al_2O_3; with the common and most important crystalline phases being α, κ, γ and θ.

The α phase of alumina is known as corundum, from which the naturally occurring mineral which consist of pure α-Al_2O comes from [1,5]. It is relatively highly ionic compound, with *+2.63e* and *-1.75e* calculated valences for Al^{3+} and O^{2-} respectively and the ionic nature of the chemical bonds between the ions accounts for its thermodynamically stable at all temperatures up to its fusion temperature of 2054 °C. Corundum has a rhombohedral structure, space group R-3c with ABAB hexagonal close packed (hcp) stacking of oxygen planes along the c-direction with Al^{3+} ions, or aluminium atoms occupying two thirds of the octahedral interstices.

The θ and γ phases of alumina are metastable. With increase in temperature, γ phase transforms into δ/θ at 700-850 °C, while θ transforms into the α-Al_2O_3 phase at about 1050 °C [1-5]. The transformations into α- Al_2O_3 is irreversible. γ – Alumina is cubic with space group Fd-3m and the Al^{3+} ions occupy both octahedral and tetrahedral positions as shown in figure 2-4 (b). Density of θ-Al_2O_3 (3600 kg/m^3) is less than that of α- Al_2O_3 (3800 kg/m^3).

Due to the structure of α- Al_2O_3, its properties are different from the other phases, and hence, provide alumina phases a wide range for applications. The atomic structure of the θ-Al_2O_3 and α- Al_2O_3 are shown in figure 2-4 below.

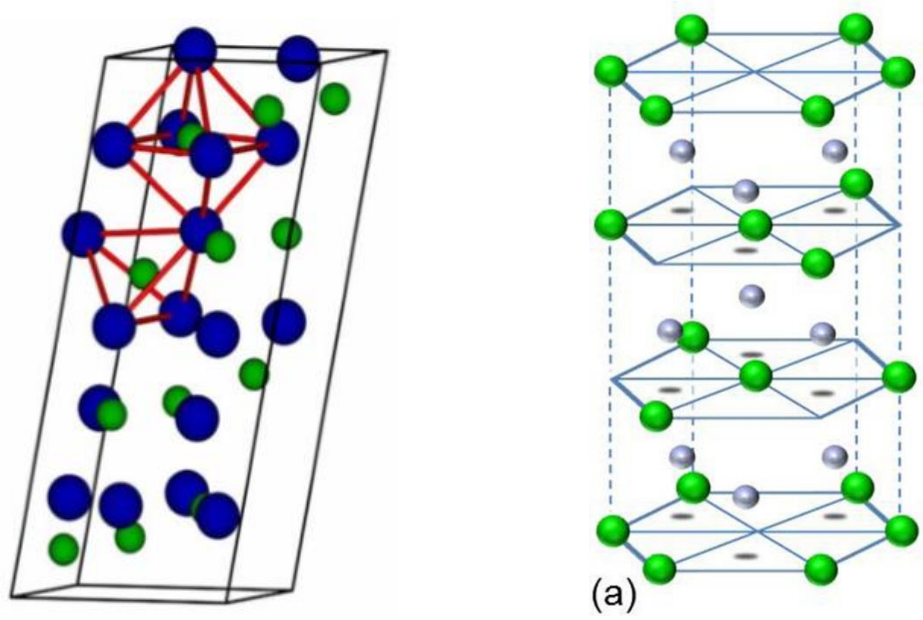

Figure 2-4: Schematic crystal structure of the Alumina polymorphs (a) ϑ-alumina; and (b) α-alumina. (a). on the ϑ-alumina monoclinic unit cell, examples of tetra and octahedral Al^{3+} positions highlighted. The large blue spheres represent O_2 atoms and the small green, Al^{3+}

Both the α-Al_2O and the κ phases are widely used as wear-resistant coatings due to their hardness and thermal stability, while, e.g., the metastable γ and θ phases with their large surface area and low surface energies find applications as catalysts or catalyst supports [1,5].

Slip casting is commonly used to fabricate alumina and alumina-based refractories [47] and can be cast in both acidic and basic slips but mould deterioration is normally accompanied with use of acidic slips. Darvan 7, a sodium polymethacrylate dispersant, which is a polyelectrolyte of the Na^+ salt of poly(methacry1ic acid), average molecular weight of 15 000 with –COOH- functional groups of the carboxylic acid groups that can dissociate to COO-.with an. Together with other anionic polyelectrolytes are commonly used in basic slips of alumina-based refractories [19].

2.2.2 Zirconia

ZrO_2 is a refractory compound that exhibits three temperature dependent allotropes and melts at 2670 °C but has limited use in high temperature applications is due to its polymorphic monoclinic – tetragonal – cubic phase transformation [5,6,21]. When cooled from a high temperature there is a 4.5% volumetric expansion from the tetragonal phase to the monoclinic that would decrease the thermal stability of the refractory [5,9, 21]; T

$$\alpha\text{-}ZrO_2\,(\text{monoclinic}) \xrightarrow{1160-1190^{\circ}C} \beta\text{-}ZrO_2(\text{tetragonal}) \xrightarrow{2300^{\circ}C} \gamma\text{-}ZrO_2(\text{cubic})$$

The high temperature use of ZrO_2 has been accomplished by the stabilisation of the cubic phase through the addition of oxides like MgO, CaO and rare-earth oxides such as Y_2O_3 and Nd_2O_3 which form fluorite type cubic solid solutions with ZrO_2 [5,9]. However, for thermal shock properties, the tetragonal – monoclinic phase transformation is accompanied by a volume expansion which arrest crack propagation and as such a fully stabilised zirconia compound is not truly desirable in refractories [5,9,21].

Yemberger [22] reported that cubic solid solutions of the (CaO-SiO_2)-(ZrO_2-Y_2O_3) and the (ZrO_2-Y_2O_3)(MgO-SiO_2) systems are predominantly stable thermodynamically and as such can be expected to be highly compatible to oxide silicate melts. From his study, the degree of stability of the cubic solid solution decreased with MgO and CaO substitution for Y_2O_3. Table 2.1 summarises the degree of stability of cubic solid solution in oxide systems. for their interaction in SiO_2 melts, no decomposition of the cubic solid solution was observed except redistribution of Y_2O_3 in ZrO_2 and lesser amounts in SiO_2.

Table 2-2: Degree of stabilization of in oxide systems at 1873K adapted from [22,25-28]

Component Content, mol %				Degree of stability for □□ZrO_2 mol.%
Y_2O_3	**CaO**	**MgO**	**SiO_2**	
7.4	-	-	7.4	100
-	10.7	-	10.7	0
-	-	10.7	10.7	100
5.7	1.9	-	6.8	60
3.7	3.7	-	5.7	55
1.9	5.7	-	6.6	100
1.9	-	5.7	6.6	40

*Rest is ZrO_2

For this study Ca-stabilised zirconia will not be used as previous studies on corrosion tests of Ca-stabilised zirconia found SiO_2 infiltration as the chief reason for the destabilization of zirconia, forming low melting point liquids, from which pseudowollastonitic crystals precipitate (during slow cooling to room temperature) next to CaO depleted ZrO_2 grains [22]. This is also in agreement with static corrosion results of 10 wt% Ca-stabilised zirconia refractories showing pitting in soda-lime silicate glass above 1300 °C in our preliminary studies.

The use of zirconia in the glass industry has been comparatively small as compared to that in vitreous or porcelain enamels, and has been considered as an opacifier; insoluble within the melt [21.23]. However, at the temperatures and melting periods employed in

the glass industries, about 20% ZrO_2 can easily be dissolved with the resultant glass having an improved chemical resistivity, viscosity and melting temperatures.

Turner et al, [22] demonstrated improved chemical resistivity of soda lime glasses towards water, acid (HCl), NaOH, and alkali ions, when alkali was replaced with the incorporation of ZrO_2 in the glass, which could not be obtained by additions of any other oxides such as Al_2O_3, TiO_2, MgO, ZnO etc. Applications of such glasses include gauge tubes for boilers. It was also noted that in enamels, when the zirconia compounds are dissolved in the vitreous component of the enamel or glaze, there was an increased chemical resistivity towards alkalis, water and acids in the same way as noted by Turner et al, [22] in glasses.

2.2.3 Zircon

Elemental zirconium does not exist in nature as a free element, mainly due to its reactivity with water, but in mineral form. It is mined mainly as zircon ($ZrSiO_2$) and baddeleyite (ZrO_2-m) but less so as zirconium bearing minerals of chemical compounds of sodium, calcium and thorium [24]. $ZrSiO_4$ is a thermodynamically stable compound, $_{\Delta}G_{1400K}$ = -1489.1 kJ/mol and has found wide spread use as a refractory material [39]. This stability is due to the high coordination number of bi-disphenoid ZrO_8 in a tetragonal structure with the SiO_4 tetrahedra. Aggressive reaction conditions are therefore required to breakdown the strong bonds between ZrO_2 and SiO_2.

Zircon is not readily attacked by aqueous alkalis and only hydrofluoric acid from the mineral acids can readily attack zircon. Figure 2-5 shows the binary phase diagram of ZrO_2 and SiO_2 and shows the thermodynamic stability of zircon at high temperatures making it a suitable refractory material.

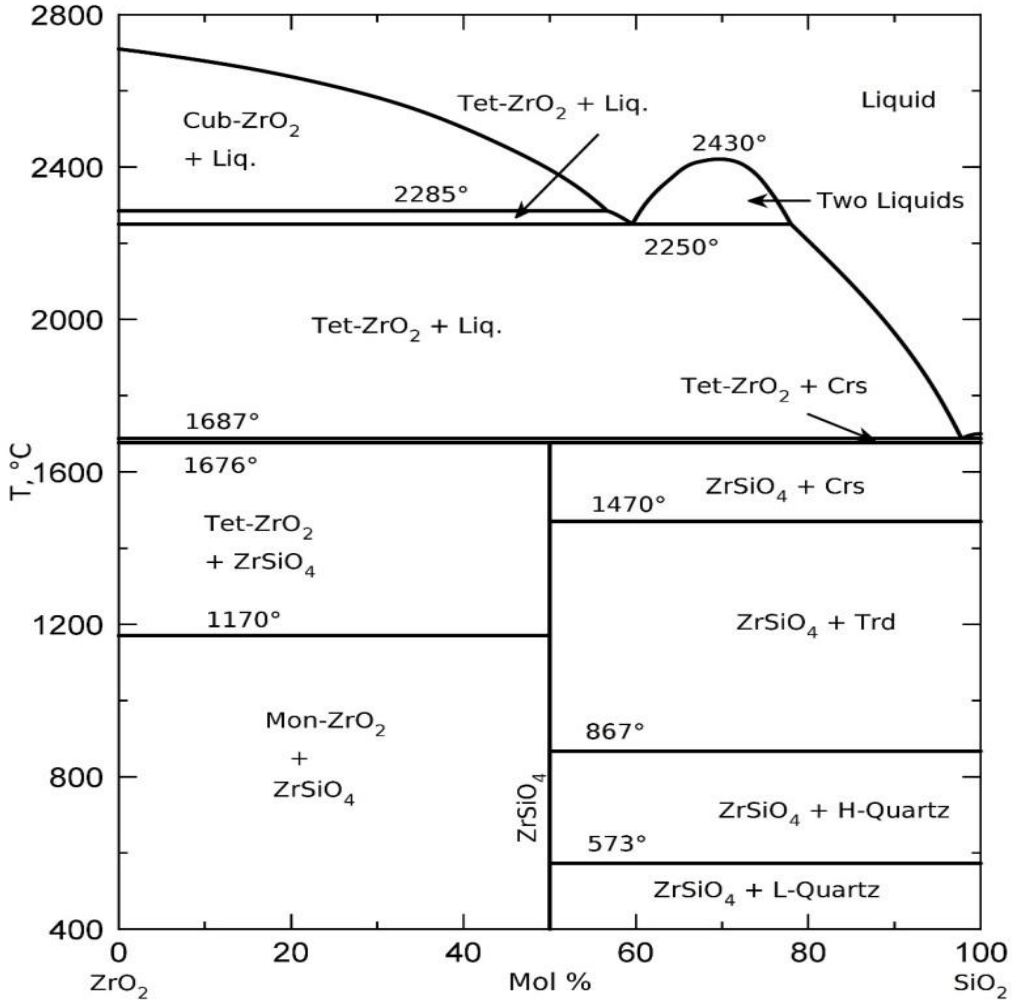

Figure 2-5: Phase equilibrium diagram of the ZrO2-SiO2 system. Taken from [48]

From the phase diagram, it shows that zircon does not melt but dissociates into zirconia and silica as expressed by the equation.

$$ZrSiO4\ (s) = ZrO2\ (s) + SiO_{2\ (s)} \quad (1)$$

Studies have shown that the dissociation of $ZrSiO_4$ is influenced by the particle size of zircon powder [12] and its purity [8,12] with decomposition temperature as low as 1285 °C reported in impure systems especially containing more concentrations of trace oxide elements such as Ti, Al, Na, Fe, Mg, and free silica [25]. Lower dissociation

temperatures of 900 °C were reported by Daher et al. [49] using 40% more than stoichiometry of fused NaOH; Na_2CO_3 and or KOH.

The excellent thermo-mechanical and chemical properties of zircon-based ceramics has seen their wide spread use such as refractory materials, grinding media as well as kiln linings for high temperature application because of the low wetting nature of ZrO_2 to siliceous and metallic melts [25, 26]. The term wetting or wettability of a solid by a liquid refers to the ability of the liquid phase forming a solid-liquid interface when coming into contact with the solid substrate [26, 27]. It is traditionally defined in terms of the contact angle formed at the gas-liquid-solid interface as shown in figure 2-6.

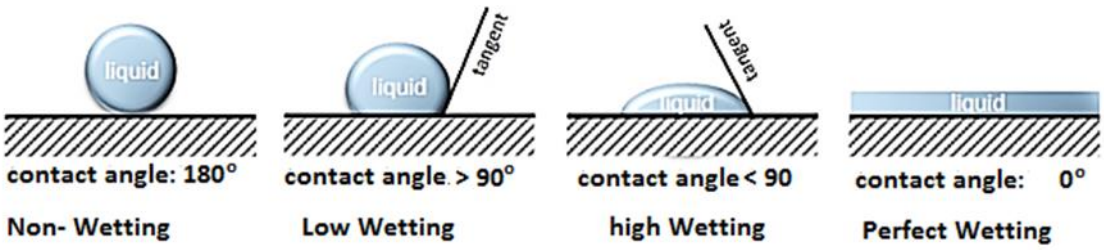

Figure 2-6: Schematic diagram characterising the contact angle and how it correspond to the wettability of a liquid on a solid substrate [25]

Active sessile drop technique tests have been employed to evaluate and quantify the contact angles and hence the tendency of a liquid phase spreading over the surface of a solid substrate [25-28].The boundary between wetting and non-wetting in liquid-solid interfaces is defined to be 90° with contact angles above Work by [26] on the wetting behaviour of feldspathic glass (Al_2O_3-SiO_2-K_2O) on the ZrO_2 substrates with time (up

to 2hr) showed high contact angles; > 90°; as shown in figure 2-7; that revealed the lack of wetting tendencies between the zirconia substrate and liquid glass melt [26].

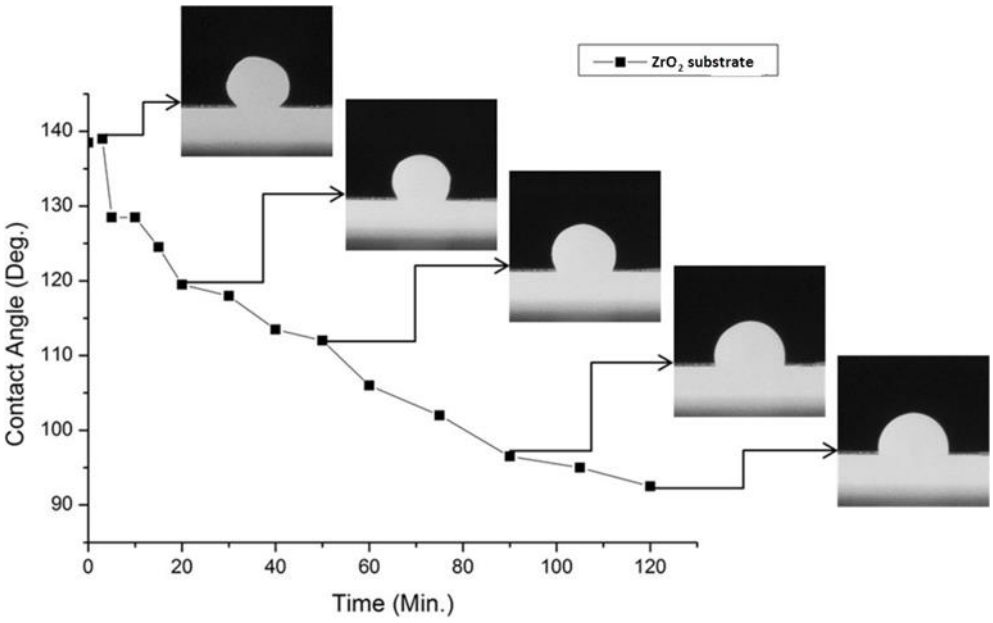

Figure 2-7: Changes in the wetting angles of molten veneer on ZrO_2 substrate blocks within a period of 120 min. Figure shows the low wetting nature of ZrO2 to siliceous glass. Taken from [26]

As highlighted earlier, zircon is cheap and readily available from beach sand and is widely used as a source of zirconia in aluminosilicate-based refractories for the production of mullite-zirconia composites.

For the standard aluminosilicate forehearth refractories, fabrication is normally done with small proportions of zircon content which has been known to improve their performance [15]. Askel et al,[15], investigated the influence of zircon in the standard slip cast forehearth refractory composition by first partially and then completely substituting the zircon with other oxide materials (alumina, silica and zirconia). From

their study, 17wt% of submicron zircon powder to relatively coarse-grained aluminosilicate refractory gave a fivefold increase in strength to room temperature, improved bonding of the matrix and reduced porosity by ~10%. The transformation toughening mechanism of zirconia from the decomposed zircon provided the increased strength. No corrosion tests were conducted on these refractories [15].

The use of zircon as a refractory requires low interstitial water content which can be influenced by the amount of deflocculants or dispersants utilised. The effects of high dispersant concentrations in the casting behaviour of zircon and zircon-alumina commercial refractory powders was investigated and found to cause deleterious cast properties by Moreno et al, [26] and they proposed the use of organic surfactants.

Gerrido L, [27] investigated effect of pH, dispersant content and solid loading slip cast parameters on alumina-zircon suspensions. Viscosity curves of 49% - 60% solid loadings in various polyacrylate based dispersant contents revealed a low viscosity stable slip at pH 9. A 0.24 wt% of dispersant used resulted in high green densities of cast samples and consequently a much denser refractory. Increased dispersant concentration was seen to exhibit an increase in viscosity (unstable slip) of the slip, as well as the number and size of agglomerates and pores which resulted in low density fired refractories [27].

2.2.4 Mullite

Mullite is the only stable intermediate solid solution phase of Al_2O_3 and SiO_2 at standard pressure and rarely occurs in nature. It is characterised by excellent temperature stability, chemical inertness and low chemical attack-corrosion by siliceous melts [28-30]. Mullite has a defect crystal structure that consist of distorted chains of

chains of Al-O octahedra which run parallel to the c-axis and linked by discontinuous double chains of Al-O and Si-O tetrahedra with randomly distributed Al^{3+} and Si^{+4} atoms. Movement of some of Al^{3+} and Si^{+4} ions into normally unfilled tetrahedral positions causes the discontinuities because of insufficient oxygen atoms unavailable to bond to them in the normal positions [30]. This results in an increase in the coordination of the remaining oxygen atoms and forces them into new positions that are slightly different from their original locations. This defect structure then accommodates no-stoichiometry.

Mullite ($Al_{4+2x}Si_{2-2x}O_{10-2x;}$ with x = 0.2 – 0.5) where x denotes the non-stoichiometric range, is the only stable crystalline non-stoichiometric solid solution composition in the Al_2O_3 – SiO_2 binary system under standard conditions [7]. Mullite compositions with x = 0.25 and 0.4 have been described as 3:2 mullite ($3Al_2O_3 \cdot 2SiO_2$) and 2:1 mullite ($2Al_2O_3 \cdot SiO_2$) respectively. For x=0; the above formula represents the composition of the three polymorphic modifications: sillimanite, andalusite, and kyanite (Al_2SiO_5), which are partially related to mullite in terms of their structure.

Figure 2-8 shows the atomic structure of mullite, which is orthorhombic, with unit cell dimensions of dimensions a = 7.540 [A], b =7.680 [A] and c = 2.885 [A] for the stoichiometric composition; projected along the [001] direction [30] and highlights the compositional variations in mullite [30,31]. An increase in the Al^{3+} solubility is achieved through substitution of the Si^{4+} and removal of an O^{2-} (3) ion resulting in an oxygen vacancy. A change in the positions of cations results in partially filled columns as shown in figure 1 by moving T to T*.

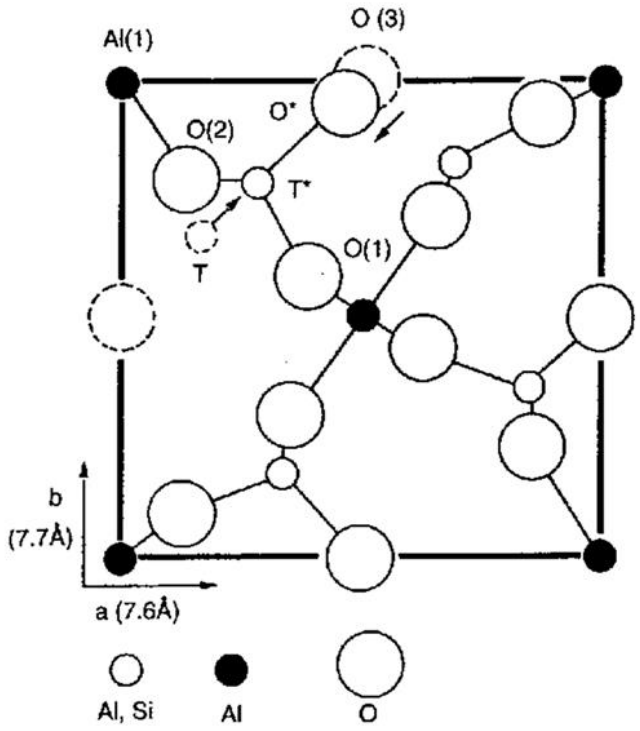

Figure 2-8: Projection of the orthorhombic mullite unit cell along the [001] direction showing T to T* transition of the cations (indicated by an arrow) which is associated with the formation of an oxygen vacancy and readjustment of oxygen in the O(3) positions.[31].)

At room temperature, mullite suffers from low fracture toughness and relatively low strength, compared to the other ceramic compounds [29]. Improvements or increase in the K_{IC} and strength property values have been shown to be realised through incorporation of ZrO_2 into the ceramic composites, thereby reinforcing the matrix [5,29].

2.2.4.1 Sources of Mullite

Reaction Sintering: (Alumina and Zircon)

Reaction sintering of zircon and alumina is a well-established more economical method for the synthesis of mullite matrix with zirconia dispersed in it according to the following reaction.

$$3ZrSiO_4 + 3Al_2O_3 = ZrO_2 + 3Al_2O_3 \cdot SiO_2 \quad (2)$$

Previous studies by [21-23] showed that reaction sintering of zircon and reactive alumina matrix mixtures provides a better distribution of ZrO_2 within the product mullite matrix phase and thereby enhancing fracture toughness values. The microstructural evolution of the crystallised fraction, composition and morphology of mullite from the conventional reaction sintering of micro to macro-sized zircon and alumina mix formulations is reported to be dependent on the firing conditions and firing cycles employed. [29,30]

Koyama et al [31] reported increased mullite phase evolution when a 2-step (sintering and annealing) optimised firing cycles were employed on reaction sintering of zircon-alumina. The microstructure of Mullite, either fused cast or formed in the presence of a liquid phase always exhibits an acicular morphology [32,36]. That formed by solid state sintering and in the absence of a liquid phase is normally granular and varies depending on the nature and purity of the starting raw materials [8,11,13]. In the absence of impurities, sintering above 1400 °C, only some detectable amounts of mullite are formed, with complete mullite conversion requiring sintering at temperatures in the proximity of 1700 °C [5,30, 33].

Work by Iqbal and Lee [43,44] led to their proposed nomenclature (based upon the morphology and relative aspect ratios) of the different types of mullite that they observed to have evolved from porcelain fired products. They named the cuboidal, granular low aspect ratio (1-3:1) grains as primary mullite "Type 1 (MI);" Secondary mullite, "Type 2 (MII)" for high aspect ratio (3-10:1) and "Type 3 (MIII)" for very high aspect ratio (30-40:1) acicular mullite [43-45].

Figure 2-8 showed the models of the atomic structures of mullite and the compositional variation characterised by the different forms of mullite is associated with a change in the lattice constants as shown in figure 2-9. From figure 2-9, a compositional change from 3/2 mullite to 2/1 mullite is characterised by an increase in the c-axis lattice parameter and reduction in the b-axis lattice constants. This explains the change in morphology and aspect ratios of the microstructures in forming 2/1 mullite from 3/2 mullite.

The microstructures of the three different forms of mullite are shown in figure 2-9(b). Another form of acicular mullite, formed in the presence of an alumina rich liquid phase and or from the edges of alumina grains into the glassy phase, was observed and named "Type 3 (MIII) tertiary mullite [45].

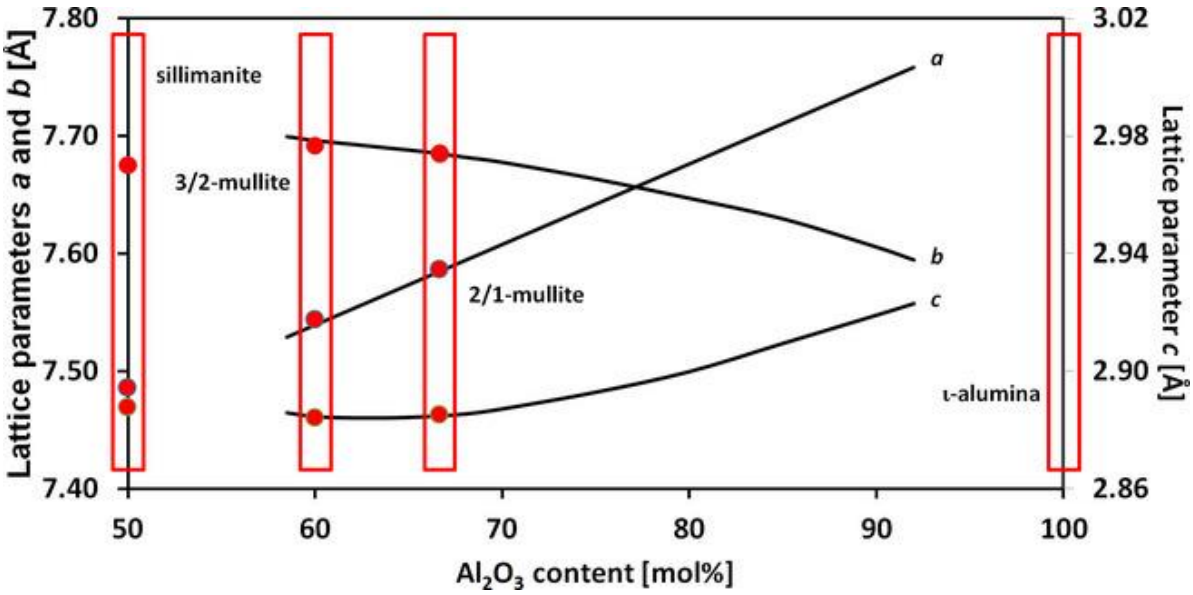

Figure 2-9: Schematic showing Lattice constants a,b and c of mullite dependent from the Al_2O content dissolved into the solid solution common phases such as sillimanite (50 mol% Al_2O_3), 3/2-mullite (60 mol% Al2O3), and 2/1-mullite (67 mol% Al_2O_3) are indicated by the red frames, with red circles representing the lattice parameters a and b (left ordinate), and c (right ordinate) [30].

Reaction sintering of stoichiometric 3:2 mullite is according to the following reaction.

$$3Al_2O_3(s) + 2ZrSiO_4(s) + \textbf{(CaO/TiO}_2\textbf{/MgO)/heat} = Al_6Si_2O_{13} + 2ZrO_2 \qquad (3)$$

Where, CaO [37], TiO_2 [38-40], MgO [41,42] La_2O_3 [43] are additives that have been used in the alumina-zircon starting formulation mixtures, as sintering agents, which have been reported in literature to enhance densification and or mullitisation through the liquid phase from the dissociated zircon. The formation of low melting liquid phase and dissolution of corundum was attributed to the lowering of the mullitisation temperature [51-57].

Among these reported additives, TiO_2 has been extensively studied and reported to enhance mullitisation at lower temperatures [52-54]. Addition of 4wt% TiO_2 was reported to improve densification and mullitisation at lower temperatures through the

formation of $ZrTiO_3$ solid solution and solid solution solubility in the evolved mullite. However, addition of the 4wt. % TiO_2 was reported to affect the hot properties of the sintered bodies at higher temperatures, with the high flexural strength deteriorated by about 25% [54].

2.2.4.1.1 Sillimanite Minerals: Decomposition of Andulusite, Kynite & Sillimanite

The three anhydrous aluminosilicates, andulusite, kyanite and sillimanite are the Sillimanite polymorph minerals that are widely used as refractory materials a source of mullite. Their chemistry and structures are related to that of mullite, and they all have the same 1:1 molar ratio of alumina to silica with a maximum Al_2O_3 content of about 62.92 wt % [30,44]. The sillimanite minerals do not form equilibrium phases at standard pressure of 1 atm, and hence are not found in the phase diagrams of the binary alumina-silica, unlike mullite, at the standard pressure.

This is because they are naturally formed at high pressures and temperatures within the earth. Of the polymorphs, Kyanite is the high pressure structure with the highest density of ($\sim 3.5 < \rho < \sim 3.7$ Mg m^{-3}); and sillimanite, the high temperature structure with a density of ($\sim 3.2 < \rho < \sim 3.3$ Mg m^{-3}). Andulusite exist at lower pressures and temperature as shown by the P-T diagram in figure 2-10 below and has a density of ($\sim 3.1 < \rho < 3.2$ Mg m^{-3}) [5,30].

Due to the nature of their formation under high pressure, all three sillimanite polymorphic materials will decompose when heated at elevated temperatures at standard pressure and their formation densities can be regarded as the driving force for the decompositions [5,30].

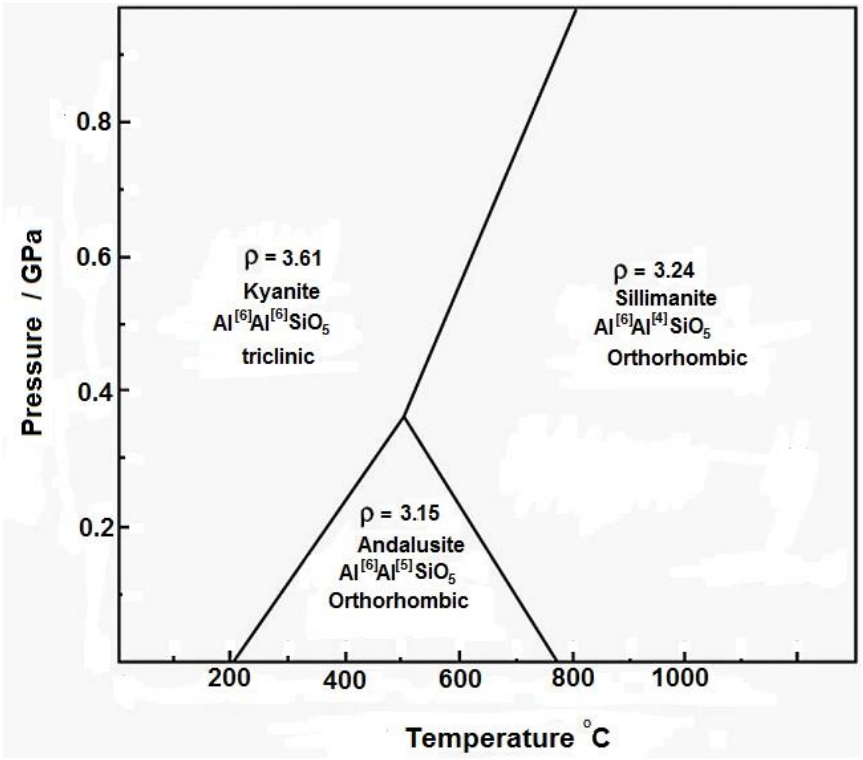

Figure 2-10: P-T diagram of $Al_2O_3.SiO_2$
Section shown highlights 1 theoretical and 3 experimental determined result at the triple point.
Taken from [22]

Their decomposition results in the reaction products of the 3:2 stoichiometric mullite and silica according to the following reaction:

$$3Al_2O_3 \cdot SiO_2 = 3\ Al_2SiO_5 = 3Al_2O_3 \cdot SiO_2 + SiO_2 \qquad (4)$$

The order of their decomposition temperature, which are time dependent starts at ~ 1.150 °C in the order Kyanite < andulusite < sillimanite at intervals. The silica phase form produced differs for the three polymorphs with kyanite producing cristobalite and amorphous for the other two. However, when the silimanite polymorphs are in submicron size, their decomposition temperature range is reduced by several hundred degrees together with their volume expansion and the amorphous silica forms as cristobalite [5,30]

2.2.5 Tin IV Oxide

Tin IV oxide (SnO_2); also known as stannic oxide is the most thermodynamically stable oxide in the Sn-O system in air at high temperatures [47-49,59]. SnO_2 melts at 1630 °C and is known by its mineral form as cassiterite [47]. It is rutile structured under ambient conditions and exist in the 2+ or 4+ oxide state as two polymorphs of SnO (Stannous oxide) and SnO_2 (Stannic oxide). Its use in the glass industry is limited to that of immersed heating electrodes in the glass furnaces due to the volatisation of SnO_2 above 1300 °C and ease of reduction by metallic elements according to the Ellingham diagrams. Therefore, its use in this study adds to the novelty of the study.

Literature on binary phase diagrams of SnO_2 and $Al_2O_3/SiO_2/ZrO_2$ systems, albeit limited, reveals no chemical reactivity in the solid state between SnO_2/Al_2O_3 and or SnO_2/SiO_2 binary systems; but only the formation of $Zr_{1-x}Si_xO_2$ – $Sn_{1-x}Zr_xO_2$ solid solutions [47,48]. These studies on the SnO_2- $Al_2O_3/SiO_2/ZrO_2$ systems are summarised below.

2.2.5.1 SnO_2 – ZrO_2 system

Work on the phase equilibria between ZrO_2 and SnO_2 was investigated by Allemande et al, (2002) by preparing pure equimolar mixtures of ZrO_2 and SnO_2 and heating, annealing the mixtures in the temperature range of 1230 – 1750 °C before fast quenching [59]. From their work, the results, presented as phase diagram showed a wide immiscibility gap between the ZrO_2 and SnO_2 phases leading to a limited solid solution of tin oxide in zirconia, $Zr_{1-x}Sn_xO_2$; and zirconia in tin oxide $Sn_{1-x}Zr_xO_2$. Their results were supported and in agreement with the limited SnO_2-ZrO_2 solid solution;

over the temperature range 1000 °C – 1600 °C, also observed by other research groups [59].

The ZrO_2 and SnO_2 binary system is presented in figure 2-11. From the binary equilibrium phase diagram, it can be seen that solubility of ZrO_2 in SnO_2 and that SnO_2 in ZrO_2 increases with increasing temperature range 1200°C - 1750°C. The maximum solid solubility of SnO_2 in ZrO_2 within the temperature range is 7.64wt. % (6.34 mol. %) to 14.43 wt. % (17.10 mol. %) respectively.

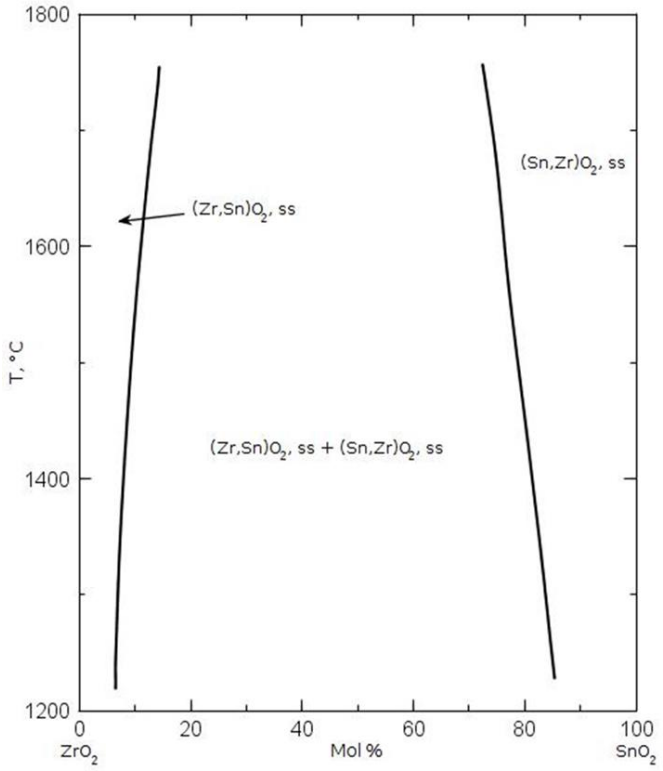

Figure 2-11: Binary phase diagram of the ZrO_2 – SnO_2 system. [59]

2.2.5.2 $SnO_2 – SiO_2$ System

Despite the relative use of SnO_2 based electrodes in glass furnace tanks and Sn-SnO melts in flat glass production, there have been limited investigations in the equilibrium phase diagram of the SnO_2-SiO_2 binary system in air [47, 48]. Yin, (2017), conducted a critical evaluation and optimization of the SnO-SnO_2-SiO_2 system by heating and quenching techniques of SnO_2 and SiO_2 mixed powders in a Rhenium crucible covered in a platinum outer crucible [48]. Rhenium has negligible solubility in liquid Sn and is not contaminated by SnO_2 at high temperature and pressure [48].

In their phase diagram experimental studies, Yin et al, observed no mutual solid solubility between solid SiO_2 and solid SnO_2 with the two oxide components existing as the only stable phases below 1500 °C. Above 1500 °C, a liquid phase formation was observed in SnO_2-SiO_2 compositions rich in SiO_2 while a solid and a liquid phase was observed to co-exist at equilibrium above 1510 °C – 1625 °C.

From the results, although limited in the range of experimental data, Yin et al determined eutectics of SnO_2 and SiO_2 in the SiO_2 rich regions at eutectic temperatures of 1500 °C - 1510 °C and a liquid miscibility gap in the SnO_2 rich regions at monotectic temperatures of 1625 °C – 1650 °C. Their findings are highlighted in Figure 2-12 which shows the calculated binary phase equilibrium diagram for the SnO_2 – SiO_2 system.

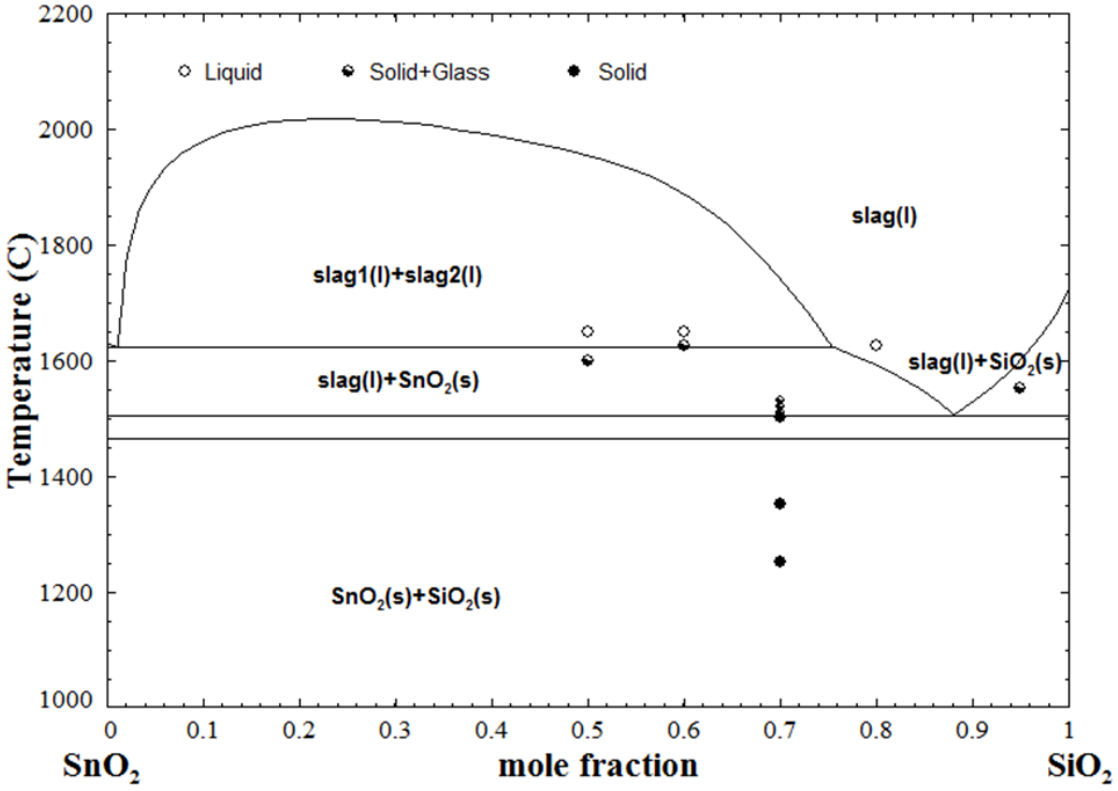

Figure 2-12: Equilibrium phase diagram for the SnO2 – SiO2 system [48].

From the data points of their critical evaluation work presented on the phase diagram in figure 2-12, it can be seen that there was no variation in the compositional range for the experiment work conducted by Yin et al, 2017; and hence validation of their results and data of the phase equilibrium diagram should be taken with caution.

However, this was the only available SnO_2-SiO_2 phase diagram from the literature survey conducted and as such was used in this research as a source of data.

2.2.5.3 $SnO_2 – Al_2O_3$ System

Figure 2-13 shows the equilibrium phase diagram for the $SnO_2 – Al_2O_3$ system.

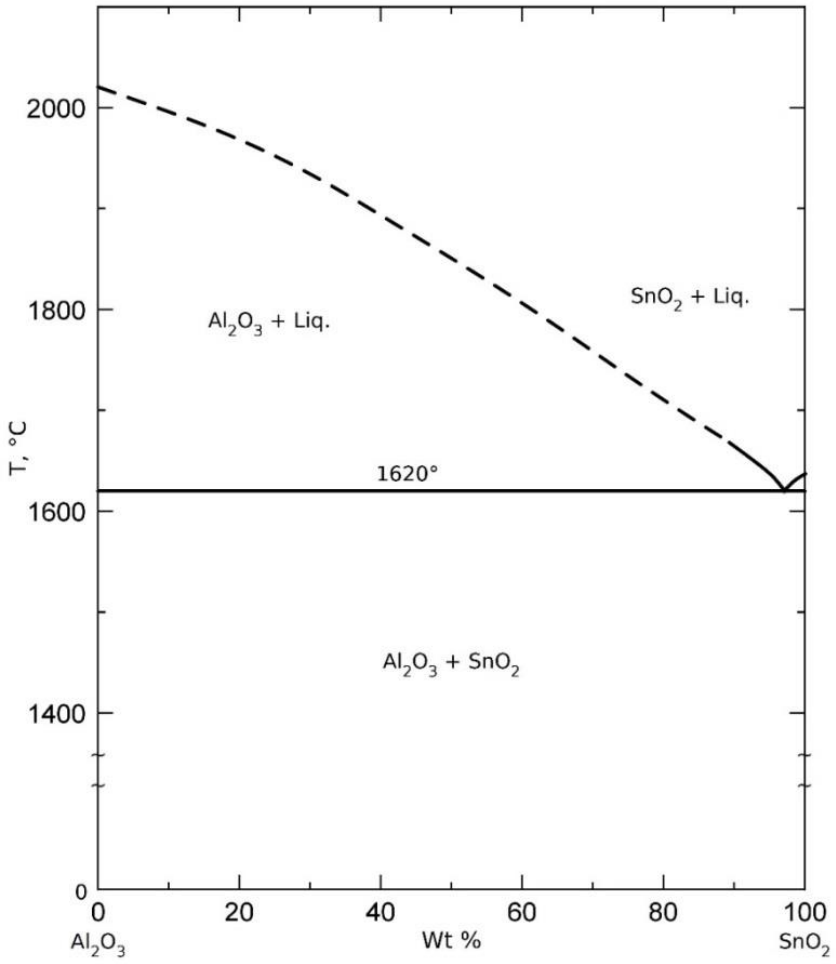

Figure 2-13: Binary phase diagram of the $Al_2O_3 – SnO_2$ system [50]

From the SnO_2-Al_2O_3 binary system, SnO_2 has no solid solubility in Al_2O_3, similarly to the SnO_2- SiO_2 system; and forms a eutectic at 98 wt. % SnO_2 (1620°C ± 5 °C); and in the presence of impurities such as in a quasi Al_2O_3-SiO_2-ZrO_2-SnO_2 system, this can be lowered to below 1828K (1555 °C) [50].

The use of SnO_2 in reaction sintering of mullite has not been extensively reported. Few publications have reported on the formation of a $Zr_{1-x}Sn_xO_2$ and $Sn_{1-x}Zr_xO_2$ solid

solution in the ZrO_2-SnO_2 binary system reactions [46,59]. Kong et al, (2003) investigated the mullitisation effects of some main oxides, SnO_2, Sb_2O_3 and Bi_2O_3 on quartz and Al_2O_3, oxide mixtures [61]. In their studies, they reported increased mullitisation from Sb_2O_3 and Bi_2O_3 additions, but negligible effect on mullite formation in the presence of SnO_2 up to 1500°C [61].

In the present study, the effect of SnO_2 as a sintering aid and mineraliser, on the reaction sintering of slip cast zircon and alumina mixtures to produce zirconia toughened mullite composites was investigated on the AZS-01 and AZS-02 refractory compositions in the temperature range 1550°C - 1550°C.

SnO_2 has the same rutile structure as TiO_2, and as such; from the materials science "structure-property" paradigm; was expected it to have comparable properties and effect on the reaction sintering of zircon and alumina raw materials akin to rutile (TiO_2). In addition, it is also known that SnO_2 has a lower solubility potential in soda-lime and borosilicate glasses with the order of solubility reported as; SiO_2 < Al_2O_3 < ZrO_2 < SnO_2 < Cr_2O_3 [23]. Therefore, any incorporation of SnO_2 into the AZS/AZM microstructure and matrix would be expected to enhance the chemical compatibility of the refractory composites in glass melts.

2.3 Slip Cast Consolidation Methods of Refractory Manufacture

2.3.1 PSD Analysis & Particle Packing modelling

Major improvements in the properties of refractories has been achieved through studies on attempts of controlling the packing densities of refractories as a result of growing

demands for refractory products with enhanced performance during service as well as efficient mixing and casting of these products [4,62]. As bonded refractories are generally made up of large aggregate grains and fine matrix grain material, the interfacial zone between the matrix and aggregate is considered an area of weakness both in terms of particle packing and bonding. This assumption is largely due to the non-organised packing of fine matrix particles near the larger aggregates grains to exhibit what is known as the Wall effects [4,5,62]. Wall effects are characterised by uneven packing and pores and de-bonding after sintering. This is highlighted in figure 2-14.

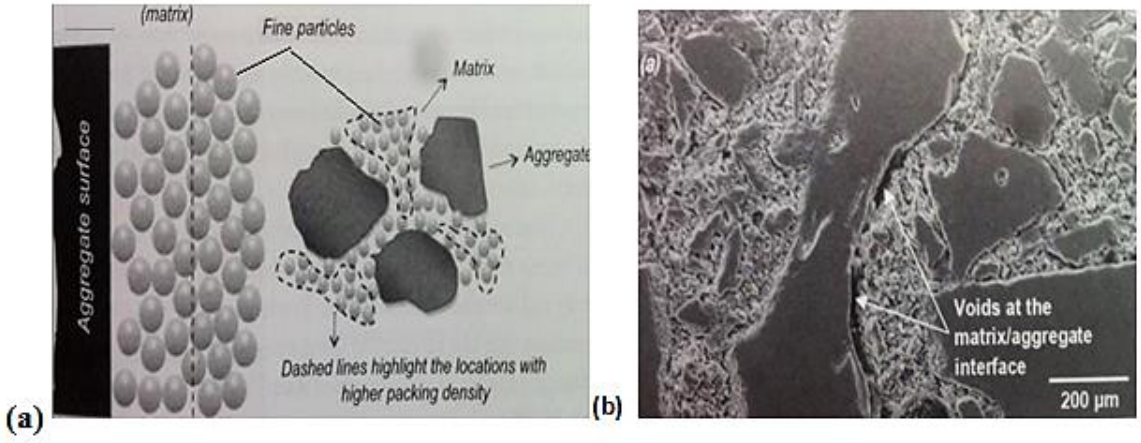

Figure 2-14: (a). Schematic representation of wall effects. (b). SEM image highlighting lack of fine particles at matrix-aggregate grain interface. Taken from [5]

A lot of research has been conducted and reported on monolithic refractories, especially the refractory castables (cement containing, CaO), to produce self-flowing refractory castables (SFRC) with optimised particle packing, reduced water content and high flowability index (FI) using particle size distribution analysis models [4,62,63] but none has been reported on mix formulations used to produce brick refractories by slip casting

consolidation methods. It has also been demonstrated by numerous studies that other physico-mechanical properties; mechanical strength [4], creep resistance [62], porosity, bulk density [4,12,63]; and physicochemical properties; corrosion [62,12,63] of refractory castables are significantly improved with optimum powder packing of selected refractory raw materials (mix formulations) with suitable sizes and fractions.

2.3.2 Slip-cast pre-Consolidation Methods

Slip casting offers a cheap ceramic forming method of using colloidal suspensions with a high solid loading to help to improve green microstructures, by minimising agglomeration through use of dispersions and increasing packing uniformity and hence lowering average pore size. The slip-casting method is used to pre-consolidate powdered ceramic formulations to a high green density of intricate near net shaped refractories and components that needs minimum machining that are not possible with the other processes such as pressing. Either a solid cast or drain cast articles can be produced by this process and larger solid cast refractories of $10ft^3$ or more are normally slip cast for glass contact [4,5,11]. The lack of expensive tooling and equipment required for the process makes slip casting a relatively inexpensive method and in general the process proceeds with the following steps;

1. A colloidal mix or slurry known as a slip is prepared from ceramic powder formulation mixed in a suspending liquid which is normally water. The particle size range of the formulation ranges from (< 100μm) for the matrix material and (<100μm – 10mm) for the grog material.

2. Deflocculants are added to the colloidal mixture to form an electrostatic double layer by cation exchange or steric repulsion of functional groups on each surrounding particle for stability.

3. Binders (e.g., clays; colloidal silica/alumina) are added to give the green cast added strength for handling prior to drying and firing

4. The slip is thoroughly mixed, cast into gypsum moulds (plaster of Paris – $CaSO_4$:$2H_2O$); dried and fired to sinter at high temperatures.

2.3.3 Rheological and Dispersion properties of Slips

As highlighted earlier, typical ceramic bodies can include both low and high solid content particle/fluid suspensions which are known as slips and slurries. Slurries are suspensions of single components, while slips are mixtures of material particulate components [4,5,11]. Ceramic slips are dispersions, and the dispersion and rheological properties of the slip are vital to the pre-consolidation processes such as mixing; green forming by slip casting as well as to the final properties of the sintered refractories [35].

The raw material particulate components are characterised by mineralogical, chemical and morphological parameters and their dispersions, sedimentation tendency, specific surface and cation exchange depend on the state of the particles [4,5,11]. With increasing particle size and density, the sedimentation tendency of the slip increases, while if the specific surface increases, this give rise to the energy of the whole system resulting in smaller particles agglomerating [4,5]. The surfaces of solids are interfaces in an unsaturated boning state, and those of ceramic oxide raw materials are composed of O^{2-} ions (from the crystal structure itself) [4,5]. In their synthesis, during milling processes, unsaturated surface bond structures are formed as well. These free bonds

have a great tendency to saturate by hydration in aqueous systems as when forming slip bodies in fluid suspension [4].

2.3.3.1 Rheology

Rheology is concerned with the deformation and flow characteristics of fluids, suspensions and forming bodies that occur over the full body of applied shear conditions. The rheology of a fluid defines its viscous behaviour as a function of applied shear and hence the viscosity of a ceramic slip measures the internal friction between particles, molecules of the dispersion. Stability of the suspensions, the absence of aggregation processes and high fluidity is vital for producing ceramics of complex geometrical shape with a defect-free microstructure after sintering [35]. Rheological measurements are of fundamental interest because of the information that can be derived from them about the structure of the colloid suspension and the specific interaction among particles [4,5,11,35]. Refractory castables, slips and particulate dispersions can exhibit either a dilatant or pseudoplastic flow behaviour [4,5, 11].

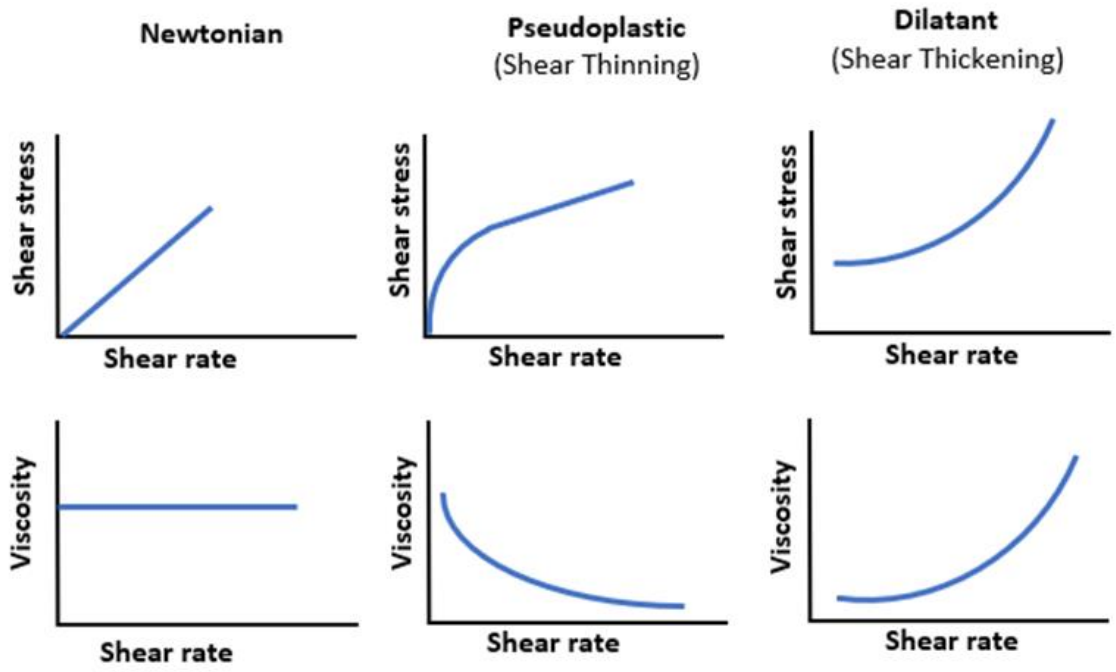

Figure 2-15: Schematic characterising the rheological classification behaviour of colloidal and suspension systems.

Under dilatancy, the viscosity of the slip increases with increasing shear force; while for pseudoplastic flow, viscosity decreases with increasing shear. In thixotropic behaviour, the viscosity decreases with time under constant stress, returning to its original value once the flow is stopped or the when stress is removed.

The rheological properties of slips are determined to a large extent by the water content as a dispersing media; solid loadings of the mix formulation and the deflocculant system of the slip [4,5]. At a pH of 7, it is known that electrolyte free water dissociates according to the following equilibrium;

$$2H_2O = H_3O^+ + OH^- \quad (5)$$

$$pH = -\log [H_3O+] \quad (6)$$

However, the water that is used as a dispersing media usually contains dissolved salts (Cl^- ; Mg^{2+}; Ca^{2+}) as natural components, and this affects the dissociation equilibrium. The dissociation equilibrium becomes defined by the pH of the system as well as the concentration of the solute ions and they all contribute and influence on the dispersion of the ceramic oxide solid particles [5]. In acidic pH range, the hydrated oxide ceramic raw materials form a positive surface charge when the hydroxyl surface groups are protonated by the excess [H_3O^+] ions [4,5,11] On the other hand, a negative surface charge is induced in the alkaline pH range as highlighted in figure 2-8.

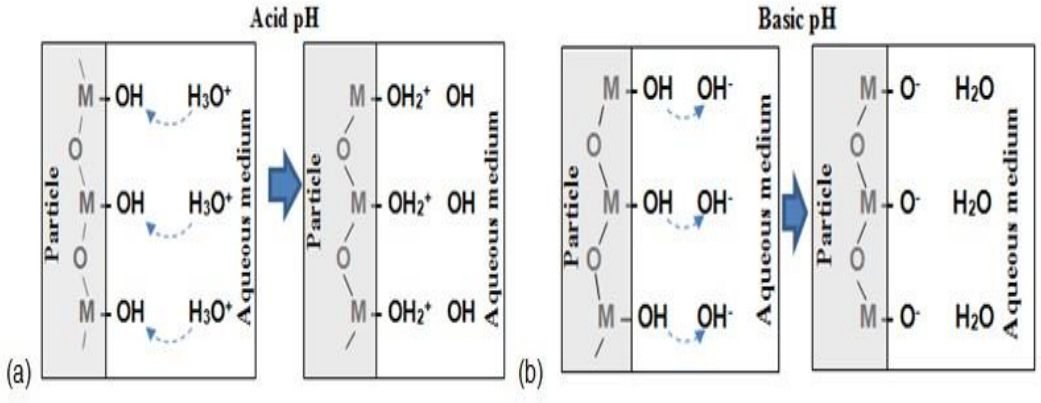

Figure 2-16: Simplified schematic drawing showing the mechanism of how (a) positive and (b) negative electric charges are generated on the oxide particle surface in aqueous medium. Adapted from [4].

2.3.4 Dispersion

2.3.4.1 Zeta Potential

The surface charges developed on the particles give rise to electrical potentials that attract oppositely charged ions (counter ions) present in solution that surround the charged particle and create a screening effect on the surface potential. An electrical double layer (a cloud of counter ions that surround the charged particle and extend into the solution) is formed which through electrostatic repulsion with neighbouring particles creates a barrier to agglomeration and the stability of the slip [4,5,66]

The bivalent cation interacts with the water and ceramic oxide solids particles by adhering to the solid particle surfaces leading to the formation of thin electrical double layers with corresponding zeta potentials and hence interferes with deflocculation at pH $\geq$ 7. However, at pH $\leq$ 6, the bivalent cations are bound and have no effect on the deflocculation [4,5, 66].

As highlighted earlier, the solid particles in the slip tend to sediment and agglomerate due to gravity and electrostatic forces respectively. Studies have shown that sedimentation tendencies increase with particle size and density while agglomeration or flocculation of the small matrix particles will tend to shift the particle size distribution (PSD) towards the larger sizes thereby reducing the particle packing efficiency [5,62,63].

2.3.4.2 Water-solid deflocculation system

As described, sedimentation and agglomeration which has an effect on the optimal rheological function of dispersions is brought about by attractive electrostatic forces.

As such, a homogenous dispersion of the mix formulation is desirable to avoid agglomeration of mainly the matrix particles. This is normally achieved by addition of dispersants or deflocculants into the water-solid particulate system through either electrostatic, steric and electrosteric mechanisms. Deflocculating using electrostatic methods is done by cation exchange of the bivalent cations (from the water) on the particle surface with monovalent ions to provide a thicker electrical double layer and thereby increase the repulsion effect between particles [5, 11,62].

For each slip, there is an optimal range of double layer thickness and corresponding zeta potential that will create a repulsive energy greater than attractive forces to produces a barrier to flocculation. In steric methods, organic polymeric compounds with functional groups act as spacers between the ceramic oxide particles providing agglomeration barriers while for electrostatic means, polyelectrolytes will impart both electrostatic and steric stabilisation to the slip. This helps in attaining a highly fluid slip with low water content and better mechanical properties before and after firing which translate to a denser cast with improved corrosion resistance properties

2.4 Experimental Studies on Corrosion of Refractories by glass melt

2.4.1 SLS Contact glass refractories

Studies by [64-69] evaluated and compared the compatibility and corrosion rates of single crystal corundum (sapphire) with polycrystalline dense α-Al_2O_3, mullite and vitreous silica in soda lime silicate glasses. From their findings, at temperatures < 1425 °C, the high purity αAl_2O_3 was corroded just slightly faster than single crystal sapphire, beyond which the polycrystalline became noticeably more easily corroded. Mullite was corroded more rapidly than silica or vitreous silica at most temperatures > 1380 °C, but

below 1380 °C, the formation of corundum at the interface provided protection against further attack [64-69].

However, the modern glass contact refractories consist of complex multiphase refractory oxide materials, not single phases and as such an accurate behavioural analysis of refractories through the use of phase diagrams is limited and not entirely predictable [1,5,12,64-76]. Since fused cast AZS refractories (from mixtures of alumina, zirconia and silica) are widely used for glass contact applications, corrosion tests of fused cast refractories have been widely reported but not much work has been reported on the corrosion of ceramic bonded AZS, alumina-zircon (AZS), mullite-zircon (AZM) refractories in soda-lime silicate and other glasses. Manfredo and McNally, [34], looked at the microstructures and corrosion resistance of high zirconia fusion cast AZS refractories in SLS glass at 1500 °C for 84 h. Askel [11,12], conducted static glass corrosion of a slip cast alumina-mullite zirconia refractory at 1370 C under ASTM (C-621) standard test guidelines for 72 h in commercial soda lime silicate glass. Zircon content of 20 wt% was used a source of zirconia to give a phase composition of ~ 57 wt% alumina, ~ 20 wt% mullite and 20 wt% zircon of the refractory. The refractory had a bulk density and apparent porosity of 2.9 g cm^{-3} and ~ 19 % respectively.

Kato and Araki, [68] conducted and reported a static corrosion study on the corrosion behaviour of zirconia containing refractories in contact with molten soda-lime silicate glasses with different compositions of varying amounts of alumina, magnesium, borate, alkali and alkali earth oxides. In their study a slip cast sintered 100 % zircon refractory (64 wt% ZrO_2 and 36 wt% SiO_2) and a fused cast ZrO_2 refractory (95 wt% ZrO_2 and 5%

aluminosilicate glassy phase) made into 1 x 1 x 2cm rectangular prism samples. The zircon refractories were fired in a platinum crucible containing crushed glass cullet and held in an electric arc furnace at different temperatures ranging from 1300 °C to 1500 °C for 24hrs before air-cooling to room temperature. The test for the fused cast refractory was similar but conducted at 1500 °C and held for 72 hours. For analysis, the pieces were sectioned at the centre and the corrosion loss measured by the percent loss of cross-sectional area while the glass-refractory interface was examined using an electron-probe micro-analyser.

In most of these studies [11,12,64,68-76] the SEM microstructural features of the glass-refractory interface reveal zirconia crystals within an alumina-silicate glassy matrix of alumina crystals that have been dissolved in the soda-lime silica glass, to form a passivating reaction layer as shown in figure 2-17.

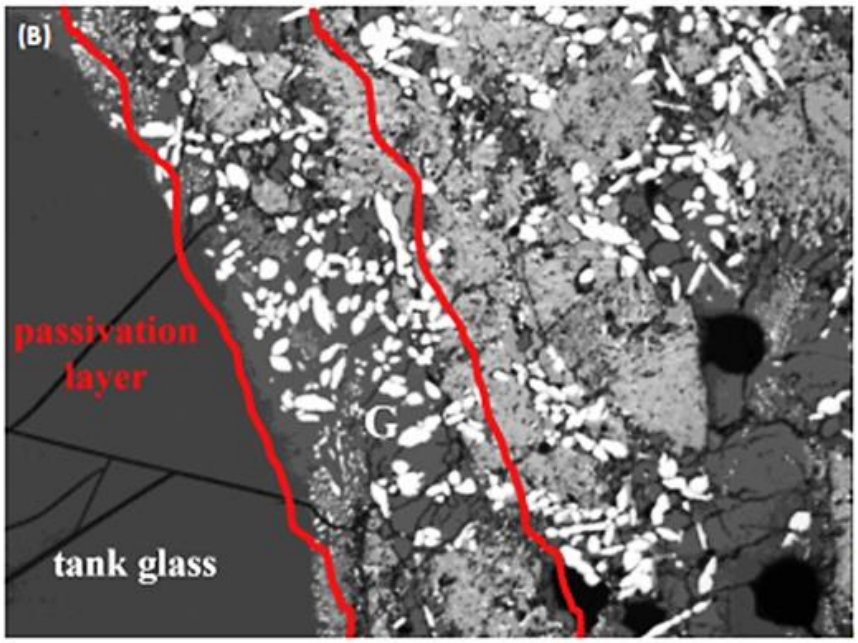

Figure 2-17: SEM electron micrograph of corroded AZS refractory. The micrograph shows the glass-refractory interface and ZrO2 crystal (white) within the passivating layer. [54]

The authors cited the presence of these zirconia crystals within the glass matrix at the refractory-glass interface as evidence of corrosion resistance improvements from zircon and zirconia additions to the refractory [11,68-76]

The corrosion mechanism of the zircon refractory was attributed to the high temperature decomposition of zircon into zirconia crystals and silica. That of the zirconia refractory was attributed to dissolution and transport of zirconia into the bulk melt. Pure zircon decomposition occurs above 1600 °C however presence of impurities is known to lower the decomposition temperatures [55] which is in agreement with the results obtained in this study, from SEM and XRD analysis, with the calculated decomposition temperatures significantly affected by glass composition and ranging from 1350 °C to 1550 °C

Increased alkali contents of Na_2O were noted to have the most effects on decomposition of zircon, but for the fused cast zirconia refractory, both CaO and Na_2O had the same effect on the corrosion rate of the refractory [64,68-76]. Though the study provided information on the effects of glass composition on corrosion rates, no useful comparison analysis could be made between the two refractories because of varying test parameters of time and temperature. No density or porosity tests were conducted on the samples and the geometry of the test pieces offered areas of increased surface area to volume ratio to the corroding medium at the edges and corners of the test samples [64,68].

The use of cylindrical specimens would offer at any one point an equal surface area to volume ratio exposure of the refractory hot face to the corroding media than the

rectangular prism. Therefore, for this study, cylindrical finger samples were used in the evaluation of the corrosion and chemical compatibility of the developed refractory compositions to soda lime silica glass and borosilicate glass compositions.

For glass-refractory dynamic corrosion tests, the corrosion behaviour of fused cast zirconia containing refractories in soda-lime silicate has been reported by many researchers; [5,68-76] but nothing has been reported on sintered zirconia containing refractories. The experiments were conducted as a function of temperature, rotation speed, contact time and duration.

Baudin et al, [70] reported on the dynamic corrosion of fused cast AZS and iso-pressed sintered chromium-based refractories in frits, (a silica based composition with varying amounts of CaO, PbO, K_2O, Na_2O, ZnO and B_2O_3 as fluxing agents), using the rotary furnace or "merry go round test" at 1500 °C. The two Cr_2O_3 based refractories were characterised by high open porosity values ~ 18 %. In their investigation, the finger samples were rotated at 6 rpm in the glass melt for 24h. Temperature of the molten frit glass was established through use of an optical pyrometer. The test samples were immersed in an index fluid with similar refractive index as the molten frit for evaluation of the remaining volume of the corroded refractory by image analysis. In "Part I" of the study, macroscopic analysis, melt-line cut or corrosion was evaluated after the test to quantify and compare the relative performance of the different refractory materials.

Before and after profile measurements were taken of the test refractory samples and in line with glass industry practice, the sample exhibiting the highest corrosion was selected as a reference R, (with a corrosion index = 1). The corrosion index of a test sample was defined as;

$$\text{Corrosion index for test sample} = \frac{(S_r/S_i)A}{(S_r/S_i)R} \quad (7)$$

Where;

S_i and S_r are initial and remaining refractory surface areas, respectively.

Part II of the study was on microstructural evaluation of the corroded regions. Their study revealed no new crystalline products demonstrating congruent dissolution mechanism and the penetration depths and widths of the corroded areas was smaller in refractories containing the highest amount of zirconia. The alkali and alkali earths penetrated through the whole reaction layers but of interest was the ZnO, which was confined to outer regions of the reaction layer. The saturation limits for the solubility of Al_2O_3 and ZrO_2 determined the dissolution process [70].The authors cited the presence of almost insoluble zirconia dispersed in a glassy phase of dissolved alumina close to the frit-refractory interface as evidence of corrosion resistance improvements from increased zirconia contents.

Corrosion of Cr_2O_3 containing refractories was controlled by ingress of molten frit into the open pores of the refractories by capillary action. Dissolution of Cr_2O_3 in the frit was followed by the precipitation of a protective spinel ($ZnCr_2O_4$) layer, which stopped further penetration of the melt frit, once saturation concentration of the spinel in the resulting glass was reached [26].

2.4.2 Non-contact glass refractories

The superstructures and crown refractories make up the non-glass contact zones of the glass furnace and during the melting of glass batch components vapour species are

produced which condensate on the refractory hot face, attach and corrode the refractories. The alkali vapours are very reactive and limit the service time of the refractories. In soda-lime silicate glasses, NaOH, KOH, Na_2SO_4, KCl are the main vapour species, while for borosilicate glasses, sodium tetra-borate and B_2O_3 predominate.

Beiler [72] evaluated the vapour corrosion tests of five types of refractories; Silica, mullite, bonded AZS, zircon and fused cast AZS, by suspending the refractory specimen over 7 molten salts that represent the vapours produced by the subsequent melted glasses, Na_2CO_3; Na-borate; Na_2SO_4; Na-Si-Fluoride; H_3BO_3; Pb monosilicate and a Na-carbonate and Pb monosilicate mixture. In the study, the specimen was exposed for 24 h at 1371 °C.

Baspinar and Kara [73] evaluated the corrosion behaviour of mullite refractories against alkali vapour at 1370 °C with 16 wt% zircon additions to the binder matrix of the refractories. Six different series of mullite refractories from three fused and three sintered aggregate (stage) grains were produced, with each from the fused and sintered grains having one of three different types of binder (matrix) to obtain a mullitic matrix. The binder matrix combinations used were; quartz/alumina (QA), kaolin/alumina (KA) and kaolin/alumina/zircon (KA16Z). In their observation, they noted that zircon addition improved the corrosion resistance of the refractories (c.a 10%) and reduced the apparent porosity. The quartz-alumina (QA) binder exhibited poor mullitisation and densification behaviour and hence had poor corrosion resistance than the KA binder which had good mullitisation and densification.

2.5 Corrosion Mechanism of Refractories for Glass Industries

The knowledge of the corrosion mechanism of refractory material and the subsequent formation of glass defects during glass production is essential as an assumption in the development of new and or improved refractory materials and compositions. The corrosion of ceramic materials has been reported by various authors [5,6,51,68-79] to occur through any one or a combination of the following mechanism;

- Chemical interaction or dissolution of refractory oxide components with the glass melt.
- Penetration or ingress of the glass melts into the refractory through pores causing breakdown of the microstructure and hence mechanical integrity of the refractory microstructure.
- Surface and Transport effects; where slag/glass melt movements, caused by free convection (density and surface tension driven) and forced convection, influence the corrosion rate of the refractory.

2.5.1 Chemical Interaction

The chemical interaction (reaction) of refractory materials with glass melts may occur by direct or congruent dissolution of the refractory components in the glass melt and or the incongruent dissolution through interaction of alkali-earth and alkali ions with the refractory oxide components to form an interface or reaction product. The chemical solution which may form a glaze on the refractory face or the interface produced from the congruent and incongruent dissolution, respectively, of the oxide components of the refractory, and the potential for corrosion of refractories can be estimated through

references of phase equilibrium diagrams from the SiO_2-Al_2O_3-Na_2O_3-CaO-ZrO_2 systems [5, 7-12]. Dissolution of a refractory in liquid slag is usually expressed in terms of dissolution rate and is governed by the diffusion of solved solute ions and, predominantly, the alkali ions from the glass melts into the refractory material through the interface and vice-versa. The dissolution rate can be expressed by Equation 8:

$$J = k(C_s - C_b) \quad (8)$$

Where: J is the rate of dissolution; k mass transfer coefficient; C_s and C_b are the saturation concentrations (g.cm-3) of refractory at interface and in bulk melt, respectively.

The saturation solution concentrations of the refractory oxide species in the glass melt or at the interface, and the diffusion coefficients of alkali/alkali earth and of the refractory oxide components, all determine the corrosion behaviour of the refractory. According to Kingery et al, [27,66] and Dunkl, [74], pure diffusion in the glass melt /refractory system without any chemical reaction or melt convection involved is not possible. It follows then that when the chemical reaction rate is quicker than the mass diffusion of reaction products; a moving solute rich phase boundary is formed through which the refractory-glass melt reactants/product species will diffuse to and from the interface. The equation that represents this rate of dissolution is expressed by the Noyes-Nernst equation:

$$J = D/\delta\ (C_S - C_b) \quad (9)$$

Where: J: Dissolution rate D: Diffusion coefficient; δ: effective boundary layer thickness Cs, saturation concentration (g.cm-3) Cb: Concentrations of reactant (g.cm-3) in the bulk melt

From the Al_2O_3-SiO_2; ZrO_2-SiO_2; SnO_2-SiO_2; ZrO_2-Na_2O; binary phase diagrams, the solubility of individual ceramic oxide components in liquid silicate glass melts can be determined from the saturation compositions at given temperatures. The liquidus lines give the *mol* or *wt* fractions at saturation as a function of temperature [66] and by multiplying the molar density of the binary phase constituents, the saturation concentrations can be obtained [67]. From equations, 8 and 9; D/δ can be defined as the mass transfer coefficient and when this is constant, the dissolution rate is dependent upon $(C_S - C_b)$. This means that as the saturation concentration decreases; the lower will be the dissolution rate. Hence, by comparing the binary phase diagrams of the Al_2O_3–SiO_2 and the ZrO_2–SiO_2 systems, it is clear that zirconia (ZrO_2), by virtue of the position of the liquidus is thermodynamically stable than alumina and does not go into solution readily with silica melts at high temperatures (> 1400 °C).

2.5.2 Porosity and Ingress of glass melt into refractory macrostructure.

The thickness of the boundary layer depends on the viscosity and fluid flow, whether free or forced convection, of the glass melt. Viscous fluids form thicker boundary layers and retard the mass transfer while high glass melt velocities will form thinner boundaries. Siebring and Franken [75] used the Laplace equation to describe the ingress of slag into the refractory wall. Their equation shows that reducing the refractory apparent porosity and increasing the boundary layer melt viscosity plays an important

factor in reducing the penetration of glass within the refractory macrostructure, according to the equation 10 below;

$$L^2 = t\,(\sigma\, d\, cos\Theta)/2\acute{\eta} \qquad (10)$$

Where;

L: Horizontal penetration depth (m)

σ: surface tension of liquid slag/glass melts

d: pore diameter (m)

Θ: wetting angle;

$\acute{\eta}$: viscosity of slag/glass melt (Pa,s);

t: time (s)

For prediction of vertical penetration of slag/glass melt into the upward facing horizontal refractory, Wanibe et al recommended the following equation;

$$L^2 = (2\,\sigma\, cos\Theta)/R\rho g \qquad (11)$$

Where;

L = Vertical penetration depth (m)

σ = surface tension of liquid slag/glass melts

R = pore radius (m)

ρ = slag density (kg/m^3);

g = gravitational constant (ms-^{2}), and

Θ = wetting angle.

2.5.3 Surface and Transport effects

As highlighted in the previous section, the flow properties (viscosity and velocity) of the glass melt influence the boundary layer thickness. The flow may be of forced convection from process flow or free convection. Thompson, 1855, [65] and later on, Marangoni [66], recognised and described strong radial surface movements of the bulk melt in contact with another liquid surface at the point of contact. This was due to density and interfacial tension gradients between the melts, a phenomenon termed the Marangoni effects. When the saturated melt is denser than the bulk glass melt, it sinks to the bottom and induces free convection of the bulk melt. Likewise, surface tension gradient between the bulk glass melt and saturated melt at the refractory-glass interface will generate surface convection due to Marangoni effects [66,75].

Furnace side walls which are vertical side facing sections further away from mechanical stirrers exhibit a glass melt-line corrosion or cut at the refractory-glass-air interface due to the free density induced convection or surface tension gradient induced convection corrosion from the refractory enriched glass melt [7, 12, 26]. This is shown in figure 2-18.

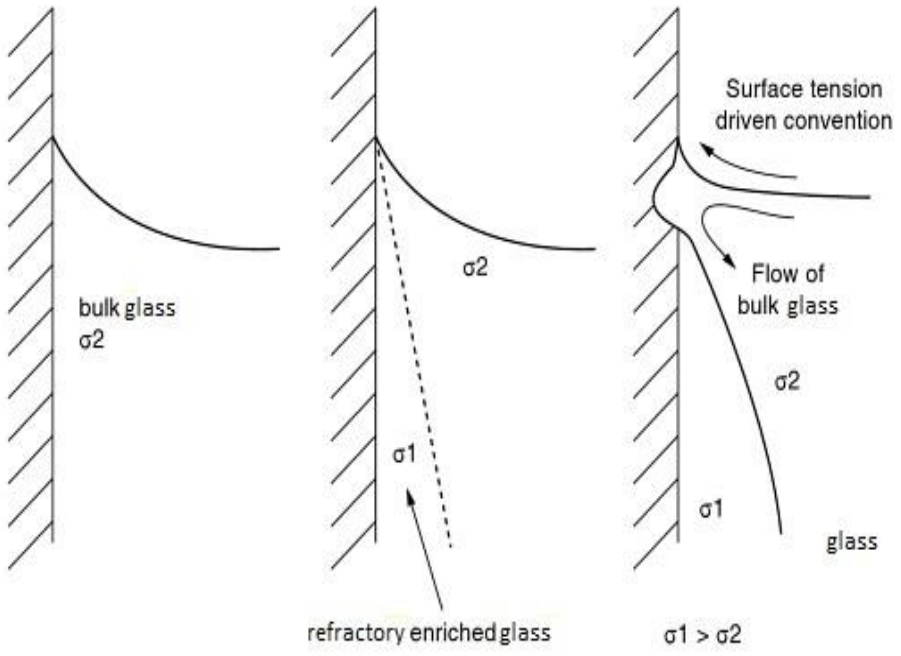

Figure 2-18: Schematic diagram of metal-line corrosion from Marangoni effects. The diagram shows the sequence of events leading to metal-line dissolution of refractories. Taken from [25]

Methods of determining the surface tension and density induced free convection effects is through static glass corrosion tests, while for forced convection, it is through dynamic corrosion tests. Forced convection on the other hand is influenced by process flow of the glass melt from the melting rates and mechanical stirrers. According to several authors, [7, 12, 26, 66] the rate in such conditions was dependent upon the velocity of the forced convection (*v)*, and more importantly to the angular velocity (*ω)*.

This would be replicated in our dynamic corrosion tests; according to Equation 7.

$$J = 0.61D^{2/3}v^{-1/6}\omega^{1/2}C \qquad (12)$$

Table 2-5 summarises the glass melt properties that influence the corrosion rate of refractories under the different convection conditions discussed.

Table 2-5: Glass melt properties that influence corrosion in refractories. Taken from [7, 8, 26]

Glass melt property	Stagnant melt convection	Free convection	Metal line corrosion	Forced convection
solubility	$C_s - C_b$	$C_s - C_b$	$C_s - C_b$	$C_s - C_b$
Diffusion coefficient	D	$D_{3/4}$	$D_{2/3}$	$D_{2/3}$
Density difference		$\Delta \rho_{1/4}$		
Kinematic viscosity		$\nu^{-1/4}$	$\nu^{-1/3}$	$\nu^{-1/6}$
Surface tension		$\Delta\sigma_{1/3}$		

2.6 Phase Diagrams and Alkali Oxide Corrosion of Ceramics

2.6.1 High alumina refractory compositions

High Alumina refractories (> 70 wt%) normally contain Al_2O_3; $Al_6Si_2O_{13}$ and a vitreous phase with the amount of the phases depending on the firing cycles [4-9, 27]. Figure 2-19 shows the Na_2O – 95% Al_2O_3 vertical section of the high alumina refractories of the Na_2O-Al_2O_3-SiO_2 system as reaction with Na_2O proceeds.

The α-Al_2O_3, $Al_6Si_2O_{13}$ and vitreous phase are reduced and eliminated to form β-Alumina, nepheline ($Na_3KAl_4Si_4O_{16}$), and $Na_2O.Al_2O_3$ respectively. Nepheline will transform to carnegiete ($AlNaSiO_4$) at temperatures above 1250 °C [67].

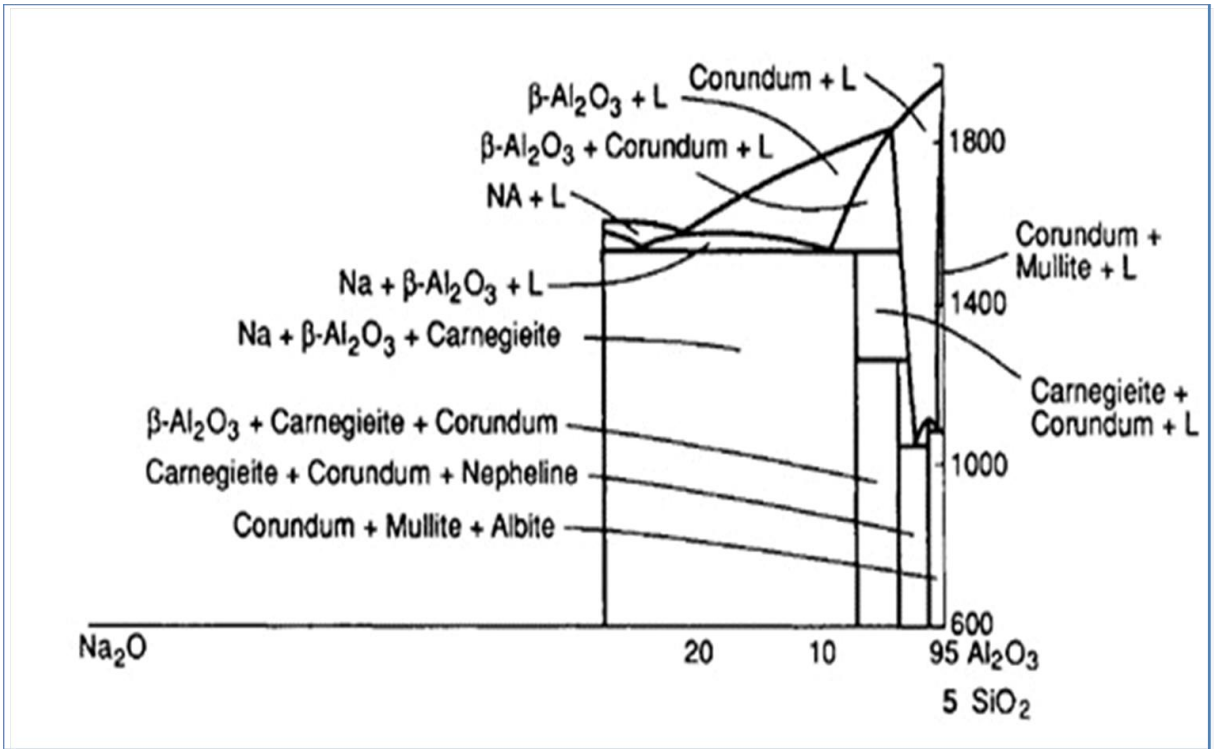

Figure 2-19: The Na_2O-high alumina vertical section of the Na2O-Al2O3-SiO2 system; [67].

2.6.2 Mullite refractory compositions:

Fig 2.20 shows the Na_2O- mullite vertical section and the phases formed are α- Al_2O_3, β-Al_2O_3, and nepheline. The mullite phase decreases in amount as the Na_2O proceeds with βAl_2O_3, and nepheline only forming at higher alkali concentrations.

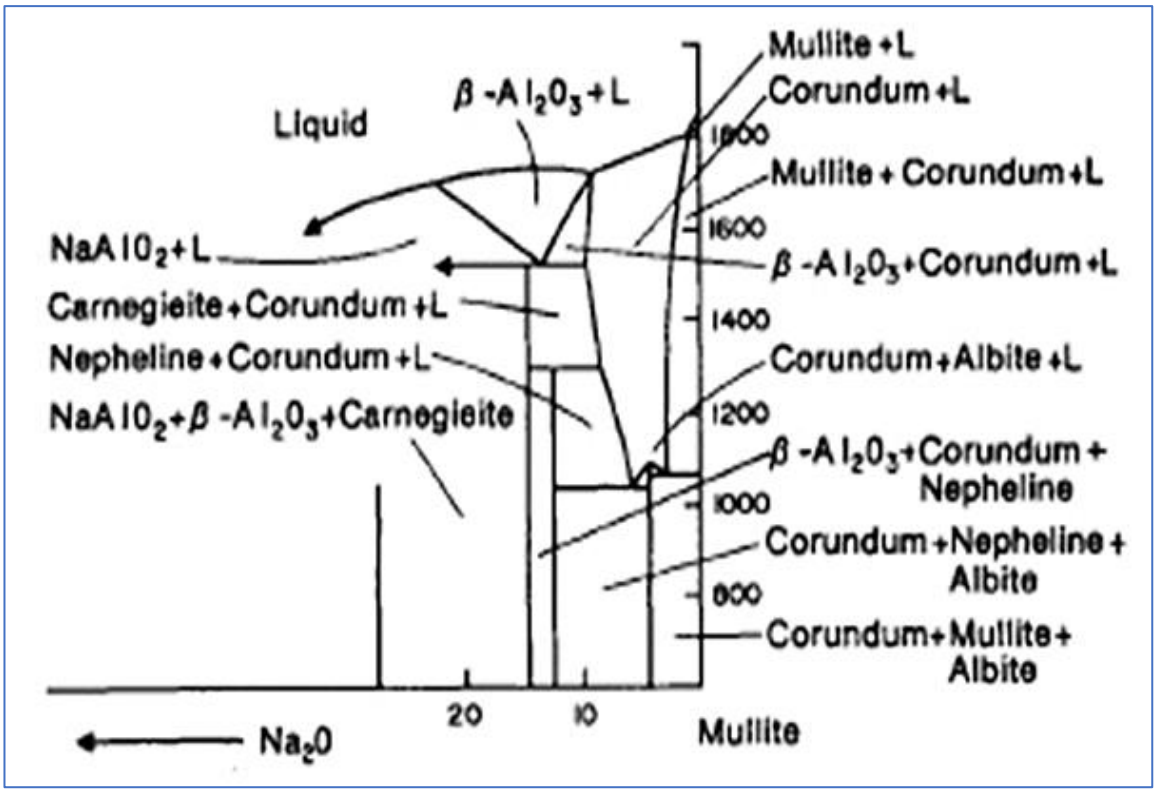

Figure 2-20: The Na2O-mullite vertical section of the Na2O-Al2O3-SiO2 system. [67]

This may mean that deeper within the refractory, with decreasing alkali content, there is less likelihood of nepheline and β-Al_2O_3 forming. Also, with increased alumina content in the refractory composition from the decomposing mullite, the amount of liquid formed decreases sharply and upon cooling this liquid crystallises than forming a glass. The findings from the work conducted by [51-53]; reviewed in the section 2.4.1; are in-line or in agreement with the above phase equilibrium relations evaluations in the Na_2O-SiO_2-Al_2O_3 system.

2.6.3 The Na_2O-SiO_2-ZrO_2 system

Fig 2.21 below shows the metasilicate – zirconia phase equilibrium relationship and stability of zirconia in glass systems with high alkali content in the Na_2O – SiO_2 – ZrO_2 system.

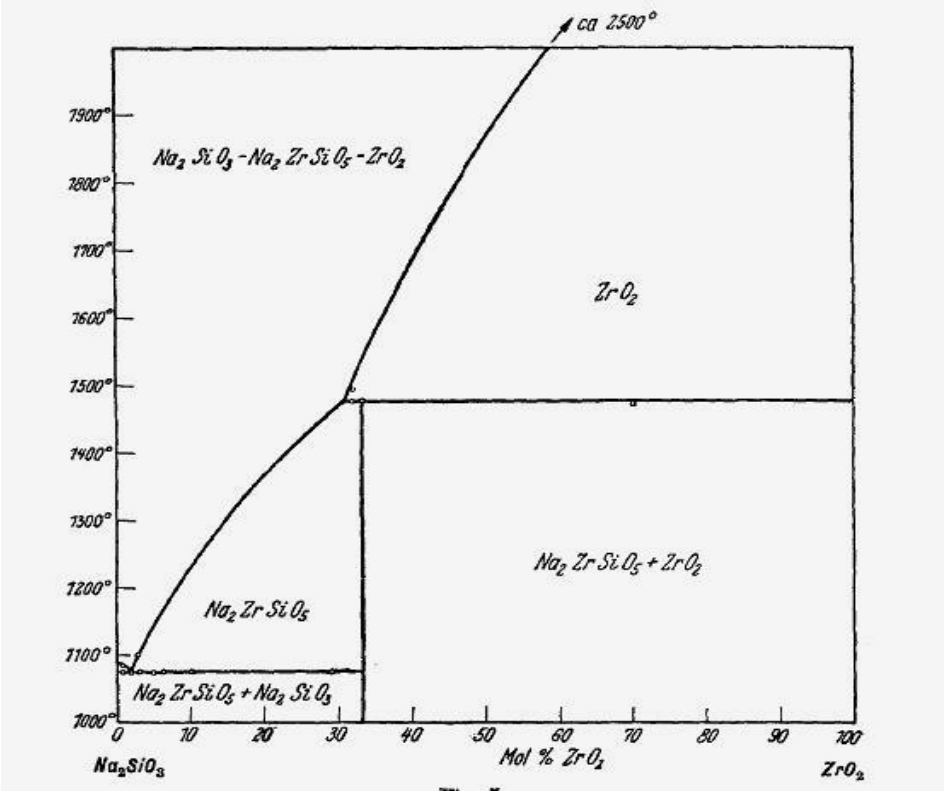

Figure 2-21: Metasilicate-zirconia phase equilibrium diagram. Adapted from [15].

Work by d'Ans and Loffler [33] on zirconia containing opacifiers looked at the equilibrium conditions in the ternary phase diagram of the Na_2O – SiO_2 – ZrO_2 system. A summary of their findings shows high melting compounds and prove the stability of zirconia and zircon in alkali-silicate glasses and hence the low solubility of zirconia in soda-lime silicate glass systems.

Three ternary compounds; Na_2ZrSiO_5 which melts incongruently at 1477C; $Na_4Zr_2Si_3O_{12}$ that melts congruently at 1540 °C and $Na_2ZrSi_2O_7$ (parakeldyshite) exist in the $Na_2O - SiO_2 - ZrO_2$ system. There exists also a binary compound Na_2ZrO_3 which melts incongruently at 1500 °C. These compounds exist at high alkali contents that are not observed in commercial silicate glasses.

Other studies [10-12] on the physical-chemical models in the form of $Na_2O - ZrO_2 - SiO_2$ and $Na_2O - Al_2O_3 - SiO_2$ ternary systems revealed that for AZS refractory systems in soda-lime silicate glasses, sodium zirconium silicates and alkali aluminosilicates ($Na_2O \cdot Al_2O_3 \cdot nSiO_2$) such as nepheline and carnegiete ($Na_2O \cdot Al_2O_3 \cdot 2SiO_2$) may form according the reactions (8) and (9) respectively. Thermodynamic calculation of the reactions shows that ZrO_2 offers the most resistance to molten glass and the possibility of existing for long periods in melts of commercial silicate glasses.

$$ZrO_2 + Na_2O + SiO_2 \longrightarrow Na_2O \cdot ZrO_2 \cdot SiO_2: \quad (13)$$

$$\Delta G = -2257.38 \text{ kJ/mol} \quad (14)$$

$$Al_2O_3 + Na_2O + SiO_2 \longrightarrow Na_2O \cdot Al_2O_3 \cdot nSiO_2 \quad (15)$$

$$\Delta G \text{ (nepheline)} = -2809.8 \text{ kJ/mol} \quad (16)$$

$$\Delta G \text{ (Carnegiete)} = -3666.5 \text{ kJ/mol} \quad (17)$$

3 Experimental Design

As highlighted earlier in chapter 1, dense refractories, when classified according to their compactness, contain porosity in the range 15 – 20 % [2]. In the literature survey and in tandem with observations from this research's preliminary static corrosion studies (discussed in section 7), most studies state a linear increase of refractory slag corrosion rates for a refractory material with an apparent porosity in the range 12 – 18 %. [15, 16]. Therefore, to answer the research question set up in section 1, this chapter highlights the scope and objectives for this research project and the experimental design taken to accomplish of the research goal of developing, synthesising improved and new sustainable AZS refractories that can offer improved corrosion and erosion resistant service life to the glass industries.

3.1 Scope and Objectives of Research

The corrosion and dissolution of refractories has been widely investigated and reported in literature to occur through the following mechanisms of;

- Capillarity – wettability of refractory by molten glass
    - Ingress of molten glass within refractory pore macrostructure.
- Chemical interaction:
    - solubility of refractory oxide in the glass melt and at interface

- Surface phenomena
  - Surface tension gradients (Marangoni effects)
- Transport phenomena
  - Mobility of dissolved refractory in the glass melt boundary phase
  - Mobility of reacting species in the glass melt

For the glass contact refractories, corrosion effects differ on the different sections of the refractory blocks but the main chemical interaction with glass melts is the interaction of alkali-earth and alkali ions with the refractory structure. As highlighted earlier in the literature review, alkali ions are the most active due to their high diffusion coefficient in glass melts as compared to the alkaline earth ions. The glass phase assemblages and open pores within the refractory macrostructure offer the weakest sites where penetration of these ions occur first, fluxing the glass phase and reducing its viscosity followed by the chemical interacting and dissolution of the mineral phases of the refractory [4-9].

The main demand placed on renowned refractory manufacturers such as PSR. Ltd-Halifax, by the glass industry are that the refractory materials meet the technical needs of the furnaces at lower costs and longer service life while providing quality glass output that is free from defects such as blisters, stone and cords [2-4]. This requires the use of a dense refractory with a low apparent porosity macrostructure that has oxide constituents with low solubility within the glass melts. The high porosity of slip-cast sintered refractories provides them with good thermal shock properties but offers zones of the refractory surface with an increased surface area to volume ratio (SA/V) to the

molten glass for an increased dissolution rates and corrosion attacks [6-9]. Most studies have found and reported that slag corrosion rates of refractory increase linearly with percentages of apparent porosity in the range 12 – 16 %; but higher at higher apparent porosities (> 20%) [62].

A research area of interest which forms the main part of this research is to reduce the apparent porosity of the slip cast sintered refractories and counteract the reduced thermal shock and spalling properties with in-situ reaction sintered mullite and the transformation toughening mechanism of dispersed zirconia within the composite matrix. Alumina has high hardness with good corrosion resistance but low fracture toughness properties while zirconia has high strength (900–1470MPa) and toughness (9–10MPam ½); excellent corrosion resistance to several aggressive environments but low hardness properties (10 – 12 GPa / Vickers Hardness HV9.807N [1-5]. Mullite has low thermal expansion, low conductivity, excellent chemical stability, creep and high temperature resistance. The presence of ZrO_2 is known to provide the increased corrosion resistance due to its low solubility within glass melts [5-9].

The main purpose of this research is to develop new/improved zircon/zirconia containing dense sustainable slip cast reaction bonded/sintered, refractory materials and compositions that offer an improved corrosion resistance to commercial glass melts. The new improved compositions will be expected to offer sustainable furnace service life of more than 10 years especially for the forehearth zones of the glass furnace.

3.1.1 Objectives:

In order to achieve this, the following research objectives were agreed upon in the pursuit of identifying a sustainable and more compatible refractory with soda-lime silicate and borosilicate glasses.

Using a standard AZS forehearth commercial refractory, PSR-315; an alumina-zircon Bucher Emhart Glass Licenced Refractory product that is widely accepted as the benchmark of the Feeder expendable product range; the effects of increasing ZrO_2 content through zircon additions in the Alumina-Zircon starting mix formulation from 35.wt% to 50 wt. % will be investigated. The composition of the PSR-315 in wt. % is; 68 % Al_2O_3, 13% SiO_2, 18% ZrO_2; 0.3% Na_2O; 0.16% Fe_2O_3 and is also highlighted in the Materials and Methods section.

This would include determining optimised packing of refractory mix formulations for the above compositions and reduced water content using Andreassen/Dinger and Funk packing models. The Andreassen/Dinger and Funk packing models are continuous approach models based on empirical theories of particle packing that are used to select proper sizes and proportions of small particles to fill larger voids and assume that all possible sizes are present in the particle distribution system, and no gaps exist between size classes.

Andreassen worked on the size distribution for particle packing with a continuous approach and proposed the “Andreassen equation” for ideal packing. Although the approach is more theoretical, it partly represents an empirical theory of particle packing Andreassen assumed that the smallest particles would be infinitesimally small. Dinger

and Funk recognised that the finest particles in real materials are finite in size and modified the Andreassen equation considering the minimum particle size in the distribution. The EMMA (Elkem Materials Mix Analyser) software is widely used to determine optimal packing structures of monolithic castables and for this study, EMMA v.3.5.1, was used to design the optimised batch formulation of the above compositions. DigiPac, a Structure-Visions packing model software from the University of Leeds was used to complement the Andreassen/Dinger and Funk empirical packing model study in modelling packed structures. The DigiPac software was used to evaluate the trend analysis of packing structures as a function of particle size distribution and shape, adding novelty to the study.

a. Testing slip rheological properties of the optimised formulations from the particle packing model studies for stable refractory castable slip that exhibits improved flowability, mixing and casting properties.
b. Synthesising, by slip cast pre-consolidation methods, of low porosity (< 12%) and dense refractory body with a tailored microstructures of in-situ reaction sintered zirconia reinforced mullite matrix. The use of SnO_2 as an sintering additive was to be evaluated.
c. Evaluate the material properties of the developed compositions by conduction physical and thermo-mechanical tests. The following tests were identified as critical and requisite to potential factory scale-up and commercialisation of the developed and promising compositions.
    - Porosity, Bulk Density,
    - Thermal shock
    - Linear thermal expansion,

- Hot modulus of rupture (HMOR) and
- Refractoriness under Load (RUL),

d. Identify the optimum composition compatible with soda lime glass melts up to 1500C by conducting static corrosion tests and dynamic corrosion tests on the above cast refractory compositions to simulate service conditions of free convention (surface tension) induced corrosion and forced convection induced corrosion of the refractories respectively.

e. Use of SEM, XRD characterisation techniques for glass-refractory interface phase analysis, refractory microstructural evolution.

3.2 Design of the Research

To accomplish the scope and objectives identified in section 3.1, the experimental method or design for this research was split into three sections, namely sections **A**; **B** and **C**. A summary of each section is briefly described below.

3.2.1 Section A: Development & Synthesis of Self-Flow Slip Cast Refractory Compositions

Work in this part of the research focussed on the development and synthesis of dense refractory compositions that would be sustainable from both the production side to service end. Literature review in chapter 2, showed that such refractories should possess a low apparent porosity micro and macrostructure < 10% (comparable to fused cast refractories, < 4%) as well as having oxide constituents and or phases with low solubility potential to alkali and alkaline earth siliceous glass melts. Therefore, the synthesized refractories would contain higher zirconia content than the standard AZS/AZM forehearth refractories widely used in the glass industries, such as PSR-315

and 333. Any loss in thermal shock properties for the refractories, as a result of the reduction in porosity, was expected to be mitigated by the evolution and enhancement of the reaction sintered mullite phase in the microstructure.

Briefly, this work initially encompassed identifying and selecting composition fields on the binary and ternary phase diagrams of the $Al_2O_3 – SiO_2 – ZrO_2 – SnO_2$ systems that would potentially provide crystalline phases that meet the required refractory properties highlighted in section 3.21 above. This was based largely on existing knowledge of the material and thermodynamic properties of the various crystalline phases found in the $Al_2O_3 – SiO_2 – ZrO_2 – SnO_2$ systems and demonstrated by a range of compositions of sintered AZS/AZM refractories. In the $Al_2O_3 – SiO_2 – ZrO_2$ system, zircon (and critically) zirconia offer the optimum physical, thermo-mechanical and chemical properties against glass melts in the production of soda-lime silicate and borosilicate glass compositions while mullite provides thermal shock properties. For this research, zirconium-silicate, $ZrSiO_4$ (zircon) was used as it is a cheap source of ZrO_2 in the production of reaction sintered AZS composites with enhanced zirconia reinforced mullite.

The next step involved slip preparation, synthesis and consolidation of slip cast AZ/AZS refractory compositions identified above. This was achieved by design of experiment (DOE) methodology, customising and optimising the Alumina-Zircon mix formulations using the particle-packing numerical concepts of Dinger and Funk particle models as well as computational modelling concepts (DigiPAC) to give an optimised mix formulation that can achieve optimum particle packing with good self-flow properties. Stable and workable refractory slips made from the optimised mix

formulations were evaluated using various slip testing/characterisation methods such as deflocculation tests and rheology tests to determine the most suitable stable refractory castable slip. The refractory slips were cast, dried and sintered before the characterisation of their microstructures as well as evaluations of their physical, thermo-mechanical and chemical properties.

3.2.2 Section B: Physical & Thermo-Mechanical Property Test

This section comprised of ASTM / BS standard tests for refractory products that were identified and conducted to evaluate the essential physical, thermo-mechanical and chemical properties of the synthesized slip cast novel refractory compositions.

3.2.2.1 Physical and Thermo-mechanical tests

Figure 3.1 shows the list of tests identified and the order of priority in which they were conducted during preliminary and development work of designing and developing the novel refractory materials.

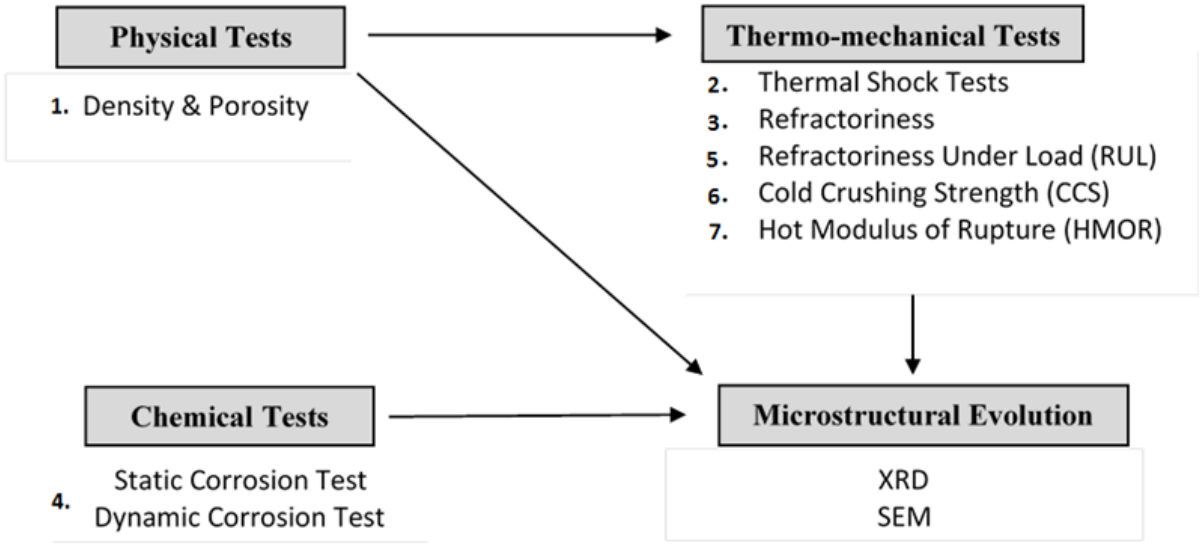

Figure 3-1: List of refractory material property tests identified and conducted in this study on the synthesised refractory products. The figure also highlights the order of testing and priority given to the testing of novel new refractory products.

The evaluated material properties of the developed compositions of interest were compared against PSR-315 and PSR-333; which are Emhart Glass Licenced compositions and PSR Ltd.'s standard commercial AZS refractories widely used in the glass industries.

3.2.3 Section C: Corrosion and Erosion of Refractories.

3.2.3.1 Corrosion of Refractories

For this study, static isothermal refractory corrosion tests were conducted on the developed AZS-01, AZS-T1 and AZS-T2 and standard PSR refractories in borosilicate glass and SLS glass melts for 72hrs according to the ASTM C-621-84 (2009) standard to evaluate refractory corrosion performance.

The static method covers the determination of corrosion resistance of refractories in contact with molten glass under static isothermal conditions that provide the most severe static corrosion environment possible at the specified test temperature. From this test, flux-line and half down corrosion calculations would constitute a measure of corrosion and the following information was obtained;

- A research and development comparison of a variety of refractory compositions could be made on their corrosion resistance to glass melts.
- The stoning potential of a refractory, presence of insoluble refractory crystals within the glass and or loosely bound at the glass-refractory interface was assessed as well as which particular refractory may provide cords and blister glass defects.
- The flux-line corrosion results provide useful indications of the relative resistance of both the upward and downward drilling corrosion of refractories.
- Service temperature use limits can be determined from the different test temperatures.

3.2.3.2 Erosion of Refractories

Refractory materials in their service life are continuously exposed to slag and glass melts and the test that best simulate the conditions the refractories are subject to in industries are those of the dynamic corrosion tests, unlike the static corrosion tests. Dynamic corrosion test simulates the forced convection in glass furnaces from mechanical stirrers and process flow.

The rotary slag test (ASTM C874) has been conducted and reported to simulate corrosion for steel-making refractories. For glass – refractory corrosion tests, some researchers have adapted the ASTM621 finger sample static corrosion test into a rotating cylindrical furnace (Rotary furnace) also known as the "merry go round" to conduct dynamic corrosion tests [16].

For this research, an adapted "merry go round" finger corrosion tests were implemented on the novel developed and modified AZS-01, AZS-T1 and AZS-T2 refractories. Before and after profile measurements for macro and microscopic analysis were conducted on the test samples of developed compositions and standard PSR refractories.

Flux-line corrosion and a comparative evaluation of the performance of the refractories was reported and conducted in line with the glass industry practice [6-9, 16].

3.3 Characterisation

The chemical and mineralogical analysis of the sintered refractory products was characterised by XRF and the XRD Bruker D8 X-ray diffractometer (Oxford UNITS).

For microstructural evolution of the developed refractory compositions, a Carl Zeiss EVO MA15 variable pressure W. SEM (Oxford Instruments) together with the Aztec Energy EDX system (Cambridge Systems) with X-Max SDD detector backscattered imaging was used for elemental mapping and point ID.

A Hitachi SU8230: high performance cold field emission (CFE) SEM with Oxford Instruments, Ultra high resolution, low kV, simultaneous SE, BSE, BF and DF imaging, with nanoscale resolution was used to evaluate the microstructural evolution of the mullite grains in the matrix region.

XRD analysis and SEM EDX analysis was also used to characterise the glass-refractory compatibility and the glass-refractory interface.

4 Materials and Methods

This chapter looks at the materials and experimental methods used in this study to identify, consolidate and test novel slip cast refractory compositions that possess both structural and chemical material properties that are compatible to high temperature, alkaline and alkaline earth, siliceous glass melts.

4.1 Materials

4.1.1 Components for Refractory production

The major raw material components used in this research were commercial grade materials from PSR-Ltd suppliers that are also currently used for commercial refractory production at PSR-Ltd. Table 3.1 lists the raw material components, used to consolidate PSR-Ltd refractory products, which were made available and used for this research.

As highlighted in section 1.2, refractory castables or materials consolidated by slip cast methods consist of aggregate grains bonded/sintered within a fine matrix material; as such, the raw materials listed in table 3.1 have been grouped according to their class size. Table 3.2 lists the materials that were used as binders, additives and dispersants.

Table 4-1: Raw material components that were made available for this research

Commercial Product Name	Material component	Source	Particle Size Distribution (µm)			Specific Surface Area (BET) (m^2g^{-1})
Aggregate Material			d_{10}	d_{50}	d_{90}	
T60 1 – 2 mm	Tabular Alumina;	Almatis		2660		
T60 0.5 – 1 mm	Tabula Alumina	Almatis		1418		
T60 0 – 0.5 mm	Tabula Alumina	Almatis		851		
T60 0 – 0.3 mm	Tabula Alumina	Almatis		324		
Duramul 1 – 3 mm	Fused Mullite	Washington Mills/Cermatco		1754		
Duramul 0.5 – 1 mm	Fused Mullite	Washington Mills/Cermatco		755.70		
M170	Calcined zircon Sand	Minchem	100.21	145.31	201.5	0.0117
Matrix Material			d_{10}	d_{50}	d_{90}	
CT9FG	Calcined Alumina	Rio Tinto Alcan (Pechiney)		4.65		
PBR	Bimodal Reactive Alumina	Rio Tinto Alcan (Pechiney)	0.61	2.45	13.44	
Zircozon 10	Calcined Zircon Flour	Minchem	0.42	2.85	4.87	2.7
Zircozon 5	Calcined Zircon Flour	Minchem, UK	0.66	2.41	6.54	2.7
Supelite Tin Oxide	Tin IV Oxide, stannic oxide	Keeling & Walker, Stoke on Trent, UK	0.10	0.80	2.40	9

Table 4-2: Raw materials that were used in formulating mixtures in this research project.

Binders		
Commercial Product Name	**Generic Name**	**Source**
Puraflo 31 -	China clay	Sibelco (WBB)
Puraflo RA –	Ball clay	Sibelco (WBB)
Alpha bond (Hydral 710B)	Hydrated Aluminium Oxide	Almatis

Table 4-3: list of Chemical Dispersant made available in the preparation of refractory suspension or slips.

Dispersants		
Commercial Product Name	**Material component**	**Source**
Darvan 7-n	Sodium Methylacrylate	Vanderbilt Minerals, llc,
Dolopix PC75	ammonium salt of polyacrylic acid	Zschimmer & Schwarz, German.
Dispex A40	Triammonium citrate,	Zschimmer & Schwarz, German.

Two PSR-Ltd commercial products, PSR-315 and PSR-333 were used as reference test materials in this research in evaluating the physical, thermo-mechanical and chemical properties of the synthesized novel compositions of interests that were produced in this research. PSR-315 is an AZS refractory while PSR-333 is from the AZM system. These AZS and AZM refractory products represent the current industrial standards for forehearth refractory products widely used in the glass industries. Table 3.3 shows the chemical composition of the two PSR standard refractories.

Table 4-4: Chemical composition of PSR-315

SiO_2	13.0
Al_2O_3	68.0
ZrO_2	18.0
Fe_2O_3	0.13
TiO_2	0.10
CaO	0.05
MgO	0.01
Na_2O	0.30
K_2O	0.14

Table 4-5: Chemical composition of PSR-333

SiO_2	15.0
Al_2O_3	73.0
ZrO_2	11.1
Fe_2O_3	0.20
TiO_2	0.17
CaO	0.10
MgO	0.10
Na_2O	0.30
K_2O	0.09

4.1.2 Glasses as corrosion media.

There are many varied glasses of different compositions currently in production worldwide. Borosilicate PYREX glass, and soda lime silicate (SLS glass) cullets were used to evaluate the corrosion characteristics of the cast refractories in this study. Flint, SLS container glass received particular attention for this research as a

source of corroding media as they represent nearly 80% of all industrial glasses and make up a major part of PSR-Ltd.'s refractories base customers for glass producing companies. As such, the flint SLS glass was chosen as the reference glass composition for evaluating the chemical compatibility of the refractories to the glass melts in the temperature range of 1200°C - 1500°C both under static and dynamic conditions. Low soda, high silica borosilicate Pyrex glass, was used for the systematic study of corrosion behaviour of refractories in Pyrex glass with varying Na_2O and CaO content finally reaching the limit close to that of Soda-Lime-Silica glass compositions.

The SLS glass cullet was purchased from Berryman Ltd (South Kirkby, UK) and GTS Ltd, (Sheffield, UK). The main chemical constituents of both glass cullet determined by X-ray Fluorescence spectroscopy (XRF) is given in Table 3.5 and table 3.6 respectively.

Table 4-6: Chemical constituents of the soda-lime silica glass cullet.

Glass	Supplier	Oxides Chemical constituents (wt. %)						
		SiO_2	CaO	Na_2O	K_2O	MgO	Al_2O_3	Others
SLS	Berryman Ltd, UK	71.53	12.78	10.78	1.53	1.41	0.59	*1.38
SLS	GTS Ltd UK	72.30	11.10	12.90	0.30	2.00	1.20	*0.351

*Others =trace (TiO_2 + Fe_2O_3 + ZrO_2 + Cr_2O_3 + SO_3)

Table 3.6 gives the chemical composition of the Pyrex glass used in this research.

Table 4-7: Chemical constituents of the borosilicate PYREX glass cullet.

Glass	Supplier	Oxides Chemical constituents (wt. %)						
		SiO_2	B_2O_3	CaO	Na_2O	K_2O	Al_2O_3	Others
Pyrex	University of Leeds.	80.89	11.67	-	4.57	0.06	2.48	*0.16

*Others = (Fe_2O_3 + ZrO_2)

4.2 Experimental Procedure

4.2.1 Section A: Development & Synthesis of Self-Flow Slip Cast Refractory Compositions

Distributor and Forehearth channel blocks as well as feeder expendable refractory products used in glass production consist of complex shapes. Slip casting, as the pre-consolidation method of refractory green bodies, was implemented for this research because slip casting represents a cheap and simple consolidation process to obtain complex shaped materials with high green density and microstructural homogeneity.

4.2.1.1 Evaluation of Ternary/Binary Phase Diagrams

4.2.1.1.1 Introduction

The development of a new ceramic material and or optimisation of the processing begin with the chemical composition and the conditions (temperature, pressure) under which pure compounds and their mixtures are stable. In line with the Materials Science physicochemical paradigm link; **Composition → Structure → Particle size → Properties**; the thermo-mechanical, chemical and physical properties of ceramic products are intrinsically related to the composition, amount and distribution of phases presents. A good understanding of the phase equilibria in ceramic systems is therefore central to the development and application of materials in metallurgical, glass and other high temperature technologies. For refractory oxide materials and glass systems, knowledge of the phase equilibria and the subsequent evaluation of their service stability in high-temperature environments can be obtained from appropriate stable and meta-stable phase diagrams. The phase equilibrium systems and tool greatly limit trial and error approaches in the development of new materials, which was the case in their absence.

4.2.1.1.2 Methodology

The binary and ternary phase diagrams of $Al_2O_3 – ZrO_2 – SiO_2 – SnO_2$ refractory oxide systems were evaluated to identify compositional fields for which the crystalline phases of the primary phase fields are known to be provide the main material properties requisite for glass-contact refractories, identified in section 3.2. These material properties include a dense, low porosity refractory body with excellent thermal shock and corrosion resistance in glass melts.

Starting with the standard AZS commercial forehearth refractory, PSR-315 composition, as a reference composition, two refractory compositions, AZS-01 and AZS-02 with increased zircon contents were initially designed and the isopleths of the compositions with increased zircon content analysed. The AcerS-NIST Phase Equilibrium Diagram pc database v. 4.2 together with the Phase Equilibrium Diagram (PED) Editor were used to aid in this methodology.

The conventional methodology for design and development of refractory compositions is to select compositions that lie on high temperature liquidus isotherms. However, for this research, selection criteria of the four compositions was made of refractory compositions within compositional fields that fall within the slightly lower liquidus projection isotherms to encourage liquid phase sintering and hence enhance densification and sintering to reduce the porosity of the refractories.

The presence of a transient liquid phase in any solid-state reactions is known to enhance the rate of reaction through dissolution –recrystallization process that provides an easier energy pathway ($- \Delta G_f$) for the reaction. Therefore, for this research, adopting this methodology of selecting composition fields that fall within lower liquidus isotherms for raw material starting mixtures of zircon and alumina, it was expected that the presence of a liquid phase from any of the $Al_2O_3 – SiO_2 –$

ZrO_2 – SnO_2 system would also ensure improved kinetics of the solid-state reactions during the reaction sintering of mullite from zircon-alumina starting mixtures.

4.2.1.2 Refractory Mix Formulation development & Optimisation

Major improvements in the properties of refractories have been achieved through studies of controlling the packing densities of refractories through efficient particle packing of the starting materials. Fine matrix particles near the larger aggregates grains are known to exhibit a non-organised particle packing to result in what is known as Wall effects [4,62,63]. This makes the interfacial zone between the matrix and aggregate an area of weakness both in terms of particle packing and bonding which results in uneven packing, pores and de-bonding after sintering. The rheological behaviour of castables is controlled by the particle size distribution (PSD), solid loading, dispersion state and the liquid content used during mixing. The rheological aspects, mixing and casting steps can be enhanced by a proper PSD selection [5, 41]. To prepare powder mix formulations that have optimum packing it is imperative to know the following criteria;

1. What the particle size distribution (PSD) for an optimum packing should look like.
2. The (PSD) of the composite mixture or mix formulation

The first criterion is met by particle packing models such as the Funas model; Andreassen particle packing model and the modified Andreassen model (also known as the Dinger and Funk Model). For this research, the modified Andreasen model for particle packing was used to optimise the PSD of the batch mix formulations of the AZS-01 and AZS-02 compositions.

4.2.1.2.1 Dinger & Funk Model for particle packing

The Dinger and funk model is a modified version of the Andreassen model approach that incorporates the smallest particle size in the distribution and is described by the continuous particle size distribution equation;

$$CPFT/100 = (d^q - d_m^q)/\ D^q - d_m^q) \quad (18)$$

Where, *CPFT* is the (Cumulative Volume Percent Finer Than); *d* is the particle size; *D* is the maximum particle size; d_m is minimum particle size in the distribution; and q is the distribution modulus/coefficient (q-value). The q-value (distribution modulus) was defined by Andreassen as a measure of the contribution of the finer fraction that could be accommodated in the mixture [4,62].The composite particle size distribution (PSD) of each mix formulation produced in the design of AZS-01, AZS-02 and the novel AZS-Sn compositions was optimised by adjusting the PSD according to the Dinger and Funk (Modified Andreassen / Alfred's) model for particle packing. This was accomplished using the Elkem Material Mix Analyzer software (EMMA v.3.5.1). The software is widely used to determine optimal packing structures of castables and uses both the Andreassen and the Dinger & Funk models [19]. Figure 4-1 shows a print screen of the EMMA modelling tool interface.

A library of the particle size distributions of the all refractory material components shown in table 3.1, used in formulating the batch formulations of the compositions was created and stored in the EMMA library bin tool, see figure 4-1. Different quantities of the individual component materials were entered into mix formulation recipes that correspond to a given composition and used to identify the size fractions in the formulation that needed to be increased or decreased to provide a formulation PSD that best follows the modified Andreassen model for optimum packing.

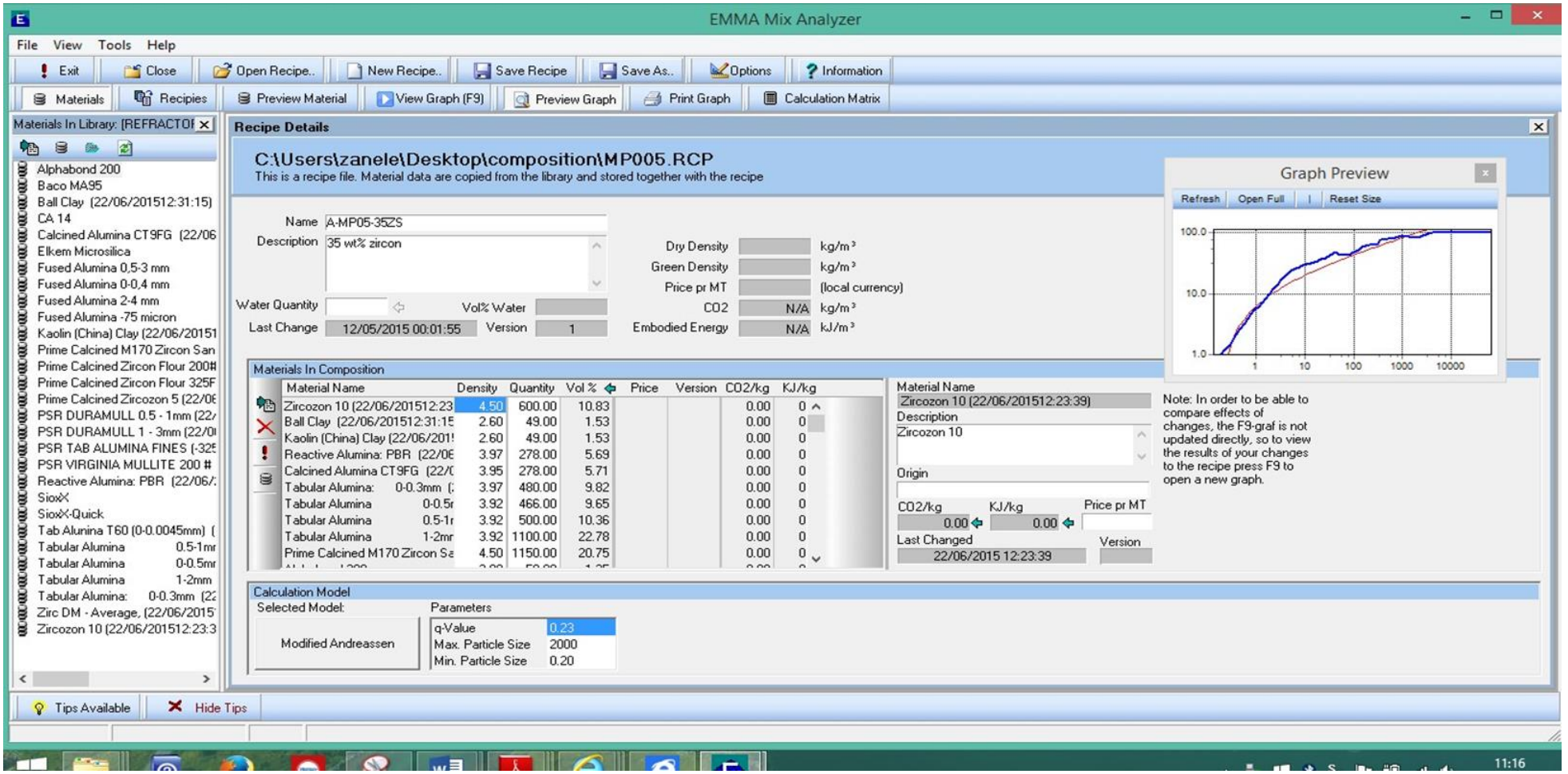

Figure 4-1: Print Screen of the EMMA modelling tool interface.
1. The material library of refractory material components that make up different refractory compositions are on the LHS;
2. At the bottom left, the parameters of selected model (modified Andreassen) are highlighted.
3. A graph preview of the modelled PSD2

4.2.1.2.2 DigiPac Model Software for particle packing

The basis of the DigiPac modelling software is the digital representation of both the particle shapes and packing environment, in the form of pixels, as lattice grid cells. This means that a particle of any shape is simply converted into a coherent collection of pixels in three dimensions (3D) together with the packing space, such as a mould, also represented as a static 3D lattice grid of pixels. Therefore, as the packing of different raw particles is simulated through their translational and rotational movement within this static 3D lattice grid of pixels, the packing is manifested as relocations of the 3D pixels (digitised particles) [46].

The modelling software utilizes 4 packing modules based on different algorithms of the software namely;

- **DigiRWP**: a **R**andom **W**alk based **P**acking algorithm for random dumping of particles and helps to see the tendency of segregation in mixtures.
- **DigiCGP**: a **C**ollision **G**uided **P**acking algorithm for simulating packed structure in small sized ratio packed columns
- **DigiRPP**: **R**andom **P**lacement **P**acking algorithm which generates a well-mixed configuration of DigiRWP and DigiCGP.
- **DigiOSP**: **O**ptimal **S**tacking **P**acking algorithm which generates an ordered packing with tight fit between the particles.

The DigiPac software was used to evaluate the trend analysis of packing structures as a function of particle size distribution and shape, as well as tendency of segregation in mixtures of different shapes and or sizes.

In the **DigiRWP** algorithm, a specified number of particles are added on top at randomly selected lateral positions, at specified intervals. At each step, each of the specified number of particle in the system undergoes a trial translational move which gets abandoned if it results in an overlap with another particle or solid boundary of container or packing environment. Equally, an accepted translational move will result when there is no overlap between two particles or solid boundary. There are 26 possible translational moves in the 3D packing of the particle (6 orthogonal and 20 diagonal).

Once a particles' trial translational move has been accepted, a rotational one is implemented and accepted or rejected on the same non-overlap criterion. This process is repeated until the best possible fit or packing of the particles is achieved. The Rebounding probability parameter was used to restrict the movement of particles in certain directions with the low non-zero rebounding probability employed to encourage quick settling of particles within local/relative minima while ensuring their translational movement to possible global minima and best fit.

4.2.1.3 Slip Preparation

For each refractory composition, preparation of the slip (castable) for slip casting was conducted by weighing accurately each corresponding raw material component size fractions that make up the refractory mix batch formulation designed in section 3.2. Depending on the total batch weight, the raw material components were weighed and added to a Hobart mixer starting with the larger aggregate material to the micro-sized matrix and binders. The Hobart Mixer, shown in figure 4-2 was used to mix 5 – 10kg batches and is a paddle-type mixer with a revolving paddle that rotates at a speed determined by fixed gears. Another Hobart mixer with a large capacity mixing drum was used to make 10 – 30kg lab mixes.

Figure 4-2: Hobart Mixer used to mix 5-10kg batches of the developed mix formulations at PSR-ltd. Picture courtesy of PSR-Ltd.

The mixing procedure of each batch formulation was divided into three steps where an initial dry mixing of the batch formulation was carried out to break up any soft agglomerates and ensure particle homogenization. This was followed by the addition of deflocculants and a two-step water addition until slip consistency or homogenisation was achieved. A two-step water addition was characterised by addition of a limited amount of the required water content (ca. 80%) at a constant rate and allowing for the composition formulation to reach a "wetting out point." The remaining water was then added intermittently until the required slip consistency was achieved.

4.2.1.3.1 Characterisation of Prepared Slips

As sintered refractories are generally made up of large aggregate grains and fine matrix raw particulate materials, for slip casting consolidation techniques, the incorporation of water into the particulate systems affects the surface chemistry effects of the matrix particulate materials as well the mobility of the particles. The prepared alumina-zircon suspensions or slips were characterised to determine the optimum dispersant using a variety of techniques that are described below.

4.2.1.3.1.1 Zeta potential and Size distributions

Zeta potential measurements and particle size distributions of suspensions of the AZS-01 composition alumina-zircon matrix raw materials dispersed using three commercially available dispersants were measured using a particle size analyser (Malvern Zetasizer ZS 1, Malvern Instruments, Worcestershire, U.K). This was done to evaluate individual dispersant efficiency and preliminarily screen for the best dispersant that provides a stable refractory slip. It was expected that a stable refractory suspension would maintain the optimised particle size distribution of the mix formulation designed in section 4.2.1.2.

The Malvin Zetasizer is an-automated integrated instrument designed to measuring the zeta potentials and particle size distribution of colloidal or particulate suspensions wet ranging from submicrons to 2000µm. In measuring the zeta potential the principle of electrophoresis is used where a charged particle will travel at a constant velocity across a voltage field and its mobility, related to the viscosity and dielectric constant of the dispersing media, and the electrical potential between the boundaries of the moving particle and dispersing media is measured and termed zeta potential.

For particle size distribution measurements using the Malvin Zetasizer, in consonance with zeta potential measurements, the moving particle passing through a laser beam will scatter light at an angle inversely proportional to its size. This scattering intensity versus diffraction angle is the primary source of information used to calculate the particle size. Therefore, any soft agglomeration of the fine particles will scatter at low angles while small particles scatter at higher angles.

For sample preparation, four dilute (0.1%) suspensions (**A, B**, **C** and **D)** of the fine particulate raw materials CT9FG, PBR and Zircozon 10 used as matrix materials for the AZS-01 compositions were prepared by dispersing the refractory powders in water and ultrasonicating the suspensions for 5 minutes to break any soft agglomerates. Three commercial dispersants, Darvan 7-N, Dispex-A-40 and Dolopix PC75 were each added to three of the four suspensions created and circulated the dispersed suspensions into the cell for zeta potential and size measurements. Three measurements were taken for each sample which were averaged.

4.2.1.3.2 Deflocculation Tests

Two 400g mix formulations of AZS-01 was added to 30g (30ml) of water to make as suspension of solid loading of 93 wt.%. To the suspensions, 0.1ml aliquots of Darvan 7-N and Dolopix PC75 were added and dynamic viscosities of the suspensions recorded from the rotational viscometer.

4.2.1.4 Slip Property and Rheology Tests

4.2.1.4.1 Self-flow test

The self-flow property of each refractory slip prepared was characterised by measuring the flowability and flow decay of the slip composition. The flowability of the slip which quantifies the self-flow properties was measured by the flow cone test described by the ASTM –C230 standard methods 28 [69]. The slip was placed into a truncated flow cone (of height, 80mm and base diameter, 120mm) on a flat board and allowed to spread out by gravity over a period of 10 minutes once the cone has been removed. The diameter of the slip as it spread out, was measured at intervals, and recorded as a free flow value according to the following equation;

$$FI = \frac{D_t - D_C}{Dc}\ \% \qquad (19)$$

Where; FI is Flowability Index; D_t: diameter of slip at time, *t*; and D_c: diameter of truncated cone.

4.2.1.4.2 Moisture; pH; Slip Temperature.

The temperature, pH and moisture content measurements of each slip were taken and recorded soon after mixing. For slip moisture content measurements, a Mettler Toledo HB43-S Halogen was used.

4.2.1.4.3 Slip Rheology (Viscosity Tests)

The rheological behaviour of the prepared suspensions or slips was measured using a Brookfield viscometer HB (Brookfield Amitek, UK). This unit is a controlled speed device that measures dynamic viscosity as a function of spindle speed (rpm), ranging 1rpm s^{-1} to 30rpm s^{-1}.

600ml of the prepared refractory suspensions or slip from each refractory composition was collected in a beaker after mixing and a 2.4cm diameter cone spindle was used to determine the dynamic viscosities of the slips at different spindle speeds or shear rates. All measurements were carried out at room temperature and dynamic viscosity readings of the slip at each spindle speed were taken after the spindle was held for a length 60s. Two trials were carried out for each prepared suspension.

4.2.1.5 Slip Casting and Sintering

4.2.1.5.1 Slip Casting & Green body strength

After the rheological property testing, each slip produced was cast into gypsum moulds for physical (density and porosity), thermo-mechanical and chemical (corrosion cup and finger) material property samples. The green cast samples were left in the gypsum moulds for 24hrs and demoulded to develop green strength before drying in a Haraeus Kiln oven dryer at 120°C for 5hr.

4.2.1.5.2 Sintering

Consolidation of the refractory green samples was conducted in either an electric fired lab kiln or the factory Kiln. Lab based samples from 5kg batches of slip cast refractories were fired in the lab Kiln at 1500C for 1hr. 12kg – 30kg mixes which were cast into expendable products were fired in the factory kilns at 1500C for 4hrs.

4.2.2 Section B: Generic Physical & Thermo-Mechanical Property Measurements

This section describes the standard physical and thermo-mechanical tests that were conducted on the synthesised and cast refractories

4.2.2.1 Bulk Density and Porosity Tests

Refractory bulk density and apparent porosity measurements is an important test for characterisation of refractories. The values from this test relate as well to other physical properties of the refractory such as strength, abrasion and gas permeability and are used to recommend and predict appropriate applications for the refractories.

The bulk density and apparent porosity of the sintered slip-cast refractory samples were measured using the standard EN 993-1 et 1SO 5017 (Determination of Bulk Density and Apparent Porosity for Dense Shaped Refractory Product), using the Archimedes water immersion method [70]

The dry, suspended and immersed weights of the samples in water were each measured. Their density and apparent porosity was evaluated from the following equations,

Bulk Density, BD**:**

$$\boldsymbol{BD} = \frac{W_d}{W_w - W_S} \times 100\% \qquad (20)$$

Apparent porosity, AP:

$$\boldsymbol{AP} = \frac{W_w - W_d}{W_w - W_S} \times 100\% \qquad (21)$$

True porosity**:**

$$true\ porosity = \frac{\rho - B}{\rho} \times 100\% \quad (22)$$

Where:

W_w: soaked weight

W_d: dry weight

Ws: suspended weight.

ρ = apparent specific gravity

ϐ = true specific gravity

4.2.2.2 Cold Crushing Strength (CCS)

The cold strength of refractories is mainly quoted in industry by refractory manufactures and the end users. In academia, the relevance of a CCS test for refractory materials that are used in hot temperature environment during service is questioned and considered irrelevant as refractory rarely fail under room temperature. However, for this study, CCS tests were used as quality control check of the adequacy of sintering of the refractory and its abrasion resistance in consonance with the physical properties (bulk density and porosity). Cold crushing strength (CCS) tests on AZS-01, AZS-T1 and AZS-T2 refractories were conducted according to the ASTM C133 standard test; a test method for determining the room temperature flexural strength in 3-point bending (cold modulus of rupture) or compressive strength (cold crushing strength), or both, for all refractory products [71]. Tests were conducted at Lucideon Ltd, Stoke-on-Trent, UK.

For sample preparation and testing, 50mm long x 50mm diameter cylindrical blocks were core drilled from sintered blocks of the refractories and a uniaxial compressive load applied until failure. Failure of the refractory will be by shear and not compression. The crushing strength values of the tested materials were evaluated from the maximum load applied at failure over the mean cross-sectional area of the refractory over which the load was applied. This is given according to the equation;

$$\boldsymbol{\sigma}\ (MPa) = {}^{\boldsymbol{F}}/_{\boldsymbol{A}} \qquad (23)$$

Where $\boldsymbol{F}$ is the applied force and $\boldsymbol{A}$ is the cross-sectional area over which load is applied.

4.2.2.3 Refractoriness (PCE)

Refractoriness is a material property at which refractory material deforms under its own weight and the softening temperature of the sintered refractory materials is expressed by the PCE (Pyrometric cone equivalent). The PCE was determined by comparing the softening of specimen pyramid cone samples with standard pyramid cones of known fusion temperature fired under similar conditions. Testing of the refractory compositions AZS-01; AZS-T1 and AZS-T2 was conducted at Lucideon Ltd, Stoke on Trent, UK.

4.2.2.4 Refractoriness under Load (RUL).

The Refractoriness under Load (RUL) of refractory material quantifies the resistance of refractory materials to deformation under load at high temperatures experienced in service. It thus provides much significant information about the high temperature strength and stability of the refractory than its refractoriness. The RUL tests of AZS-01, AZS-T1 AND AZS-T2 refractories were also all

conducted at Lucideon Ltd in accordance to the BS EN ISO 1893:2008 standard [72].

Sample specimen for the RUL test consisted of a core drilled 50mm diameter x 50mm length cylindrical refractory block with a central axial hole of 12.5mm diameter. The top and bottom faces of the specimen sample were ground flat and parallel. A vertical cylindrical furnace (CARBOLITE, UK), with a maximum temperature capability of 1600 °C was used and had eight vertical axial PYROX S heating elements with a central 350 mm long hot zone spaced evenly on an 80 mm radius around the test specimen and loading column. A constant compressive axial stress of 0.2MPa was applied to the test specimen and the temperature raised at a rate of 5 °C min^{-1} up until sagging and complete failure of the material was reported.

Figure 4-3 shows a schematic representation of a typical RUL curve highlighting the rate of sagging of a refractory material under load with temperature. The figure also shows the significant high temperature material properties that are calculated from the RUL curve. These parameters are the $T_{0.5}$ (Ta) and $T_{1.0,}$ which are defined as the onset of softening of the refractory and the end of softening of the refractory before failure respectively. The Dmax gives the maximum expansion of the refractory and temperature range at which this occurs.

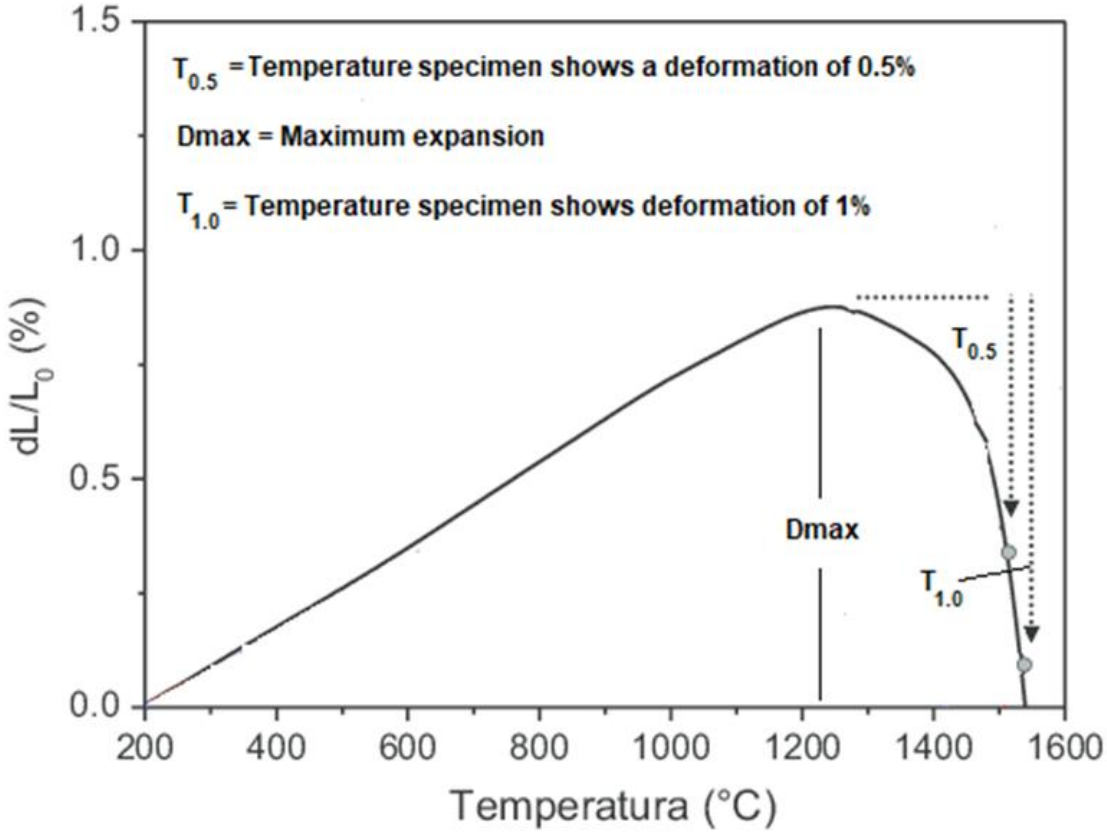

Figure 4-3: Schematic representation of a typical RUL rate of sagging with temperature curve

4.2.2.5 Hot Modulus of Rapture (HMOR)

The hot modulus of rupture standard test (ASTM C-133 and C-583) provides information on the flexural strength of the refractory material at high temperatures respectively [73]. The values from this test are indicative of the strength of the bonding matrix of the refractory at the test temperatures.

For this study, HMOR tests were conducted on the AZS-T1 and AZS-T2 compositions sintered at 1550 °C to evaluate the effect of the sintering agent, SnO_2, on the high temperature flexural strength properties of the refractories. This would cover a research gap on the use of SnO_2 above 1550 °C, where from the literature review; it was cited to have negligible effect on mullitisation and thermo-mechanical properties when sintered up to 1500 °C. As well, recapping

the literature review in section 2.3, the use of TiO_2 as sintering agent in Alumina-Zircon reactive sintering was reported to have lowered the high temperature strength by 32%.

HMOR tests were conducted at Lucideon Ltd, Stoke-on-Trent, and 2 specimen per bar samples measuring 100mm x 25mm x 15mm sectioned from sintered blocks and tested for Modulus of Rupture (& MOE) by 3 point flexure at test temperatures of 1300 °C and 1400 °C. Each specimen was heated to the test temperature at a rate of 3000 °C h^{-1} and soaked for 20 min before being loaded to failure. The modulus of elasticity was of the refractory was calculated between 25% and 75% of the modulus of rupture.

4.2.2.6 Thermal Shock

15mm x 15mm x 150mm prism block samples of AZS-01, AZS-T1, AZS-T2 refractory compositions and PSR-315 and PSR-333 commercial refractories, as reference materials, were either slip cast in 15mm x 15mm x 150mm prism block gypsum moulds or sectioned from sintered refractory blocks and thermal shock tested using the ASTM C-1100 standard test [74].

The samples were heat treated at 1200 °C for 15 min in a lab kiln before being immersed and quenched in water. After 10 min, the heat treatment cycle was repeated for up to 10 thermal and quench cycles. The test was used to compare the performance of different refractory compositions. The integrity of the bars were visually analysed after each cycle.

4.2.2.7 Determination of Thermal Expansion

Testing for the determination of linear thermal expansion of refractory materials was conducted at Lucideon Ltd, Stoke on Trent, UK.

Specimen samples measuring 50mm x 8mm x 8mm were heated from room temperature to 1400°C and cooled back, at a heating rate of 5 °C/min in according to the BS 1902: Section 5.14/1: 1992 standard to determine the linear thermal expansion and calculation of the coefficient of thermal expansion (CTE) for the optimised (AZS-01) and novel compositions (AZS-T1 and AZS-T2).

4.2.3 Section C: Corrosion and Erosion of Refractories

4.2.3.1 Static Corrosion

The chemical compatibility of refractories in SLS and Borosilicate glasses were determined using a variant of the ASTM standard test method for Isothermal Corrosion Resistance of Refractories to Molten Glass, ASTM C-621 – 84 []. This test method covers determination of corrosion of refractory materials that are in contact with glass melts under static conditions and isothermal conditions which are not encountered during service.

As such, this test was used as a comparative tool to compare the corrosion resistance of the developed compositions AZS-01, AZS-T1 and AZS-T2 to the standard commercial refractories, PSR-315 and PSR-333, widely used in the forehearth and feeder of glass furnace.

For this research, slip-cast corrosion cup samples and core drilled finger samples from sintered blocks of each refractory composition were used to conduct static isothermal corrosion tests and determine the corrosion resistance of the respective

refractory compositions. Figure 4-4 shows the static corrosion cup sample from a slip cast AZS -01 refractory.

In the ASTM C – 621 – 84 methods, a platinum crucible is used as a glass melting crucible to which refractory test finger samples are inserted. However, for this research, PSR-333 and PSR-315 slip cast crucibles were used as glass melting pots/crucibles for static and dynamic corrosion using finger samples. This is described in detail in the next section on the dynamic corrosion experiments.

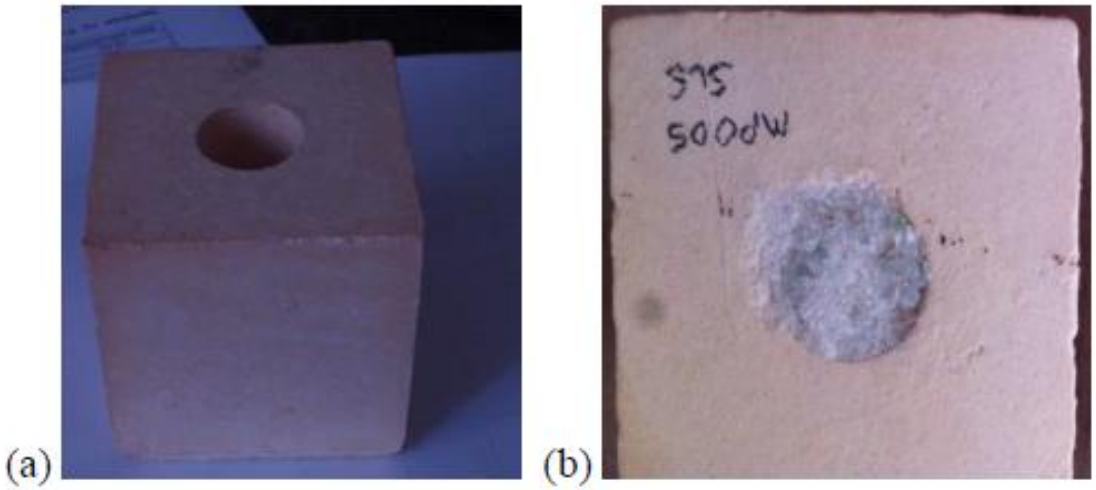

Figure 4-4: Corrosion cup samples used for static isothermal glass corrosion and to determine the corrosion resistance of the refractories to the glass melt. (a) Shows the cup sample with recess in the middle where the crushed glass cullet is placed before corrosion tests. (b) Cup sample with crushed SLS glass cullet filled in the recess of the cup sample.

The region of melt or flux-line corrosion of the refractories was used as the main result to evaluate the relative resistance of the refractory to corrosion as well as the upward and downward drilling corrosion mechanisms. In determining the flux-line cut, both the cup samples and finger samples (when possible) were sectioned in half as shown in figure 4-4 and the flux line corrosion calculated according to the ASTM – C621 - standard as follows [74];

$$Gc = [G - \tfrac{1}{2}\, g_1 + g_2] / 2 \qquad (24)$$

Where:

Gc = Flux-line or melt-line corrosion.

G = Width or diameter of specimen at glass line before test, mm.

g_1 and g_2 = Width (cup samples) or diameter (finger samples) of the two halves of the cut specimen at the flux line measured on the cut face of the specimen after static test.

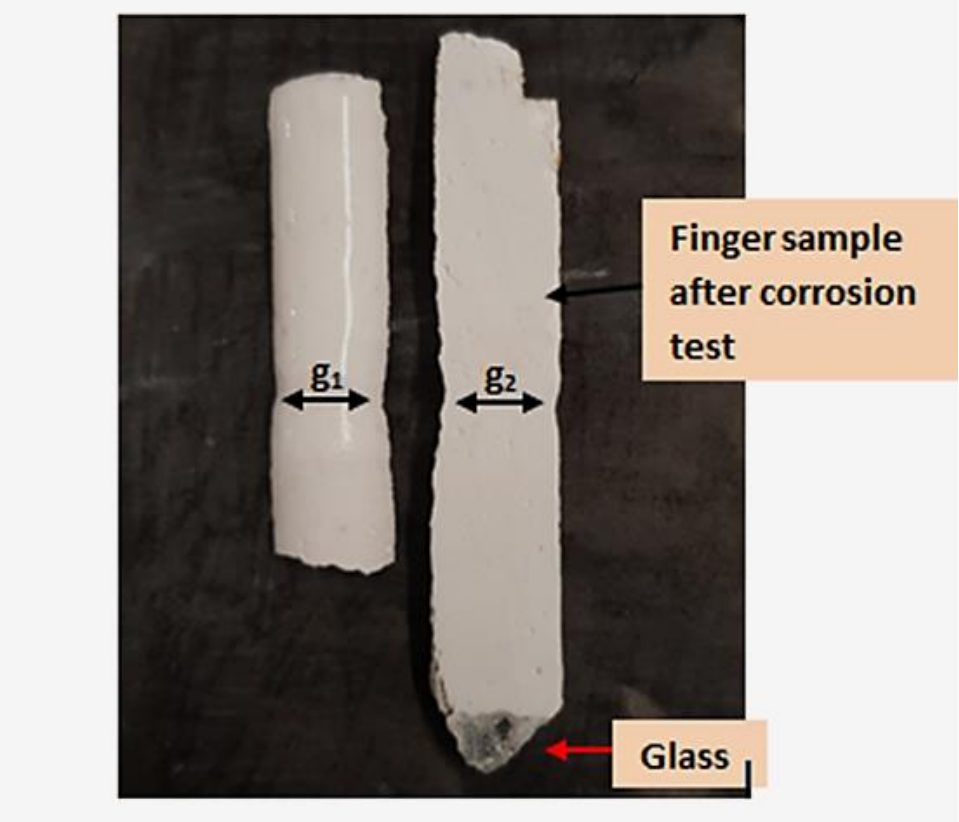

Figure 4-5: Finger sample after corrosion and sectioned in half and showing how flux- line corrosion measurements were taken.

Flux-line corrosion measurements were conducted a Digital measuring microscope, Cooling-Tech (model USB SO1) as well the use of a digital Vernier calipers and average readings taken. The set-up for measuring the flux-line corrosion is shown in appendix page C.

4.2.3.2 Dynamic Corrosion

Exposure of refractory material to slag and glass melts is one in which the process is continuous and to which the refractory undergoes both chemical corrosion and erosion. The tests that best simulate these conditions that refractories are subject to in industry are those of dynamic corrosion tests, unlike the static corrosion tests. The glass-refractory dynamic corrosion tests were conducted on the refractory compositions, AZS-01, AZS-T1 and AZS-T2 in identifying the corrosion and erosion resistance of the developed novel refractory compositions in soda lime silica glass melts.

4.2.3.2.1 Metal Frame & Furnace Unit for Dynamic Corrosion

A specifically designed and fabricated apparatus for the dynamic corrosion test was used in this study. This is shown in figure 4-6 below. A top loading furnace (Lenton Thermal Designs Ltd, Market Harborough, UK) was employed for melting glass during the dynamic corrosion test at different temperatures.

An adjustable frame connected by a winch was used to control the lowering or lifting of the sample position before and after the experiment, respectively. The rotation speed was controlled by a motor (Parvalux Electric Motor Ltd, Dorset, UK), which was mounted on the adjustable sample holder frame.

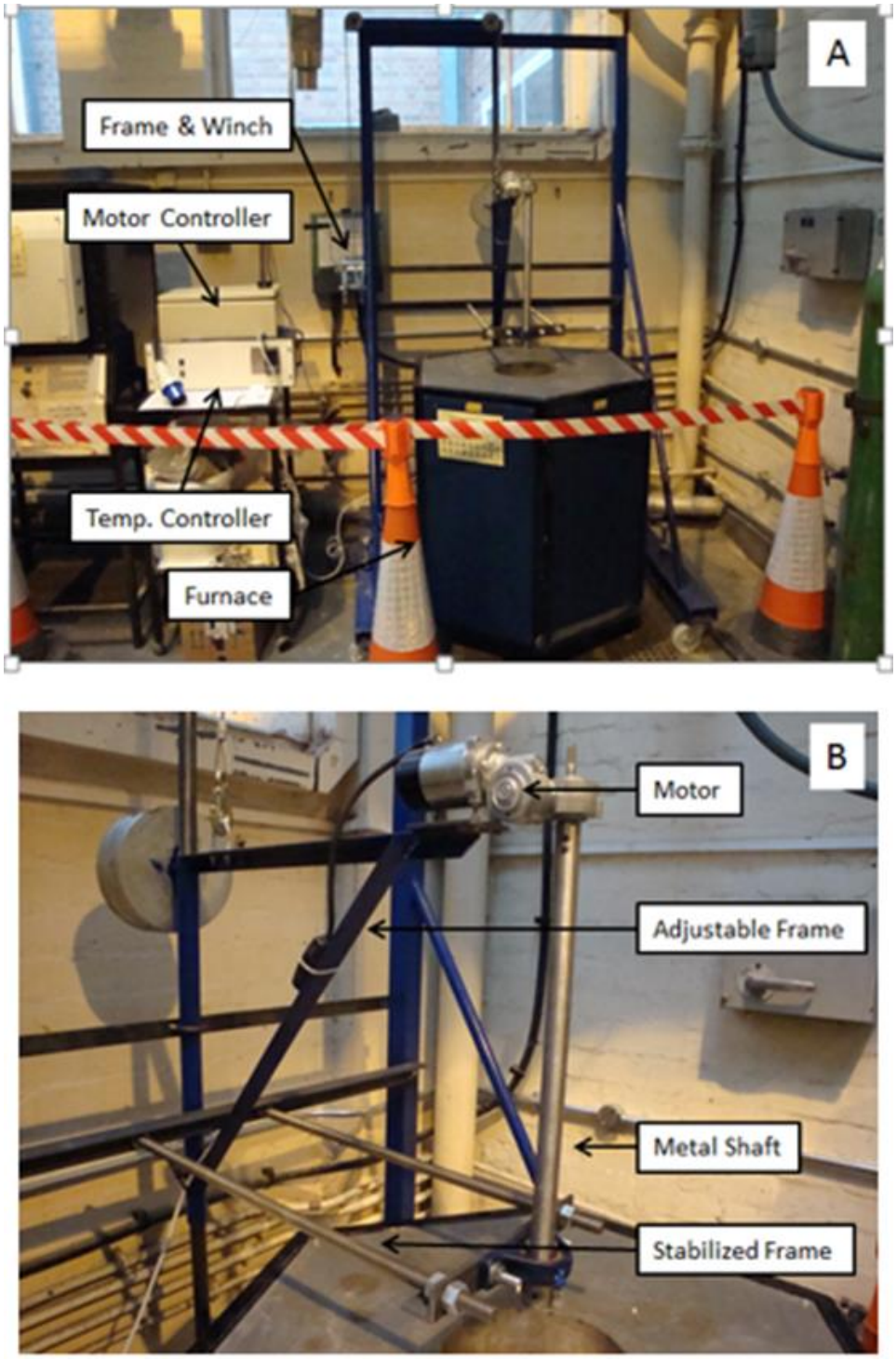

Figure 4-6 (a) and (b): Bespoke dynamic corrosion rig, designed and fabricated apparatus that was used for the dynamic corrosion test

In order to avoid over-heating of the motor, a stainless-steel shaft was used to connect the motor and, the ceramic sample holder and ceramic shaft. A

supporting bar with a ball bearing was used to maintain a stable position of the rotating shaft and sample holder assembly during the experiment.

4.2.3.2.2 Sample Preparation

Finger samples of the developed AZS-01, AZS-T1 and AZS-T2 refractory compositions were core drilled from sintered blocks or either made by casting in a bespoke made plaster to produce dumbbell shaped finger samples. The samples were cylindrical in shape with 100 (±0.02) mm lengths and 15 (±0.02) mm diameters.

A sample holder made from a mullite based refractory was assembled to a 300 mm length and 25 mm diameter ceramic shaft, obtained by core drilling by cement and connected to the metal shaft. The sample holder and ceramic shaft were used to hold the test finger samples in place during corrosion testing. This is shown in figure 4-6.

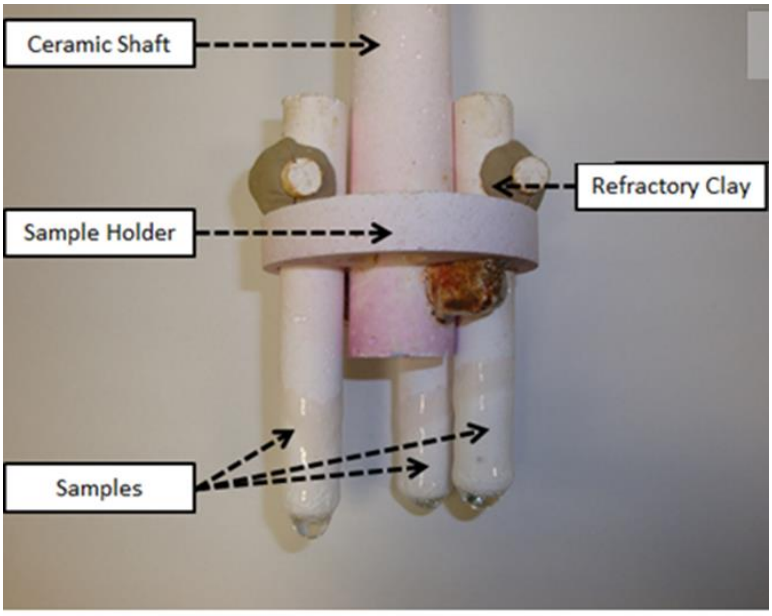

Figure 4-7: Ceramic sample holder with finger samples.

The use of dumbbell finger samples helped negate the need to notch the samples as in the core drilled samples. The dumbbell head provides the support to the test body and helps to maintain it in an upright position during dynamic corrosion experiment at high rpm. This helped to provide a clear melt line that could be easily measured.

Figure 4-8: dumbbell shaped finger samples for dynamic corrosion on a sample holder.

4.2.3.2.3 Experimental Process

Commercial soda-lime-silica (SLS) cullets are from Berryman Ltd (South Kirkby, UK) or GTS, Leeds, with compositions given in table 4-7 were used to determine and evaluate the corrosion resistance and compatibility of the developed refractories for this study. Before the experiment, an Al_2O_3-ZrO_2-SiO_2 (AZS) crucible was filled with 600g cullet and placed inside the furnace and heated to the desired temperature. The AZS-01, AZS-T1 and AZS-T2 were tested under dynamic conditions at test temperatures of 1370C and 1420C. Fibre insulation

was placed around the keyhole opening to prevent any heat loss and to maintain a constant temperature during experiment (see Figure 4-8).

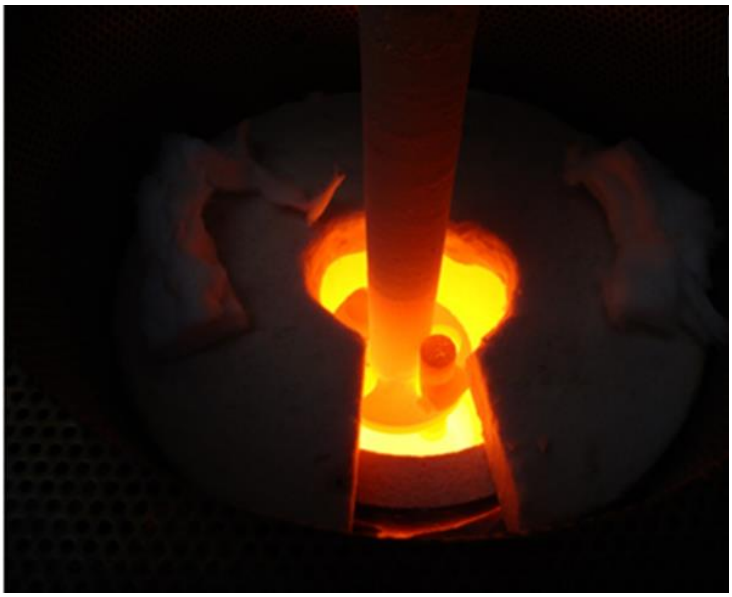

Figure 4-9: Part of the dynamic corrosion test rig showing samples being immersed in molten SLS glass at 1370 ºC during dynamic corrosion test.

4.2.3.2.4 Measurement

In this study, the relative corrosion rate of the PSR-315 commercial refractory was taken as the reference with corrosion index = 1 (100%). The corrosion index for a test specimen sample for AZS-01, AZS-T1 and AZS-T2 was identified as:

$$Corrosion\ index\ for\ test\ sample = \frac{\left[\pi\left(\frac{D_i}{2}\right)^2 \Delta l - \left(\frac{D_r}{2}\right)^2 \Delta l\right]_A}{\left[\pi\left(\frac{D_i}{2}\right)^2 \Delta l - \left(\frac{D_r}{2}\right)^2 \Delta l\right]_R}$$

$$= \frac{(D_i - D_r)_A^2}{(D_i - D_r)_R^2} \qquad (25)$$

Where; D_i and D_r are the initial and remaining diameter of the test piece, respectively. Δl is the length of the specimen. $\boldsymbol{A}$ and $\boldsymbol{R}$ are the test piece and reference (PSR-315 or PSR-333) piece, respectively.

4.3 Characterisation and Testing

4.3.1 XRD

XRD is an important technique used in the characterisation of ceramics and many other crystalline materials. It is made up of 3 basic elements, X-ray tube, sample holder and a detector. With minimum sample preparation required, sample purity, crystallinity, identification of crystal structures and phase composition quantitative analysis using Reitveld refinement can be achieved. Both powder and bulk sample analysis can be conducted.

The XRD works on the principle of diffraction occurring by constructive interference of the monochromatic incident X-rays ($K_{\alpha \text{ and }} K_{\beta}$) with the sample lattice spacing satisfying Bragg's Law;

$$n\lambda = 2d \sin \theta \quad \ldots\ldots\ldots\ldots\ldots\ldots\ldots\ldots\ldots\ldots\ldots \text{(26)}$$

Where; λ is the wavelength;

d is the lattice spacing and;

θ the diffraction angle.

This is highlighted in Fig. 4-9. The diffracted X-rays are detected and scanning the sample over a range of 2θ angles will determine all possible lattice parameters of the crystalline material. Each material has a unique set of d-spacing and conversion of diffraction peaks to d-spacing will identify the material from a library of reference materials.

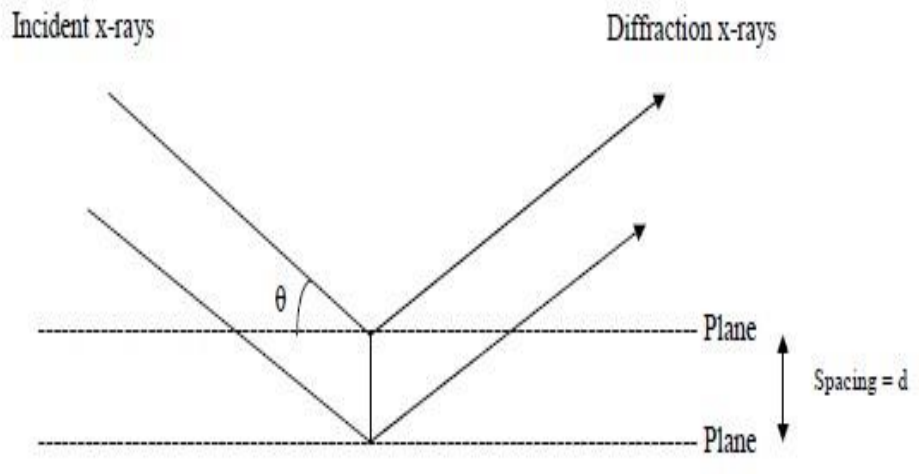

Figure 4-10: Schematic diagram for Bragg's Law Diffraction

4.3.1.1 Phase Analysis and Quantification of Synthesised Refractory Bodies

For this research, the bulk sample ambient temperature XRD analysis using the X'Pert MPD, P'Analytical, Almelo, Netherlands was conducted to identify the refractory phases, completion/non-completion of reaction sintering of alumina – zircon compositions and the subsequent phase evolution from such processes. As described earlier in the literature review section Exceptionally for the AZS refractory materials, they are characterised by a glassy phase, partly due to the presence of SiO2 and the non-completion of the reaction sintering processes; in the case for sintered products; or cooling rates in the fused cast process. The proportion of the glassy phase in the refractory microstructure will define or influence much of thermo-mechanical properties as well as corrosion behaviour in glass melt [5, 7-12]. Therefore, quantification of the evolved mineral (crystalline) and glassy (non-crystalline) phases present in the synthesized refractories was important. Quantification of the crystalline and non-crystalline phases was conducted based on the application of the internal standard Reitveld methodology.

4.3.1.1.1 Theory of Reitveld Methodology:

The Reitveld method is an effective methodology that has been demonstrated to quantify phase analysis in different materials according to the equation;

$$W_i = \frac{S_i\,(ZMV)_i}{\tau_i} \Big/ \frac{\sum S_p (ZMV)_P}{\tau_P} \quad \ldots\ldots\ldots\ldots\ldots\ldots (27)$$

Where; W_i is the weight fraction of the i-phase for all the phases present; Si, Zi, Mi, Vi and i are the scale factor; molecules per unit cell; molecular weight; unit cell volume and τ_i the mass absorption correction factor of the i-phase respectively.

With Reitveld analysis, the crystalline structure of each phase should be known and as such the quantification of glassy or amorphous phase was difficult to evaluate. However, several authors [74-77] demonstrated the quantification of non-crystalline phases using the Reitveld method by either; employing a fully crystalline internal standard component (SiO_2(s) or Al_2O_3) in known proportions or using the structural model where the inclusion of the glassy phase to the refinement can be understood as the widening of the peaks as a result of an extreme decrease in the crystallite size of a quartz phase.

4.3.1.2 Methodology.

Sintered refractory samples from synthesised compositions of interest; AZS-01 – AZS-03; and the Tin oxide doped compositions AZS-T1 and AZS-T2; together with the standard PSR refractories, PSR-315 and PSR-333 were ground to <50µm size powder for powder XRD analysis and quantification of phases using the Conconi et al, Reitveld internal standard method [89].

15 wt. % of milled (SiO_2) quartz was used as internal standard aggregate before Rietveld quantification. For any non-crystalline phase present in the refractory sample, the wt.% of the internal; standard would result in an over-estimate and therefore, quantification of the amorphous/glassy phase present in the sample would be easily evaluated from the equation;

$$NC_{IS}(\%) = 10^4[\frac{(1-W_s)}{R_s}/100 - W_s] \quad \ldots\ldots\ldots\ldots\ldots\ldots (28)$$

Where; NC_{IS} (%) is the glass phase content by the internal standard method, W_s is the internal standard proportion aggregated (%) and R_s is the internal standard evaluated by the Rietveld method.

4.3.1.3 Phase Analysis and Quantification of Synthesised Refractory Bodies

It was also used more importantly to identify the phase evolution at the glass-refractory interface, penetration zones in the refractory block and evaluate the dissolution mechanism at play during the corrosion of refractory in glass melts. For the glass-refractory interface analysis, the sample was mounted on a bracket and the beam width reduced and focused to a 10 x 1mm beam by use of slit.

Beam position and alignment was conducted on a graphite disc before placing the sample mounted on a bracket into the X'Pert machine. Accurate detection of the interface was done by conducting a partial XRD pattern covering the angular range of interest from the glass region and moving towards the refractory area until the interface was reached.

4.3.2 SEM

Scanning Electron Microscopy (SEM) is a powerful imaging tool that compliments other characterisation techniques in microstructural and mineralogical analysis. SEM with energy dispersive X-ray spectroscopy (EDS) was used for microstructural and mineralogical analysis of the modified refractory compositions of PSR-315/333 before and after glass corrosion tests. For microstructural characterisation of the refractory composition consolidated from both optimised and non-optimised formulations, several samples from different regions of the refractory brick were taken, sectioned and mounted using cold setting resin. Mounting in cold set resin was done to allow for venting and vacuum in the SEM chamber to be reached quicker and save time as the refractory brick were porous.

For phase evolution and microstructural analysis after static corrosion test, cross sections of refractory crucible, i.e. sections normal to the glass-refractory interface were cut by a diamond saw, mounted in cold set resin, ground and polished according to standard ceramographic techniques. Micro-chemical analysis techniques such as mapping, point ID and line scanning were carried out using SEM-EDS to evaluate the compositions of the phases as well as identify the diffusion profile of the glass and refractory elements.

5 Development, Preparation & Synthesis of Slip Cast AZS Refractories.

5.1 Introduction

As highlighted in chapter 1, the aim for this research was to develop and synthesise refractory compositions by slip cast methods that are more sustainable from a production stand point as well as during service than the current PSR-Ltd standard refractories widely used in the forehearth and as “Expendables” at the forming section of the glass furnace. To attain this, the objectives for this study was to develop self-flow slip cast refractories that, when sintered, possess the main material property requisites of low porosity, high temperature flexural strength, thermal shock and improved corrosion resistance in glass melts.

From the literature review, in section 2.5, it is widely known and shown that while increased porosity in a refractory or ceramic material enhances the thermal shock properties of the material, the corrosion resistance of the material to slags and glass melts is dramatically reduced. Design engineers and developers in ceramic or refractory development, have always faced this trade-off in material properties [ ]. However, for this study, it was expected that in developing a dense, low porosity refractory where a reaction sintered in-situ zirconia-reinforced-Mullite phase is evolved within the microstructure, would help counteract the loss of thermal shock properties from the reduced porosity.

Literature review in the previous chapter showed that the refractory physical material property of low porosity and high bulk density are a result of the particle packing of the starting raw materials while the thermo-mechanical and chemical properties of the consolidated refractory body are intrinsically related to the composition, amount

and distribution of the phases present. In the Materials Science, physicochemical paradigm link; **Composition → Structure → Particle size → Properties**; the "structure-particle size" relates to the phases present in the material. Therefore, using the methodologies described in section 3.3, this chapter aims to present how binary and ternary phase diagrams evaluation was implemented in identifying and developing new refractory compositions from Alumina -Zircon starting raw materials that would provide the above-mentioned properties. The chapter also discussed how the Dinger and Funk model for particle packing and DigiPack were used to design mix formulations that exhibit self-flow properties and produce workable slips with low water demand. Slip properties of the developed AZS refractories and the standard reference composition, PSR-315, together with the physical and thermos-mechanical properties were compared and evaluated.

5.2 Development of Optimised Slip Cast AZS Refractory Compositions.

5.2.1 Characterisation of Commercial Standard PSR-Ltd Refractories.

5.2.1.1 PSR-315

In order to develop improved refractory materials that would offer enhanced physical, thermo-mechanical and chemical properties than the current standard PSR-Ltd refractory compositions, two standard refractories, PSR-315 and PSR-333, that were used in this study as reference materials were characterised. Table 5-1 below lists the batch formulations of the two reference compositions. From table 5-1, the starting raw material batch formulations reveals that PSR-315 is a Alumina-Zircon refractory, classified as an AZS, while PSR-333 produced from an Alumina-Zircon-

Mullite mix formulation is classified a AZM refractory. The mix formulations of PSR-315 and PSR-333 have not been optimised for optimum particle packing.

Table 5-1: Mix formulation of standard PSR-Ltd widely used as forehearth refractory materials.

PSR-315	**PSR-333**
Zircozon	Zircozon 10
PBR	Tabular Alumina 325#
CT9FG	35# Virginia Mullite -
Tabular Alumina -0.3mm	Fused Mullite 0.5 -1mm
Tabular Alumina -0.5mm	Fused Mullite 1-3mm
Tabular Alumina -0.5 -1mm	Tabular Alumina 1-2mm
Tabular Alumina 1-2mm	China Clay
China Clay	Ball Clay
Ball Clay	
Alphabond	

Table 5-2: Physical properties of PSR-315 and PSR-333

Property	**PSR-315**	**PSR-333**
Bulk Density (g/cm^3)	3.111	2.82
Apparent Porosity %	20	21
Cold Crushing Strength	154	87.3 MPa
Refractoriness	Cone 35 (1775 C)	Cone 33 (1745 C)
Reversible thermal expansion	1% (20 – 1000C)	0.63% (20 – 1000C)
Thermal Shock	>10 cycles with minor hairline cracks at edges	>10 cycles

As mentioned earlier in section 1.1, PSR-315 and PSR-333 refractories are international standards for feeder expendable refractory materials. As Emhart licensed products, they are known world wide and find wide use in Feeder and Forehearth applications for Flint glass production.

PSR-315 products find their application as feeder expendables (spouts, plungers, tubes, stirrers and orifice rings) at the working end of the glass furnace mainly due to the good corrosion properties against glass, as a result of the increased ZrO2 content (19 wt%) as compared to the PSR-333. PSR-333, find most applications as forehearth and channel blocks, acting as a conduit for glass conditioning from the melting furnace to the working end. From table 5-1, PSR-333, has primary mullite (virgin mullite) in its starting formulation as as such presents excellent thermal shock properties and low corrosion rate (< 0.5cm/year) that can accommodate the current 10+ year service life expectancy of most container glass forehearths [14]. As well due to its lack of glassy phase, low ZrO_2 content (11 wt%); it is an unlikey source of zircon/zirconia related cat-scratch cord glass defects that will present in the final product [14].

Table 5-2, shows the typical physical properties of the two PSR comercial products, as per product data sheets provided of the respective refractories. Both refractories are classified as dense refractories and contain average apparent porosities of ca. 20%.

Figure 5-1 shows a low magnification SEM micrograph of the microstructure of PSR-315 which is typical of refractory castables. The figure shows two aspects of the microstructure, that it is composed of alumina grog grains bonded in an fine

matrix material. The alumina grog grains coming from the tabular alumina size fractions in the batch formulation. Figure 5-1 further shows the SEM EDX mapping of the microstructure and reveals the matrix to be a zircon-mullite matrix which is confirmed by XRD pattern of the PSR-315 refactory presented in figure 5-2.

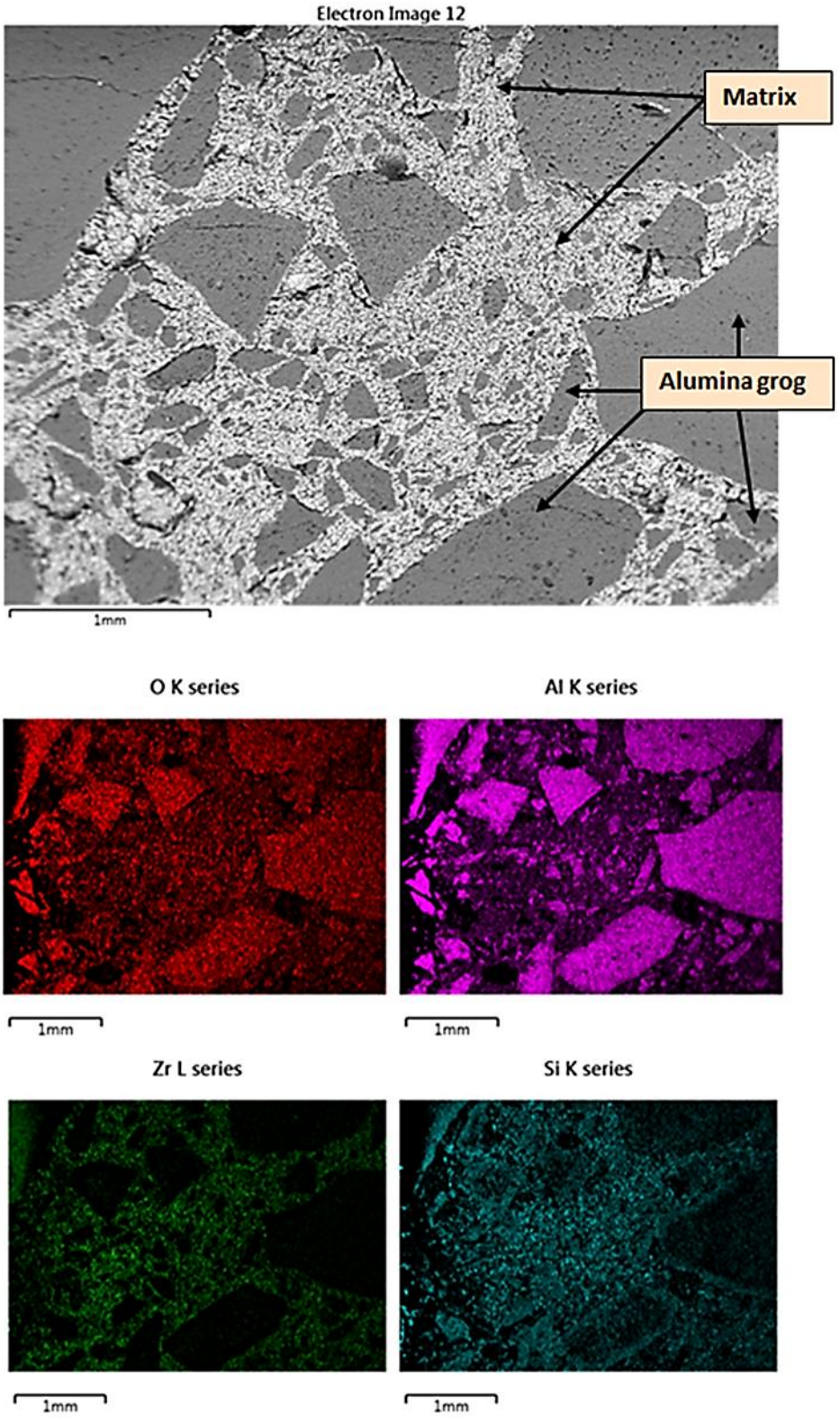

Figure 5-1: Microstructure of the PSR-315 refractory. (a) Low magnification and (b) SEM EDX mapped microstructure region of PSR-315 refractory.

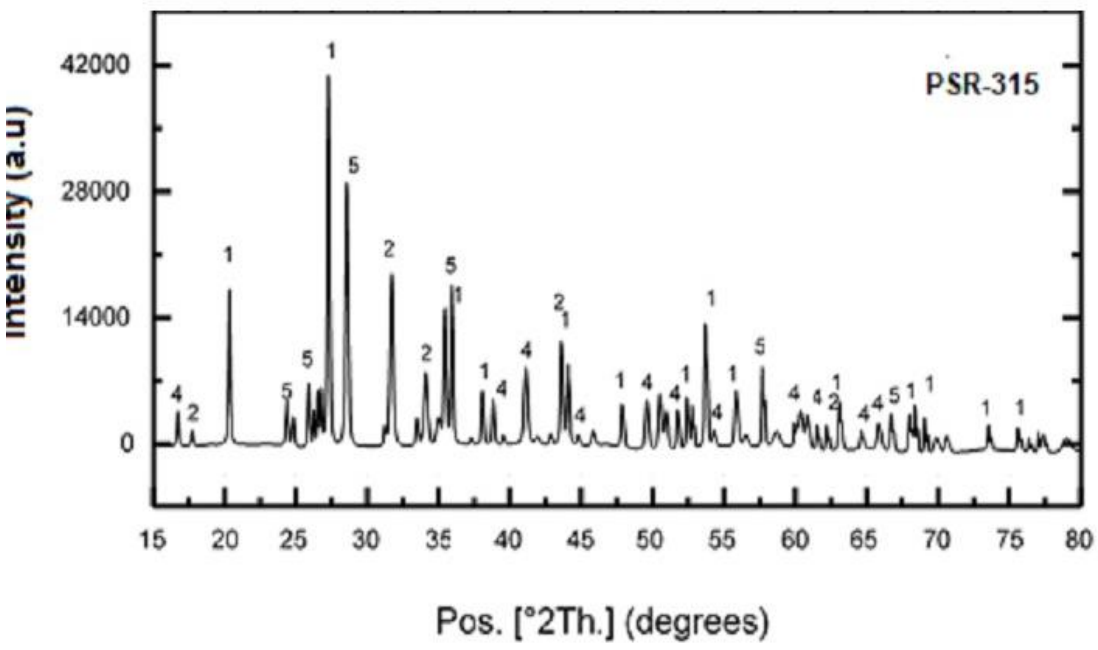

Figure 5-2: XRD pattern of PSR-315 refractory zone area sintered at 1500°C.

1= ZrSiO4 [ref code: 04-008-8667]; 2 = ZrO2-m [ref code: 04-008-]; 3 = ZrO2-t [ref code: 04-008-];

4 = Al6Si2O13; [ref code: 04-010-3002]; 5 = α-Al2O3; [ref code: 04-005-4502]

As explained previously, the matrix represents the weakest region of the refractory and as such has the greatest effect on the thermo-mechanical stability as well as chemical compatibility in slags and or siliceous melts. Figure 5-3 shows the matrix region of PSR-315 from a high magnification SEM micrograph. The figure shows some regions of the micristructure where debonding of the matrix from alumina grog grains has occurred resulting in cracks and pores. This is normally a result of a phenomenon known as wall effects from packing flaws between the fine matrix materials and the large grog grains. The presence of such packing flaws leaves the refractory prone to ingress and attack by glass melts within these pores. Therefore, it was realised that to avoid such packing flaws in the developed compositions, the

partcle side distributions of mix formulation would need to be optimised. This was done and is discussed in detail in the folowing sections of this chapter.

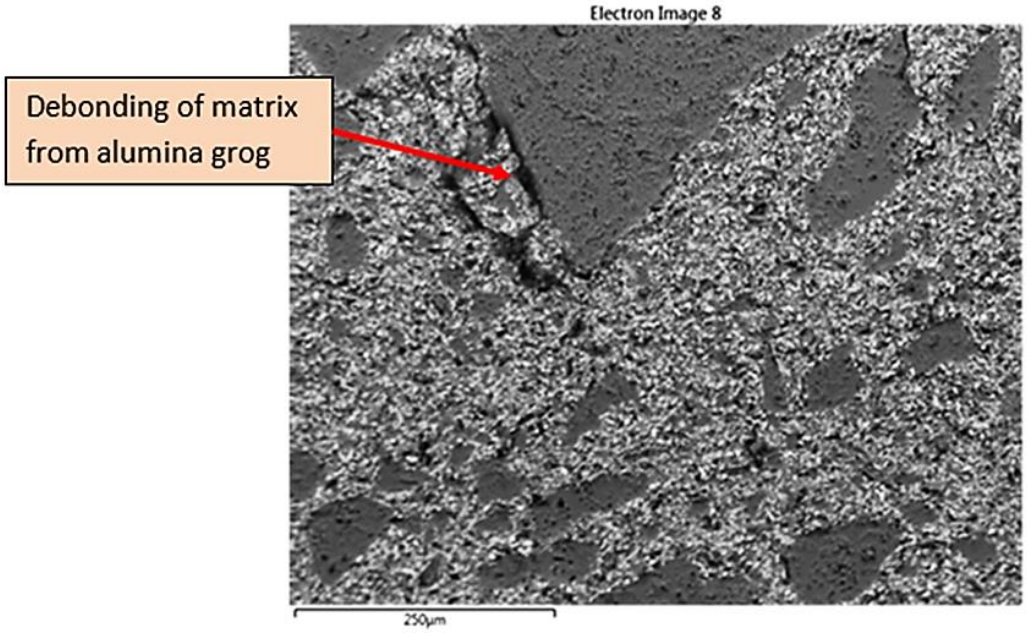

Figure 5-3: Low SEM magnification of the PSR-315 microstructure showing the debonding between the matrix and grog grains due to wall effects.

5.2.1.2 PSR-333

Figure 5-4, show the microstructure of PSR-333..

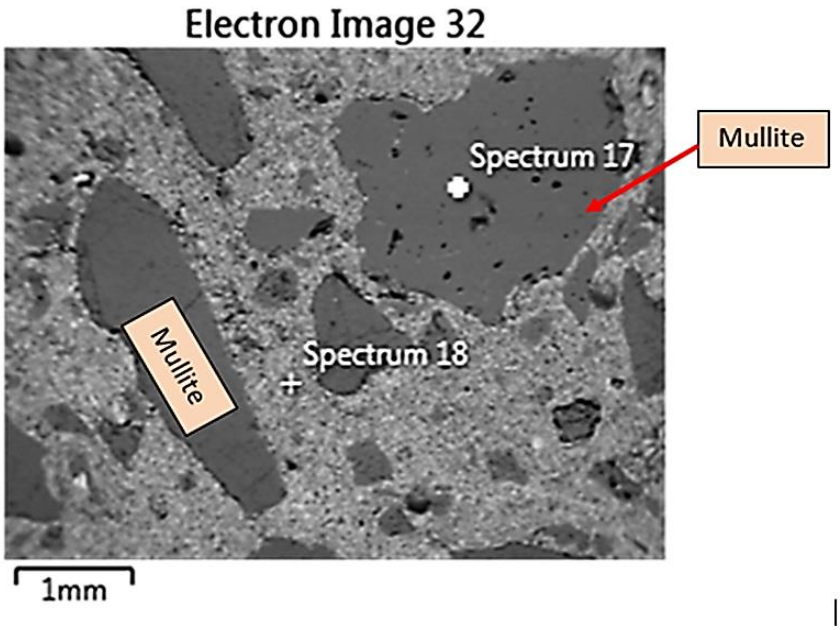

Figure 5-4: SEM micrograph showing the microstructure of PSR-333 refractory.

From figure 5-3, it can be seen from the morphology that the mullite phase exists within the microstructure as single grains, coming from the primary mullite in the starting batch raw material

Table 5-3, shows the semi quantitative point analysis of the mullite phase and shows the grain in spectrum as the fused 1-3mm Virginia mullite, with Al_2O_3 content of 78 wt.% which typical of mullite produced from melt.

Table 5-3: SEM Semi quantitative point analysis of PSR-333 refractory shown in figure 5-4

Element	Spectrum 17	Spectrum 18
	wt.%	wt.%
O	49.2	48.5
Al	34.1	40.5
Si	16.5	12.0
Zr	0.00	0.00
Total	100.00	100.00

Mullite is known for high temperature stability thermal and thermal shock properties. However, [37-40] from the thermomechanical properties of the ceramic body studied, their results showed a 13 -16% increase in the flexural strength as well as improved thermal shock properties when the mullite exist as acicular and interlocked within the matrix microstructure [37-40]. This indicates that the type of mullite has significant effects on the thermomechanical properties of the refractory body. Therefore, for the development of the compositions of interest in this research, their evolved microstructure would need to possess mullite in the form of acicular grains to improve the thermo-mechanical properties of the developed refractories. Hence it was decided not to use Virginia mullite in the starting mix formulation of the trial compositions as is the case with the PSR-333 formulation. Rather, the reaction

sintering route of an Alumina-zircon staring mixture as in the case of PSR-315 formulation was preferred with the aim of trying to evolve an acicular mullite based microstructure that would enhance the thermo-mechanical properties of synthesised refractories.

5.2.2 Evaluation of Phase Equilibrium diagrams

5.2.2.1 Al_2O_3-ZrO_2-SiO_2 system

The principal raw materials used in the production of the reaction sintered, zirconia reinforced, mullite refractory bodies in this study were α-Al_2O_3 and $ZrSiO_4$ meaning that the sintered composites would be of the Al_2O_3-ZrO_2-SiO_2 system. From the material properties of the standard reference refractories PSR-315 and PSR-333, characterised and presented in the previous section, a clear picture was presented of what the new developed compositions of interest, with increased ZrO_2 content should possess in terms of microstructure, mineral phases and their microstructural evolution.

PSR-333 presents good thermal properties from the inherent mullite phase in its microstructure. Therefore the new trail compositions of interest were selected to lie within primary phase fields that contain mullite on the AZS ternary phase diagram.

Figure 5-5 shows the ternary phase diagram and the primary phase fields of a Al_2O_3 – SiO_2 – ZrO_2 system at 1500C. The figure also highlights the selected range of compositions (red eclipse) for preliminary studies of this research project.

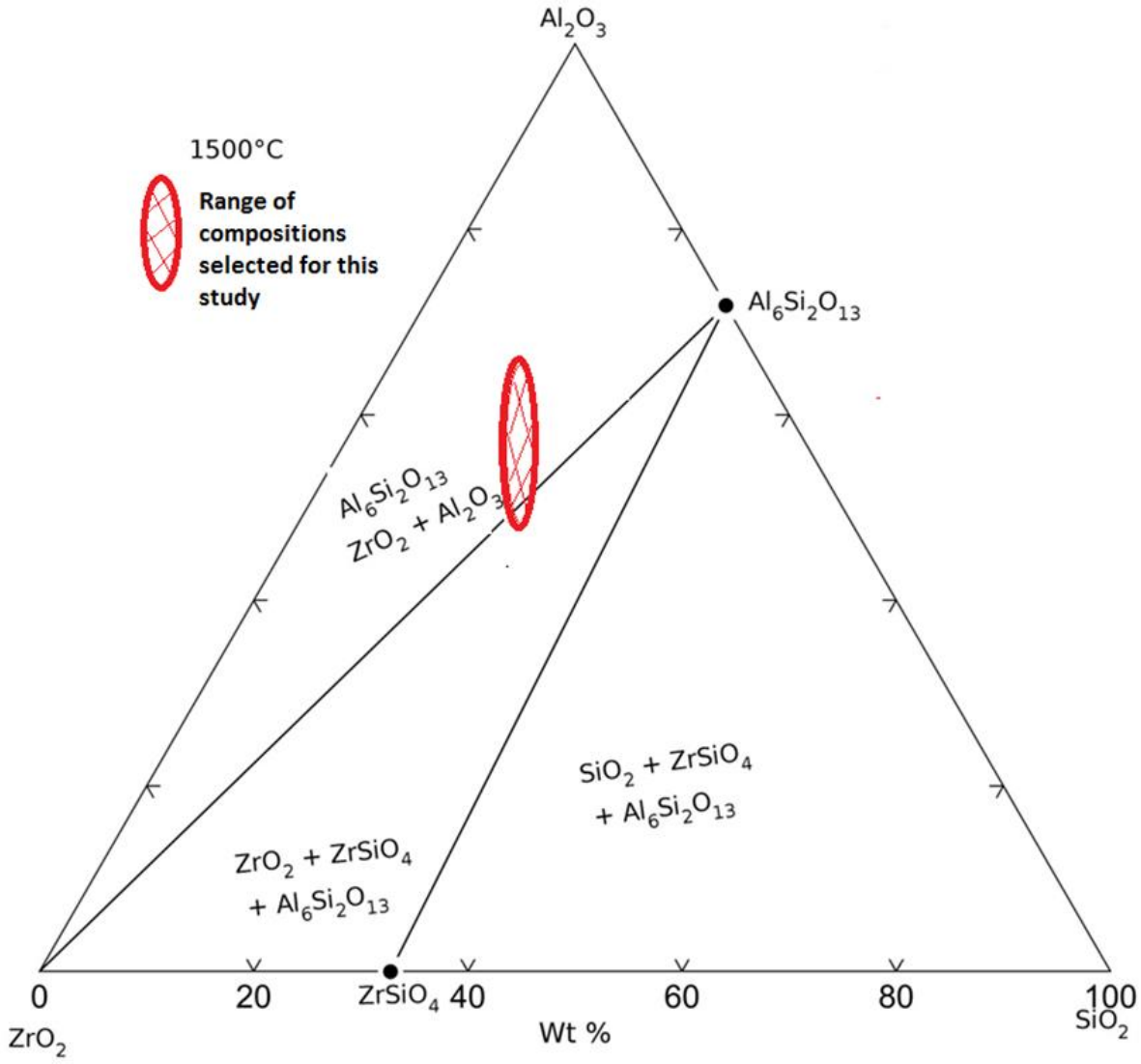

Figure 5-5: Ternary phase diagram of the Al2O3 – SiO2 – ZrO2 system showing the primary phase fields at 1550C [11]

Figure 5-6, shows the isopleths, within the liquidus isotherms, of the standard refractories compositions PSR-315 and PSR-333. From the ternary phase diagram, it can be seen that the standard refractories PSR-315 and PSR-333 the standard refractories have a high refractoriness. Their isopleths are located within high temperature liquidus isotherms and away from the eutectics.

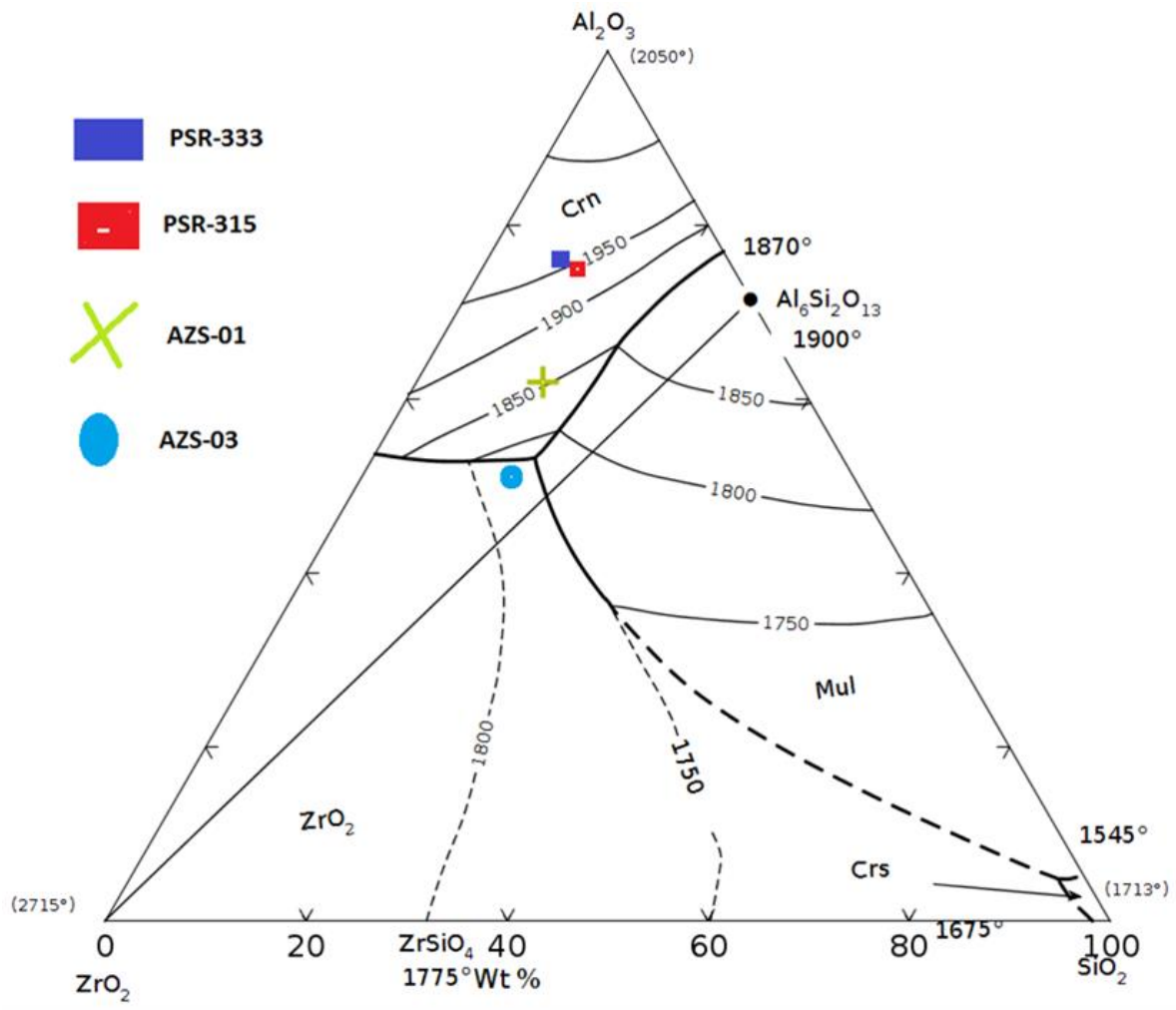

Figure 5-6: Ternary phase diagram of the Al_2O_3 – SiO_2 – ZrO_2 system. The isopleths of the standard reference refractories PSR-315, PSR-333 and the developed compositions of interest, AZS-01 and AZS-03 are shown on the Al_2O_3-SiO_2-ZrO_2 liquidus ternary isotherms [11].

Figure 5-6 also highlights the isopleths of the three trial composition batches in this research, AZS-01, AZS-02 and AZS-03, with increased zircon ($ZrSiO_4$) content, up from the standard PSR-315 to 50 wt.%. As highlighted in the previous section, the evolution of acicular mullite was determined as requisite in developing refractories with improved thermo-mechanical properties, hence the new trial compositions were selected to lie at lower liquidus isotherm to enhance liquid phase sintering.

5.2.2.2 $Al_2O_3 – ZrO_2 – SnO_2 – SiO_2$ system

No phase equilibria experimental studies were conducted in this research. Rather, proven work and studies from literature was used to justify and investigate the effects of SnO_2 as a sintering aid on the reaction sintering of Alumina – zircon mixtures.

The ZrO_2-SiO_2 system has been extensively studied and from the binary phase diagram shown in figure 2-3, the composition of $ZrSiO_4$ falls in the two phase ZrO_2 + liquid from 1680 °C and dissociates in the temperature range of 1550 °C according to the reaction;

$$ZrSiO_4\,(s) \longrightarrow ZrO_2\,(s) + SiO_2\,(s)$$

$$\Delta G,_{1400K} = 1489.1\ kJ/mol \qquad (26)$$

From the tabulated Gibbs free energy data, this means Zircon is stable by a narrow margin up to the temperature where a liquid phase appears, and the above reaction will proceed in the forward direction when the product SiO_2 (s) is replaced by the descriptor SiO_2 (l). This means zircon will decompose only in concurrence with melting as the activities of SiO_2 (l) component is reduced. Also, it has been shown that in the presence of impurities, the dissociation temperature of zircon is reduced.

As described earlier in section 2.2.5.1; work on the phase equilibria of the ZrO_2 and SnO_2 system by various workers and presented by Allemande et al, (2002) as a phase diagram showed a wide immiscibility gap between the ZrO_2 and SnO_2 phases leading to a limited solid solution of tin oxide in zirconia, $Zr_{1-x}Sn_xO_2$; and zirconia in tin oxide $Sn_{1-x}Zr_xO_2$ in the temperature range of 1230 – 1750 °C.

In the SiO_2-SnO_2 system, phase equilibria studies by [48] above 1500 °C, showed the formation of a liquid phase in SnO_2-SiO_2 compositions rich in SiO_2 while a solid and a liquid phase was observed to co-exist at equilibrium in the temperature range 1510 °C – 1625 °C. From the results, [48] determined eutectics of SnO_2 and SiO_2 in the SiO_2 rich regions at eutectic temperatures of 1500 °C - 1510 °C and a liquid miscibility gap in the SnO_2 rich regions at monotectic temperatures of 1625 °C – 1650 °C.

Therefore, from the above evaluations, it would suggest that in the Al_2O_3 – ZrO_2 – SnO_2 –SiO_2 system, a liquid phase produced from the reaction between SiO_2-SnO_2 above 1510 °C would favour the forward reaction of the dissociation of $ZrSiO_4$ as shown in equation 26.

5.2.2.3 Compositional studies

To determine whether the phase diagram analysis and compositional evaluations concluded in the above section on the effects of SnO_2 as a sintering agent, compositional studies were conducted on the alumina-zircon refractory matrix mixture. In these studies, calcined alumina (CT9FG) and zircon (zircozon 10) mixtures with 1wt% and 5wt% SnO_2 added were pressed into pellets. Figure 5-7 shows the XRD pattern of the pressed pellet sintered at 1550 C.

The XRD pattern in figure 5-7 revealed the presence of corundum, $Zr_{1-x}Sn_xO_2$ solid solution, baddeleyite and mullite as the major phases. No zircon peaks were observed in the sintered pellet.

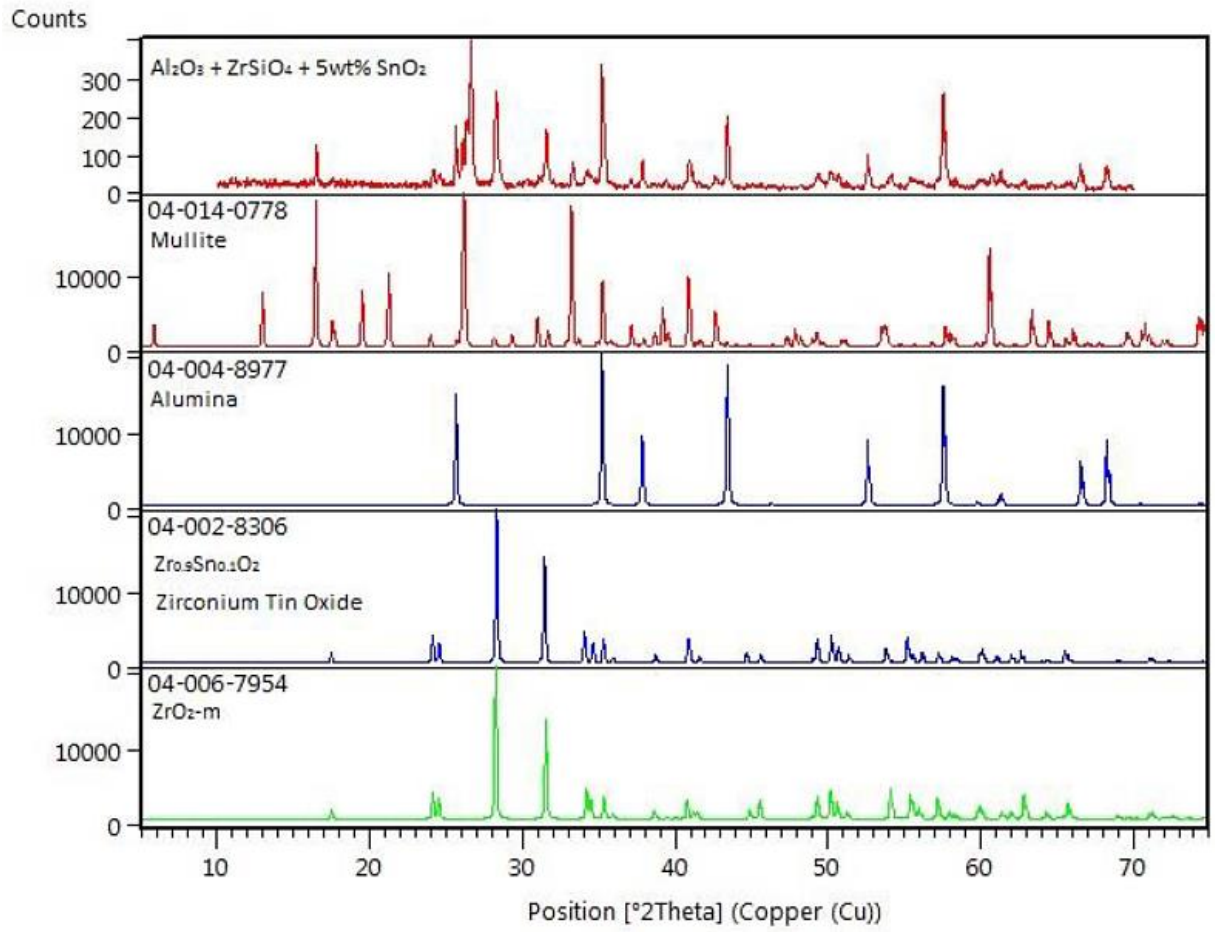

Figure 5-7: XRD pattern of pressed pellet of Al_2O_3+$ZrSiO_4$+SnO_2 mixtures sintered above 1500 °C. Reference XRD patterns of Mullite: $Al_6Si_2O_{13}$ (04-014-0778); Corundum: α- Al_2O_3 (04-014-0778); Tin-Oxide solid solution: $Zr_{0.9}Sn_{0.1}O_2$ (04-002-8306); and Baddeleyite: ZrO_2 (04-006-7954) are also presented.

This highlighted a complete dissociation of zircon from the starting material and enhanced reaction sintering of alumina-zircon through the increased mullite phase evolution as evidenced by the numerous mullite diffraction peaks under conventional sintering.

5.2.3 Mix formulations Design and Optimisation

5.2.3.1 Dinger & Funk PSD analysis Results

Using the standard PSR-315 batch formulation as reference, trial batch formulations of the AZS-01, were created and optimised to determine an optimum mix formulation that would present self-flow properties of the prepared suspensions or refractory slip.

The formulations of AZS-02 and AZS-03 were then later derived from the optimised formulation of AZS-01. To achieve this, the composite PSD of the PSR-315 refractory mixture was determined from each individual material component's particle size distribution and the corresponding composite CFTP from each size class of all the material components using the modified Andreassen model (Dinger and Funk) equation.

From Figures 5-8 (a) – (d), the distributions modulus (q-value) of the current PSR-315 mix formulation was observed to be the one which followed the q-values of the Dinger and Funk curves in the range of 0.08 to 0.20.

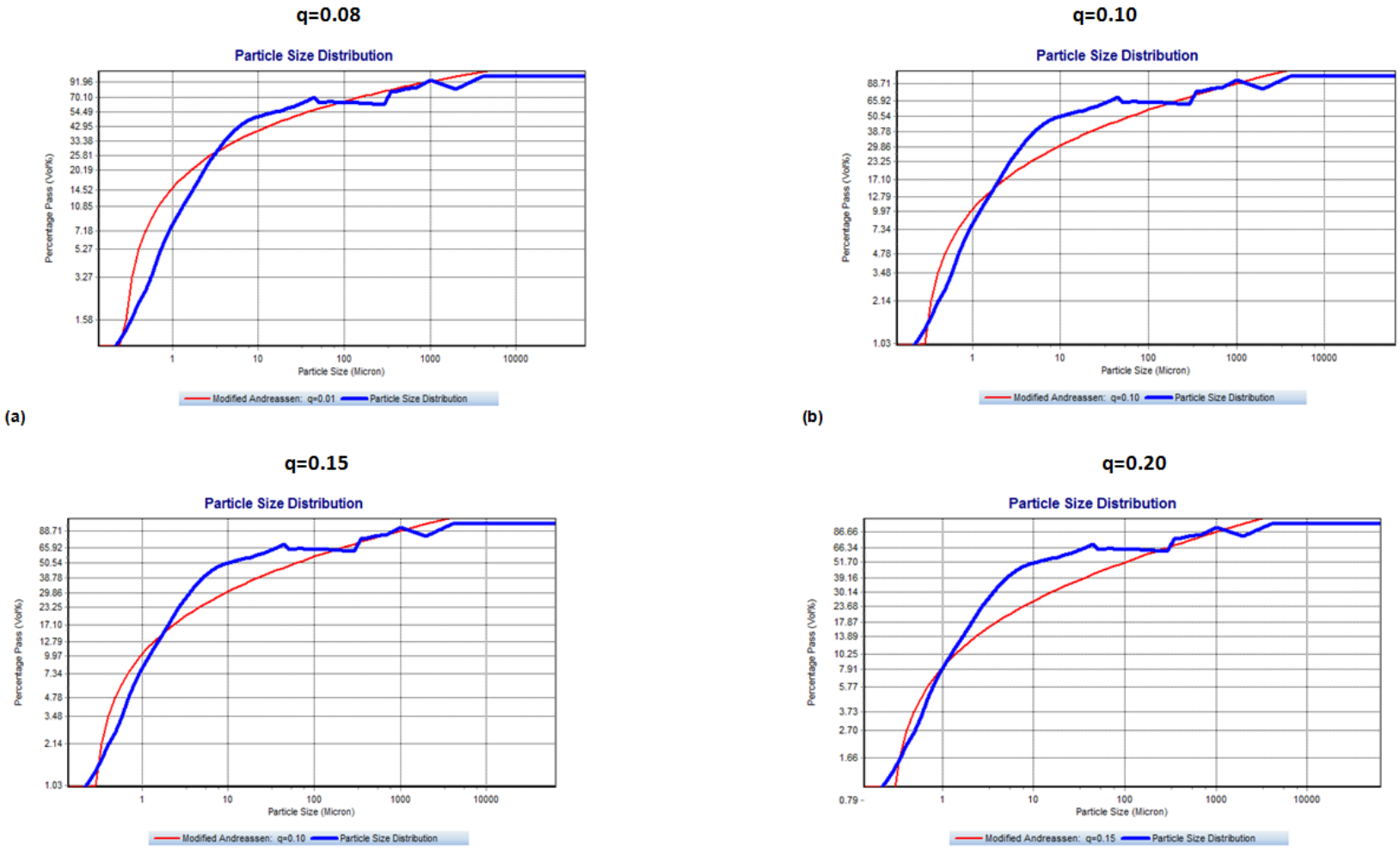

Figure 5-8: Corresponding composite CFTP, from each size class of all the material components of the PSR-315 formulation modelled against the Dinger and Funk distribution curve at different packing modulus (q-values) modelled so as to determine the packing modulus of PSR-315.

From literature review, the distribution modulus, q, for a 100% packing density of infinite distribution was found to be 0.37 or lower by Dinger and Funk. However, for self-flowing castables with optimum packing density, research results from systems based on the Dinger and Funk model indicated the q-values to be in the range between 0.20 – 0.25 [53, 55]. Therefore, using the PSR-315 formulation at q-value of 0.20 as reference, AZS-01, AZS-02 and AZS-03 formulations were designed in preliminary studies. In the preliminary study, seven formulations based on q-values of 0.19 to 0.25 were designed using the Elkem Material Mix Analyser software.

A q-value of 0.23 has been reported in literature to provide self-flow properties for refractory castables of > 80%. This is agreement with findings in our preliminary studies on the AZS-01 formulations where an (OFAT) design of experiment (DOE) methodology was implemented to determine the optimum q-value of the AZS-01 formulation that exhibits a self-flow or flowability index of > 80 % with minimum water demand.

Figure 5-3 shows the composite PSD curve of the AZS-01 trial mix formulation (01) modelled to the Dinger and Funk particle packing curve at a q-value of 0.23, with zircozon 10, (d50 = 2.85µm and d90 = 13.44 µm) as the only zircon additive in the mixture and the corresponding batch mix formulation. The smallest particle size in the formulation was 0.2µm and the largest particle size 2mm. From the figure, the red curve represents the modified Dinger and Funk model curve for optimum packing at q = 0.23. The blue curve represents the composite PSD of the mix formulation of composition AZS-01.

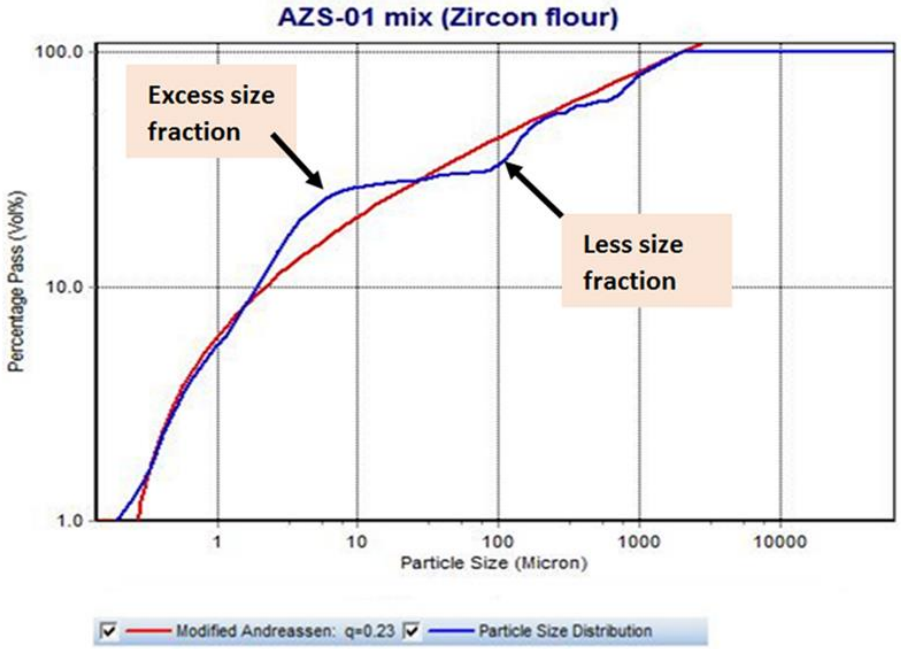

Materials In Composition

Material Name	Density	Quantity	Vol %
Zircozon 10	4.50	1752.00	31.22
china clay	2.62	49.00	1.50
Ball Clay	2.62	49.00	1.50
Calcined Reactive Alumina: PE	3.95	278.00	5.64
Calcined Alumina CT9FG (08/(	3.95	278.00	5.64
Tabular Alumina: 0-0.3mm (13	3.92	618.00	12.64
Tabular Alumina 0-0.5mm (13.	3.92	469.00	9.59
Tabular Alumina 0.5-1mm (13.	3.92	322.00	6.59
Tabular Alumina 1-2mm (13/0	3.92	1190.00	24.34
Alphabond 200	3.00	50.00	1.34

Figure 5-9: Trial mix formulation of AZS-01 with zircon flour as the only zircon source material in the formulation and Its corresponding PSD curve modelled to Dinger and Funk model for particle packing at q-value of 0.23.

From figure 5-4, it can be seen that in the composite PSD curve of AZS-01, there is an excess of the cumulative percent finer than (CPFT) distribution for the size fraction 2.12µm – 12.45µm that make up the matrix, and less of the size fractions with a median diameter d_{50} = 120µm. As such, size fractions of zircon sand M170 were added to the formulation by reducing the size fraction of zircozon 10 to

optimize the particle packing. From the list of commercial raw materials components that were available for the batch mix formulations of the designed refractories, shown in table 4-1, the size fraction with a d_{50} = 120µm, represents the size fraction of zircon sand M170. As such, the size fractions of zircon sand M170 were added to the formulation by reducing the size fraction of zircozon 10 to optimise the particle packing.

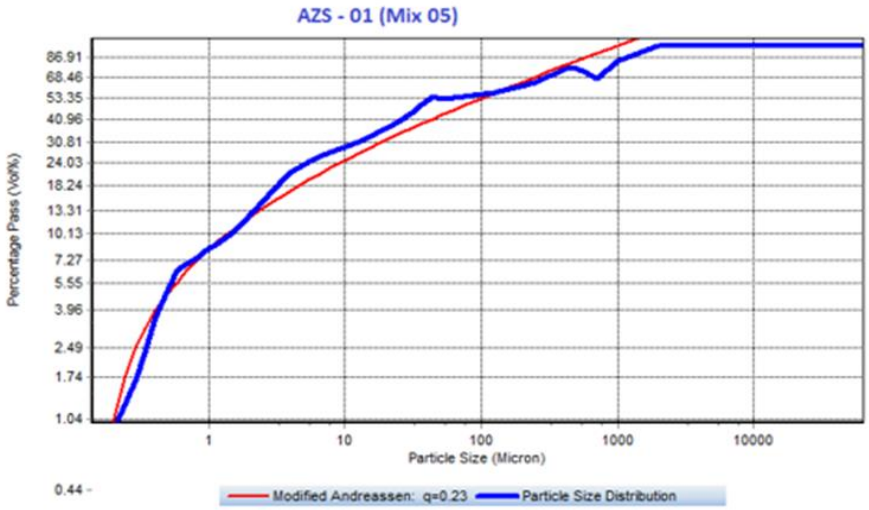

Materials In Composition

Material Name	Density	Quantity	Vol %
Zircozon 10	4.50	452.00	7.74
china clay	2.62	49.00	1.44
Ball Clay	2.62	49.00	1.44
Calcined Reactive Alumina: PE	3.95	278.00	5.42
Calcined Alumina CT9FG (08/(	3.95	278.00	5.42
Tabular Alumina: 0-0.3mm (13	3.92	418.00	8.22
Tabular Alumina 0-0.5mm (13.	3.92	369.00	7.25
Tabular Alumina 0.5-1mm (13.	3.92	522.00	10.26
Tabular Alumina 1-2mm (13/0	3.92	1489.00	29.27
Alphabond 200	3.00	50.00	1.28
M170 Prime Calcined Zircon Sa	4.50	1300.00	22.26

Figure 5-10: Trial mix formulation (05) of AZS-01 with zircon sand added to the formulation and Its corresponding PSD curve modelled to Dinger and Funk model for particle packing at q-value of 0.23.

Figure 5-4 shows the optimised mix formulation (05) at q-value of 0.23, after some of the prime calcined zircon sand (d50 = 140µm) has been substituted for the zircon flour (d50 = 2.5µm and d90 = 13.44µm) in the formulation. The formulation had the requisite or suitable proportions of zircon sand and zircozon 10 size fractions that would provide optimum packed distributions with self-flow properties and was selected for slip preparation. Table list the determined optimised formulations of AZS-01, AZS-02 and AZS-03.

Table 5-4: Developed and optimised mix formulation of AZS-01, AZS-02 and AZS-03

Raw material component	vol. % fraction		
	AZS-01	AZS-02	AZS-03
Zircozon 10	10.3	10.9	12.1
Zircon sand M170	22.3	23.5	34.5
PBR	9.4	8.9	7.6
CT9FG	7.9	8.4	7.2
Tabular Alumina -0.3mm	6.7	7.0	3.6
Tabular Alumina -0.5mm	5.6	5.9	3.6
Tabular Alumina -0.5 -1mm	6.7	5.9	3.6
Tabular Alumina 1-2mm	28.4	26.5	24.6
China Clay	1.5	1.6	1.6
Ball Clay	1.5	1.6	1.6

5.3 Slip Preparation & Optimisation

The pre-consolidation of ceramic bodies using wet forming processes such as slip casting requires the dispersion of mix formulation raw material powders in an aqueous medium to form slurry known as a slip. As highlighted earlier in the previous section, the prevailing trend in producing refractory castables is for the mix

formulations of the refractory composition to consist of a wide particle size distribution to enhance particle packing, reduce the mixing size scale and more importantly, produce a dense green body. This was the case for the mix formulations of the trial refractory compositions AZS-01, AZS-02 and AZS-03, shown in table 5-1, whose particle size distribution ranged from 1µm - 2000µm and were designed and optimised for optimum particle packing.

As discussed earlier in section 5.3, a high solid loading for the AZS-01 refractory composition was requisite to allow for low water demand refractory slip with good casting rates which would lead to sustainable production from reduced energy consumption in drying. However, incorporation of water to particulate systems is well known to affect the surface chemistry of the fine matrix particulate materials which tend to agglomerate because of intra-particle Van der Waals forces [5,30, 53]. The agglomerates trap water within and this results in an increased solid loading (vol. %) of the system. A high solid loading, together with fine particulates and agglomerates enhances more particle – particle interaction which results in dilatancy of the dispersed system that becomes characterised by an increase in the viscosity of the slip. This makes the slip un-workable and requiring of an increase in the slip water demand.

The grog, coarse particles and some soft agglomerates may also sediment which would lead to segregation resulting in density and microstructural inhomogeneities in the green and sintered bodies. Therefore, the stability of the AZS-01 refractory slip was paramount to the final ceramic or refractory body possessing the requisite material properties highlighted in section 5.2. As such, for this study, the AZS-01 slip had to fulfil several requirements such as maintaining a homogenous well

dispersed slip that is easily reproducible even with slight changes in the solid loading and raw material batches.

Various dispersants are used in stabilising refractory slips or suspensions and for this part of the study, three commercial dispersants, Darvan 7, Dolapix PC725 and Dispex A40 were tested and evaluated to identify the best dispersant and its optimum concentration ideal for AZS-01 slip stability. Zeta potential and particle Size measurement techniques were used to preliminarily screen between the three dispersants. Deflocculation evaluation tests of the AZS-01 slip properties were then conducted to validate the choice of dispersant. This section highlights and discusses the results of the study.

5.3.1 Zeta Potential

Zeta potential tests were conducted on Preliminary screening evaluation to determine the most suitable dispersant in producing stabilised dispersions of the compositions AZS-01, AZS-02 and AZS-03 designed with increasing zircon content designed and selected in section 5.2. Zeta potential and particle size measurements were conducted according to the methodology described in **section 4.3.1.1.**

From the prepared dilute aqueous solutions of the fine raw material particulate components of the AZS-01 mix formulation that make up the matrix (<100µm), 0.1ml aliquots of the commercially available dispersants, Darvan 7, Dolapix PC75 and Dispex A40 were added and zeta potential and size measurements taken to evaluate and use a guide for the selection of suitable and efficient dispersant. All three dispersants were supplied from the manufacturers in aqueous form and are water soluble.

Table 5-3 shows the measured zeta potentials of the dispersed refractory suspensions of the blended AZS fine particulate raw materials, CT9FG, PBR and Zircozon 10 that make up the matrix raw materials of the AZS-01, AZS-02 and AZS-03 refractory compositions.

Table 5-5: Zeta potential measurements for the AZS-01 matrix suspensions dispersed in 3 commercial dispersants.

Suspension	Dispersant added	Zeta Potential (mV)	pH
A	None	-5.54	8.1
B	Darvan 7-N	-32.8	6.8
C	Dolopix PC75	-35.2	6.2
D	Dispex -A40	-5.54	8.9

Recalling from the literature review, in section 2.3, the interaction of adjecent particles in slips is determined by changes in the Van der Waals attraction forces and or electrical repulsion forces brought about by the added electrolytes. Surface dissociation or ion adsorption of the oxide particles from the fine mix formulation brings about the electrical repulsion forces resulting in a net surface charge on the particle.

The results show that the zeta potential value of suspension **A**, without any dispersant added to it, is low and close to zero, at -5.54mV. Since the magnitude of the zeta potential of a dispersed particulate solution infers to the possible stability of the suspensions. This means that the particles in suspension A, with a zeta potential of -5.54 have no adequate electristatic force to prevent floculation and thus the suspension is not stable.

This can be seen when the size distribution of the dispersed particles is ploted, as shown in figure 5-2. The size distribution of the suspended mixture shows a monomodal distribution that is shifted to the right having a d_{50} of that is greater than the d_{50} of the starting particles. This shows that flocculation of the fine AZS matrix particles has occurred in the absence of a dispersant, and as such, the use of a dispersant to produce a stabilised slip was paramount.

Suspensions, B and C, containing the dispersants, Darvan-7N and Dolopix PC75, presented high zeta potential values of -32.8mV and -35.2mV respectively. From table 5-2, the addition of the two dispersants Darvan 7-N and Dolopix PC75 brought the suspensions' pH from alkaline to an acidic range.

Suspension D containing the dispersant Dispex A-40 had a low zeta potential value of -2.58mV and its addition to the suspension pushed the pH to be more alkaline. From the zeta potential values, it was clear that of the three dispersants tested, Darvan 7-N and Dolopix PC-75 were the suitable dispersants for the AZS-01 batch formulation that would provide well dispersed suitable, stable and workable slips.

Size distribution measurements confirm these findings deduced from the zeta potential values. In figure 5-2, suspension D, with Dolopix A-40, exhibits a broad multimodal size distribution with the third size intensity peak showing a d_{50} of 824.5µm. This shows that the three matrix materials used in suspensions were agglomerating. Suspensions B and C, containing Darvan 7-N and Dolopix PC 75, respectively showed trimodal peaks indicating good dispersion of the materials in suspension.

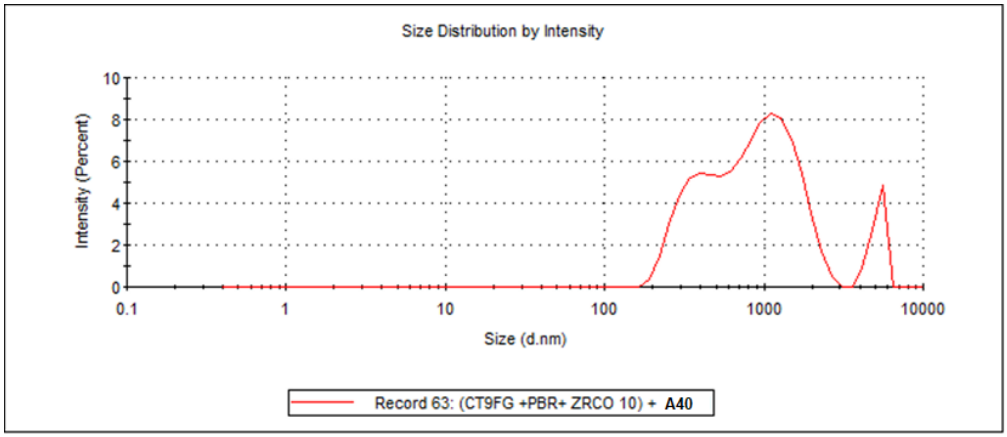

Figure 5-11: Size distribution of dispersed AZS-01 matrix suspension under the deflocculation with Dispex-A40 added to the suspension. The corresponding zeta potential was -35mV

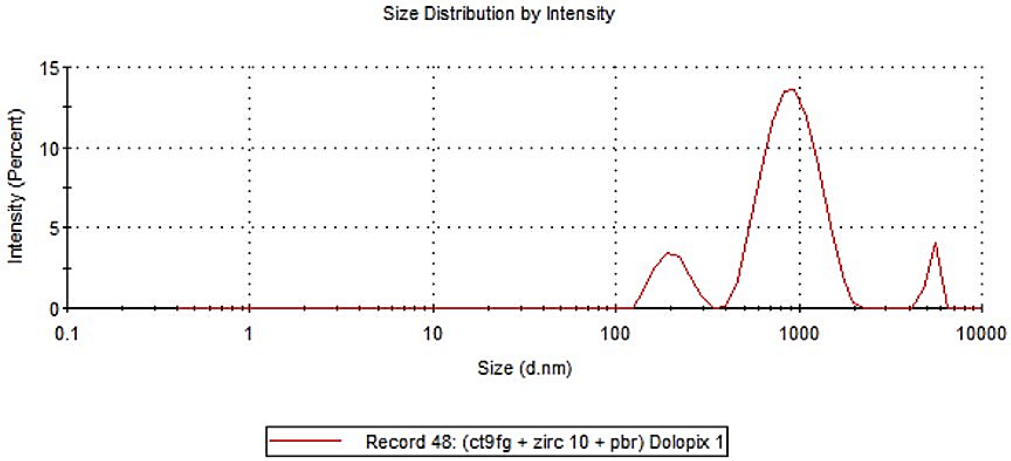

Figure 5-12: **Size distribution of dispersed AZS-01 matrix suspension under the deflocculation with Dolopix PC75 added to the suspension. The corresponding zeta potential was -35mV.**

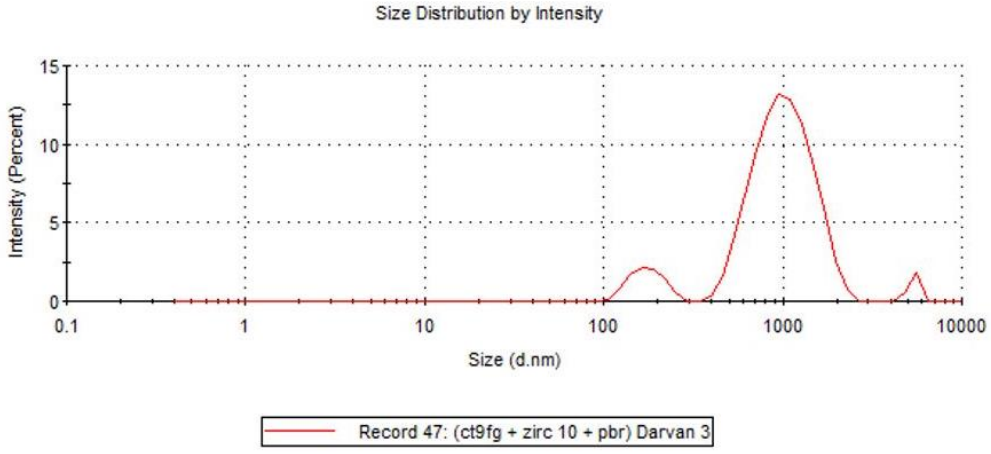

Figure 5-13: Size distribution of dispersed AZS-01 matrix suspension under the deflocculation with Darvan 7-N added to the suspension. The corresponding zeta potential was -32.8mV.

From literature, the iso-electric point of alumina is within the 8.3 - 9.6 pH while zircon is around 4.5 [30]. Therefore, it seems that the alumina matrix materials were the main particle that were agglomerating in suspsension D as the pH of suspesion was within the isoelectric point of alumina at 8.9 pH. For suspensions B and C, the pH of suspesions was shifted towards the acidic range, out of the iso-electric point of alumina thereby creating an electrostic repulsion between the surface particle and ensuring a well dispersed and stable suspension.

5.3.2 Deflocculation Tests

Deflocculation tests on high solid loadings of 93wt. % (which correspond to vol. % of 83%) of AZS-01 formulations were conducted according to the viscometry methodology described in section **4.3.1.2** for the rheological characterisation of the suspensions. Two 400g mix formulation of AZS-01 was added to 30g (30ml) of water to make as suspension of solid loading of 93 wt.%. To the suspensions, 0.1ml aliquots of Darvan 7-N and Dolopix PC75 were added and dynamic viscosities of the suspensions recorded from the rotational viscometer.

Figure 5-7 shows the deflocculation curves of the AZS-01 refractory suspension and from the figure, it can be seen that the lowest viscosity minima is produced by Darvan 7-N. For Dolopix PC75, with additional increments of the dispersant to the refractory suspension results in an increase in the dynamic viscosities of the slip. which would render the suspension or slips un-workable or requiring more water demand which would negate the main requisite for the design of the new developed formulations.

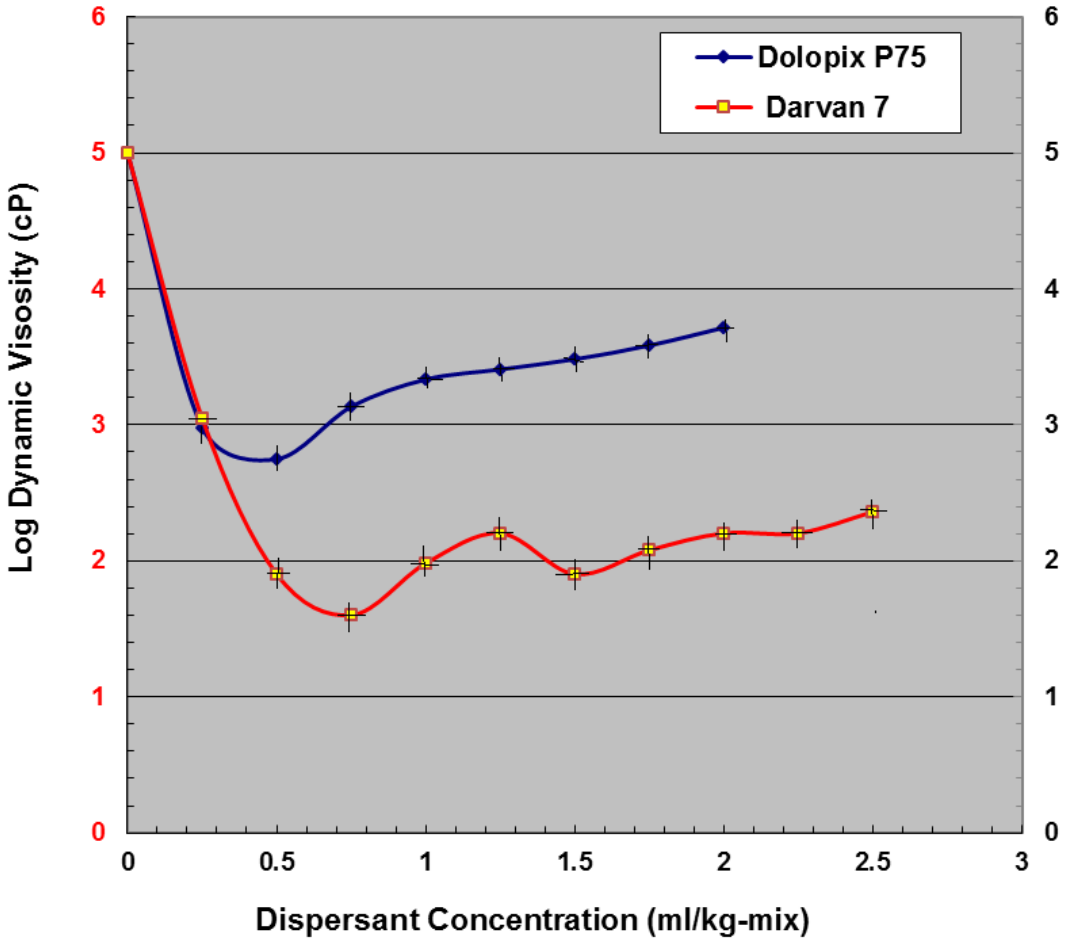

Figure 5-14: Deflocculation curves of AZS-01 mix formulation at different solid loading. The effect of two commercially available dispersants, Darvan 7-N and Dolopix PC75 on the AZS-01 mix formulation was evaluated to identify the optimum

5.4 Synthesis of Slip cast AZS compositions

For this part of the research a preliminary study was conducted on three designed refractory compositions AZS-01, AZS-02 and AZS-03 to evaluate the effect of increased zircon contents up to 50 wt. % slip casting method. The study focussed on identifying compositions for which zircon content (and critically ZrO_2) offer optimum physical, thermomechanical and chemical properties as compared to the standard commercial refractories PSR-315 and PSR-333.

5.4.1 Materials and Methods

Table 5-4 shows the raw materials used to produce the refractory products and the mix formulations of the slip cast refractories. The mix formulations were developed and optimised in the previous section.

For each refractory composition, preparation of the slip (castable) for slip casting was conducted according to the methodology described in section **4.2.1.4.2**. For this study, 5kg batches of formulations of AZS-01, AZS-02 and AZS-03 were produced by weighing accurately each corresponding raw material component size fractions that make up the refractory mix batch formulation. The 5kg optimised batch mix formulations were each dry mixed in a Hobart mixer for 3 minutes. Darvan 7, a sodium polymethacrylate dispersant, and water added and the mixture wet mixed for 5 minutes until a homogenous slip was formed. The standard PSR-315 refractory was also slip cast its slip properties used for comparison with the slip properties of the developed compositions.

After mixing, each prepared slip was cast into 50mm diameter x 50mm long cylindrical blocks plaster of Paris moulds for consolidation of density and porosity samples to evaluate the effect of increased zircon addition in the developed compositions. Chemical compatibility of the developed refractory compositions was also evaluated by conducting static isothermal glass corrosion tests using SLS flint glass, from GTS, UK, composition presented in table 4-6.

For static glass corrosion testing, 150mm x 150mm square crucible cup test samples with a 25mm Ø x 25mm depth recess in the centre were prepared by slip casting the prepared refractory slips into gypsum moulds. All slip cast samples were de-moulded after 24h, before drying and sintering to a temperature of 1500C for 1 hr.

5.4.2 Effect of Zircon addition

5.4.2.1 Slip properties

The main slip properties that were considered in this part of the study were ease of mixing (time taken to reach a homogenous slip), water demand and rheology.

Table 5-6 presents the averaged mixing test data results recorded after mixing and preparation of refractory slips of the developed trial compositions AZS-01, AZS-02, AZS-03 and the standard refractory PSR-315. Table 5-7 show the averaged slip property measurements taken from the prepared refractory slips of the above compositions with increased zircon additions.

Table 5-6: Averaged mix test data results recoded in preparing refractory slips. of the developed compositions and PSR-315.

Composition	Batch Weight (kg)	Total Water added ml	Average Mixing Time (minutes)
PSR-315	5	430 ± 25	15 ± 3
AZS-01 (MP05)	5	325 ± 10	14 ± 3
AZS-02-(MP10)	5	360 ± 30	18 ± 3
AZS-03 (MP12)	5	415 ± 30	20 ± 4

Table 5-7: Averaged slip property measurements of the developed and synthesized refractory AZS compositions taken over 10 mixes. The standard PSR-315 was as a reference for comparison.

Composition	Batch weight (kg)	Zircon (ZrO_2) Content %	Slip Density Kg m^{-3}	Flow cone mm	Moisture (Water Demand) (%)
PSR-315	5	27 (17.01)	3.120 ± 0.02	325 ± 45	8.30
AZS-01 (MP05)	5	35 (22.70)	3.378 ± 0.04	320 ± 30	6.04
AZS-02-(MP10)	5	40 (26.00)	3.108 ± 0.02	326 ± 40	6.86
AZS-03 (MP12)	5	50 (33.1)	3.345 ± 0.06	280 ± 40	8.06

During the study, The AZS-01 formulation exhibited good mixing properties, requiring only 325ml of water in a 5kg batch, see table 5-6. Mixing of the AZS-03 formulation in the Hobart mixer was laboured, lasting on average about 20 minutes of mixing and requiring further additions of water to acquire a homogenous workable slip. PSR-315 took on average 15 minutes to mix to a homogenous slip. This was acknowledged by the Technical Manager and experienced personnel at PSR-Ltd as at the upper limit of the optimum and allowable maximum mixing period. Beyond this mixing time period, the slip temperature has been observed to rise and this is known to affect the casting rate as well as the flow properties of the slip. In general, a drop, in the flow properties of slips is observed with a reduction in slip temperature.

From table 5-6, the mixing times of AZS-01 were comparable to those of the standard refractory, PSR-315, used as a reference. It can be seen that AZS-01, had the lowest water demand with slip moisture of 6.04% as presented in table 5-5 while the slip of refractory composition AZS-03 had the highest water demand of 8.46% and exhibited dilatant behaviour. Moisture content of the slip was measured using a moisture analyser, the Mettler Toledo HB43-S Halogen. The mechanism for a low water demand in an optimized packed fraction of particles, discussed in the literature review section, has been ascribed to the added water first filling up the interstitial voids between particles. The excess water, known as the non-pore/void water, then covers and forms a film around the particle surfaces, (which corresponds to the “ball formation and wet out time” of the mixture during mixing), and results in separating the particles for self-flow characteristics of the slip. Therefore, given that the refractory mix formulations of AZS-01, AZS-02 and AZS-03 were all optimized for particle packing as highlighted in the previous section. It suggests then that the

suspensions of the AZS-02 and AZS-03 were not well dispersed, for the given high solid loading of 94 wt. %, even with the optimum dispersant concentration evaluated in section 5.32. Therefore, formation of flocs in the AZS-02 and AZS-03 suspensions entrapped water and increased the solid loading of the slip resulting in a dilatant slip rheology as shown in table 5-7.

AZS-01 also had the highest slip density of 3.378kgm^{-3} suggesting optimum packing of particle. The slip densities of AZS-02 and AZS-01, with increased zircon contents than AZS-01, were lower than that of AZS-01 suggesting flocculation of the particles resulting in an increased solid loading and reduced particle packing. This can be seen when considering the water demand of the prepared slips of the developed compositions presented in table 5-6. The slips of all the three developed compositions presented good self -flow properties with flowability Index of more than 120%.

After mixing and slip preparation, the refractory was cast into gypsum moulds for density and porosity samples as well as corrosion cup samples to evaluate the physical properties, as well as chemical compatibility to SLS Flint glass, of the developed refractory compositions.

5.4.2.2 Physical Properties

Table 5-8 shows the physical properties of the sintered AZS-01, AZS-02 and AZS-03 developed refractory compositions and the commercial reference refractory PSR-315 used in this study. From table 5-8, the AZS-01 refractory sintered at 1500 °C had apparent porosities of ca. 14% and bulk densities of 3380kg m^{-3}.

Table 5-8: Physical properties of the sintered AZS-01 and AZS-02 refractories

Refractory Sample	Physical Properties	
	***BD (g/cm^3)**	***AP (%)**
PSR-315	*3.11 ± 0.1*	*20.0 ± 2.3*
AZS-01	*3.38 ± 0.06*	*13.8 ± 0.3*
AZS-02	*3.28 ± 0.1*	*17.5 ± 0.3*
AZS-03	*3.17 ± 0.2*	*19.2 ± 0.5*

This shows the developed refractory body had improved physical properties than the reference AZS-01 refractory, with porosity of ca. 20% and bulk density of 3300kg m^{-3}. This translates to a reduction in porosity of about 30 rel. %, in comparison with the commercial PSR-315 refractory. Apparent porosity results, from table 5-5, also reveal that the sintered AZS-02 and AZS-03 refractory compositions had high apparent porosities of ca. 18% and 19% which are comparable to PSR-315 apparent porosities.

The AZS-01 refractory with higher zircon content (35wt. %) also presented an increased bulk density than the AZS-02, AZS-03 and the commercial PSR-315 refractory for AZS refractory compositions sintered at the same temperature. This can be attributed to the enhanced particle packing of the AZS-01 formulation, low water demand and workable homogeneous slip, as presented in table 5-5, which yielded a higher initial green density. Numerous studies have shown that the dense particle packing and hence; a higher initial green density; enhances densification at low temperatures through uniform sintering [19,21]. Therefore, for the AZS-01 refractory, the enhanced particle packing from an optimized PSD provided a path for enhanced sintering and densification of the refractory resulting in improved physical properties shown in table 5-5.

5.4.2.3 Corrosion Resistance Properties

From literature review, the measured high apparent porosity values of AZS-02, lie at the upper limit of the range of apparent porosity that [11] observed results in a linear increase of refractory slag corrosion rates for an apparent porosity % in the range 12 – 18 %. AZS-03 and PSR-315 refractories contained porosities that lie outside this range and hence were expected to exhibit higher refractory slag corrosion rates. Therefore, the next part of the study investigated the effects of increased zircon content on the chemical performance of the developed compositions in SLS glass.

Crushed SLS glass cullet was filled into the recess of the static corrosion cup samples of the PSR-315, AZS-01, AZS-02 and AZS-03 as described by the isothermal static corrosion methodology in section 4. The samples were placed in an electric kiln and fired at 1370 °C for 72h at a heating and cooling rate of 3 °C/min. After the test, the samples were sectioned, and the flux-line cut measured. Figure 5-11 shows a sectioned half section of the AZS-01 refractory after static corrosion.

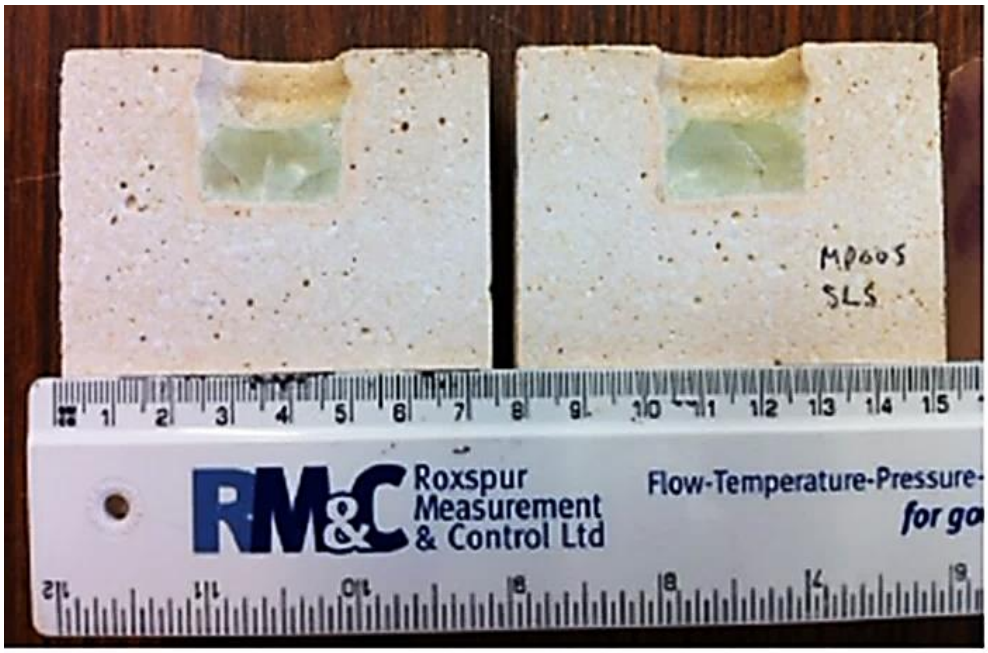

Figure 5-15: Sectioned corrosion cup sample of AZS-01showing glass-refractory compatibility and flux-line cut.

The flux-line corrosion of each refractory composition was measured and the corrosion rate at the flux line was plotted as a function of increased zircon composition as shown in Figure 5-12. From figure 5-12, it can be seen that an increase in zircon content of about 8 wt. % in AZS-01 from that of the standard PSR-315 composition showed a significant low melt-line cut rate under the same furnace atmospheric. This means that AZS-01 had better glass corrosion resistance than the standard PSR-315 refractory. Therefore, zircon additions and optimised particle packing had the effects of reducing the melt line cut of the refractory in AZS-01 refractory. This can be attributed to the increased densification of the refractory and reduced porosity from the zircon addition, which was also observed by Askel, [9, 12] in his study.

However, further increases in zircon content of 5wt% additions in the other compositions, AZS-02 and AZS-03, did not result in any significant reduction of the melt line cut rate as can be seen in the figure 5-12. The flux-line corrosion of AZS-02 and AZS-03 were comparable with the standard PSR-315 refractory despite an increase in the ZrO_2 content of the compositions which is thermodynamically stable in alkali and alkaline earth silica melts. Both refractories contained apparent porosities 18% and 19% respectively which are comparable to the PSR-315 porosities of 20%. Therefore, this shows that apparent porosity in refractory macrostructure is an important physical property that has adverse effects on the corrosion resistance of sintered refractories to glass melts.

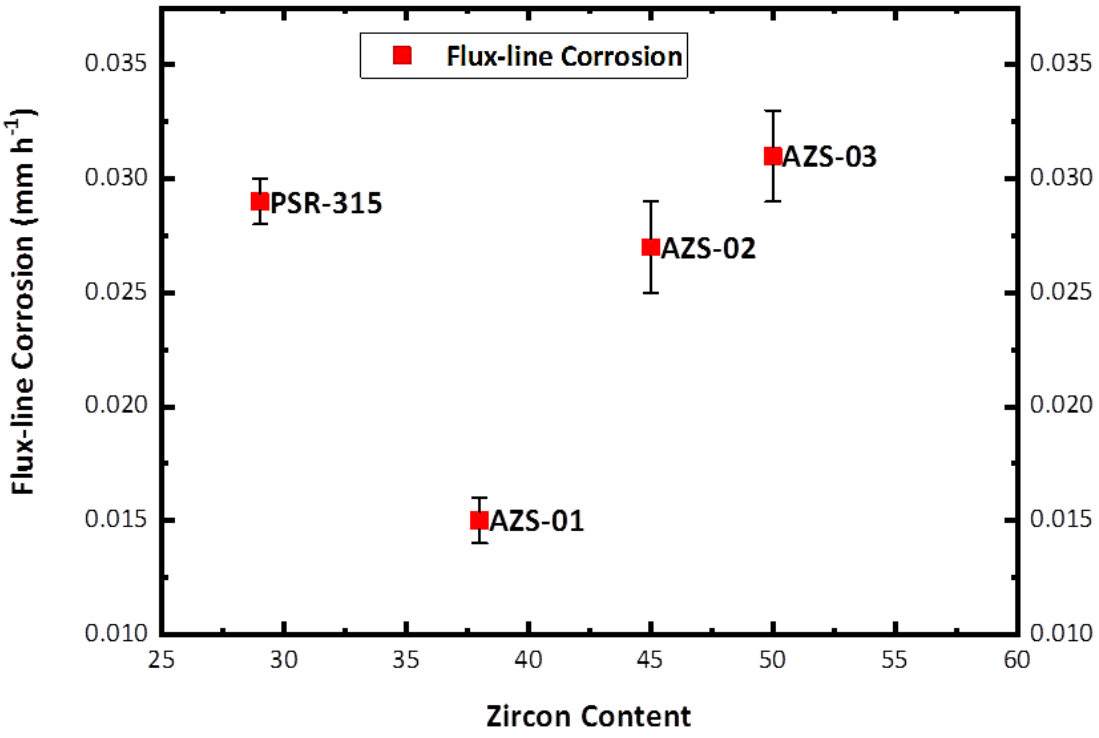

Figure 5-16: Flux-line rate of corrosion as a function of added zircon content in AZS refractory compositions

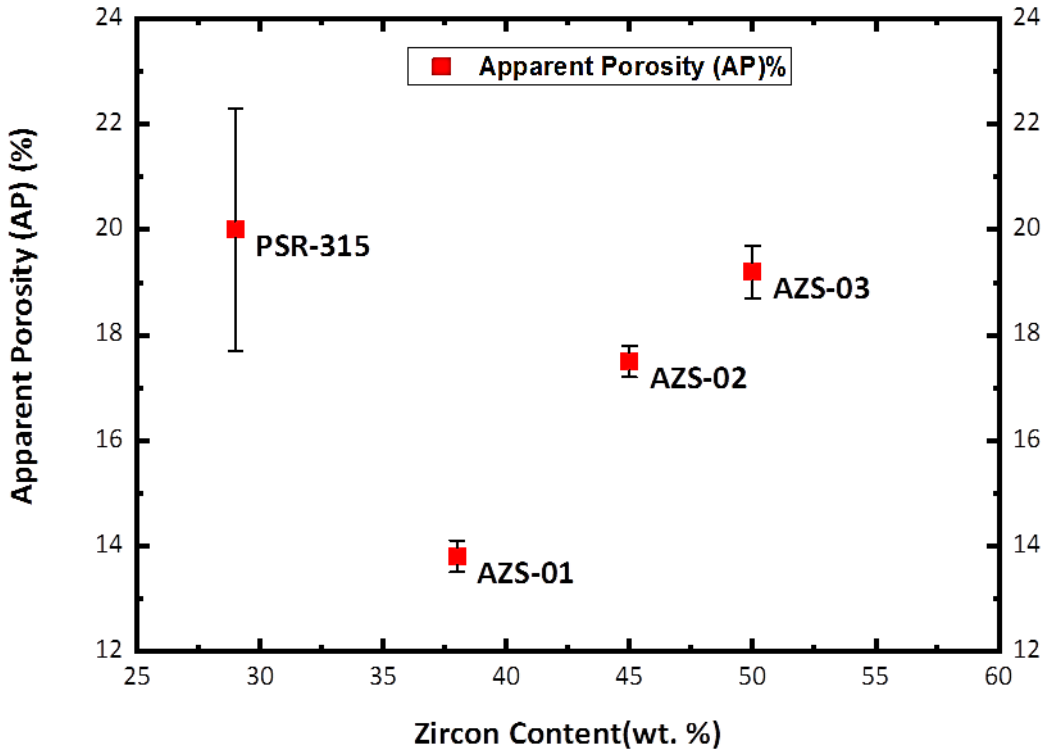

Figure 5-17 Refractory apparent porosity (AP) as a function of starting zircon content (wt. %) in AZS refractory compositions

As discussed in the literature review section, corrosion of refractories by liquid melts is through either ingress of glass melt into the refractory through the pores by capillary action and or congruent/incongruent dissolution of the refractory oxides into the glass melt. By reducing the apparent porosity in the AZS-01 refractory, the corrosion mechanism of the refractory was limited to the interaction of the glass with the refractory mineral phases at the hot face. Therefore this means that for the AZS-02 and AZS-03 refractories that contained high porosities, corrosion was facilitated through ingress of glass into the refractory.

5.4.3 Development & Manufacturability of AZS-01 Refractory

From the preliminary studies conducted in the previous section, refractory composition AZS-01 was identified as the having the a good workable slip that translated into a dense and low apparent porosity refractory body after consolidation when compared to the other developed compositions and the reference PSR-315 and PSR-333 refractories. Therefore, the next part of the research looked into further developing the AZS-01 refractory, evaluating its manufacturability, microstructure and thermo-mechanical properties.

5.4.3.1 Optimization of AZS-01 using DigiPac Modelling Software.

As previously stated, particle packing is defined by the PSD, shape and cohesion forces of the particulate raw material components. In the last section, optimised formulations of AZS-01 to AZS-03 refractories were designed using the empirical equation of the Dinger and Funk packing model utilizing the PSD of the raw material components. In using the Dinger and Funk model for particle packing, the

particle shape is not taken into account and assumes all spherical particles in the packing structures. Therefore, the next study looked at further optimizing the particle packing of the AZS-01 raw material formulation using the DigiPac software as described in **section 4.1.2.2.**

Although DigiPac is a geometrical packing algorithm with no explicit consideration of particle interactions (forces), it has been validated by to predict quite accurately the packing structure of particulates whose shapes are commonly encountered in industry [68]. The packing fractions of AZS-01 raw material components were grouped into three size groups based on their PSD, namely 0-60µm; 60 – 600µm and 600 - 2000µm. However, due resolution limitation after reconstruction of the scanned particles into voxels for simulation in DigiPac, only the size group > 60µm could be simulated. The X-ray tomography scanned particles are presented in appendix C. Therefore this meant that only the Zircon M170 particles (60 - 600µm size group) and α-Al_2O_3 (0-0.3mm – 1-2mm size particles) that fall into the 600 - 200µm size groups were used for simulation. There were limitations to this part of the study as only two packing simulations were managed and completed due to issues faced in acquiring a computer with better processing power. As such, the two simulation runs were not adequate to provide enough statistical data to validate any of the experimental work. Therefore, this work or study has been flagged for future work of this research.

5.4.3.2 Evaluation & Validation of the Manufacturability of AZS-01

To evaluate the commercial impact of the research and investigate the manufacturability of AZS-01, factory scale mixes were produced and a list of expendable products cast. 480kg mix and 500kg batch mixes were made and cast in a small Eirich mixer, used for commercial production of the PSR-Ltd refractory

products. For the 480kg mix, 450ml of dispersant chemical, (Darvan 7) and was used. A total mixing time of 12 minutes was taken and required for AZS-01 slip consistency to be reached.

Table 5-9 below presents the slip properties and rheology of the AZS-01 pilot scale up mix together with the average slip and rheological properties of similar standard PSR-315 mixes taken over the a production calendar year. From table 5-9, it can be seen that while AZS-01 mix has less water demand (6 %) and chemical (0.1 %) compared to PSR-315 mix of 8 % and 0.2 % respectively; it however exhibits similar flow properties (> 300mm) as the standard PSR-315 slip.

Table 5-9: Slip and Rheological properties of AZS-01 (420KG) mix and PSR-315 (450KG) mixes. (Amount of Deflocculant used is in percentage of total batch weight).

Sample & (Batch Weight)	Slip density kg/m^3	Viscosity (cP)				Water %	Darvan 7-N (%)	Flow (mm)
		2.5rpm	5.0rpm	10rpm	20rpm			
MP5 (420KG)	3331	310	220	215	208	6.28	0.11	315
315 (450KG)*	3083	271	225	220	228	8.2	0.15	326

*Average values of 2017 test data of

Table 5-9, from the slip rheology and water demand properties of AZS-01presented, further shows that the slip produced from the AZS-01, 420kg factory scale mix, had the same consistency, stability and homogeneity as previous lab based 5kg – 30kg mixes, presented in table 5-7. The AZS-01 slip presented no separation of grog material from fines characteristics from both the flowability test and during casting of expendable products demonstrating the stability of the AZS-01 slip.

The stability of the slip can be attributed to the optimised PSD of the mix formulation that is well dispersed from the deflocculation studies conducted in the previous sections which resulted in tailored rheology of the slip to exhibit high viscosities at very low shear rate (rpm) and low viscosities at high shear rates.

This phenomenon is known as shear thinning. High shear rates (high rpm such as 20rpm) on refractory slips are experienced during mixing in industrial mixers such as the Eirich mixer, while low shear rates (low rpm such as 2.5rpm) on the refractory slips are experienced when the slip has been cast in the mould to set.

Therefore the rheological properties of AZS-01 allow ease of mixing of the suspensions at high rpm (as is the case in the Eirich mixers) due to the low viscosity of the slip; and good stability with no separation of the slip in the moulds after casting due to the high viscosity of slip at low rpm. The high viscosity of the slip at low rpm or in the mould retards the settling of large grog material and maintains the packing structure of the designed PSD of the mix.

This highlights the excellent workability and manufacturability of AZS-01 mix due to the optimisation and process control even with changes in batches of the fine matrix material and grog tabular size fractions.

Figure 5-18: Feeder tubes cast from AZS-01 factory-scale mix.

Figure 5-18 shows feeder tubes and plungers that were part of the Expendable Feeder products that were cast from AZS-01 composition. To evaluate whether optimising the particle size distribution of the AZS-01 mix and the deflocculation studies were effective to ensure a homogeneous dispersal of the raw material components from mixing to slip homogeneity and casting, sintered AZS-01 plungers were marked and cut into five sections as highlighted in figure 5-19 below. Bulk density (B.D) and apparent porosity (A.P) measurements were taken across each of these sections.

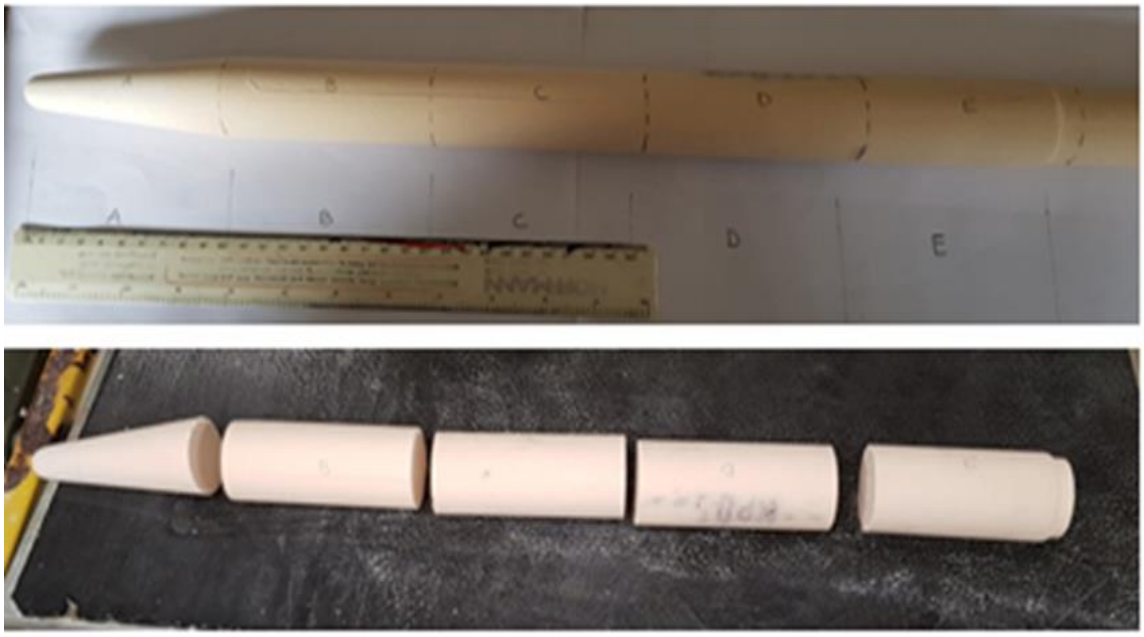

Figure 5-19: Figure 2: AZS-01 (144-15106) plunger marked and sectioned for Bulk density and porosity measurements

A comparison was made with results from the lab samples. Studies by [35, 36], showed that inadequate mixing and homogeneity of the mix and slip may result in micro-regions of varying compositions and packing due to agglomeration which may result in varying porosities and densification across the fired cast [35,36].

Table 5-10: Table 2: Bulk density and Apparent Porosities of PSR-315 and AZS-01 fired off-cut plungers and lab samples. (Error given in %)

	PSR-315 plunger Fired off-cut		**Region/Section**	**AZS-01 plunger Fired off-cut**	
	A.P %	**BD kg m-^{3}**		**A.P %**	**BD kg m-^{3}**
	17.70	3.00	A	13.86	3.34
	17.60	3.17	B	13.47	3.35
	17.70	3.00	C	13.89	3.34
	18.00	3.20	D	13.35	3.35
	18.80	3.20	E	13.80	3.33
Mean	17.96 ± 0.84	3.11 ± 0.08		13.67 ± 0.2	3.34 ± 2.4

From the physical property results presented in table 5-10, it can be seen that there are no significant variation in the bulk densities and porosities across the sections of the plungers for both PSR-315 and AZS-01 products. As well, the AZS-01 fired off-cut plunger has similar physical properties to the lab samples shown in table 5.10. The next study then work looked at the developed microstructure of AZS-01 and evaluate the effect on thermo-mechanical properties.

5.4.3.3 Microstructural Evolution of AZS-01 Refractory

Figure 3 shows the XRD patterns of PSR-315 and AZS-01 refractories respectively. The XRD patterns for both the PSR-315 and AZS-01 refractories exhibits similar mineralogy whereby the main primary phases of each refractory are corundum, monoclinic zirconia (baddeleyite), mullite and zircon, which is typical of AZS products sintered below 1600 °C.

Above 1600 °C, zircon is known to dissociate into zirconia and an amorphous silica phase. There is, however, a discernible difference in the intensities of the mullite peaks between the two AZS materials. It can be seen that AZS-01 presents mullite peaks at higher intensity when compared to that of reference PSR-315 refractory especially when comparing their relative intensities in the [110] and [121] mullite reflections.

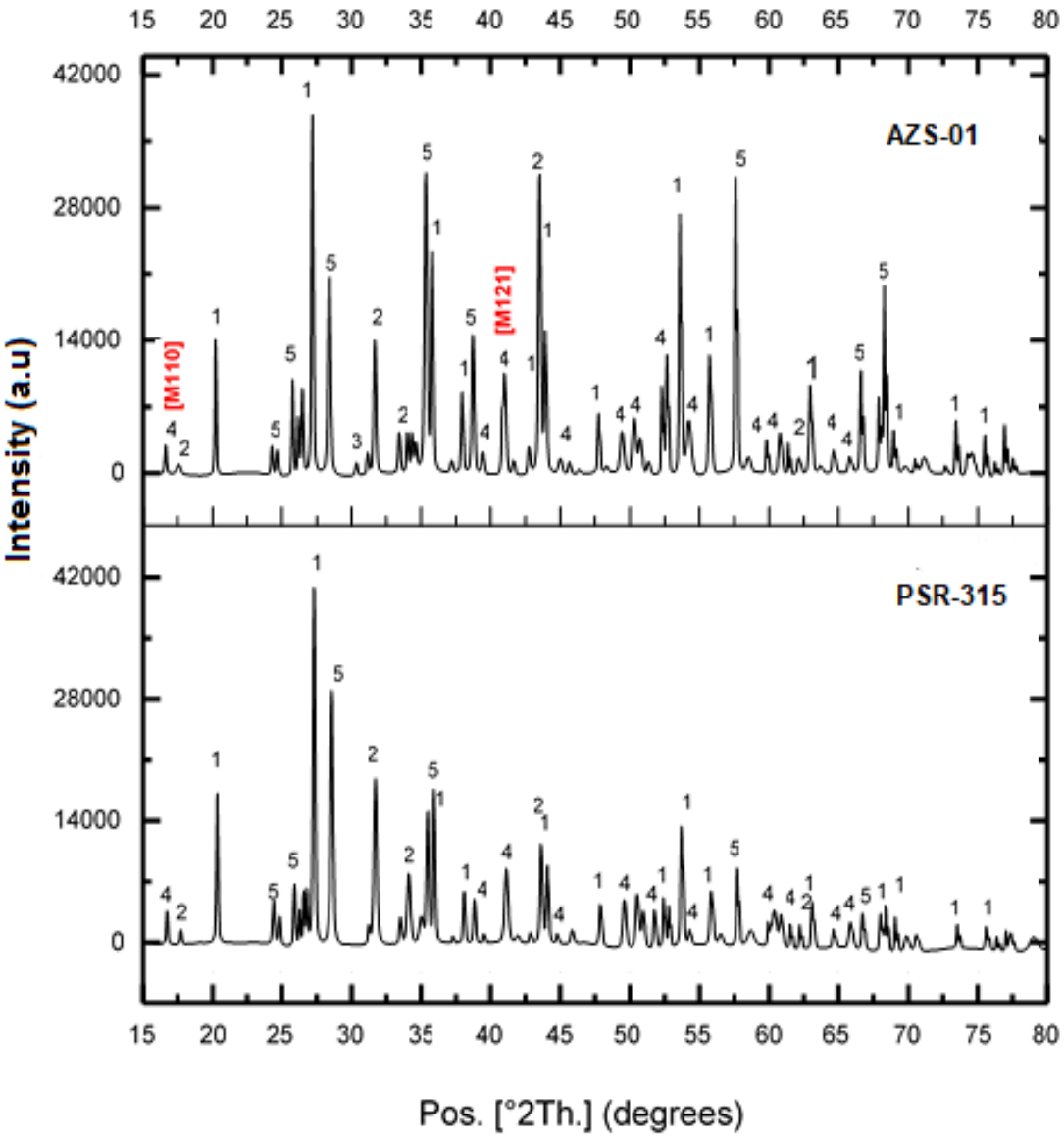

Figure 5-20: XRD pattern of PSR-315 refractory body sintered at 1500°C.

1 = $ZrSiO_4$ [ref code: 04-008-8667]; 2 = ZrO_2-m [ref code: 04-008-]; 3 = ZrO_2-t [ref code: 04-008-]; 4 = $Al_6Si_2O_{13}$; [ref code: 04-010-3002]; 5 = a-Al_2O_3; [ref code: 04-005-4502]

This is also shown and confirmed in the quantified mineralogical composition of the two refractories, shown in table 5-7. The quantified XRD mineral phases of the AZS refractories shown in table 5-7, reveal that standard reference refractory, PSR-315 consist of about 50 wt.% Al_2O_3 and a high proportion of amorphous phase (19 wt. %) in contrast to the AZS-01 refractory with 9 wt. % amorphous phase.

Table 5-11: Mineralogical composition of the sintered PSR-315 and AZS-01 refractories sintered at 1500°C.

Sample	**Mineral Composition (wt. %)**					**Microstructural Evaluation** Ratio of ZrO_2: $Al_6Si_2O_{13}$
	α-Al_2O_3	ZrO_2	$Al_6Si_2O_{13}$ *(3:1 and 2:1)*	$ZrSiO_4$	*Amorphous*	
PSR-315	*50.5*	*7.2*	*13.1*	*10.1*	*19.0*	*1:1.8*
AZS-01	*44.8*	*11.6*	*20.5*	*12.3*	*10.8*	*1:1.8*

Table 5-11 further shows that from a comparison of the ratios or proportions of the zirconia (ZrO_2) phase (evolved from the dissociation of zircon) to $Al_6Si_2O_{13}$, (evolved mullite phase from the reaction sintering of SiO_2 and Al_2O_3); it can be seen that both PSR-315 and AZS-01 refractories have similar relative ZrO_2**:**$Al_6Si_2O_{13}$ ratios or proportions of the mineral phases within their microstructures. However, from the two consolidated refractories PSR-315 and AZS-01; both derived from a starting alumina-zircon mixtures; there is more reaction sintered mullite fraction (20.5 wt. %) evolved in the AZS-01 refractory mineral composition than the standard refractory PSR-315 (13.1 wt. %).

Thus, this would suggest that AZS-01 has undergone increased microstructural evolution than AZS-01 from to the greater reaction sintered mullite. Therefore the increased mullite formation is possibly because of the greater particle-particle contacts as a result of optimized particle packing and hence leading to more grain boundaries and shorter diffusion paths for rapid matter transport. This infers that there is improved reaction kinetics from the primary zircon dissociation to yield amorphous SiO_2 as a dissociation product which softens and dissolves Al_2O_3 to form an aluminosilicate glass.

Mullite then is evolved after a critical Al_2O_3 concentration in the glassy phase reaches saturation. This can be shown by the reaction;

$$ZrSiO_4\,(s) / (1500°C) \longrightarrow ZrO_2\,(m/t) + SiO_2\,(l) \quad (27)$$

$$SiO_2\,(l) + \alpha\text{-}Al_2O_3 / (1500°C) \longrightarrow SiO_2 + x\cdot Al_2O_3 + (1\text{-}x)\cdot\alpha\text{-}Al_2O_3 \quad (28)$$

To give a net reaction;

$$ZrSiO_4\,(s) + \alpha\text{-}Al_2O_3/(1500°C) \longrightarrow 3Al_2O_3\cdot 2SiO_2 + ZrO_2(m/t) + (1\text{-}x)\cdot\alpha\text{-}Al_2O_3 \quad (29)$$

From the semi-quantitative EDS, the mullite evolved in both PSR-315 and AZS-01 had Al_2O_3:SiO_2 wt. % ratio in the range 71:19 to 74:16 which is in agreement with other studies and expected for ceramics solid state sintering at or below 1500°C [8, 25].

Figure 5-21 shows the SEM microstructures of the PSR-315 and AZS-01 refractories after sintering and reveals the phases present, with both confirming the phase constituents as seen from the XRD pattern in figure 5-10. The microstructure of the reference PSR-315 refractory reveals ‘wall effects’ due to uneven packing resulting in the generation of crack-like pores and regions of differential densification giving the refractory an un-textured microstructure.

The resulting AZS-01 microstructure in contrast, as shown in figure 5-11; reveals a denser and textured microstructure with relatively low pore size distribution.

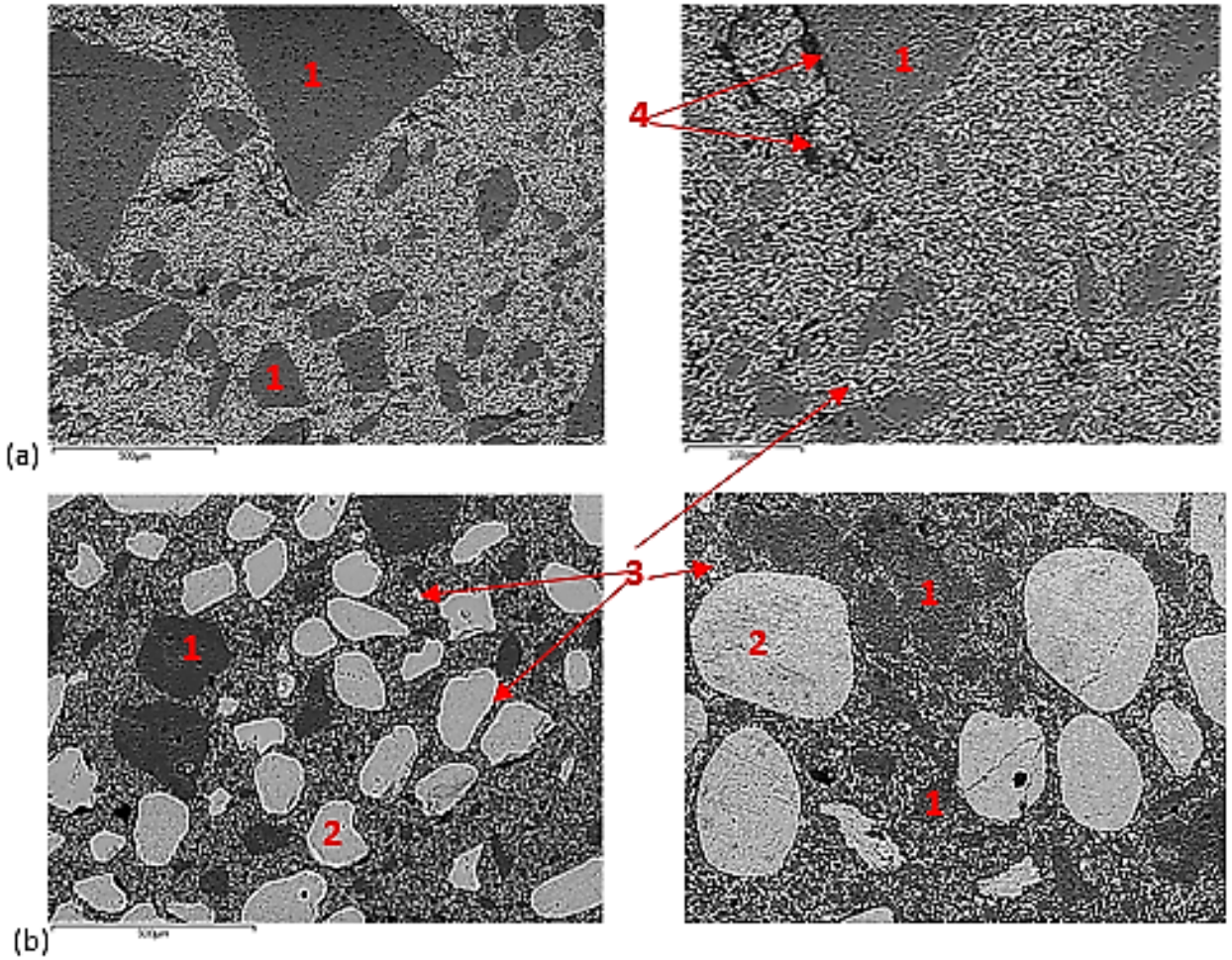

Figure 5-21: Low to high magnification BEI SEM micrograph microstructures of (a) PSR-315 and; (b) AZS-02 refractories after sintering. (1). Corundum; (2). Zircon; (3). Baddeleyite; (4). Pores.

The mullite evolved in both PSR-315 and AZS-01 microstructures has an equiaxed morphology and semi-quantitative EDS revealed that the Al_2O_3:SiO_2 wt.% ratio to be 71:19 to 74:16 which is in agreement with other studies and expected for ceramics solid state sintering at or below 1500°C [8,25]. No characteristic acicular mullite structures (type II and III mullite), a feature of mullite evolved from a liquid phase; was resolved even at high magnification considering the presence of a high amorphous phase within the microstructures of both the AZS refractory materials.

5.4.3.4 Effect of Sintering Temperature

The effects of sintering at higher sintering temperatures were investigated on the AZS-01 refractories. At PSR-Ltd, 1500C represents the maximum temperature used to fire PSR-Ltd products and therefore, sintering above this temperature would be non-sustainable. However, the study was conducted to evaluate if raising the sintering temperature on the AZS-01 refractory would result in complete dissociation of the zircon grains and evolution of a reaction sintered mullite microstructure that would enhance the physical properties of AZS-01.

Figure 5-16 shows the XRD pattern of AZS-01 refractory after sintering at 1570°C for 1 hr.

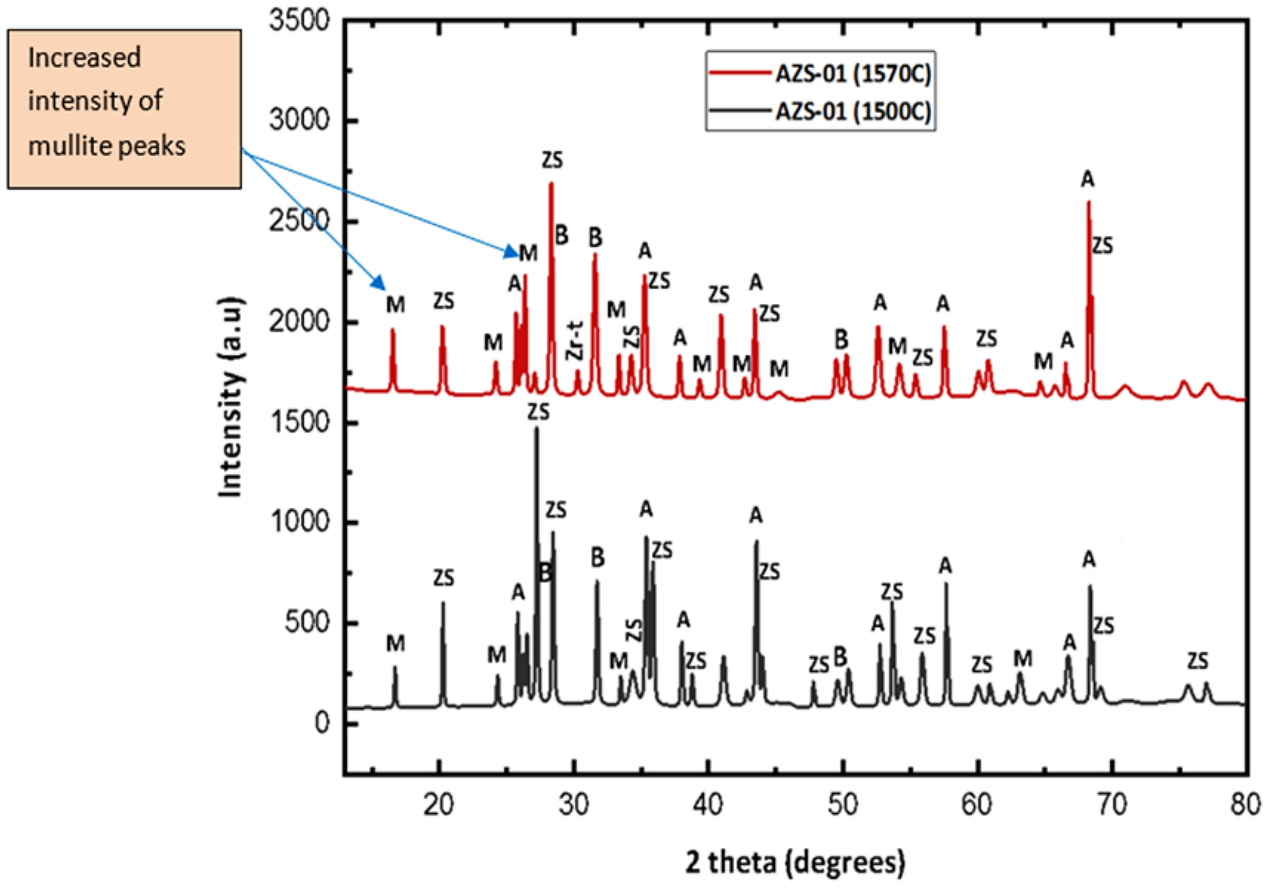

Figure 5-22: XRD pattern of AZS-01 refractory sintered at 1500C and 1570C for 1hr.

(M =Mullite, ZS = Zircon, A= α-Al_2O_3, B (Baddeleyite) =monoclinic ZrO_2, Zr-t = Tetragonal ZrO_2)

From the XRD pattern presented in figure 5-22, it can be seen that while there as an increased mullite evolution as evidenced by the increased intensity in the mullite peaks, reaction sintering reaction does not go to completion as there is no complete dissociation of the zircon grains.

Figure 5-17 shows a SEM micrograph of the AZS-01 microstructure after sintering at 1570 °C. In the figure, it can be seen that raising the sintering temperature from 1500 °C to 1570 °C cracks appear within the matrix microstructure.

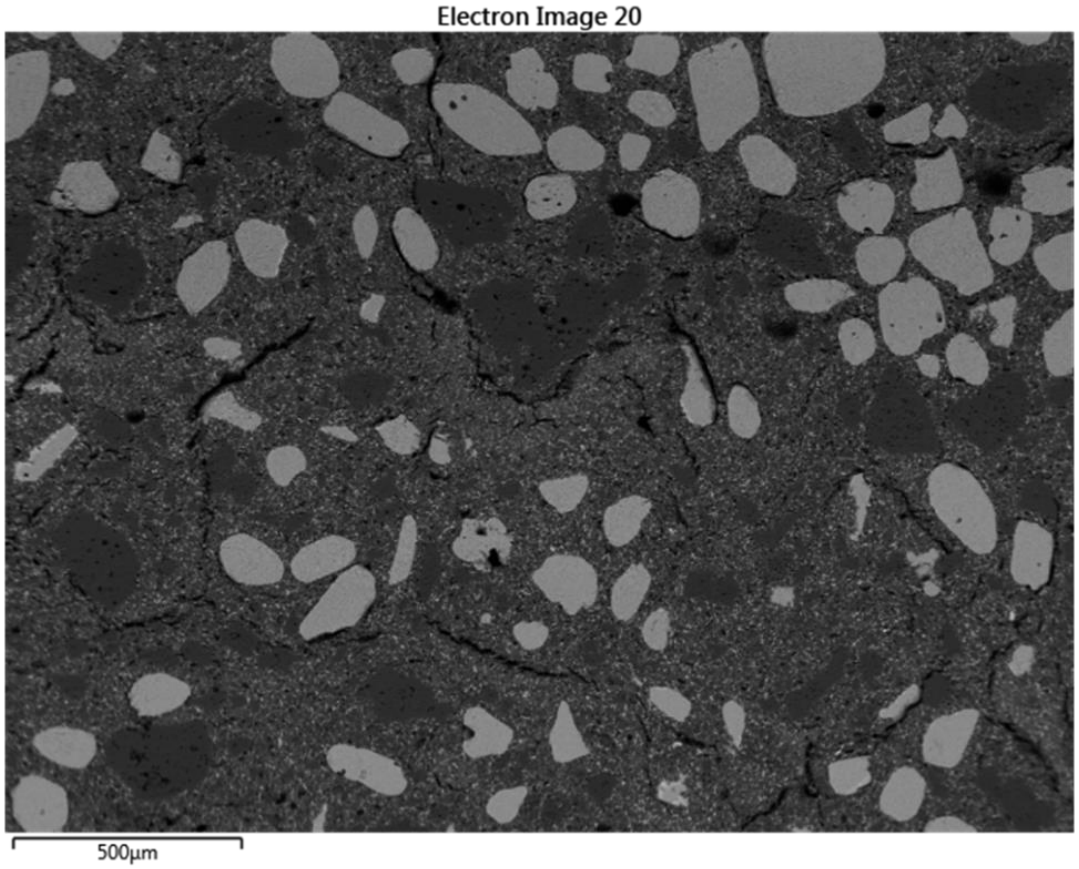

Figure 5-23: SEM micrograph showing the microstructure of AZS-01 fired at 1570 °C.

This evolution of cracks within the microstructure suggest to a mismatch in the coefficient of thermal expansion of the existing major phases in AZS-01 at 1570 °C. Zircon remains as the major phase as well as alumina and some evolved mullite. The appearance of cracks can affect the physical and thermomechanical properties of the refractory body.

This was highlighted in the physical properties of the AZS-01 refractory samples sintered at 1570 C. The bulk density and apparent porosity of the AZS-01 refractory samples sintered at 1570 are presented in table 5-12. From table 5-12, sintering of AZS-01 above 1500 °C does not improve densification of the refractory, as seen from the bulk density of samples sintered at 1570 °C, of 3.29 kg m^{-3} compared to samples sintered at 1500 °C, of 3.38 kg m^{-3}.

Table 5-12: Bulk density and apparent porosity values of AZS-01 sintered at 1570 °C and the benchmark, Emhart licenced PSR-Ltd standard refractories, PSR-315 and PSR-333 also sintered at 1570 °C.

Physical Property	Bulk Density (B.D) / kgm^{-3}	Apparent Porosity (A.P)/ %
AZS-01	3.29 ± 0.3	13.0 ± 0.2
PSR-315	3.13 ± 0.03	16.4 ± 0.4
PSR-333	2.89 ± 0.01	17.5 ± 0.8

Rather, there is a slight reduction in the bulk density of circa 3 %, possibly from partial dissociation of zircon (ρ = 4.8 kg m^{-3}) by increased thermal input to form and zirconia some reaction sintered mullite (ρ = 2.8 kg m^{-3}) from the viscous amorphous SiO_2 on reaction with alumina. The apparent porosity of AZS-01, was increased, as a result of the cracking and shrinkage of the zircon grains as they partially dissociate.

5.4.4 Thermo-mechanical Properties of AZS-01

Only qualitative results can be, and were, obtained from the heating and quenching cycling (Thermal shock) tests that were conducted on the PSR-315, PSR-333 and AZS-01 refractories. Table 5.7 shows the results of thermal shock tests performed on slip cast samples as well as sectioned test samples from sintered blocks of AZS-01 and the commercial reference refractories PSR-315 and PSR-333, as described the methodology in **section 4.2.2.6**. Sectioned samples from a bulk sintered block may introduce stress concentrations and defects such as micro-cracks from the saw blade, hence why slip cast samples were used in determining the thermal shock properties of the refractories.

Table 5-13: Results and report of thermal shock tests conducted on AZS-01 and reference refractories. The coefficient of thermal expansion of the refractory samples are also provided from Revisable linear expansion tests.

Refractory	CTE α (10^{-6} m/m °C) (0 – 1400 C)	Thermal shock behaviour of test Sample produced as		Visual observations
		Slip cast	Section from refractory block	
PSR-315	7.38	> 10 cycles	> 10 cycles	No spalling or discernible cracks on surface
PSR-333	6.7	> 10 cycles	> 10 cycles	No spalling or discernible cracks on surface after 10 cycles
AZS-01	7.32	> 10 cycles	> 10 cycles	No spalling or discernible cracks on surface

* CTE = Coefficient of thermal expansion from Reversible linear expansion tests conducted at Lucideon

In the thermal shock tests conducted, AZS-01 exhibited excellent thermal shock behaviour comparable to the standard refractories, with no visual cracks or spalling occurring or being observed on the refractory surfaces after 10 thermal cycles. While the cycling heating-quenching thermal shock test method provides adequate information on the performance of the refractories in service, it does not provide enough comparative data about the thermal shock properties of AZS-01 and the standard refractories. Therefore, to provide more information on the thermal stability and properties of AZS-01, the reversible linear thermal expansion properties of PSR-315 and AZS-01 were analysed.

Figure 5-13 shows the reversible linear thermal expansion test of PSR-315 and AZS-01 refractories during a heating and cooling cycle.

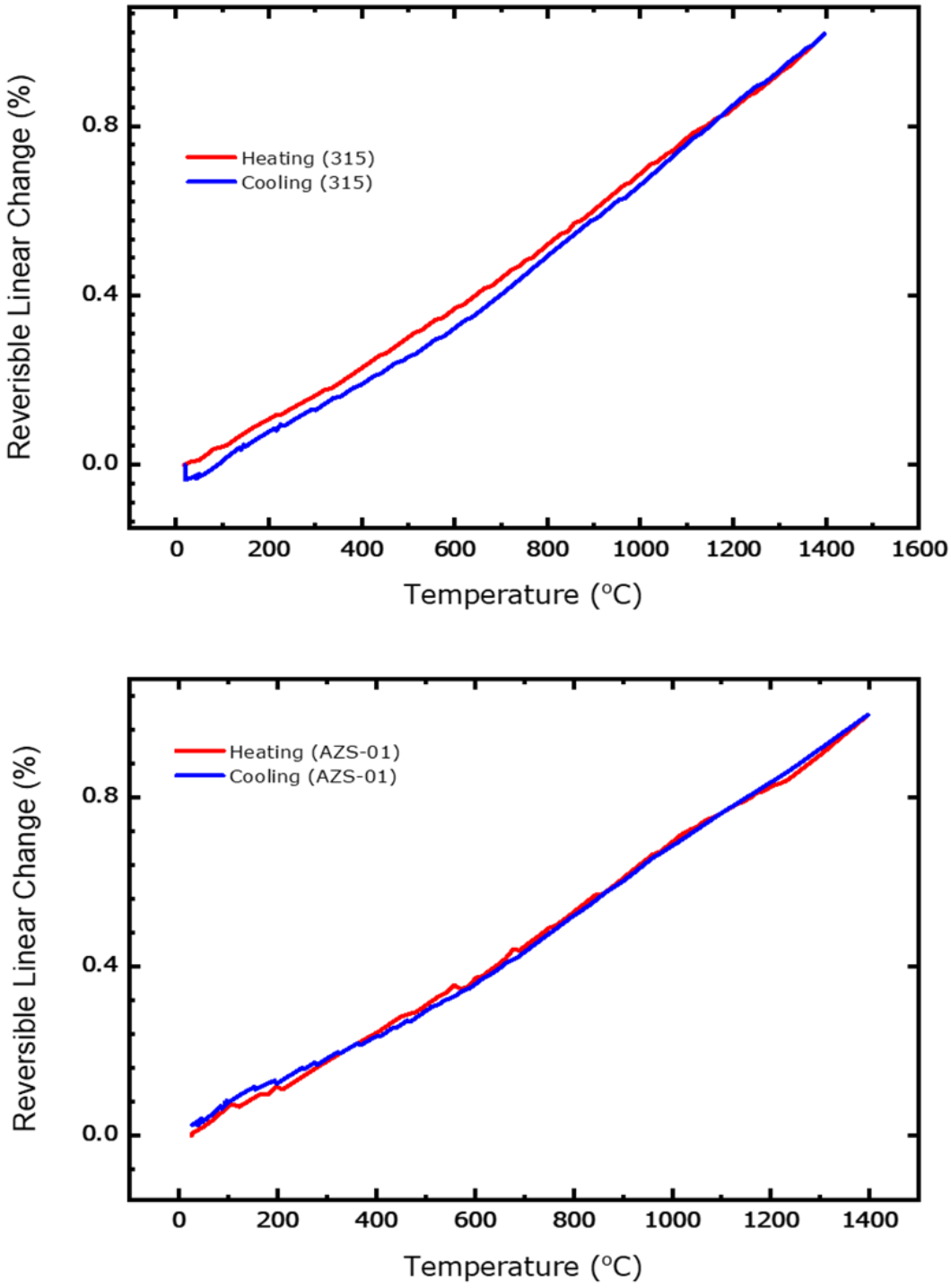

Figure 5-24: Linear Thermal expansion curve of PSR-315 and AZS-01. The figure highlights the thermal hysteresis of the heating and cooling curves of the two refractories.

The test highlights the expansion and shrinkage behaviour of the refractories and its evaluation can be used to provide the thermal stability of the refractory body and significant material property such as thermal shock.

During heating and cooling cycles of ZrO_2 based materials, the ZrO_2-m to ZrO_2-t on heating and vice-versa during cooling produces a hysteresis area as a result of volume changes associated with the phase transformation [P Kumar et al, 2016]. Figure 5-13 shows the thermal hysteresis of PSR-315 and AZS-01 from their heating and cooling curves and may be thought to represent a single thermal shock cycle.

In figure 5-13, it can be seen that PSR-315 exhibits a discernible and larger thermal hysteresis area (~3 cm^2) than AZS-01(1 cm^2). This means that on cooling after heating, PSR-315 does not follow a similar contraction path as during expansion. This thermal expansion hysteresis is normally due to formation of micro-cracks, evolution of phase changes during the heating cycle and or softening of the glassy phase present. This means that PSR-315 on repeated thermal cycling, will exhibit a volume change that may affect its structural integrity and result in spalling. However, since duration of the thermal shock tests, PSR-315 did not spall or show surface cracks after 10 cycles, this may mean that the viscous glassy phase helps in providing thermal healing of the micro cracks and thermal stress relaxation.

In contrast, the AZS-01 contraction path follows the same path during expansion and result in a thermal hysteresis area close to 0. This means that during thermal cycling, there is negligible volume change of the refractory and this helps it to maintain its structure and resist spalling. Although this analysis does not quantify the thermal shock properties of the two refractories, it provides an insight into how we can

justify that AZS-01 possesses excellent thermal shock properties than that of PSR-315.

5.5 Summary of Discussions.

It has been shown that an increase in zircon additions to the AZS-01, AZS-02 and AZS-03 compositions, sintered at 1500C did not translate into increased densification and improved physical properties. AZS-01 exhibited physical and glass corrosion properties that were better than the standard commercial refractory PSR-315. This was presented in the isothermal glass corrosion test studies where only AZS-01 presented the lowest flux-line corrosion in soda lime silica glass, at standard test temperatures of 1370°C for 72hr. AZS-02 and AZS-03 had comparable flux line corrosion as PSR-315.

Due to the low improvements in their physical and glass corrosion resistance properties, development of AZS-02 and AZS-03 compositions was not taken any further. AZS-01 refractory was further developed by optimising its formulation particle packing further using the DigiPac software, although only one simulation run of the modelling was conducted due to the limitations of time and processing speed. Sintering AZS-01 above 1570 °C did not improve the physical properties and cracks were observed within the matrix microstructure.

The Factory scale mixes of AZS-01 that were conducted showed the manufacturability of AZS-01 slips and the potential commercial impact of this research. From static and dynamic corrosion tests that were conducted, and are discussed in detail in the next chapters, the denser and less porous AZS-01 refractory had excellent glass compatibility with very low glass defect potential in soda lime

glass and shows promising thermo-mechanical properties (discussed in detail in the next chapter) and summarised below.

Physical & Mechanical Properties

Bulk Density **3380 kg/m^3**

Cold Compressive Strength **190 MPa**

Apparent Porosity **13 %**

Refractoriness **1775°C**. (Cone **34-35**)

Refractoriness Under Load (**RUL**).

Reversible Thermal Expansion. 20-1000°C **0.68 %**

CTE = 6.00 x 10^{-6} °C^{-1} (20°C – 200°C)

CTE = 7.25 x 10^{-6} °C^{-1} (200°C – 1200°C)

CTE = 9.00 x 10^{-6} C^{-1} (1200°C – 1400°C)

6 Development and Evolution of a Novel $(Zr_{1-x}Sn_x)O_2$ Toughened Mullite Alumina Slip Cast Refractory: Effect of SnO_2.

6.1 Introduction

Zirconia reinforced mullite refractories from the Al_2O_3-ZrO_2-SiO_2 (AZS) and Al_2O_3-ZrO_2-$Al_6Si_2O_{13}$ (AZM) systems have a wide range of application in the glass industries, both as structural (crown) and glass contact applications (channels blocks, forehearth and glass feeder application) [1-4]. This is due to their excellent thermo-mechanical properties such as; the high-temperature, low thermal expansion and low creep rate (inherent from the mullite phase); and the excellent fracture toughness as well as chemical stability in alkaline siliceous melts (coming from the zirconia phases) [2-5]. It is well known that ZrO_2 is not easily wetted by siliceous melts and the addition of ZrO_2 to the mullite based refractory composites enhances their chemical stability in similar melts or slags [25-28]. Reaction sintering of Al_2O_3 and zirconium silicate ($ZrSiO_4$) bearing compounds is a cheaper and extensively explored method of producing zirconia reinforced mullite composites [10,11,36-41]. Zircon ($ZrSiO_4$), is available in abundance and a cheap source of zirconia.

However, in our previous studies, highlighted in the section 5.43, it was seen that consolidated AZS refractory compositions, AZS-02 and AZS-03 with starting zircon contents of > 38wt%; (without the use of any mineralisers); exhibited a deterioration in their physical and chemical corrosion resistance material properties. This was highlighted by the increase in the apparent porosities and subsequent decrease in the bulk densities of the refractories, see table 5-4. This deterioration in the physical properties also affected the chemical compatibility of the AZS-02 and AZS-03

refractories in glass melts as was seen in the increase in the flux line corrosion of the refractories against SLS glass as compared to the AZS-01 refractory.

The microstructural evolution of the crystallised fraction, composition and morphology of mullite from the conventional reaction sintering of micro to macro-sized zircon and alumina mix formulations is reported to be dependent on the firing conditions [5,32-41]. The microstructure of Mullite, either fused cast or formed in the presence of a liquid phase always exhibits an acicular morphology [5,32-44]. That formed by solid state sintering and in the absence of a liquid phase is normally granular and varies depending on the nature and purity of the starting raw materials [5,32-,44]. In the absence of impurities, sintering above 1400 °C, only some detectable amounts of mullite are formed, with complete mullite conversion requiring sintering at temperatures in the proximity of 1700 °C [32-44]].

As highlighted in the literature review, the use of SnO_2 in reaction sintering of mullite has not been extensively reported.

In the present study, the effect of SnO_2 as a sintering aid on the reaction sintering of slip cast zircon and alumina mixtures to produce zirconia toughened mullite composites was studied. SnO_2 has the same rutile structure as TiO_2, and as such we expected it to have comparable properties and effect on the reaction sintering of zircon and alumina raw materials akin to rutile (TiO_2). In addition, it is also known that SnO_2 has a lower solubility potential in soda-lime and borosilicate glasses with the order of solubility reported as; $SiO_2 < Al_2O_3 < ZrO_2 < SnO_2 < Cr_2O_3$ [23]. Therefore, any incorporation of SnO_2 into the AZS/AZM microstructure and matrix would be expected to enhance the chemical compatibility of the refractory composites in glass melts.

6.2 Methods

In the previous studies, it was shown that consolidation of AZS refractory compositions, AZS-02, AZS-03 with an initial starting zircon content of > 35wt%; (without the use of any mineralisers); exhibited a loss of densification of the refractories. Therefore, for this study, with the use of SnO_2 as a sintering aid and mineraliser, refractory compositions with higher ZrO2 contents were formulated, representing an initial starting zircon content of more than 35wt%.

Table 6-1 shows the material formulations of the tin-oxide doped compositions that were designed and used in this study.

Table 6-1: Developed and optimised mix formulation of AZS-T1 and AZS-T2 used in this study.

Raw material component	% fraction	
	AZS-T1	AZS-T2
Zircozon 10	11.0	10.9
Zircon sand M170	27.0	23.5
SnO_2 Superlite Tin Oxide	5.0	5.0
PBR	12.5	8.9
CT9FG	5.0	8.4
Tabular Alumina -0.3mm	8.3	5.0
Tabular Alumina -0.5mm	7.3	5.9
Tabular Alumina -0.5 -1mm	5.3	3.9
Tabular Alumina 1-2mm	21.6	23.5
China Clay	1.5	1.6
Ball Clay	1.5	1.6

To evaluate the effects of SnO_2 as a sintering aid, the 5kg batches of AZS-01 and AZS-03 were each doped with 5 wt. % SnO_2 to form two compositions, designated AZS-T1 and AZS-T2 respectively, by removing 5 wt.% of the alumina fractions while keeping the zircon contents of the AZS-01 and AZS-03 composition constant. Therefore, the AZS-T1 and AZS-T2 compositions, as tin-oxide doped derivatives of AZS-01 and AZS-03, were produced from an alumina-zircon-cassiterite starting mix formulation ratio by wt. % of 57**:**38**:**5 and 45**:**50**:**5 respectively. The batch sheets of AZS-T1 and AZS-T2 are shown in appendix E (pages i and ii).

China and Kaolin clays were used as binders and sources of mullite seed nuclei. Pure Reagent grade (>99.9%) SnO2 (Keeling Walker Ltd, Stoke-on-Trent) was used as the sintering aid.

The corresponding composite mix formulations of the SnO_2 doped, AZS refractory compositions, AZS-T1 and AZS-T2, were then optimised using the Dinger and Funk model for particle packing to attain optimally packed self-flowing mix fractions as described in section 5.2.

The normal slip preparation and casting procedures described in section 4 and section 5.4 were used to prepare the refractory slips for casting. Going with the preliminary study results highlighted and discussed in section 5.2 that had shown that a mix formulation with a *q* value of 0.23 provided an optimised refractory slip system that had self-flow characteristics with low water demand and optimal packing properties, the slips of AZS-T1 and AZS-T2 compositions were prepared and their flow and rheological properties tested before consolidation by slip casting methods. For slip preparation, the optimised mix formulations of AZS-T1 and AZS-T2

compositions were respectively dry mixed in a Hobart mixer for 3 minutes. Darvan 7, a sodium polymethacrylate dispersant, and water was added and the mixture wet mixed for 5 minutes until a homogenous slip was formed.

The prepared slips of AZS-T1 and AZS-T2 refractory compositions were slip cast into 50mm depth × 50mm diameter gypsum moulds to consolidate for bulk density and porosity test samples, and into a 300mm×200mm prism gypsum block moulds for the use of core drilled RUL and CCS test samples. They were left overnight to develop green strength, a batch from each composition was sintered for 1h at 1500 °C and another at 1550 °C, at a heating and cooling rate of 3° C/min.

6.2.1 Analysis of Self-flowing properties

The flow decay and the flowability index (FI) of the prepared AZS-T1 and AZS-T2 refractory slips, were measured by the flow cone test described by the ASTM –C230 standard methods [25].

6.2.2 Physical Property & Mechanical tests

For physical properties, the bulk density (BD) and % apparent porosity (AP) of the sintered refractory samples were determined using the Archimedes water-immersion technique [84]. Cold Crushing strength (CCS) tests were conducted according to the ASTM C133 standard [85] to evaluate refractory performance and the adequacy of sintering and abrasion resistance in consonance with the physical properties (bulk density and porosity). The CCS values of the sintered refractory AZS-T1 and AZS-T2 compositions were compared with the cold strength values of AZS-01 composition to evaluate the effect of SnO_2 on the mechanical properties of the AZS refractory.

To evaluate the effect of SnO_2 on the thermomechanical properties, The Refractoriness under load (RUL - Differential method with rising temperature) of the sintered refractory compositions AZS-T1, AZS-T1 were determined according to the BS EN ISO 1893:2008 standard [87] and compared with the RUL of AZS-01.

Additional 25×25×150mm3 bars were sectioned from the 300mm×200mm cast blocks of AZS-T1 and AZS-T2 refractories for the measurement of 3-point bending strength, hot modulus of rupture (HMOR) and dynamic elastic modulus at test temperatures of 1300°C and 1400°C.

6.2.3 Characterisation

Chemical and mineralogical analysis of the sintered AZS-T1 and AZS-T2 refractory products, was conducted by XRF and the XRD Bruker D8 X-ray diffractometer (Oxford UNITS). A Carl Zeiss EVO MA15 variable pressure W. SEM (Oxford Instruments) together with the Aztec Energy EDX system (Cambridge Systems) with X-Max SDD detector backscattered imaging was used for elemental mapping and point ID.

A Hitachi SU8230: high performance cold field emission (CFE) SEM with Oxford Instruments, Ultra high resolution, low kV, simultaneous SE, BSE, BF and DF imaging, with nanoscale resolution was used to evaluate the microstructural evolution of the mullite grains in the matrix region.

6.3 Results and Discussions

6.3.1 Analysis of Self-flowing properties

Table 6-1 shows the measured self-flow and calculated flowability index of the AZS-T1 and AZS-T2 refractories. The self-flow and FI of the AZS-01 composition, which did not contain SnO_2 is also shown for comparison.

Table 6-2: Averaged self-flow measurements and calculated flowability index FI of the slips of AZS-T1, AZS-T2 and standard refractories PSR-315 and PSR-333.

	AZS-T1	AZS-T2	PSR-315	PSR-333
Self-flow after 10min (mm)	335 ± 25	330 ± 30	330 ± 15	330 ± 30
Flowability Index, FI (%)	145	135	140	140

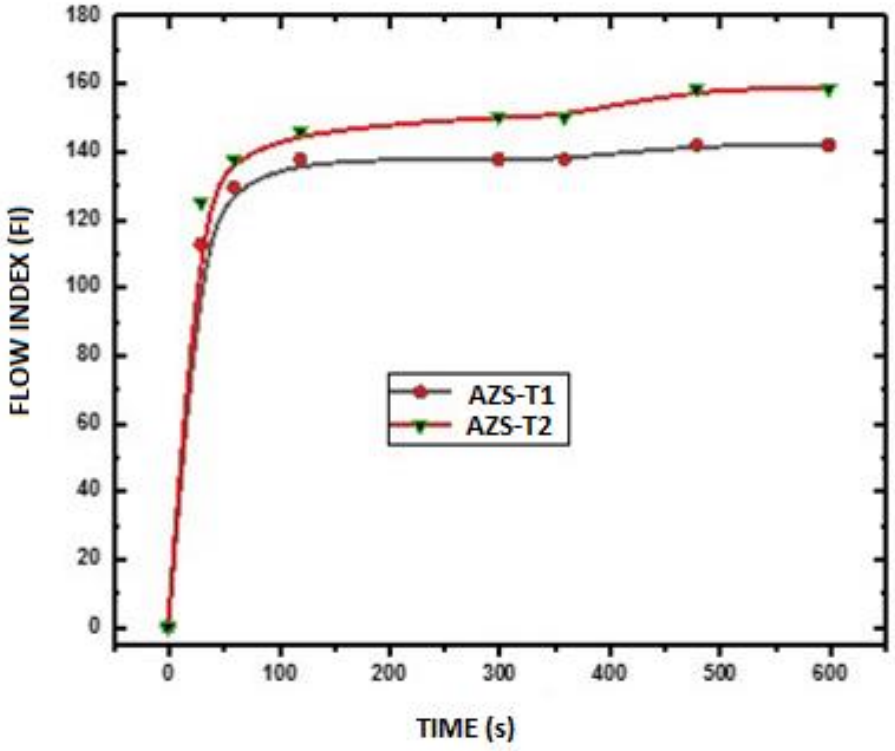

Figure 6-1: Flow decay characteristic curves of AZS-T1 and AZS-T2 refractory slips.

Figure 6-1 shows the flow decay/flowability characteristic curves of composition AZS-T1 and AZS-T2 slip systems measured over a period of 10 minutes. For shaped or brick casts, this represents an adequate period for the installation or casting and sufficient filling into the mould of the slip. From table 6-1, the flow characteristics of both slip systems, with a solid loading of 94.5% and reduced water demand (< 5.5%), exhibited excellent free flow properties, having a FI ≥ 80%; which are comparable to the standard PSR-315 and PSR-333 refractory slips with water demand of (>8%) including low cement self-flow castables (LCC) and no cement self-flow castables NCC [4,35,83]. Lower water demand is deemed to be advantageous for improved mechanical and physical properties of sintered products.

6.3.2 Effect of SnO_2 on Microstructural Evolution

Figure 6-1 shows the phase evolution, XRD pattern, of the refractory compositions AZS-T1 and AZS-T2 sintered at 1500°C and 1550°C for 1hr. When considering the mode and relative peak intensities of each phase from the diffraction pattern of AZS-T1 sintered at 1500C, corundum and primary zircon are the major phases; with new phases, mullite and $Zr_{1-x}Sn_xO_2$ solid solution peaks, appearing as intermediate to minor phases. The $Zr_{1-x}Sn_xO_2$ phase is in monoclinic form and no high-temperature tetragonal phase is retained which is in agreement with observations reported in publications from other workers [21, 59, 60]. The presence of some zircon peaks suggests to the partial dissociation of zircon from the starting material and thus no complete mullitisation was achieved at these temperatures even in the presence of SnO_2.

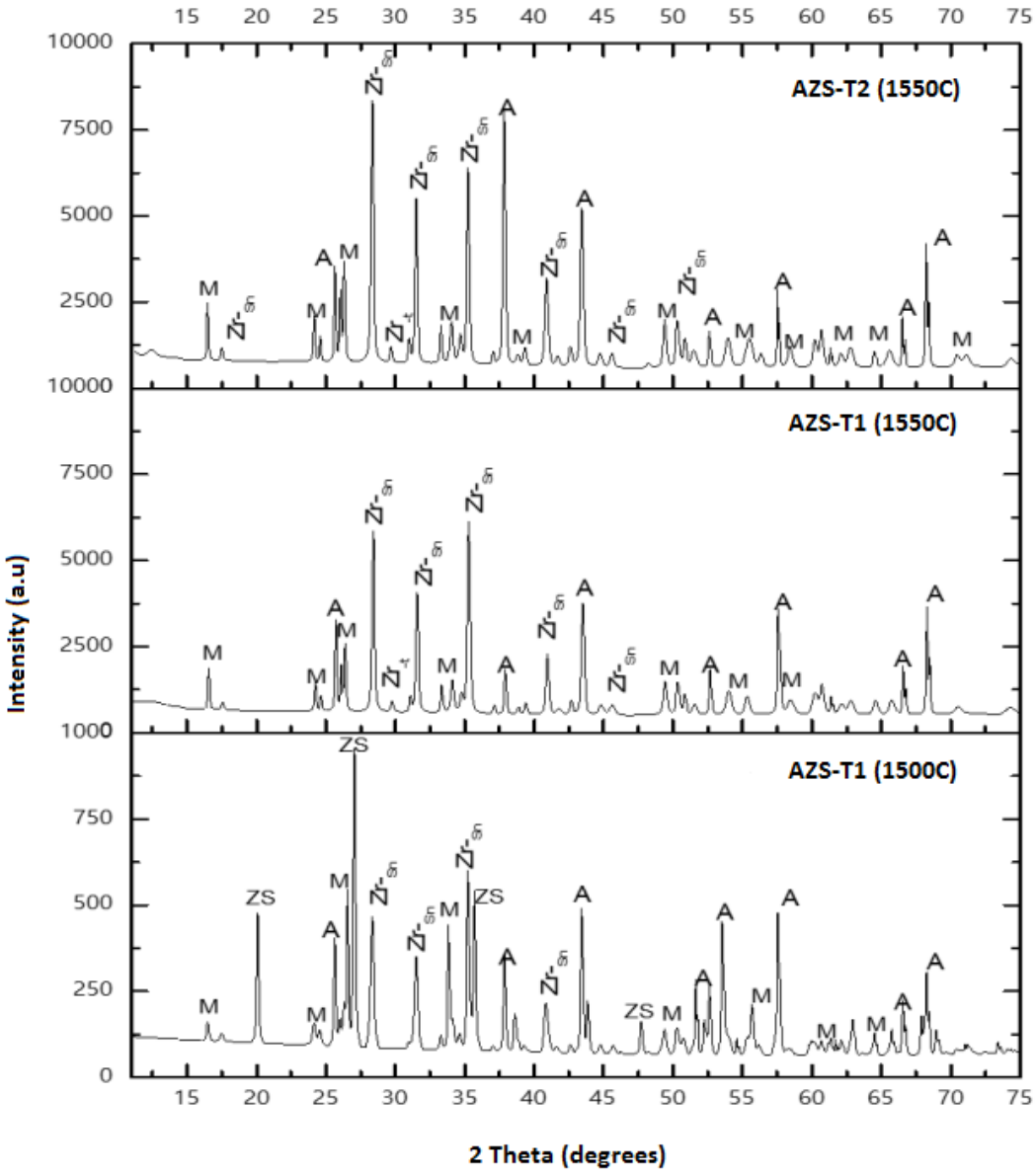

Figure 6-2: XRD pattern of refractory AZS-T1 and AZS-T2 sintered at 1500C and 1550C.

A = α-Al_2O_3; [ref code: 04-005-4502]; Zr-Sn = $Zr_{0.9}Sn_{0.1}O_2$ [ref code: 04-002-8306]

M = $Al_6Si_2O_{13}$; [ref code: 04-010-3002]; ZS = $ZrSiO_4$ [ref code: 04-008-8667]

Evidence of this can be seen from the SEM EDX microstructural analysis of the AZS-T1 refractory highlighted in the SEM micrograph, figure 6-3; which shows an elemental mapping of the AZS-T1 refractory microstructure after sintering at 1500°C.

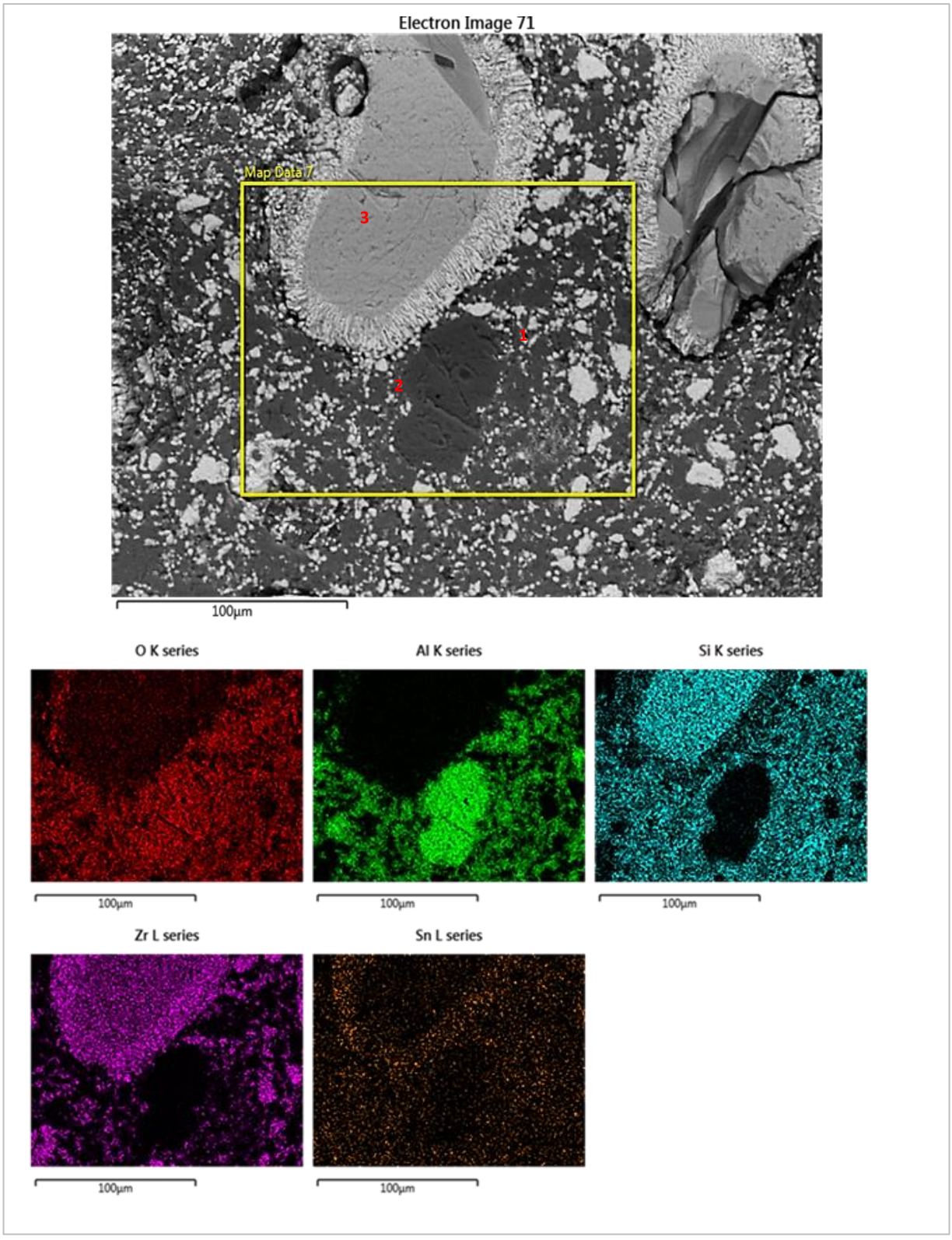

Figure 6-3: SEM EDX elemental mapping of AZS-T1 refractory microstructure (Sintered at 1500C for 1h). Zircon (light grey grains); (2) α-Al_20_3 (Corundum dark grey grains); (3) $Zr_{1-x}Sn_xO_2$ solid solution (bright light grains);

From the micrograph, the microstructure reveals a dense matrix which is comprised of composite grains of zirconia-tin oxide solid solution (bright/light grains), corundum grains (dark grey), mullite (lighter dark grey) and partially dissociated large zircon grains (light grey grains). From figure 6-3, it can be seen that the fine-grained zircon (d_{50}~ 2.4µm) have undergone a complete solid-state dissociation while the large zircon grains (d_{50}~ 140µm) are partially dissociated at the edges. The solid-state dissociation products, ZrO_2 and amorphous SiO_2, reacts with SnO_2 and α-Al_2O_3 to form a $Zr_{(1-x)}Sn_xO_2$ solid solution and equiaxed mullite (MI, type 1 mullite) respectively.

This was also seen in the previous chapter, section 5.4 in the microstructure of the AZS-01 refractory composition, without SnO_2 doping, sintered at 1500°C. SEM phase quantification of the granular mullite evolved, revealed the Al_2O_3:SiO_2 ratio to be 72.06:27.94 wt. %; indicating a near stoichiometric 3:2 Mullite. This would suggests that SnO_2 has negligible influence in the sinterability and mullitisation of alumina-zircon mixtures when sintered up to 1500°C, which agrees with findings by Kong et al, [61].This is in good agreement with observations made by other studies in literature and expected from a solid-state reaction at such low sintering temperatures and in the presence of excess Al_2O_3 in the Al_2O_3:SiO_2 ratio from the starting batch mixture.

Figure 6-2 further shows that the partial solid-state dissociation of the large “zircon sand” grains has occurred with decomposition initiating from the zircon grain edges towards the centre. This is in good agreement with similar observations made by other groups on the thermal dissociation of zircon and the conventional accepted theory that solid-state reactions occur faster with decreasing particle size [29]. At these zircon grain edges, precipitated SnO_2 enriched ZrO_2 dendritic grains appear

where SiO_2 is depleted. This suggests that SnO_2 diffuses towards the zircon region and reacts with the solid-state dissociation product, ZrO_2 dissolved in the amorphous SiO_2, and because of the limited solubility of either SnO_2 or ZrO_2, a $Zr_{(1-x)}Sn_xO_2$ solid solution is precipitated out in the form of dendrites. The α-Al_2O_3 then reacts with the SiO_2 to form an equiaxed type 1 or primary mullite (MI,).

However, when the sintering temperature of AZS-T1 and AZS-T2 refractories is raised to 1550°C, there are increased mullite peaks and monoclinic $Zr_{(1-x)}Sn_xO_2$ solid solution peaks at high intensities together with corundum making up the main phases of the microstructure, as can be seen from the XRD patterns of AZS-T1 and AZS-T2 refractory materials, in figure 6-1. Figure 6-1 further shows that in both the AZS-T1 and AZS-T2 refractories sintered above 1500°C, partially stabilised zirconia as tetragonal $Zr_{(1-x)}Sn_xO_2$ appears as a new minor phase. As well, no $ZrSiO_4$ peaks appear in the XRD patterns indicating a total complete dissociation of the large zircon grains.

It follows then that above the sintering temperature of 1500°C, the large zircon grains are completely dissociated from the grains edges towards the centre leading to an increased amorphous silica and free zirconia phase fraction which reacts with the SnO_2 to form a solid solution that has limited solubility in the siliceous phase and thereby precipitating the $Zr_{(1-x)}Sn_xO_2$ solid solution as dendritic grains. This indicates that SnO_2 has a marked influence in aiding the dissociation of zircon. The marked influence of SnO_2 in mullitisation above 1500°C sintering temperature can be seen when comparing the XRD pattern of the refractory composition AZS-01, sintered at 1570°C, shown in figure 5-8. In the figure, AZS-01 sintered above 1550°C still contains zircon peaks indicating incomplete dissociation and mullitisation in the absence of SnO_2.

For the AZS-T1 and AZS-T2 compositions sintered above 1500°C, no cassiterite (SnO_2) peaks appear in the XRD pattern for both refractories. Table 6-2 shows the bulk chemical composition of AZS-T1 and AZS-T2 refractories, sintered at 1550°C, by XRF analysis. A mass balance of the SnO_2 added to the starting batch mixtures of AZS-T1 and AZS-T2 from the XRF bulk chemical compositions of the refractories, shown in table 6-2, reveals that there was negligible SnO_2 loss due to volatization. SnO_2 is known to decompose and volatise in air above 1500°C according to reaction,

$$SnO_{2(s)} \longrightarrow SnO_{(g)} + O_{2(g)} \quad \text{.....(30)}$$

In the starting mix formulations of AZS-T1 and AZS-T2, 5 wt..% of SnO_2 was added.

Table 6-3: Chemical composition of AZS-T1 and AZS-T2 refractories sintered at 1550°C by XRF. Trace elements are (Na, Ca, Ti, Fe)

Sample	Chemical Composition (wt. %)								
	Al_2O_3	SiO_2	ZrO_2	SnO_2	R_2O	RO	Fe_2O_3	TiO_2	Others
AZS-T1	57.79	12.96	24.55	4.02	0.20	0.08	0.06	0.10	<0.32
AZS-T2	47.97	15.85	30.82	4.89	0.16	0.09	0.08	0.09	<0.12

*$R_2O = Na_2O + K_2O$; RO = CaO + MgO; Others = trace compounds < 0.01%

This can be explained from the phase equilibrium analysis and considerations discussed in section 5.1 on experimental studies in literature on binary phase diagrams of SnO_2 and $Al_2O_3/SiO_2/ZrO_2$ systems, albeit limited, that revealed no chemical reactivity in the solid state between SnO_2/Al_2O_3 and or SnO_2/SiO_2 binary systems; but only the formation of $Zr_{1-x}Si_xO_2$ – $Sn_{1-x}Zr_xO_2$ solid solutions from the

SnO_2-ZrO_2 binary system. In the SnO_2-SiO_2 system, phase equilibria experimental studies by [48], above 1500 °C, a liquid phase formation was observed in SnO_2-SiO_2 compositions rich in SiO_2, while a solid (SnO_2) and a liquid slag phase was observed to co-exist at equilibrium above 1510 °C – 1625 °C. A SnO_2-SiO_2 eutectic was determined at temperature range of 1773 - 1783K (1500 - 1510 °C) and liquid miscibility of SnO_2-SiO_2 above 1625 °C. In the sub-liquidus region of the Al_2O_3-SnO_2 system, a eutectic is observed at 98 wt. % SnO_2 at a eutectic temperature of 1893 ± 5 K (1620 °C) and in the presence of impurities such as in a quasi Al_2O_3-SiO_2-ZrO_2-SnO_2 system, this can be lowered to below 1828K (1555 °C).

Therefore, the presence of both ZrO_2 and amorphous SiO_2 from the dissociated zircon grains, plus a transient pro eutectic Al_2O_3-SnO_2.ZrO and SnO_2.SiO_2 liquid phase, may be thought to adversely affect the volatisation of SnO_2 through the formation of ZrO_2-SnO_2 solid solution and or reduced SnO_2 diffusivity in the amorphous SiO_2. High magnification SEM analysis of the AZS-T2 microstructure, as shown in figure 6-3 proves our theory.

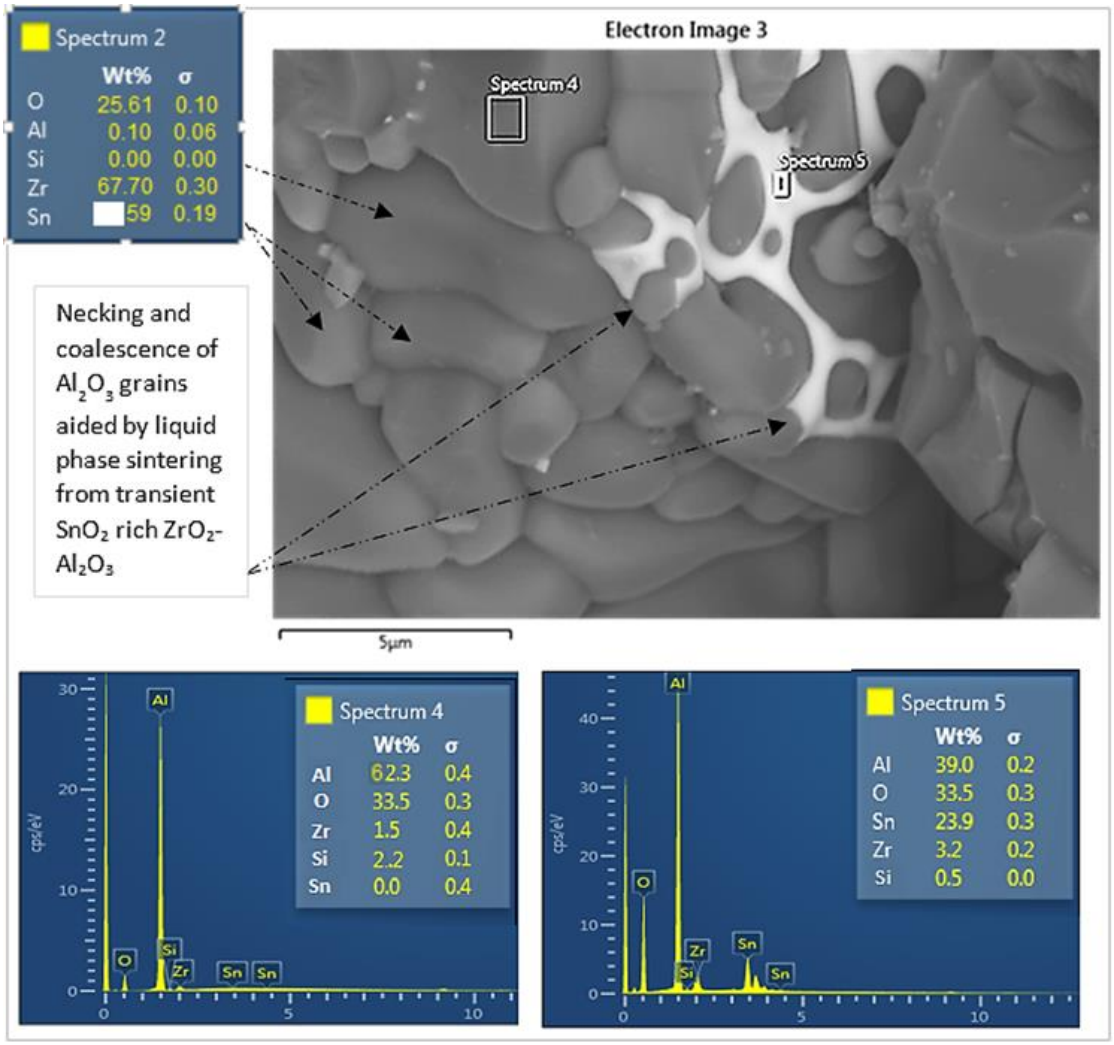

Figure 6-4:High magnification SEM(Hitachi SU8230) micrograph of the matrix region of the AZS-T1 refractory. A Tin oxide rich alumina-zirconia amorphous phase (white) can be seen at the grain boundaries of alumina grains (grey). Coalescence and gain growth of the alumina grains is cleary discernable and is enahanced by liquid phase sintering.

From figure 6-4, EDX semi-quantitative point analysis reveals the dark-grey grains (spectrum 4) as alumina grains and the white amorphous phase at the alumina grain boundaries as a SnO_2 rich, ZrO_2 and Al_2O_3 amorphous phase. Figure 6-4 further shows the coalescence of alumina grains of differing sizes, with the large grains

absorbing the small grains, enhanced by an attractive capillary force from the SnO_2 rich ZrO_2-Al_2O_3 liquid phase sintering leading to densification and coarsening of the alumina grains. Coalescence occurs as grains of differing size come into contact, where neck formation and growth of neck with a grain boundary ensues, leading to grain boundary migration through the smaller grain to form a single large grain [93,30]. Our findings are in good agreement with results from other workers where for high-solid content mixtures, boundary migration was the typical mechanism and grain boundary migration was through a transient liquid layer [98-100].

The presence of a liquid phase in sintering is known to permeate the microstructure leading to densification. For our study, this was highlighted in the physical properties of the AZS-T1 and AZS-T2 refractories both sintered at 1500C and 1550C respectively, as seen in table 2.

Table 6-4: Bulk density and apparent porosities of AZS-T1 and AZS-T2 refractories.

Sample	After sintering at 1500°C		After sintering at 1550°C	
	B.D (gcm^{-3})	**A.P** (%)	**B.D** (gcm^{-3})	**A.P** (%)
AZS-T1	3.37	12.8	3.41	8.5
AZS-T2	3.38	11.2	3.42	7.2

Density and apparent porosity measurements, shown in table 2 show a decrease in apparent porosities of AZS-T1 and AZS-T2 composites from c.a 13% to 8% and 11% to 7% respectively. This proves the marked effect of SnO_2 on the mass movement due to plastic flow which enhances sinterability and a reduction in the open pore. There is only about 1.4% increase in the bulk densities of the AZS-T1 and 2.3% in the AZS-T2 refractories when sintered above 1500°C to 1550°C. From

literature survey, it is known that the densification mechanism and chemical reactions, in alumina-zircon reaction sintering, during firing compete against each other [38-43]. In the earlier sections, it was shown that sintering above 1500°C to 1550°C, there was complete dissociation of zircon grains under the influence of the doped SnO_2 resulting in an amorphous phase of SiO_2 with ZrO_2 and SnO_2 dissolved plus the presence of some SiO_2 –SnO_2 and Al_2O_3 – SnO_2 transient liquid phase. Therefore, the relatively low increase in the bulk density of the refractories can be attributed to the relative increase in liquid phase formation from the dissociated zircon grains, plus the pro-eutectic SnO_2-Al_2O_3 –ZrO_2 and SnO_2-SiO_2 transient liquid phase and the volume expansion from the evolved mullite ($\rho = 3.63 gcm^{-3}$) from the reaction between SiO_2 and x-Al_2O_3, shown in equation 26.

6.3.2.1 Mullite Microstructural Evolution

The next part of this study looked at analysing the microstructural evolution of the reaction sintered mullite. Mullite formation in reaction sintering of Al_2O_3 and SiO_2 is known to be dissolution-precipitation controlled. Therefore, based upon the above observations and analysis made in the previous section, the morphology of the evolved mullite in the microstructures of AZS-T1 and AZS-T2 refractories sintered at 1500 °C would be expected to vary from the ones sintered at 1550 °C.

SEM microstructural analysis of the AZS-T1 and AZS-T2 refractory products sintered at 1500 °C, shown in figure 3, revealed that the evolved mullite has an equiaxed granular structure.

Figure 5 shows the microstructure of the AZS-T1 refractory matrix region after sintering at 1550C. From the figure, it can be seen that three types of mullite, based

upon their morphology and aspect ratios as defined by Iqbal and Lee **[35-37]** have evolved.

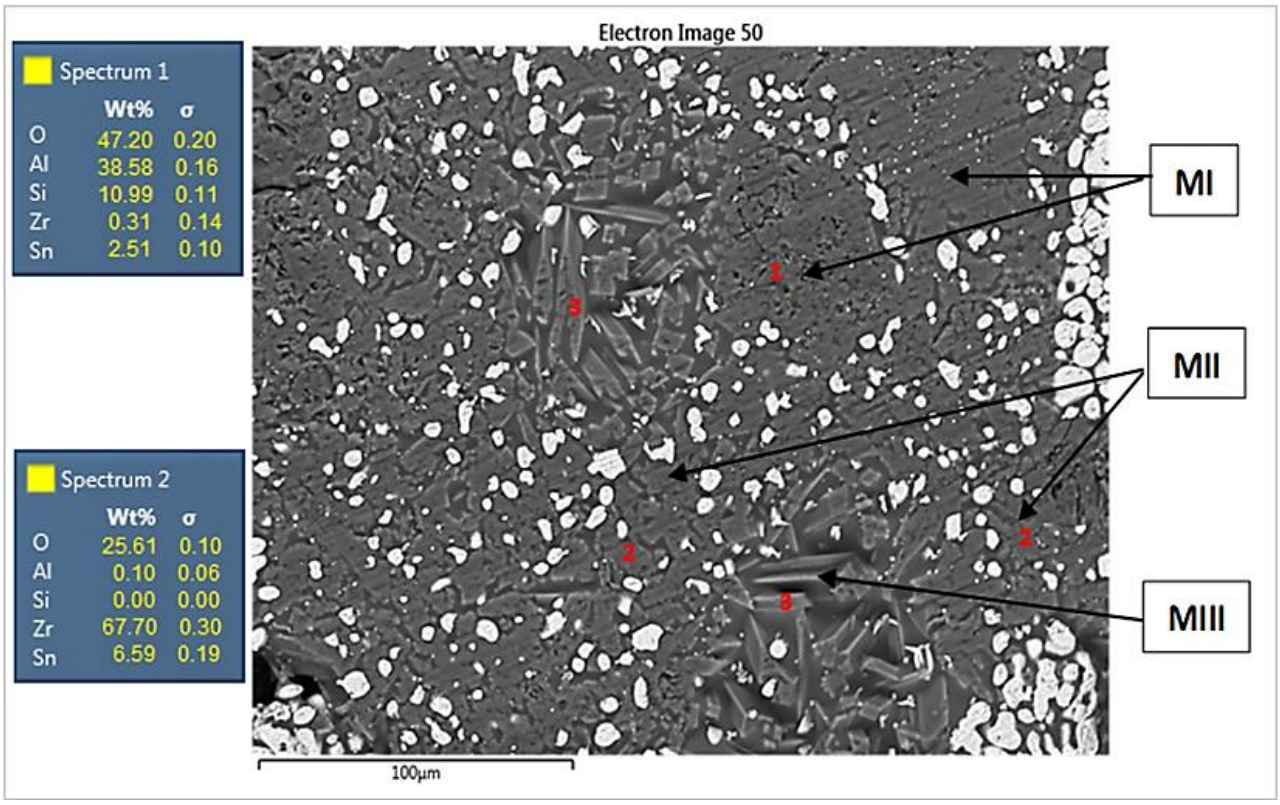

Figure 6-5: SEM micrograph showing the microstructure of the AZS-T1 refractory and the three types of evolved mullite.

MI = type 1 (primary mullite); MII = type 2 (secondary mullite); MIII = type 3 (tertiary mullite)

The proportion of the equiaxed primary mullite MI is reduced as there is grain growth of the primary, MI, mullite grains, which have increased in size with their aspect ratio reaching the maximum 3:1. The grain coarsening is due to the rise in sintering temperature from 1500C to 1550C as well as an increase in a transient less viscous amorphous phase from the decomposing zircon grains, SnO_2-Al_2O_3 –ZrO_2 and SnO_2-SiO_2 transient liquid phase which favours mass transport and grain growth.

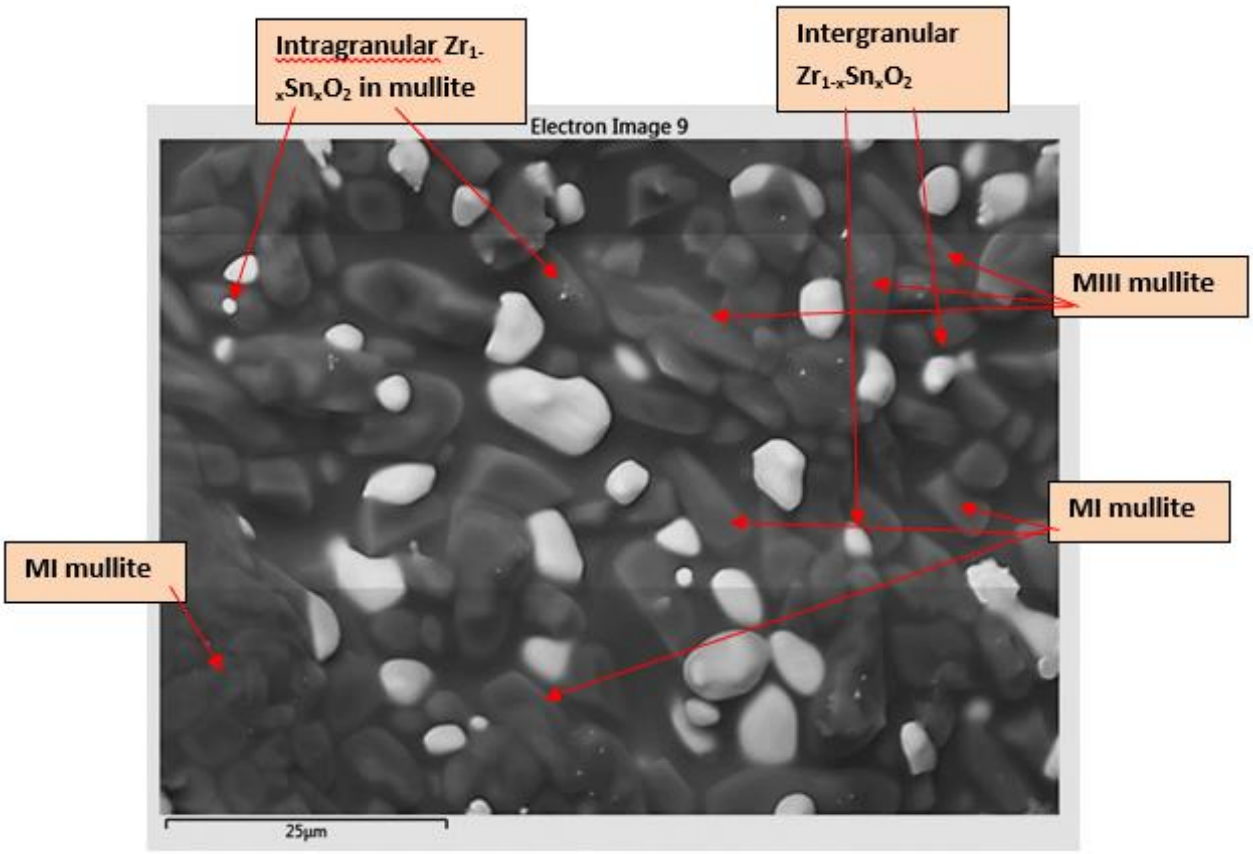

Figure 6-6: High magnification SEM micrograph of AZS-T1 microstructure. Microstructure shows the evolved matrix of the AZS-T1 microstructure with acicular grains of mullite reinforced by a dispersed intragranular and intergranular $Zr_{1-x}Sn_xO_2$ solid solution grains.

The spatial arrangement of the MI and MII mullite, shown in figure 6-5 and figure 6-6suggest that the primary mullite MI transforms into MII with the increase in sintering temperature and amorphous phase from the dissociating zircon grains which increase mass transport and the potential for unhindered grain growth.

Adjacent the secondary MII mullite are the tertiary MIII mullite grains, distinguishable by the needle like morphology and their very high aspect ratio grains. From figure 5, it can be seen that the tertiary acicular MIII mullite occur near agglomerates of $Zr_{1-x}Sn_xO_2$ crystals, evolved from the dissociated zircon grains. EDX semi-quantitative analysis reveals the Al_2O_3:SiO_2 ratios of MIII and MII to be 77.8:22.2 wt. % and 75.5:24.5 wt. % respectively; an increase of Al_2O_3 content in

the mullite structure from the MI mullite Al_2O_3:SiO_2 ratios. This means that the mullite composition varies from the 3:2 mullite from the primary MI to a 2:1 mullite from the secondary MII and tertiary MIII mullite. This suggests, in good agreement with numerous other studies [11-13, 99], the held view that the occurrence and growth of MII and tertiary MIII mullite is due to a fluid matrix. Wherein the case of this study, is an alumina rich siliceous phase from corundum dissolved in the amorphous silica from the dissociated zircon which allows nucleation and enhanced unhindered growth of the Mullite crystals to high aspect ratios. As well, SEM EDX semi quantitative analysis, see figure 6-6, reveal that the MII and MIII mullite incorporates within their structure both ZrO_2 and SnO_2 atoms. This would be expected to impart better corrosion resistant properties to the mullite grains in siliceous melts or slags.

Table 6-3, shows the quantified XRD mineralogical analysis of the AZS-T1 and AZS-T2 refractories sintered at 1550 °C, calculated according to the Internal standard (IS) Reitveld method [89-91]; and confirm these findings. From table 6-3, it can be seen that no $ZrSiO_4$ fractions are present in either refractory after sintering at 1550°C and the $Al_6Si_2O_{13}$ and ZrO_2 phase fractions are increased while the corundum fraction is reduced in comparison to the starting material.

Table 6-5: Mineralogical composition of AZS-T1 and AZS-T2 refractory composites after sintering at 1550 °C.

Mineralogical Composition (wt. %)		
Phase	*AZS-T1*	*AZS-T2*
α-Al_2O_3	*38.3*	*29.7*
$ZrO_{2\text{-}m}$	*26.3*	*31.0*
$ZrO_{2\text{-}t}$	*0.1*	*0.3*
SiO_2	-	-
$Al_6Si_2O_{13}$ (3:2 and 2:1)	*27.7*	*26.1*
$ZrSiO_4$	-	-
Amorphous	*6.6*	*11.2*

Figure 6-7 (a) - (d); shows SEM micrographs of the resultant microstructures of AZS-T2 after sintering at 1550°C. From the figure 6-7(a), the microstructure consists of aggregate tabular alumina grains within a mullite matrix reinforced by a dispersion of zirconia agglomerates from dissociated zircon grain relicts. The mullite matrix shown in figure 6-7 (b) reveals the homogenous dispersion of $Zr_{(1\text{-}x)}Sn_xO_2$ within the M1, MII and MIII crystals. AZS-T1 also exhibited a similar microstructure, having good homogeneity in the $Zr_{(1\text{-}x)}Sn_xO_2$ grains dispersion in the mullite matrix, albeit with relatively less zircon relict grains due to complete dissociation of zircon grains in the matrix. Figure 6-7, (c) and (d); further reveal that the tabular alumina aggregate grains are reinforced by precipitated $Zr_{(1\text{-}x)}Sn_xO_2$ solid solution grains, possibly from the transient liquid phase filling the tabular alumina pores. Therefore, the microstructures of the AZT-1 and AZS-T2 refractories evolve to a monoclinic $Sn_{(1\text{-}x)}Zr_{(x)}O_2$ reinforced mullite and alumina composite with some

tetragonal $Zr_{(1-x)}Sn_xO_2$ (that has not transformed), remaining as a minor phase when sintered above 1500°C to 1550°C.

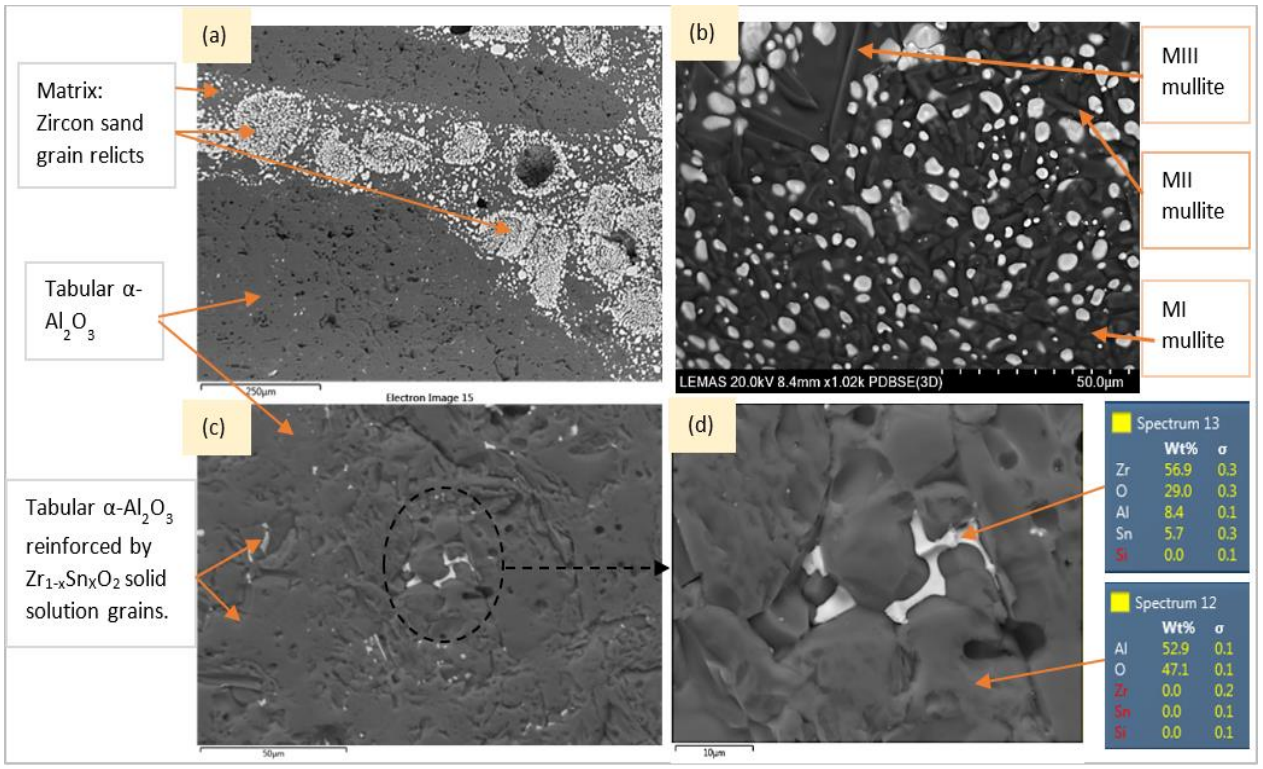

Figure 6-7: High - low magnification SEM micrographs of AZS-T2 refractory microstructure after sintering at 1550C.

- ***(a) Micrograph shows the aggregate - tabular (α-Al_2O_3) grains in zirconia reiforced mullite matrix.***
- ***(b) Micrograph shows homegenous dispersion of zirconia grains within the mullite matrix.***
- ***(c) Tabular α-Al_2O_3 aggreagte grain with $Zr_{(1-x)}Sn_xO_2$ dispered within the pores of the grains.***
- ***(d) High mag. SEM micrograph of Tabular α-Al_2O_3 aggregate grain reinforced by $Zr_{(1-x)}Sn_xO_2$ grains.***

6.3.3 Effect of SnO_2 addition on Thermomechanical Properties

It has been suggested by [39,42-45], from the improved thermomechanical properties of refractory bodies containing acicular mullite within their microstructure that the high aspect ratio mullite, MII and interlocking MIII mullite crystals increase the strength and thermal shock resistance of ceramic composites [39,42-45]. Therefore, based on the evolved acicular mullite structures in the microstructures of AZS-T1 and AZS-T2 refractories from the addition of SnO_2; the next part of this study looked at the effect of SnO_2 addition on the thermos-mechanical properties of the

AZS-T1 and AZS-T2 refractories to evaluate whether our results would be in agreement with those of [39,42-45].

6.3.3.1 Cold Crushing Strength

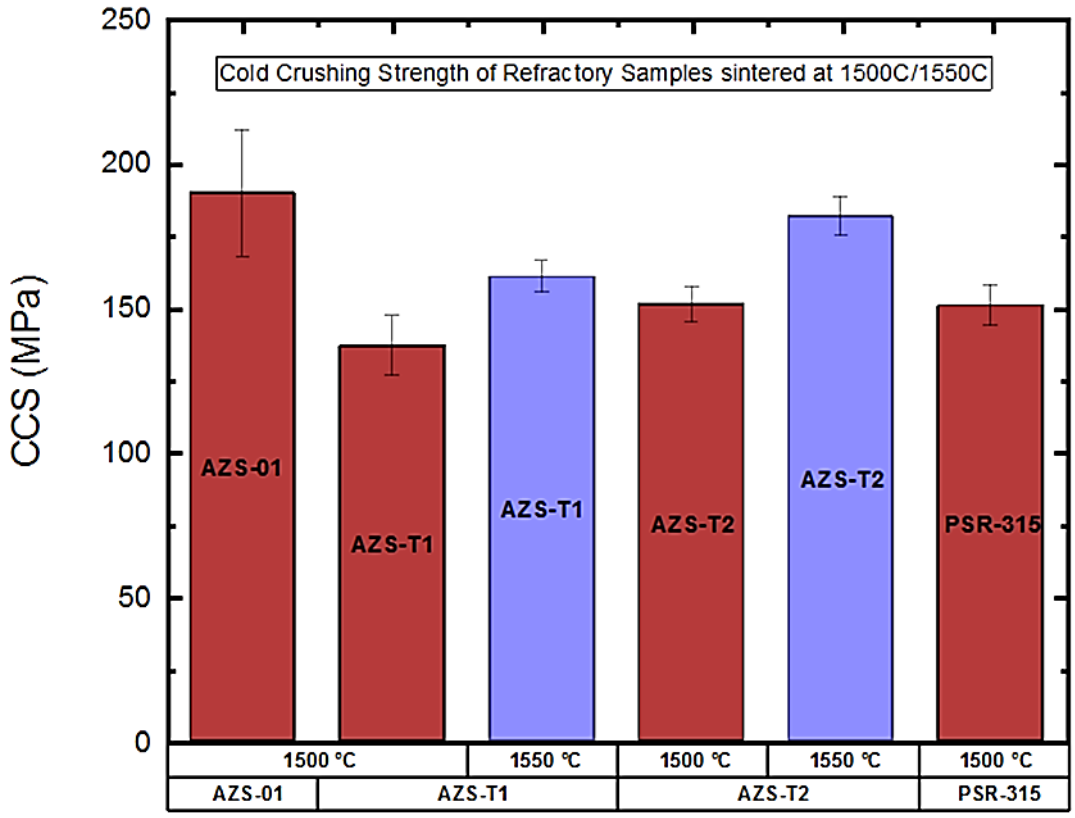

Figure 6-8: Cold Crushing Strength values of AZS-01, AZS-T1 and AZS-T2 refractories sintered at 1500 °C and 1550 °C. The CCS of a commercial refractory widely used in the glass industry PSR-315 was used as a comparison.

Figure 6-8 shows the cold crushing strength of AZS-T1 and AZS-T2 refractories sintered at both 1500°C and 1550°C and that of AZS-01 refractory sintered at 1500°C. The cold strength properties of AZS-01 were compared with AZS-T1 to evaluate the effect of SnO_2 on the cold strength of the refractories.

From figure 6-8, for refractories sintered at 1500°C, the AZS-01 refractory has higher cold strength properties than the tin oxide doped refractory AZS-T1 and AZS-

02. The cold crushing strength of AZS-01 is 190 MPa, while that of AZS-T1 (AZS-01 doped with SnO_2 and also sintered at 1500°C) is 136MPa. The cold strength value of AZS-T2 refractory, with 50 wt. % of zircon in its starting mixture, is 146MPa. This shows that the addition of SnO_2 has a significant effect on the cold crushing strength properties of AZS refractories. The addition of SnO_2 results in a reduction in room temperature strength values of about 30%. However, when the AZS-T1 and AZS-T2 refractories are sintered at 1550°C, Figure 6-8, further shows that their cold crushing strength values increases considerably by 17.5% and 25.4% respectively.

This, despite the fact that is the relative mullite phase content of AZS-T1 is higher than that in AZS-T2, as shown in table 2. It has been observed in this study that when sintering above 1500°C, there is an increase in the evolution of secondary MII and tertiary MIII, at the expense of the primary MI mullite grains. This means that for the AZS-T2 refractory, a higher liquid phase content, conducive for a tertiary MIII mullite evolution, was expected from the complete dissociation of the higher zircon content from the initial starting mix formulation as compared to the AZS-T1 refractory. This explains the relatively higher amorphous phase content in the AZS-T2 refractory (11.2 wt. %) as highlighted in mineralogical analysis shown in table 2. This suggests that the increase in the cold crushing strength of the AZS-T2 (183 MPa) over that of AZS-T1 refractories when sintered at 1550°C could be as a result of the evolved interlocked high aspect ratio MIII mullite. This observation is in agreement with similar observations by Khadelwal and Cook [99]. However, Lee and Iqbal [44], in their observations, concluded that mullite content alone is not the only factor that can affect the refractory/ceramic product strength but rather the proportions and morphology of the types of mullite evolved as well as other

mineralogical phases (e.g., monoclinic and tetragonal ZrO_2 and Al_2O_3) available within the microstructure.

In the case of our study, the presence of ZrO_2 and $Zr_{1-x}Sn_xO_2$ polymorphs interlocked within acicular mullite matrix microstructures of AZS-T1 and AZS-T2 after sintering at 1550°C, as shown in figure 6-6, appears to enhance and improve the cold crushing strength properties of the two refractory products respectively. Therefore, doping of SnO_2 as a sintering aid in the reaction sintering of alumina-zircon mixtures does seem to offer significant cold crushing properties when sintered above 1500C where the evolution of acicular mullite and complete dissociation of zircon grains has been shown to occur.

6.3.3.2 Refractoriness & Refractoriness under Load

The refractoriness or fusibility temperature range of a refractory body, as discussed in the section 1, is a material property in which the refractory body will deform under its own load at high temperatures. The refractoriness of a material therefore shows the heat resistance of the refractory material and is generally expressed in terms of the Pyrometric cone equivalents (PCE). In industry, refractoriness is an important material property that is often quoted in the product data sheet and used to gauge the suitability of a refractory body for a given service temperature. However, refractoriness of refractory body decreases when refractory is under a load which is common in most of its service applications. Therefore, testing the refractoriness under load (RUL) of a refractory is thus more important rather than just the refractoriness or PCE.

For this part of the study, the refractoriness of the developed compositions AZS-01, AZS-T1 and AZS-T2, described and discussed in the earlier sections, were compared

with the standard PSR compositions PSR-315 and PSR-333. The refractoriness under load properties of the developed compositions were also evaluated and compared to investigate the effect of SnO_2 on the hot flexural strength properties of the novel AZS refractories.

Table 6-5 shows the refractoriness or fusibility temperature range and the determined PCE values of the developed AZS-01, AZS-T1 and AZS-T2 refractories. The refractoriness and PCE values of the standard commercial PSR refractories, PSR-315 and PSR-333 are also given for comparison. Table 6-6 shows the typical chemical compositions of the standard commercial refractories and the developed refractories.

In general, as explained earlier, refractoriness of AZS bricks is a function of the alumina and zirconia contents of the refractory composition. The higher the alumina content, normally, the higher the refractoriness.

This was highlighted in section 5.2, when considering the compositions or isopleths of the standard commercial refractories and the developed compositions from the $Al_2O_3 – ZrO_2 – SiO_2$ ternary system. The standard refractories, PSR-315 and PSR-333, were designed to have high refractoriness, from their high alumina contents, as highlighted in table 6-6, while the new developed compositions in this research, AZS-01, AZS-T1 and AZS-T2 were designed with lower alumina content and selected to lie within lower liquidus isotherms to encourage densification through liquid phase sintering.

The presence or development of a liquid phase in the refractory microstructure during sintering, as utilised and highlighted in this research, enhances densification and sinterability of the refractory. However, its presence, particularly from the effect

of impurities such as R_2O, RO, TiO_2 and Fe_2O_3 inherent in the starting raw materials affects and is detrimental to the thermal stability of the material.

Table 6-6: Refractoriness (fusibility temperature range) and PCE values of standard PSR refractories and developed compositions.

Refractory - Sample	**Refractoriness (°C)**	**PCE**
PSR-315	1775 °**C**	34 – 35
PSR-333	1745 °**C**	33
AZS-01	1775 °**C**	34 – 35
AZS-T1	1724 – 1743 °**C**	32.5 – 33
AZS-T2	1724 – 1743 °**C**	32.5 – 33

Table 6-7: Chemical compositions of the commercial refractories used as reference materials in this study and the developed compositions of interest.

Sample	Chemical Composition (wt. %)								
	Al_2O_3	SiO_2	ZrO_2	SnO_2	R_2O	RO	Fe_2O_3	TiO_2	Others
PSR-315	68.00	12.96	17.97	-	0.44	0.06	0.13	0.10	<0.32
PSR-333	73.00	15.00	11.10	-	0.45	0.20	0.20	0.17	<0.32
AZS-01	61.80	12.80	24.90	-	0.21	0.08	0.06	0.09	<0.12
AZS-T1	57.79	12.96	24.55	4.02	0.20	0.08	0.06	0.10	<0.32
AZS-T2	47.97	15.85	30.82	4.89	0.16	0.09	0.08	0.09	<0.12

From table 6-6, it can be seen that the developed composition, AZS-01, together with the tin oxide doped compositions AZS-T1 and AZS-T2 have high refractoriness, typical of high alumina refractories [11,28,42,101].

AZS-01 has similar refractoriness, PCE of 35, as PSR-315. This is mainly due the relative increase of the zirconia phase into the AZS-01 microstructure from the dissociated zircon and evolved mullite and lower glassy phase, as discussed and highlighted in table in section 5.4. The evolved interlocked zirconia grains in AZS-01 enhances the refractoriness of material, zirconia being the most refractory phase in the AZS system with a m.p of 2715 °C.

As well, according to the typical chemical composition of the refractories, in table 6-6, AZS-01 contains low impurity concentration levels of alkali and alkali earth compounds (R_2O and RO), as well as TiO_2 and Fe_2O_3 than PSR-315. These impurity compounds are known to introduce low melting liquid phases which affect the thermal stability of the refractory. This is seen when considering the refractoriness of PSR-333 refractory, which despite having a higher alumina of 73 wt. % has a refractoriness of 1745 °C, PCE 33 – 35, lower than AZS-01. This is because PSR-333 contains higher concentrations of alkali, alkali earth and TiO_2 and Fe_2O_3 impurities.

The tin doped refractories, with low alumina contents, have similar refractoriness as PSR-333. When considering the refractoriness of AZS-T1 refractory (1745 °C max) and the AZS-01 (1775 °C), it can be concluded that the addition of SnO_2 (m.p 1625 ± 5 °C) does not significantly lower the refractoriness of the AZS refractories, with a reduction of about 1.7%. This can be related to the observed evolution of the acicular mullite grains (MII and MIII mullite) as shown in the previous section, see

figure 6-5 and figure 6-6. The evolved acicular mullite yields a three dimensional reinforcement network of the microstructure, which can be thought to enhance the thermal stability and resistance to shearing or deformation at high temperatures [44,45,106-108].

Under service however, refractories are constantly subjected to loads and as explained earlier, their refractoriness is lowered. The refractoriness under load (RUL) is a critical hot material property for refractory materials that is used to evaluate the behaviour and softening temperature range and thus the suitability of the refractory material in service at high temperature applications. Therefore, the RUL behavioural properties of the developed refractories, AZS-01, AZS-T1 and AZS-T2 were evaluated from the RUL tests conducted at Lucideon Ltd, Stoke on Trent, UK.

Testing was done according to the methodology described in section 4.2.2.1. The RUL test was also used to evaluate the effect of SnO_2 as a sintering aid on the hot properties of the developed AZS refractories given that in their development, the use of liquid phase sintering had been favoured route and design of this research scope to evolve zirconia reinforced interlocked acicular mullite matrix in an AZS refractory.

Figure 6-9 shows a schematic representation of a typical RUL curve highlighting the rate of sagging of a refractory material under load with temperature. The figure also shows the significant high temperature material properties that are calculated from the RUL curve. These parameters are the $T_{0.5}$ (Ta) and $T_{1.0,}$ which are defined as the onset of softening of the refractory and the end of softening of the refractory before failure respectively.

The Dmax gives the maximum expansion of the refractory and temperature range at which this occurs.

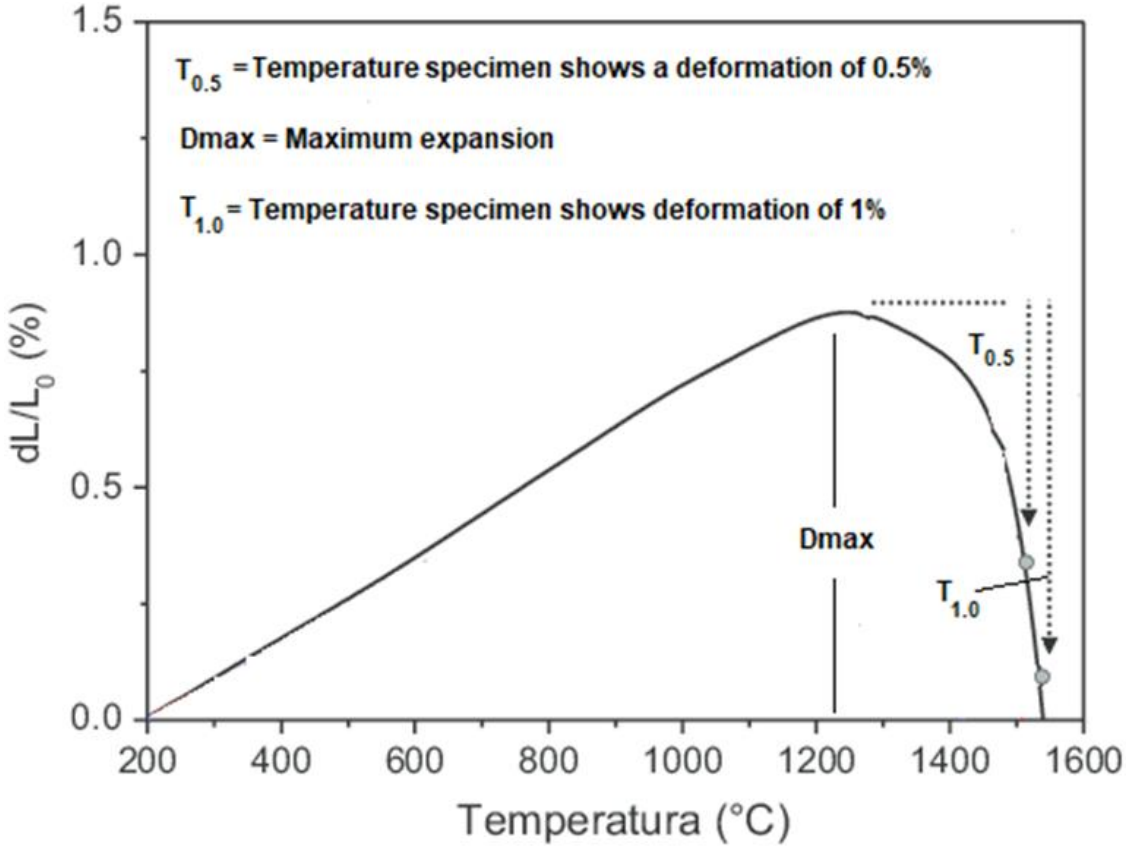

Figure 6-9: Schematic representation of a typical RUL rate of sagging with temperature curve.

Figure 6-10, shows the RUL curves of the developed refractory compositions AZS-01, AZS-T1 and AZS-T2 from room temperature to 1700 °C. Table shows the calculated RUL values of the tested refractories.

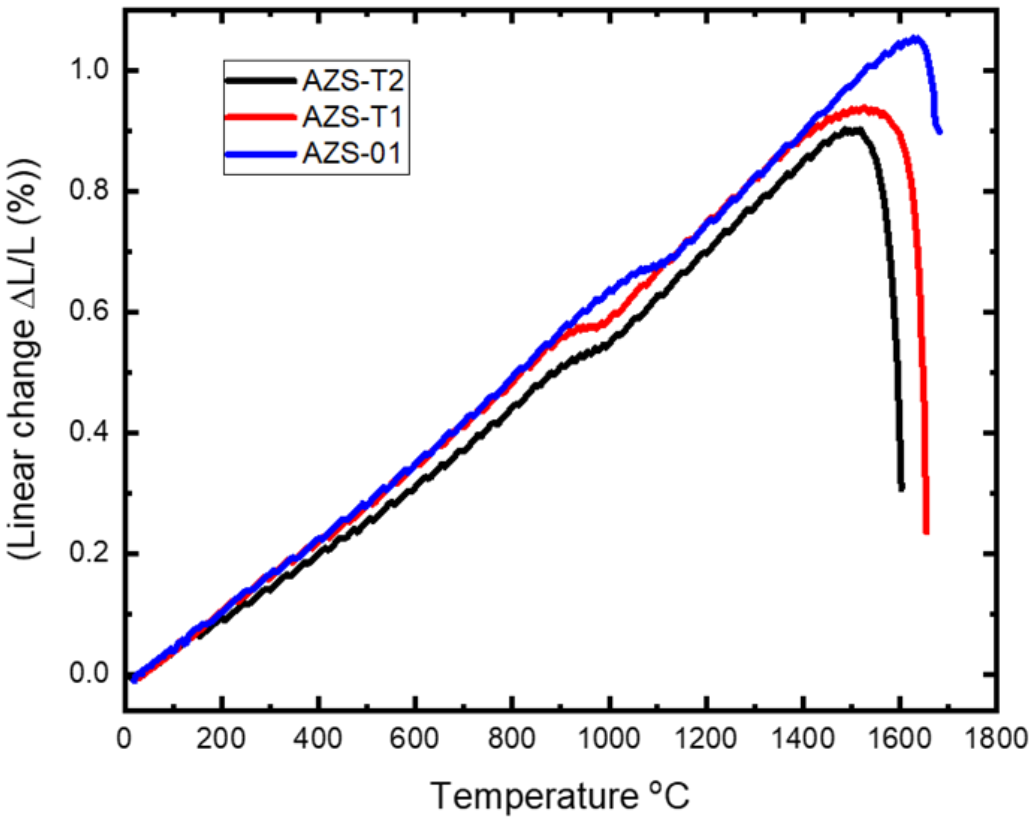

Figure 6-10: Refractoriness under load curves of AZS-01, AZS-T1 and AZS-T2 refractories.

The calculated RUL results presented in table 6-7 show that AZS-01 has high refractoriness under load strength than the SnO_2 doped compositions. This is expected, considering the refractoriness or PCE values of the refractory compositions presented in table 6-5. The temperature range within which subsidence of the AZS-01 occurs is >1681 °C. This represents a temperature range that is ca. 100 °C lower than the PCE values of AZS-01 presented in table 6-5. This is in agreement with literature where the RUL values of High Alumina refractories are quoted about 100 °C lower than their corresponding PCE values. The temperature of the onset of subsidence ($T_{0.1}$ or 10% of refractory slagging) of AZS-T1 (AZS-01 with SnO_2 addition), is ca. 1522 °C up to 1622 °C. This suggests that SnO_2 dopant affects and lowers the hot temperature stability of the AZS refractories by 3 – 7 %.

AZS-T2, with similar amount of SnO_2 concentration added to a 33 wt% ZrO_2 bearing AZS refractory composition has RUL values of 1540 °C. These results show that the SnO_2 doped AZS refractories AZS-T1 and AZS-T2 have reduced upper service temperature. However, although, SnO_2 as a sintering aid does have an effect on the hot properties of the AZS refractories, the effects are not as significant as those imparted by TiO_2 which were reported to be reduced by up to 25%. Also, it should be noted that these temperatures are still way above the maximum temperatures channel and forehearth refractories would face in service.

Table 6-8: Calculated RUL values of the developed refractory compositions.

Refractory	D_{max} %	D_{max} Temperature °C	$T_{0.5}$ °C	$T_{1.0}$ °C
AZS-01	1.06	1620	>1681	>1681
AZS-T1	0.94	1500 - 1560	1622	1659
AZS-T2	0.9	1450 - 1585	1540	1614

However, from figure 6-10, there are two significant temperature domains on the RUL curves of the refractories that are emphasised and presented. These are;

- Points of inflection that correspond to the zirconia allotropic phase transformation; and.
- The region of subsidence of the AZS-01 and AZS-T1 compositions on the RUL part of the curve from 1350 °C – 1700 °C that present the maximum expansion and beginning and end of the softening temperature range (i.e, the RUL of the refractories).

Figure 6-10 shows inflection on the AZS-01curve at higher temperature range than observed on the AZS-T1 and AZS-T2 refractories. The inflections are a result of the zirconia allotropic phase transformation from monoclinic to tetragonal that are known to occur in the temperature range of 980C to 1180C.

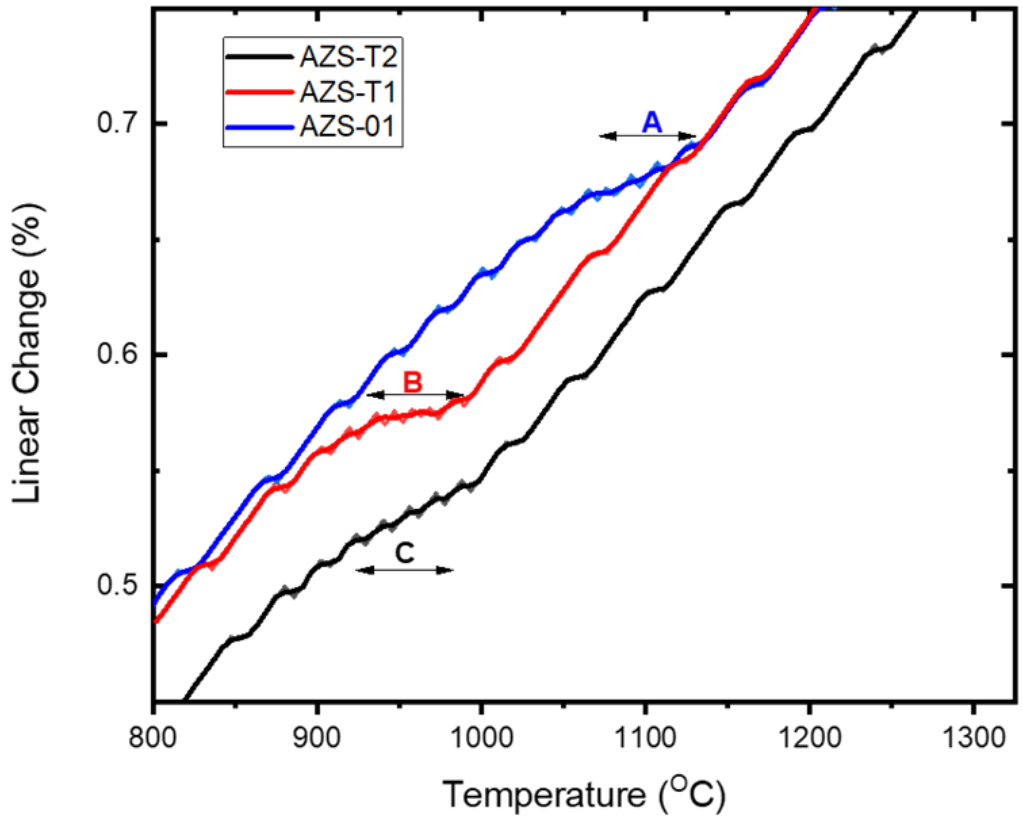

Figure 6-11: RUL heating curve showing three inflections points (A, B and C) on the curves of the developed refractories. The highlighted inflection points A, B and C represent the monoclinic – tetragonal phase transformation of the ZrO2 phase in the microstructures of the developed refractories AZS-01, AZS-T1 and AZS-T2.

Figure 6-11 shows an inflection on the AZS-01curve at higher temperature range than observed on the heating curves of AZS-T1 and AZS-T2 refractories. These inflections are a result of the zirconia allotropic phase transformation from monoclinic to tetragonal that are known to occur in the temperature range of 950C to 1180C. From figure 6-11, which highlights the temperature range of this phase transformation of the developed refractory compositions, it can be seen that in AZS-

T1 and AZS-T2 compositions, with SnO_2 dopant, the transformation occurs at a lower temperature range, highlighted B and C (910 °C – 980 °C) respectively. Whereas for the AZS-01 (without any SnO_2 additions) the phase transformation occurs in the temperature range 1080 °C – 1180 °C, highlighted C.

This decreased monoclinic – tetragonal transformation can be attributed to the formation of solid solution of SnO_2 in t-ZrO_2 which transforms to monoclinic $Zr_{1-x}Sn_xO_2$ detected in the XRD pattern of AZS-T1 and AZS-T2 presented in figure 6-12.

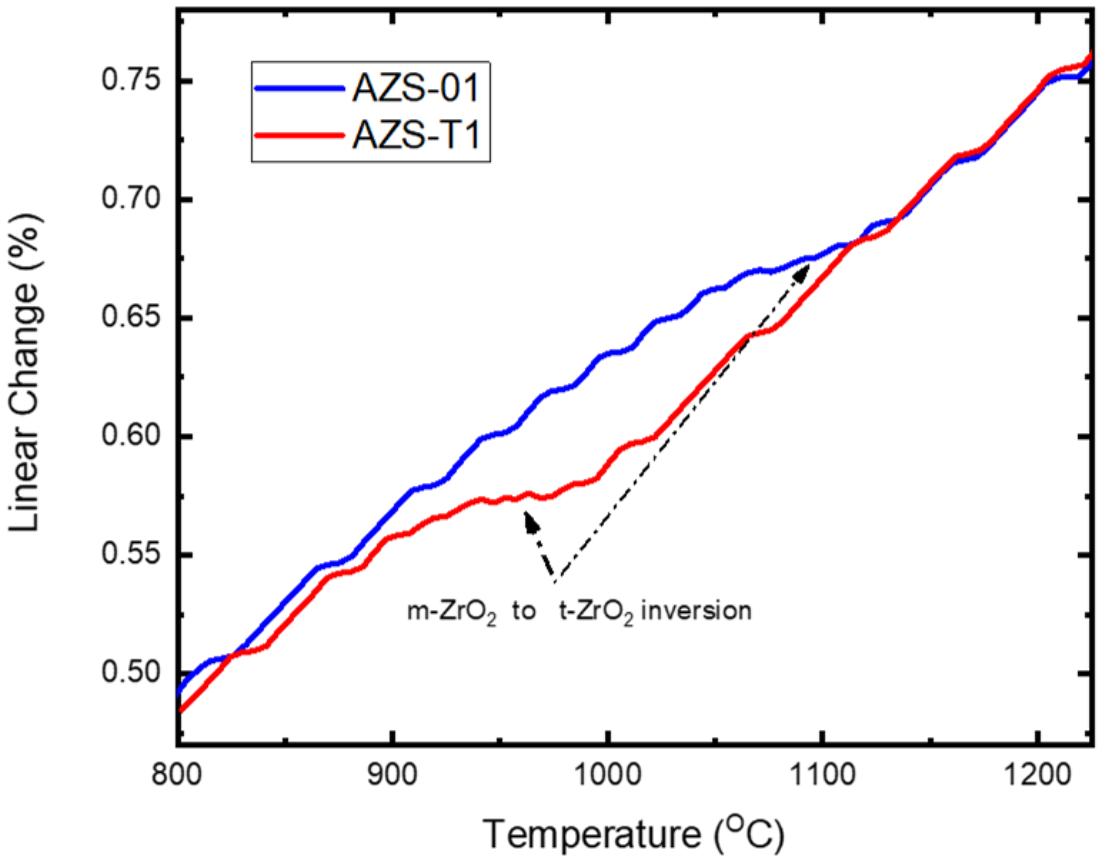

Figure 6-12: Linear expansion curve of AZS-01 and AZS-T1 refractories during an RUL test. The curve shows the expansion paths of the two AZS refractories and the effect of dopant SnO2 in AZS-T1 on the respective temperature ranges for the zirconia allotropic phase transformations of the refractories.

This occurrence is analogous to observed decreased zirconia allotropic transformations from TiO_2 additions [12,76,79,85]. When considering the linear

expansion curve of refractory composition AZS-01 and AZS-T1, the pronounced effect of SnO_2 on the phase transformation can clearly be distinguished. This is clearly highlighted in figure 6-11. In the figure 6-12, it can be seen that both refractory, AZS-01 and AZS-T1, follow the same expansion path with the exception being at the phase inversion temperatures.

From microstructural evaluation studies of the SnO_2 doped compositions, it was shown and discussed how SnO_2 reacted with the ZrO_2 from the dissociated $ZrSiO_4$ to form a SnO_2-ZrO_2 solid solution $Zr_{1-x}Sn_xO_2$. This shows that SnO_2 has a marked effect in stabilising the tetragonal phase to a much lower transformation temperature range of 910 °C – 980 °C from 1050 °C – 1120 °C. The shift in the allotropic monoclinic-tetragonal phase change temperature range from 1080 °C – 1180 °C to 910 °C – 980 °C has wider technological benefits for forehearth and feeder expandable products that experience service temperatures in the range of 1100 – 1260 °C. This means that at within these service temperatures, the refractories are not subject to the volumetric changes associated with the > 6% monoclinic – tetragonal transformations which may be detrimental to the thermal shock behaviour of the refractory body [11,12,104,106]. As well, the AZS-T1 and AZS-T2 refractories whose transformation occurs at the lower temperature range of 910 °C – 980 °C will possess tetragonal zirconia phase that is crucial in strengthening mechanisms and will enhance the thermal and strength properties of the refractories [12,60, 104-108].

When considering the region of subsidence of the refractories on the RUL curve, as highlighted in figure 6-13, the effect of SnO_2 on the thermal stability behaviour of SnO_2 doped AZS compositions AZS-T1 and AZS-T2 can be seen from the slope of the AZS-T1 RUL curve.

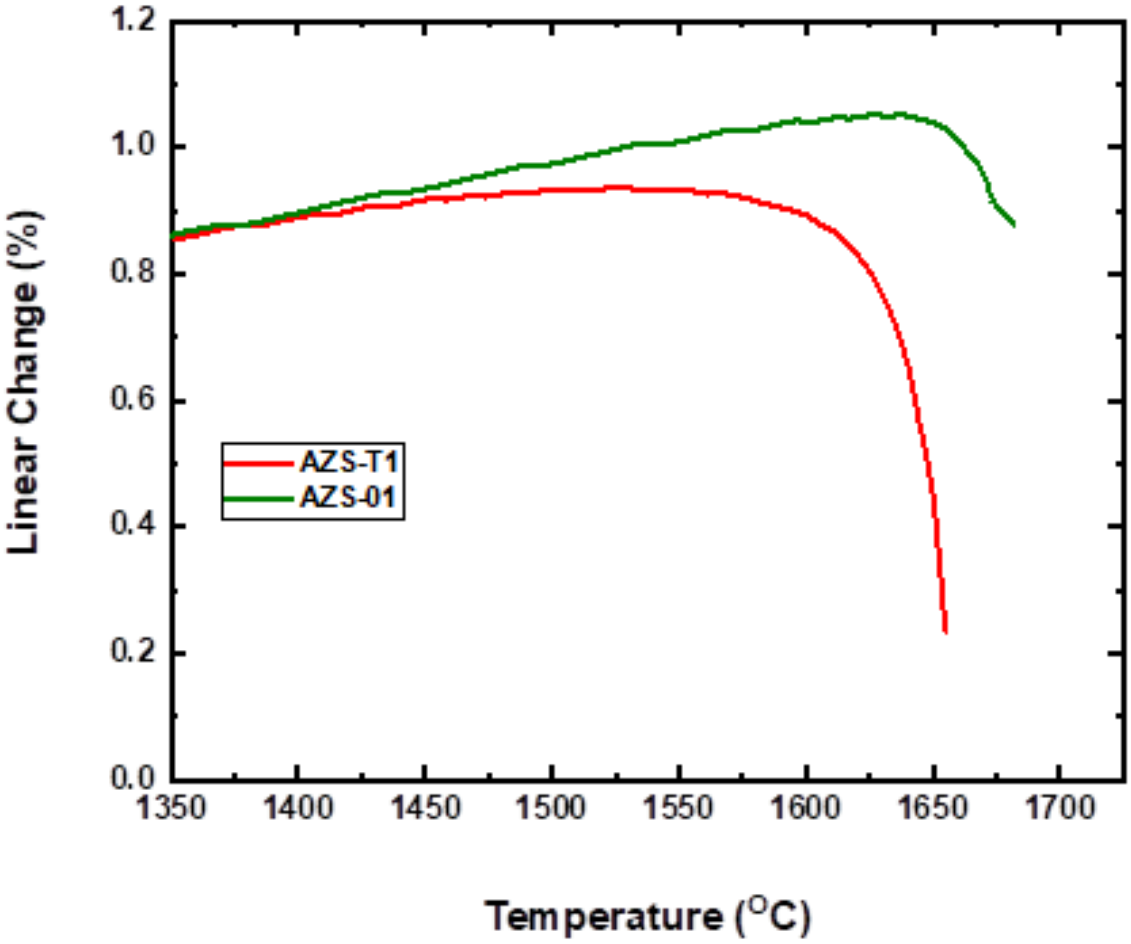

Figure 6-13: Refractoriness under load curves of AZS-01, AZS-T1 refractories in the temperature range of maximum expansion and end of subsidence.

From table 6-7, the maximum expansion of AZS-T1 is reached at 1560 °C under a 0.2N Load and is maintained until 1645 °C, where subsidence of the refractory starts. This T0.5 is quoted as the RUL value of a refractory as this represents changes in the phases of the refractory microstructure, normally as a result of formation of low melting liquid phases. In contrast, AZS-01 reaches maximum expansion at 1640 °C and up to 1672 °C where the curve starts to taper signalling the beginning of subsidence of the refractory. This means that the AZS-01 refractory, without any SnO_2 doping, has a limited temperature range in which it resists against high temperature stresses before subsiding. While for the AZS-T1 refractory, the

temperature range of thermal stability is wide spread and this is attributed to the formation of the acicular mullite that forms a reinforcing network of the refractory.

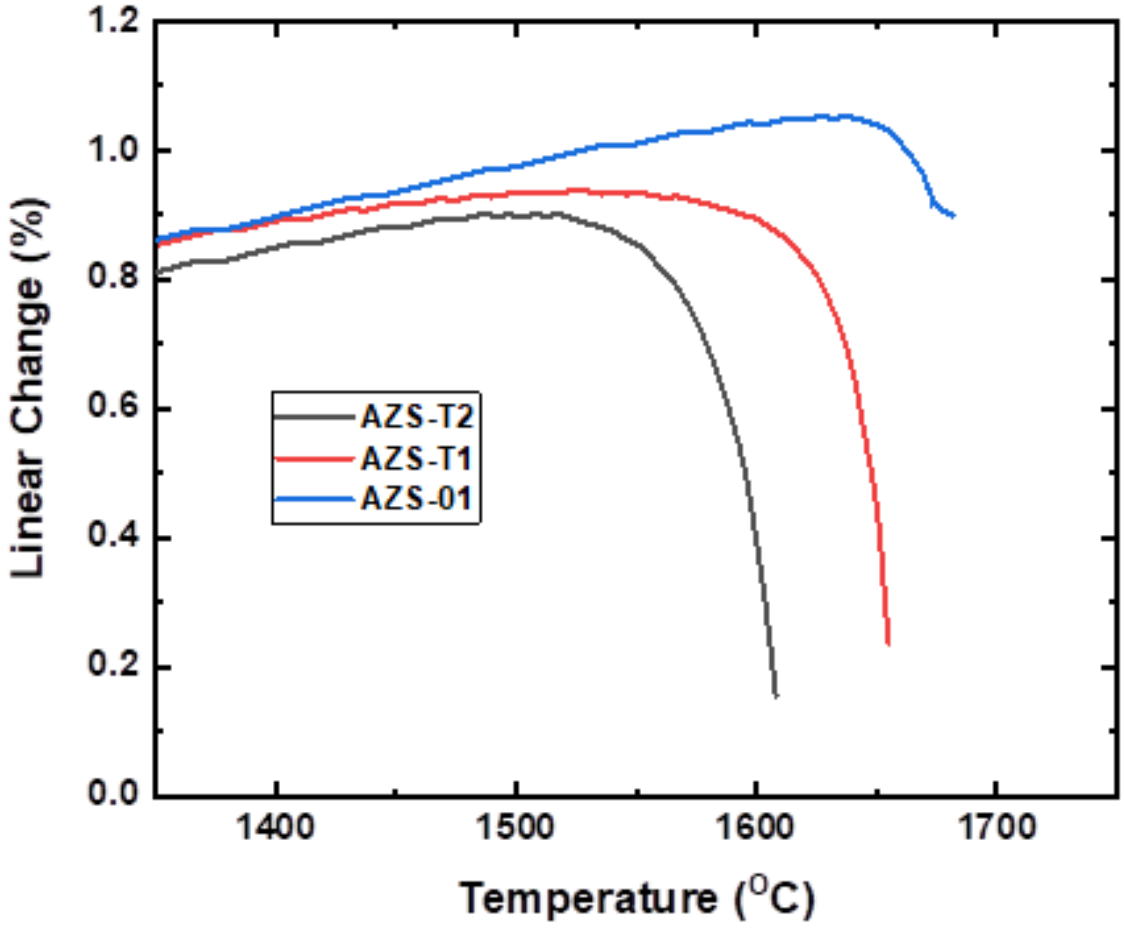

Figure 6-14: Refractoriness under load curves of AZS-01, AZS-T1 refractories in the temperature range of maximum expansion and end of subsidence

Figure 6-14, shows the RUL curve of the two doped AZS refractories, AZS-T1 and AZS-T2. It can be seen both from table 6-7 and figure 6-13 that AZS-T1 has better RUL than AZS-T2. This can be attributed to the large glassy phase in the AZS-T2 microstructure of 11.2 wt. % compared to AZS-T1 with 6.60.

6.3.3.3 Hot Modulus of Rupture (HMOR)

Table 6-8 shows the hot modulus of rupture (HMOR) and modulus of elasticity (MOE) test data at test temperatures of 1300 °C and 1400°C, respectively, of the developed refractory compositions AZS-T1 and AZS-T2 sintered at 1550 °C.

Table 6-9: Hot Modulus of Rupture values of AZS-T1 and AZS-T1 at test temperatures of 1300 °C and `1400 °C

Sample Reference	Temperature	Modulus of Rapture	Modulus of Elasticity
		(MPa)	(GPa)
AZS-T1	1300	20.3	19.5
AZS-T2		17.2	14.8
AZS-T1	1400	*23.4	
AZS-T2		*17.3	

*tests conducted at Reliance Ltd, India and no MOE values were provided.

From table 6-8, it can be seen that between the test temperatures of 1300 – 1400 °C, which represent the expected service temperatures in forehearth and feeder sections of the glass furnace, the hot flexural strength of AZS-T1 increases with temperature and this can related to the RUL behaviour of AZS-T1 highlighted in figure 6-14. For AZS-T2, there is only a slight increase in the HMOR values from 17.2MPa to 17.3MPa. No HMOR tests were conducted on AZS-01 and as such no comparisons and effect of SnO_2 additions to the flexural strength properties of reaction sintered AZS refractories.

6.4 Conclusion

The research results have shown and proved successfully the use of SnO_2 as sintering additive to develop and evolve reinforced alumina and mullite refractory composites AZS-T1 and AZS-T2 of the Alumina-Zirconia-Mullite system, from reaction sintering of Alumina and zircon starting mixtures having higher zircon content. The research objective of synthesising dense refractory bodies with relatively low apparent porosities of less than 10% were achieved by sintering the SnO_2 doped compositions above 1500 °C to 1550 °C. The presence of a liquid phase enhanced densification and mullitisation of the refractories and SnO_2 has a considerable influence in the enhancement of the kinetics of dissociation of zircon and subsequent reaction sintering of alumina and zircon.

Three types of mullite crystals, namely primary mullite (MI); secondary mullite (MII) and acicular tertiary mullite MIII, based on the morphology and aspect ratios, were evolved to form zirconia reinforced network of the matrix microstructure. The MII and MIII mullite crystals evolved in regions of aluminosilicate amorphous phases from the decomposed zircon grains and widely contribute to the hot flexural strength values of the refractories.

Addition of SnO_2 as a sintering aid had the effect of lowering the monoclinic – tetragonal phase transformation temperature. It however did not significantly lower the high temperature flexural and strength properties of the AZS refractoriness. SnO_2. While refractoriness and refractories under load was lowered by less than 2% from AZS composition without SnO2 doping, the hot temperature behaviour of AZS compositions doped with SnO_2 exhibited flexural strength properties after reaching maximum expansion that can be related to good creep properties.

The physical and thermo-mechanical properties of the developed refractories compositions from this research were superior to the reference PSR-315 and PSR-333 compositions proving the commercial research impact of this research. Therefore, the next part of the study set up to investigate the chemical properties of the developed compositions and compatibility in glass melts by conducting static and dynamic corrosion tests.

7 Static & Dynamic Glass Corrosion of AZS/AZS-Sn Refractories

7.1 Introduction

In answer to the part of the research question of producing a sustainable refractory composition with superior physical, thermos-mechanical and chemical properties than the standard refractories widely used in the forehearth and as expendable products for the glass industry, Chapters 5 presented an optimised slip cast refractory compositions, AZS-01, that had a stable slip properties which exhibited enhanced physical and thermomechanical properties upon firing as compared to the standard commercial PSR-315 and PSR-333 refractories used as reference materials.

In chapter 6, the study presented two novel slip cast compositions; SnO_2 doped AZS refractories, AZS-T1 and AZS-T2, which are derivatives from the AZS-01 and AZS-03 refractory compositions, which exhibited tailored interlocked mullite-zirconia microstructures of the matrix analogous to the fused cast skin microstructure highlighted in section 1. The AZS-T1 and AZS-T2 refractories also demonstrated more enhanced physical properties and thermo-mechanical properties than the AZS-01 refractory. These physical and thermo-mechanical properties of the developed refractories compositions from this research show and prove the commercial research impact of this research.

In this chapter, the chemical properties of the developed composition AZS-01, AZS-T1 and AZS-T2 were evaluated to determine their chemical compatibility in SLS and Borosilicate glass to answer the last part of the research question on producing sustainable refractories during their application in the glass furnace. From the literature review, it has been shown that the main properties that determine refractory application in glass furnaces are;

- The rate of dissolution of the refractory;
- The defect potential of the refractory; and
- The chemical contamination potential of the refractory

The dissolution or corrosion of the refractory determines its service life span while the defect potential of a refractory in producing glass defects such as stones (insoluble refractory crystals in glass), blisters/seeds/bubbles and cords (local glass of different composition and refractive index) will determine the quality of the glass [5,12,102-104].

Therefore, the first section of this study evaluated the refractory-glass compatibility of the developed refractories and their defect forming potential. This was accomplished by conducting static corrosion studies of the refractories in borosilicate and SLS glass melts. For the second and final part of the study, the corrosion and erosion of the refractories were evaluated and compared against the PSR commercial refractories as references.

7.2 Corrosion of Refractories

7.2.1 Effect of Alkali and Alkaline Earth

7.2.1.1 Methodology

Three borosilicate glass compositions (A; B & C) with increased Na_2O content were used to evaluate the corrosion behaviour of the two AZS refractories. The chemical properties of the glass compositions used in this static corrosion studies are given in table 4-7. Crushed cullet of a borosilicate (PYREX 7740) glass was used as the reference base glass and identified as composition A in this study.

Thereafter, subsequent batches of Pyrex glass compositions B and C, with increased Na_2O content of ~ 9wt. % and 12wt. % respectively, were prepared by adding soda ash ($NaCO_3$) to the powdered Pyrex glass cullet.

Normal glass batch calculations were used to determine the subsequent glass batch compositions with increasing soda content. Na_2CO_3 (99.9%, Aldrich Chemicals); was used as a source of Na_2O and as such a gravimetric factor of 1.71 was used to determine the batch weight of soda needed to make up the desired molar glass composition.

7.2.1.2 Analysis of corrosion profiles.

Preliminary visual analysis of the sectioned PSR-315 and AZS-01 static corrosion cup samples, see figure 5; do not show any noticeable corrosion for both refractory materials to the borosilicate glass composition A. This indicates excellent glass-refractory compatibility of both refractories at the test temperature of 1370 °C.

For the AZS-01 refractory, glass/refractory interface profile does not give any discernable melt line corrosion or upward drilling on the vertical side walls of the refractory to all three-borosilicate glass compositions (A, B and C) which showed good glass/refractory compatibility with all 3 glasses. For the reference refractory, PSR-315, only slight significant flux line corrosion was noticeable in the glass composition C with about 13wt% Na_2O.

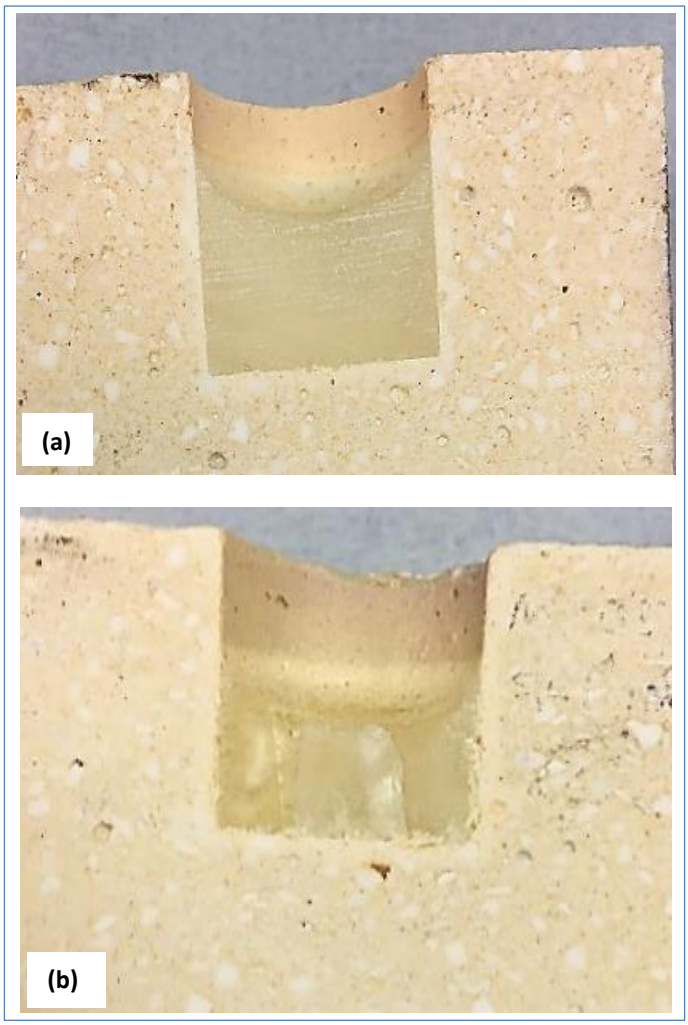

Figure 7-1: Sectioned static corrosion cup test samples highlighting the glass-refractory interaction.
(a) MP5 in Pyrex glass composition A;
(b) PSR-Ltd in Pyrex glass composition A;

Glass-refractory flux line corrosion at the triple point is known to be a melt, surface tension and density gradient, driven refractory corrosion mechanism (Marangoni effects); that occurs in the meniscus of the glass melt and its rate, according to Hrma [107], is proportional to the viscosity terms (η^{-3} and $\eta^{-3/2}$) of the glass.

Therefore, the absence of any significant flux line corrosion on the two refractories suggest that the relatively high glass viscosities, η, of glass compositions (A – C); are not significantly reduced by concentration changes from dissolved refractory to affect the rate of flux line corrosion, buoyancy and surface tension free convections.

The viscosities (η), of the three borosilicate glasses A, B and C at 1370 °C, with calculations based on a Global Statistical Modeling Approach, are 2.0 Pa.s; 1.7 Pa.s and 1.6 Pa.s respectively. This is plausible given the non-linear composition-viscosity effects of most common glasses; where any further additional increase of alkali to the glass composition do not significantly change the viscosity of the glass than from the initial alkali addition [12,13].

Viscosity of glass, however, is known to be significantly reduced from mixed modifier effects resulting in enhanced flux line corrosion which agrees with results from the second part of this study (to be presented in a future paper) where visible and measurable flux line corrosion appear in refractory samples tested in Pyrex glass composition with added lime (CaO) content.

Figure 7.2 shows the post mortem analysis of the glass-refractory corrosion profiles of PSR-315 and AZS-01 refractories in borosilicate Pyrex glass compositions, A – C, with increasing alkali content.

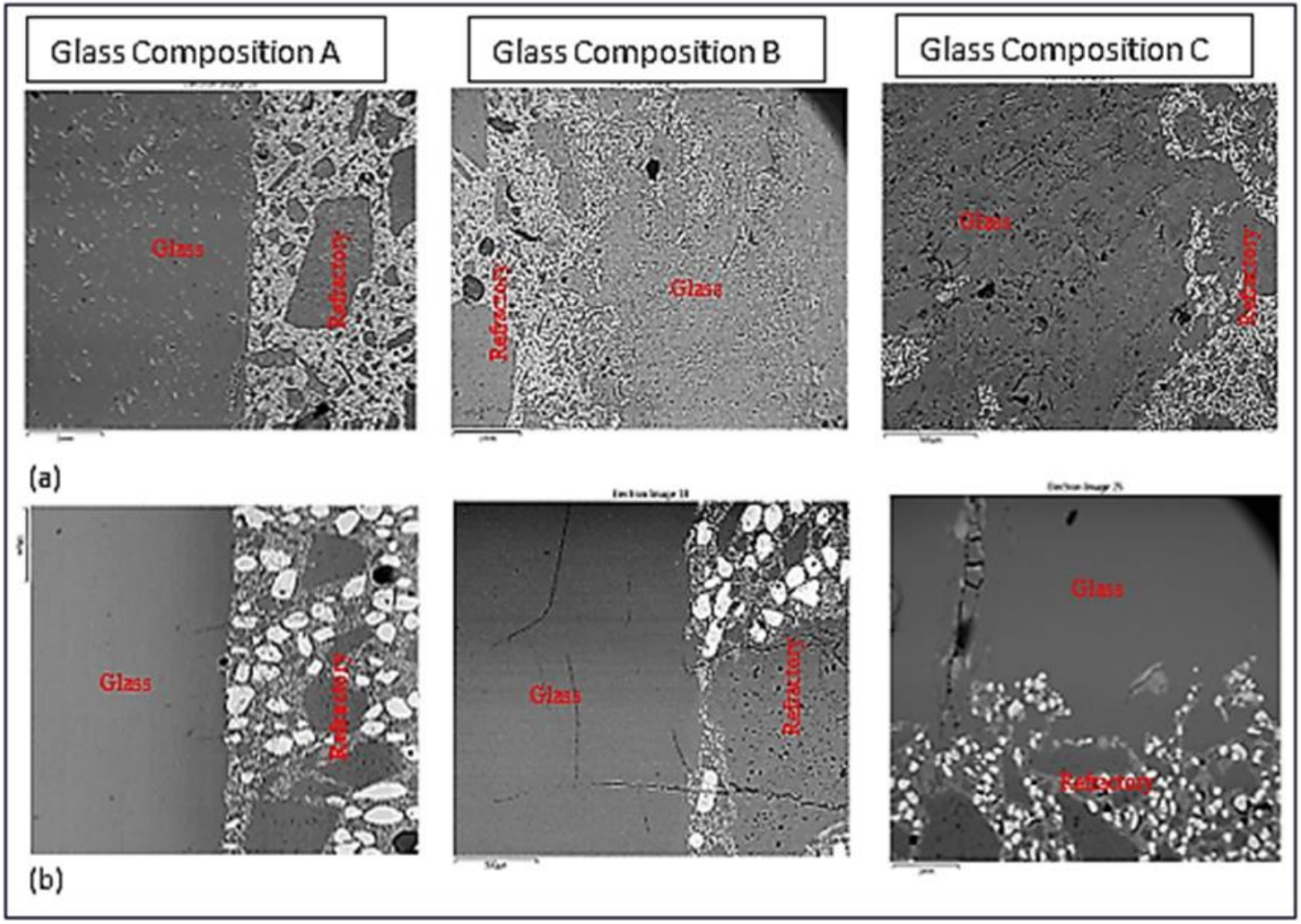

Figure 7 2: Glass-refractory compatibility. SEM micrographs of (a) PSR-315 and (b) MP05 refractory showing the glass-refractory interface profiles after static corrosion test to standard Pyrex glass compositions A; B and C; (i.e., with 4.7wt%; 8.2wt% and 11.6wt% Na2O content respectively).

They reveal four distinct regions or zones that are similar to the schematic described by Lee and Zhang [61]; as well as those highlighted in post mortem examination of refractories in CAS, SLS and Lead Silicate glasses [73-76,96,112]. These are the unaltered refractory; interaction/penetration zone; glassy boundary phase; and the parent glass regions respectively. In glass composition A, both refractories exhibit similar, smooth glass-refractory interface profiles showing relatively no localized corrosion over the entire length of the interface.

However, in glass compositions B and C, with the increased soda content, some extensive localized corrosion on the glass-refractory interface of the PSR-315 refractory has occurred which results in the formation of rough glass-refractory interface profile. In contrast, the AZS-01 refractory, still shows a smooth glass-refractory interface with no localized corrosion for all glass compositions (A, B and C) used in this study. High magnification SEM analysis and EDX mapping of the refractory regions adjacent the glass-refractory interfaces of the two AZS refractory products, are shown in Figure 7.3; showing the 'penetration/interaction glass/refractory zone'. This zone represents and is regarded as the zone of interest when studying the corroded region of the refractory. EDX elemental mapping and linescan analysis was used to show evidence and the extent of corrosion of the refractories, as a function of glass constituents' penetration into the refractory region and for any dissolution of refractory mineral phases into the glass.

The composition and microstructure of the parent refractory within this region, for the two AZS refractory products, is severely altered. The crystalline (α-alumina) phase corundum grains from the PSR-315 refractory in the penetration zone are completely dissolved, with Al^{3+} ions diffusing across the interface into the glass

region and the Na^{+}; $B_2O_3^{2-}$and SiO_4^{-}glass constituents, have diffused or penetrated the subsurface of the AZS refractory-glass interface toward the refractory region. Semi-quantitative EDX reveal an increased Al_2O_3 content in the glass (5.1 wt. %) when compared with the initial glass composition (2.3wt. %).

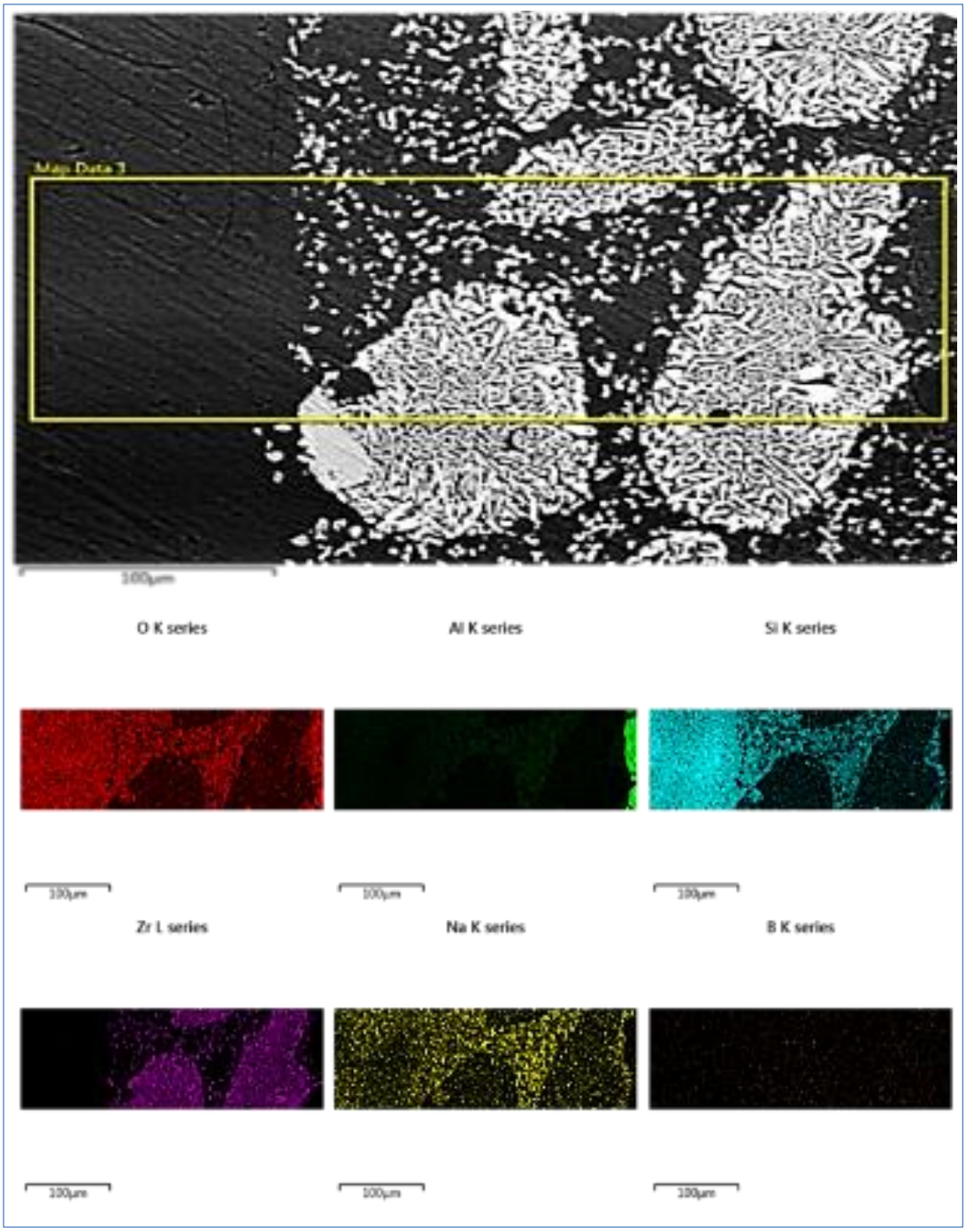

Figure 7-2: SEM EDX mapped regions of the glass-refractory interface and penetration zone of (a) AZS-01 Elemental mapping highlighting the ingress of glass constituent into the subsurface of the refractory regions. ZrO_2 (bright white grains); $ZrSO_4$ (light grey); Glass phase (dark grey-black)

Figure 7.3 further shows that considerable dissociation of zircon grains to SiO_2 and ZrO_2 with EDX identifying the bright white grains as zirconia and the remaining undissociated primary zircon are seen as light grey and the glass as dark. Zircon grains have dissociated into amorphous SiO_2 and ZrO_2 crystals according to the zircon dissociation reaction:

$$ZrSiO_4 = ZrO_2 + SiO_2. \quad (31)$$

Therefore, in this study, the dissociation of zircon grains occurring in the two AZS materials when in contact with molten glass over a long period can be thought to be have been influenced by the reaction with Na^+ and $B_2O_3^-$ ions from the glass melt and the excess free Al^{3+} ions from the dissolved crystalline alumina, reducing the activity of the free SiO_4 from the glass. The resulting microstructure varies significantly between the two AZS refractories although they have similar initial mineralogical makeup.

The resulting microstructure of the penetration zone for the PSR-315 refractory consists of interspersed small monoclinic zirconia crystals within a sodium aluminosilicate glass matrix. For the AZS-01, the penetration zone consists largely of large interlocked monoclinic zirconia crystals with thin siliceous glassy phase between the crystals and some interspersed small zirconia crystals analogous to the microstructure of a High Zirconia Fused Cast (HZFC) refractory [74].

Figure 7.4 shows the EDX linescan analysis that was conducted on the same regions of the PSR-315 and AZS-01 as the elemental map regions highlighted in figure 7, to evaluate the depth of the penetration zone and the relative concentrations of the glass constituents within this zone.

Figure 7-2 shows that the depth of corrosion for the PSR-315 refractory is more extensive than that of the AZS-01 refractory with $B_2O_3^-$ ions having penetrated farthest than Na^+ or SiO_2^- from the glass. This is because B^{2+} has a higher diffusivity than Na^+ or SiO_2^- ions in glass. The depth of slag penetration through refractory pores or capillaries, expressed as an integral solution of Poiseulle's law (equation 2); has been shown by various studies to be dependent and proportional to the pore diameter under isothermal conditions [75-79].

$$h^2 \ \alpha \ \{d^{\cdot}\sigma_{LV} \cos\theta / (4\eta)\} \ldots\ldots\ldots\ldots\ldots\ldots\ldots\ldots\ldots\ldots\ldots\ldots\ldots\ldots\ldots\ldots\ldots\ldots\ldots\ldots. (32)$$

where; h, is the liquid penetration depth; d, is the pore diameter; η, the dynamic viscosity; and σ_{LV}, the melt surface tension; and θ, the contact angle. Under isothermal conditions, η; σ_{LV}; and θ, are all constant, and hence from eqn. 2;

$$h^2 = k \cdot d \ldots\ldots\ldots\ldots\ldots\ldots\ldots\ldots\ldots\ldots\ldots\ldots\ldots\ldots\ldots\ldots\ldots\ldots\ldots\ldots\ldots\ldots\ldots\ldots\ldots\ldots\ldots. (33)$$

Therefore, for the commercial AZS-01 refractory with a higher apparent porosity and amorphous phase content in the microstructure, there is enhanced glass melt ingress into the refractory region and exposure of the mineral phases of the refractory to corrosion. As well, a great depth of penetration of a large amount of slag is evidence that the texture of the refractory is poor [14]. Another reason for the difference in the depth of penetration in the PSR-315 and AZS-01 refractories may be due to the higher mullite content of the AZS-01 refractory. Boron is known to form a solid solution with mullite and has been used as a furnace lining for boron rich glasses [30]. Therefore, it can be thought that higher mullite content can react with B_2O_3 to form boron-mullite solid solutions reducing the chemical activity of B^{2+} ions in the glassy phases, thereby mitigating the corrosive/fluxing effects of borosilicate glass.

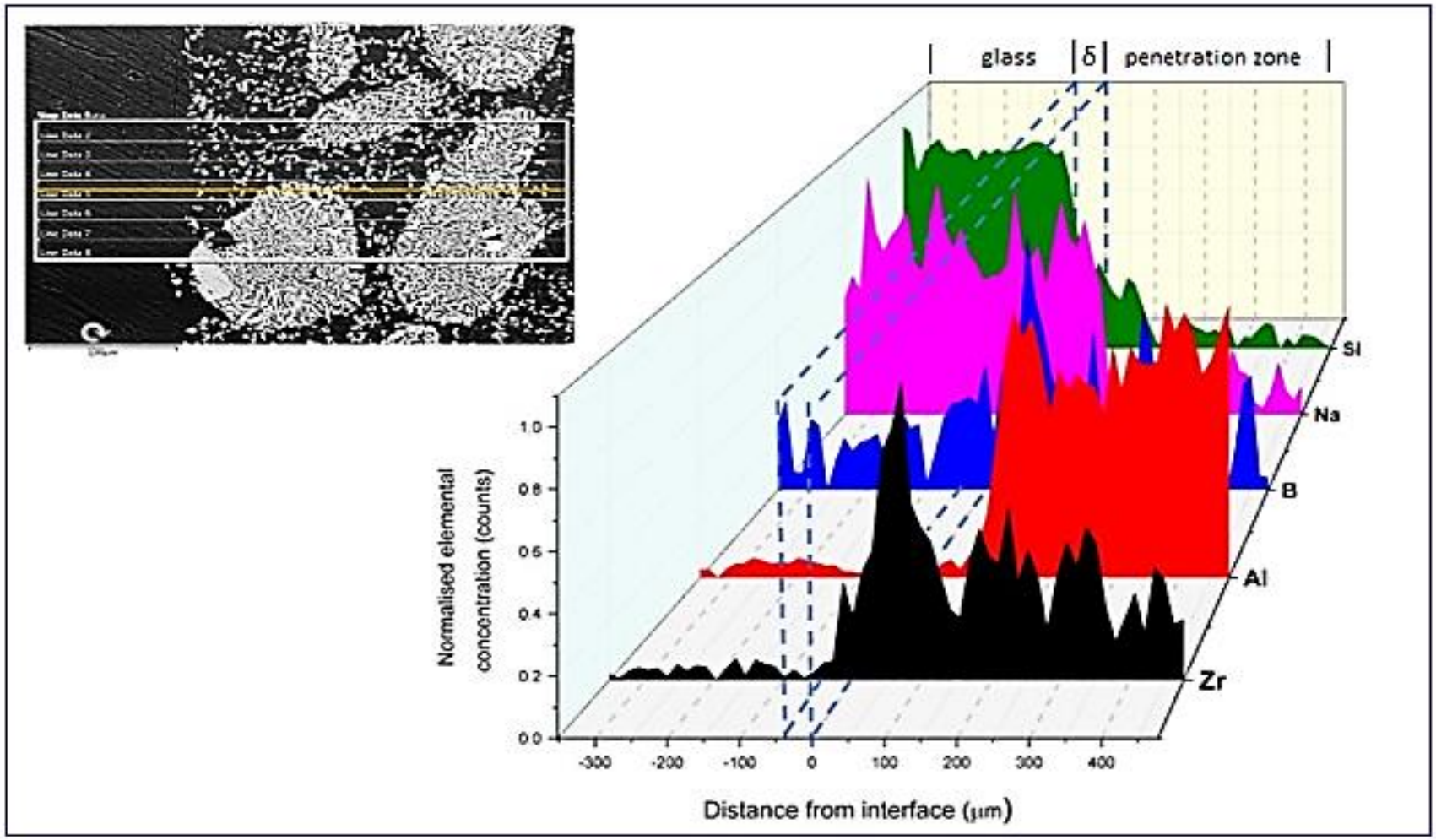

Figure 7-3: EDX elemental concentration profiles along the orange scan line over the same mapped region of the AZS-02 penetration zone highlighted in figure 7-3

Figure 7.4 further shows the presence of a ZrO_2 rich sodium-aluminosilicate boundary glassy layer, δ, adjacent the glass-refractory interfaces of the PSR-315 and AZS-01 refractories. For the PSR-315 refractory, the thickness of the glassy layer is ca.120µm while that of the AZS-01 is ca.30µm. When the rate of chemical reaction is faster than the rate of reaction product removal from the interface, a solute rich boundary layer is formed [75,79,81]. This boundary layer is a reaction product interlayer from the reaction between the glass melt and refractory constituents. Therefore, the thin boundary layer can be attributed to the resulting coarse grained interlocked zirconia microstructure phase at the glass-refractory interface (the so-called zirconia rich barrier region) which provide a chemical barrier acting two-fold diffusing ions towards the reaction front and the reaction products from the refractory into the bulk glass.

7.2.1.3 Corrosion Mechanism

Refractory dissolution or corrosion mechanisms and the formation of a boundary layer in different glass-refractory systems have been extensively described by Dunkl; Lee and Zhang; and, Cooper and Kingery [61,74,81,104]. Corrosion is known to proceed through microstructural regions/phases of weakest resistance. Therefore, the matrix region which contains much of the porosity and amorphous phase content of the refractory microstructure offers the weakest points within the microstructure for ease of glass attack and subsequent penetration into the subsurface layer of the refractory-glass interface by capillary action through the open pores of the refractory. [61, 81, 104].

This means that in this study, at the glass melt/refractory reaction front, when the two PSR-315 and AZS-01 refractory materials were in contact with the standard

borosilicate Pyrex glass composition **A**, initial wetting of the refractory hot face by the glass occurred at and around the pores and glassy phase regions of the refractory. Therefore, the PSR-315 refractory hot face was more wetted by the glass resulting in the Na^{+}, $B_2O_{3,}$ and SiO_2 glass constituents penetrating within the subsurface of the glass-refractory interface, reacting with and dissolving the refractory mineralogical phases present.

When the PSR-315 refractory mineral phases were exposed to such aggressive fluxing environments, the amorphous phase was the first to be attacked and easily fluxed by $B_2O_3^{2+}$ and (Na^{+}, Ca^{2+}..,) ions forming variations in local melt compositions adjacent to the crystalline phases present (i.e., mullite, alumina, zirconia, zircon...,) each with differing solubilities [20,29]. Depending on the relative fractions and extent of dissolution of each mineral phase that make up the refractory microstructure, selective dissolution of the glassy, mullite, corundum and to a lesser extent, zirconia phases of the refractory, would result in the increase of these pockets of localized corrosion at and beyond the reaction front.

Therefore, when the Na_2O content of the borosilicate glass was increased from glass A – C, the viscosities of the fluxed glassy phases are further reduced, which influences and enhances the ionic diffusivities of the B_2O_3, Na_2O, SiO_2 glass constituents leading to their penetrating farther into the refractory region and corroding the refractory. This explains the smooth interface profile exhibited by both the AZS-01 and AZS-02 refractories to the low alkali borosilicate Pyrex glass composition A and manifestation of a rough interface profile from the AZS-01 refractory to borosilicate glasses (B and C) with an increased Na_2O content as shown in figure 3.

7.2.1.4 Effect of Increased Alkali content and Glass Defect forming Potential

The next stage of the study focused on the effect of increasing the alkali content of the borosilicate glass on the rate of corrosion of the PSR-315 and AZS-01 refractories and any potential of forming glass defects. The rate of corrosion of the AZS refractories in borosilicate glass with increased alkali content was plotted in figure 9 as a function of the depth of penetration by Na_2O.

Results of the measured maximum depth of penetration of Na_2O in the penetration zones of PSR-315 and AZS-02 refractories from each of the three borosilicate glasses (A, B and C) were used to plot figure 7.5. The results show that the extent of penetration was greater for the standard PSR-315 refractory when compared to the AZS-01, exceeding 2500µm in depth from the glass-refractory reaction front compared to 1200µm for the AZS-01 in borosilicate glass C. Increased alkali content results in more glass fluidity and penetration of fresh glass constituents across the boundary layer into the refractory region.

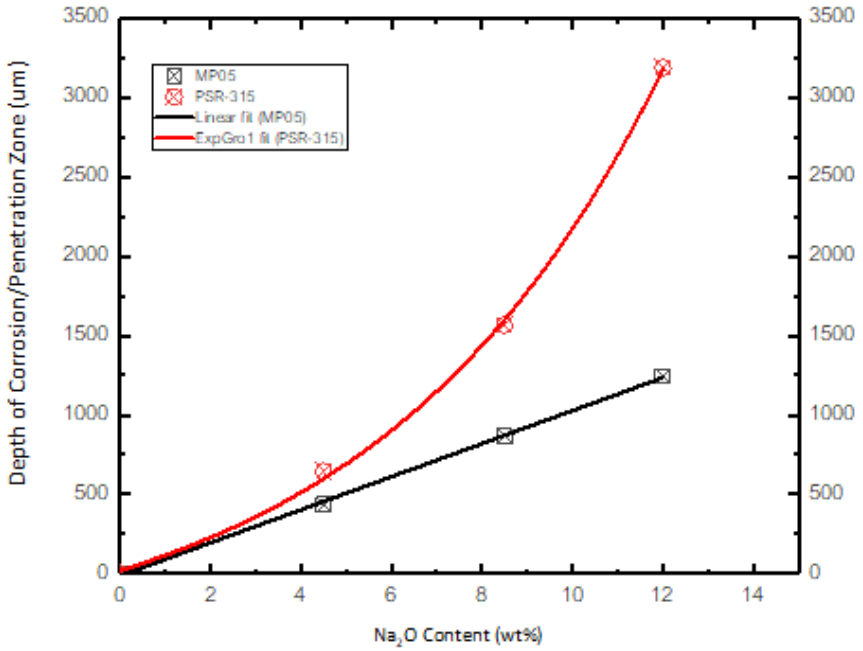

Figure 7-4: Hot corrosion of PSR-315 and MP05 refractories in borosilicate glass melt as a function of depth of glass penetration with increased alkali content at 1370C for 72hours.

Figure 7.5 shows that AZS-01 with lower porosity (14%) and higher bulk density follows a linear rate of corrosion whilst PSR-315 follows a parabolic corrosion rate. This correlation is in agreement with observations made by many other workers [7, 14,15, 31] which showed that a linear rate of increase in refractory slag corrosion for an apparent porosity in the range of 12 – 18 %. The reference refractory PSR-315 with a higher porosity of 20% and an amorphous phase content of 19wt.% in its microstructure presented a weaker region for glass attach and this was attributed to a greater penetration zone' as a function of Na_2O content for borosilicate glasses. With an increasing alkali content, decreasing viscosity of the borosilicate glass melt ensues and the viscous boundary layer is reduced as a result. This can lead to further penetration of the glass constituents into the refractory.

The effect of improved densification, lower porosity and microstructural texture as a result of an optimized particle packing in the AZS-01 refractory can be clearly seen. Figure 3.5 highlights potential glass product defects such as stoning in the PSR-315

refractory exposed to the borosilicate glass compositions B and C respectively because of extensive localized corrosion at and beyond the glass-refractory reaction front leading to a rough or non-uniform interface. For the AZS-01, as corrosion rate increases with increase in alkali content in the glass, the localized fluid pockets adjacent to the refractory mineral phases, act to dissolve the mineral phases thereby further degrading the cohesiveness of the refractory structure and allows the gradual separation of recrystallized fine grain zirconia grains. This follows the same observation made by Guyolan and Pustyl'nikov [76]. However, for the AZS-01, the interlocked coarse insoluble zirconia crystals at the interface and penetration zone act to prevent further corrosion of the refractory.

According to Woolley [111], the corrosion rate of a refractory corroded by various glasses of the same chemical family is approximately proportional to the glass melt viscosity/fluidity. Trier [115], observed that both the corrosion rate and glass fluidity doubles for each 50 – 100°C increase in interface temperature. Therefore, considering these observations, the corrosion rate data, as a function of glass constituents' penetration depth into the refractory subsurface for each of the borosilicate glass compositions A – C, was extrapolated and plotted over the melting temperature range of borosilicate glasses as shown in figure 7.6.

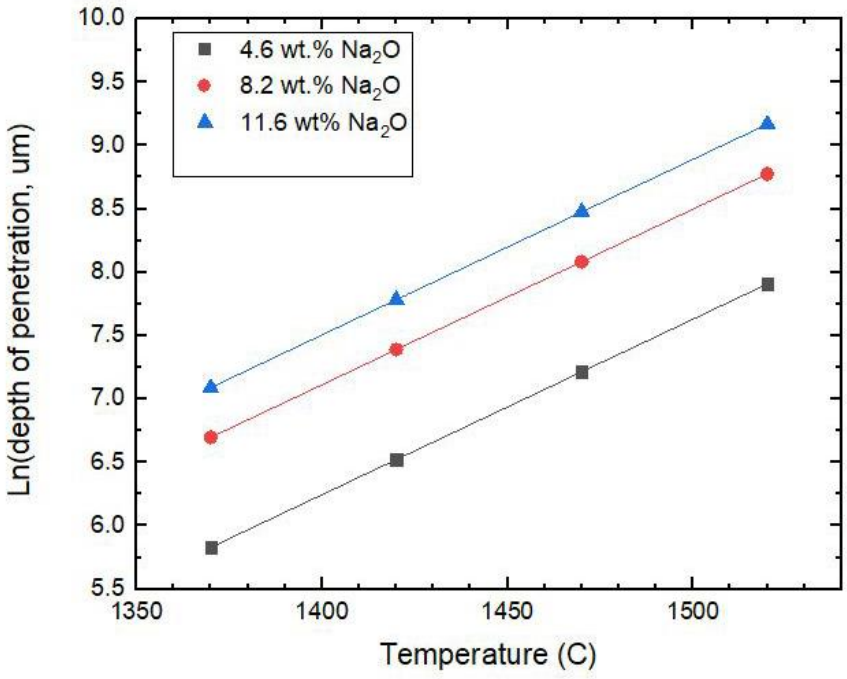

Figure 7-5: Extrapolated data showing the effect of increased temperature on the corrosion of an AZS-01 refractory as a function of glass penetration

The plot highlights possible glass compositions and service temperature ranges to which the AZS-01 can offer excellent glass-refractory compatibility. From the extrapolated plot, figure 7.6, the AZS-01 refractory is expected to exhibit excellent glass compatibility with low glass product defect potential for borosilicate glass composition with an alkali content of 12 wt. % up to a temperature of 1450C.

7.3 Seeding/Bubbles Defect forming Potential

Refractory AZS-01 was evaluated for its compatibility in soda-lime silica and borosilicate glasses against any glass defect forming potential due to seeding or bubble formation. A zircon refractory that is commonly used for borosilicate glass contact applications was also used as a reference refractory together with PSR-315. Potential glass defects in the form of bubbles were only visible and present in the zircon refractory, PSR-966, for both the two glass melt compositions A and B tested as shown in figure 7-7.

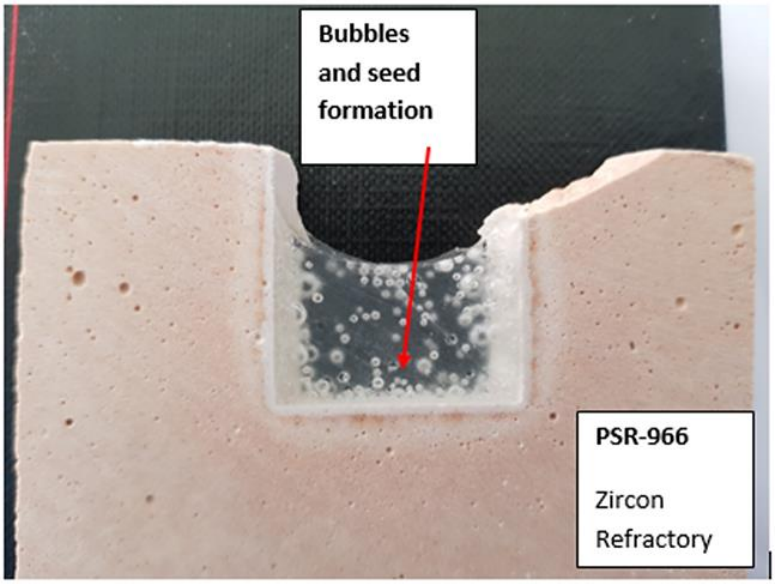

Figure 7-6: Section static corrosion cup sample of a standard zircon refractory composition, PSR-996. Figure shows the formation of bubbles and seeds in the borosilicate glass composition A tested at 1370C for 72hrs.

The sizes of the bubbles range from micron size to a few mm, which is large enough for products to be rejected as defects [3, 6, 23]. Glass bubble formation within glass melts is well known to be caused by glass batch material decomposition at temperature and or electrochemical reactions between the glass and refractory ions. Hence, the addition of Na_2CO_3 to the Pyrex glass cullet in producing the borosilicate glass composition B, could have been the source of bubble formation in the glass.

However, the occurrence of bubble glass defects in Pyrex borosilicate glass composition A, suggests that the major source of these bubble formation as originating from either; the redox reactions between the glass constituents and the polyvalent ionic impurities (e.g., $Fe^{3+\ /\ 2+}$; $Ti^{4+\ /\ 2+}$) of zircon, concentrated in the siliceous glassy phase of the refractory; and or the trapped gases in the refractory pores [23, 24]. Glass-refractory interaction at the interface results in cations from the glass migrating into the subsurface of the refractory and with it, electrons from the interface, to balance the positive charge induced in the refractory. The polyvalent

ionic impurities such as Fe^{3+} are reduced by the electrons and oxygen is given off [23, 24].

An interesting observation is that the two AZS refractories, consolidated from the same zircon batch raw material used to consolidate the zircon PSR-966 refractory, do not form any potential glass defect bubbles in all the three borosilicate glass compositions A, B and C tested.

We have not investigated on this further and can only suggest that probably the presence of high α-Alumina content in the AZS refractories' formulation may aide in scavenging the siliceous phase to form mullite. Now, as point defects in both these structures results in oxygen vacancies, oxygen $O_{2(g);}$ adsorption or incorporation into their structures to form lattice O^{2-} is possible through migration of these vacancies and the subsequent reduction reaction of the surface vacancies and the adsorbed oxygen. This is the mechanism for oxygen incorporation in solid oxygen fuel cells (SOFC). Also, since it follows that bubble formation within glass results only when the $O_{2(g)}$ from the redox reaction diffuses through the interface and boundary glass layer into the glass, the presence of alumina together with the zirconia crystals form a diffusion barrier to the glass cation constituent's and oxygen migration and thereby limits bubble formation.

7.4 Upward Drilling Corrosion Resistance

The upward drilling resistance of PSR-315, AZS-01 and the SnO_2 doped compositions AZS-T1 and AZS-T2 were evaluated by conducting static glass corrosion of the finger samples suspended in borosilicate glass with a zircon block at the base. Upward drilling corrosion is commonly observed in glass furnace,

especially in the refractory that is located above molten glass, for example, facer block of the throat.

Zircon refractories (ZS) are known to generate bubbles or seeds in borosilicate glass due to the reaction mechanism which is based on an internal reduction of polyvalent ionic impurities of ZS and an oxidation of oxide ions of the melt at the ZS surface as discussed in the previous section. The redox reaction proceeds via a reaction layer below the ZS surface, which forms an inherently short-circuited, internal, galvanic cell with a growing thickness [92,112,113]. The generated bubbles can give rise to upward drilling or corrosion of refractories as a result of the gas bubbles escaping. The escaping bubbles also increase glass convection which will bring fresh un-equilibrated glass to the refractory glass interface thereby increasing corrosion.

Another explanation provided for bubble generation or seeding is outgassing from the closed refractory pores in the refractory macrostructure that open up after chemical reaction of the refractory subsurface with glass constituents resulting in a potential pull of fresh gases from the refractory [54,92,111]. Therefore, to evaluate the corrosion resistance of PSR-315, AZS-01 and the AZS-T1 compositions against the alkaline borosilicate glass, the test pieces were immersed in a crucible containing borosilicate glass with a zircon block at the base and heated to and held at 1370°C for 72hrs. The samples were sectioned and analysed to evaluate the upward drilling corrosion resistance in borosilicate glass. All refractory samples of PSR-315, AZS-01 and the AZS-T1 doped compositions did not show any upward drilling holes or pitting and suggested to their upward drilling corrosion resistance in borosilicate glass. This is highlighted in figure 7-8 which shows the after corrosion test profiles of the test samples.

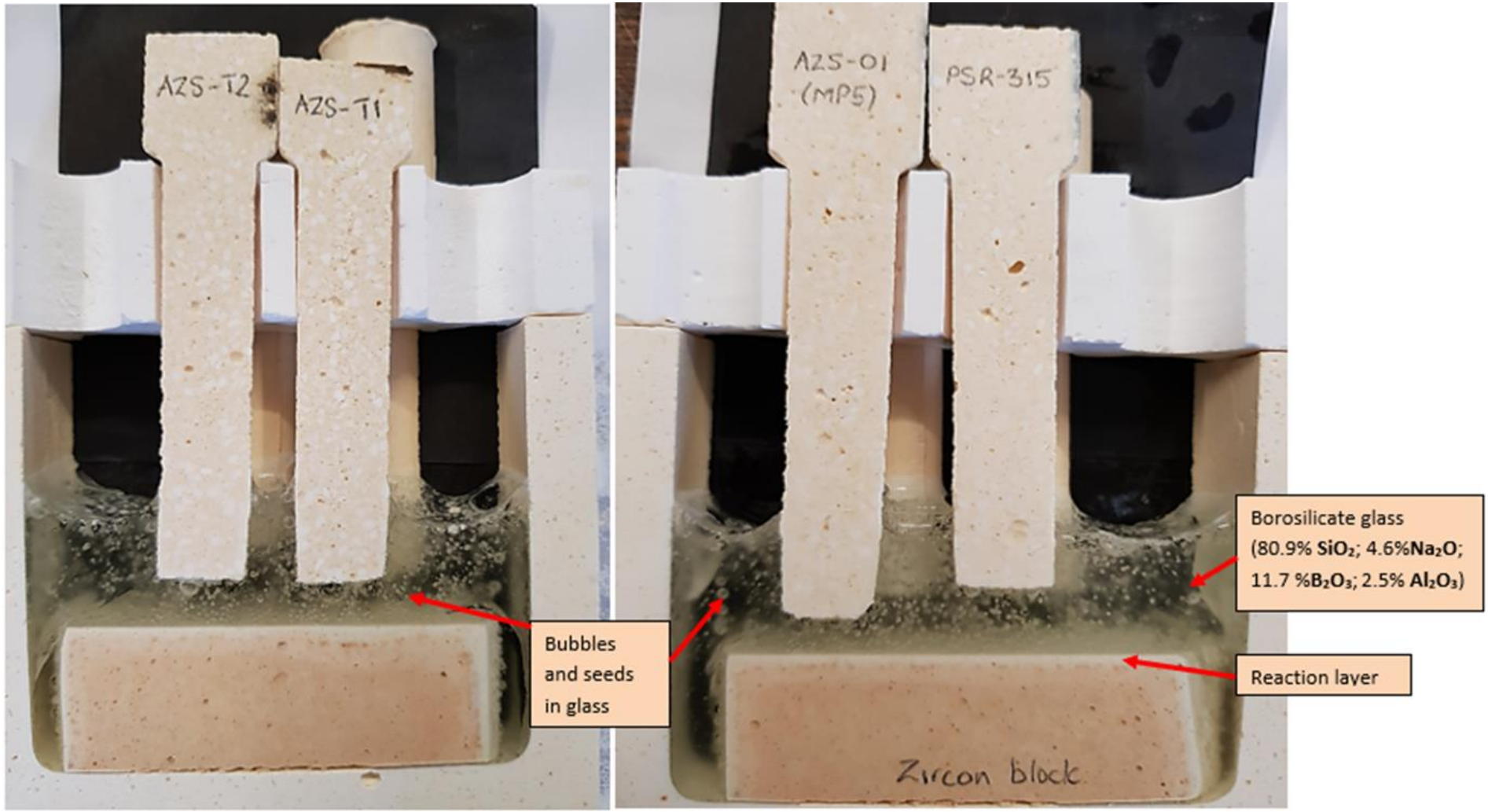

Figure 7-7: Finger samples of PSR-315, AZS-01, AZS-T1 and AZS-T2 after upward drilling corrosion tests in borosilicate glass

7.5 Effects of SnO_2 on Refractory Glass Corrosion and Service Life of the AZS refractories.

In the previous study in sections 7.1 to 7.4, we have shown how the modified refractory AZS-01, with interlocked large zircon grains and insoluble zirconia crystals of the modified AZS-01 refractory offer better protection to further corrosion of the refractory as well as low glass defect forming potential than the standard reference refractories PSR-966 and PSR-315 in borosilicate glasses with Na2O contents up to the levels of SLS glass compositions.

This next study focused on evaluating the corrosion resistance of the developed compositions AZS-01, AZS-T1 and AZS-T2 under corrosion and erosion and thereby determining the expected service life of the new developed refractories in reference to the standard refractories PSR-315 and PSR-333.

The effect of dopant, SnO_2, on the corrosion resistance of AZS refractories was achieved by conducting static and dynamic corrosion tests on the developed compositions of interest (AZS-01, AZS-T1 and AZS-T2) and the standard reference compositions in SLS glass melt, as described sections 4.2.3.1 and 4.2.3.2 respectively.

7.5.1 Methodology.

Initially, the corrosion resistance of AZS-01, AZS-T1 and the standard refractories PSR-315 and PSR-333 were evaluated through static isothermal glass corrosion of finger samples, as well as static cup samples of the respective refractory compositions as described sections 4.2.3.1 and 4.2.3.2 respectively. The flux line corrosion on the refractories was used as the point of measure of the corrosion resistance of the respective refractories. “Before and after” corrosion dimensions of

the finger samples and cup test samples were taken and the refractory with the least flux line cut presented the most corrosion resistant properties.

After, static isothermal tests, the extent of service life of the refractories were determined from dynamic isothermal corrosion tests conducted on finger sample samples of the AZS-01, AZS-T1 and standard reference refractories PSR-315 and PSR-333. The tests that best simulate the service conditions that refractories are subject to in the glass industry and can help determine the service life of the refractories are those of the dynamic corrosion test. The isothermal dynamic corrosion tests were conducted as a function of rotation speed at standard test temperature of 1370C. The rotation speeds used were 0; 1.5; 3.5; and 5.5 rpm, which corresponds to a linear flow rate of 0, 188, 438, and 688 mm min^{-1} of molten glass, respectively. Note that the standard glass flow in the glass industry is typically 180 mm min^{-1} [1,14]. The length of time for each corrosion test run was 72h.

7.5.2 Effect on Glass Corrosion Resistance

Although, static isothermal conditions are not experienced in actual service by refractory materials during glass production, they were used in this initial study, simply to compare the corrosion resistance of the refractories. In addition, as described earlier in the literature review, from [9,18,23], SnO_2 has a low solubility potential in siliceous glass melts as highlighted by the order of solubility of ceramic/refractory oxides in SLS and BSG glass melts of; $SiO_2 < Al_2O_3 < ZrO_2 < SnO_2 < Cr_2O_3$. Therefore, the study would help validate the hypothesis presented in our project objectives, that any incorporation of SnO_2; (because of its low solubility potential0; into the AZS/AZM microstructure and matrix would be expected to enhance the chemical compatibility of the SnO2-doped AZS refractory compositions in both the BSG and SLS glass melts.

Figure 7-8 shows the static cup test samples and finger samples of AZS-01 and AZS-T1 after static glass corrosion in SLS glass at 1370C for 72hr. AZS-01 presents enhanced flux line corrosion from both the sectioned static test cup samples and the finger sample, as compared to AZS-T1. This comparison shows clearly the increased corrosion resistance effects of SnO_2 doping on the corrosion resistance of AZS refractories.

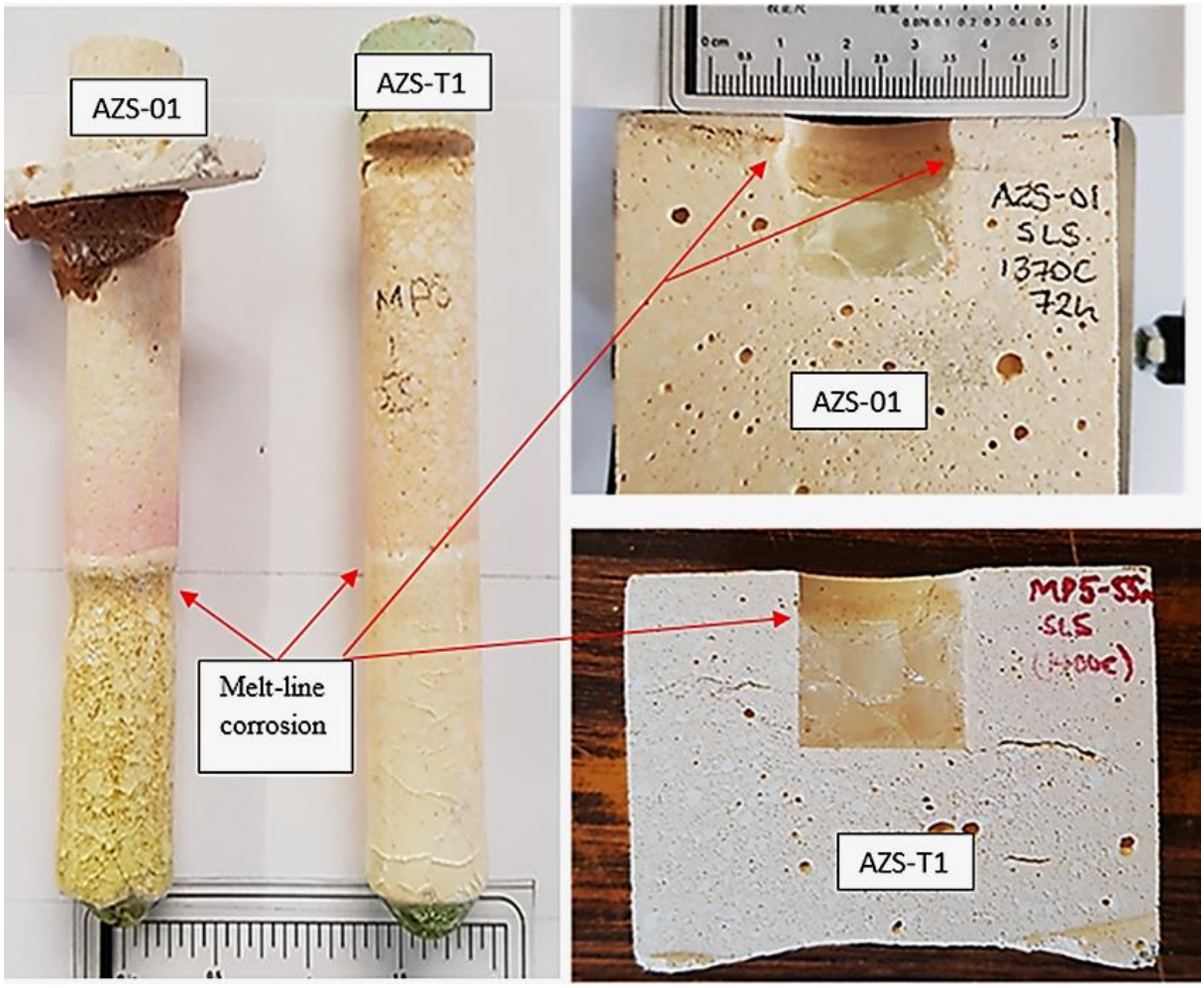

Figure 7-8: Static cup test samples and finger refractory samples of AZS-01 and AZS-T1 after static corrosion glass test in SLS glass. The increased corrosion resistance of the AZS-T1 refractory, doped with SnO_2 compared to the AZS-01 is shown by presenting the flux/melt line corrosion cuts on the respective refractories.

AZS-01 was characterised by a flux line corrosion, in SLS glass under isothermal static conditions, of circa 7.5%; while AZS-T1, had negligible flux corrosion of

about 0.3% highlighting the enhanced effects of SnO_2 on the corrosion resistance of the refractory.

The effect of SnO_2 on the corrosion resistance of the AZS compositions doped with Tin oxide was also evaluated and validated by investigating the $Zr_{1-x}Sn_xO_2$ solid solution grain from the AZS-T1 composition and the ZrO_2 grain from the AZS-01 composition that have come to chemical equilibrium with the glass after the static glass corrosion tests.

Figure 7.9 and figure 7-10 shows the AZS-01-SLS glass interface and AZS-T1-SLS glass interface respectively. Table 7-1 shows the SEM point ID semi-quantitative analysis of the zirconia grains at equilibrium with the glass.

Table 7-1: SEM EDX semi-quantitative analysis Zirconia grain in equilibrium with SLS glass highlighted in figure 7-8 and 7-9.

Element	AZS-T1	Interface	AZS-01	interface
	Grain	Glass	Grain	Glass
	Spectrum 44	Spectrum 43	Spectrum 34	Spectrum 35
	wt.%	wt.%	wt.%	wt.%
O	26.2	46.9	26.7	46.9
Al	0.00	13.2	0.0	5.8
Si	26.7	26.7	1.2	31.9
Zr	66.3	1.1	72.2	4.9
Sn	5.6	0.0	-	-
Ca	0.0	2.8	0.0	5.6
Na	0.9	9.3	0.0	4.9
Total	100.0	100.0	100.1	99.9

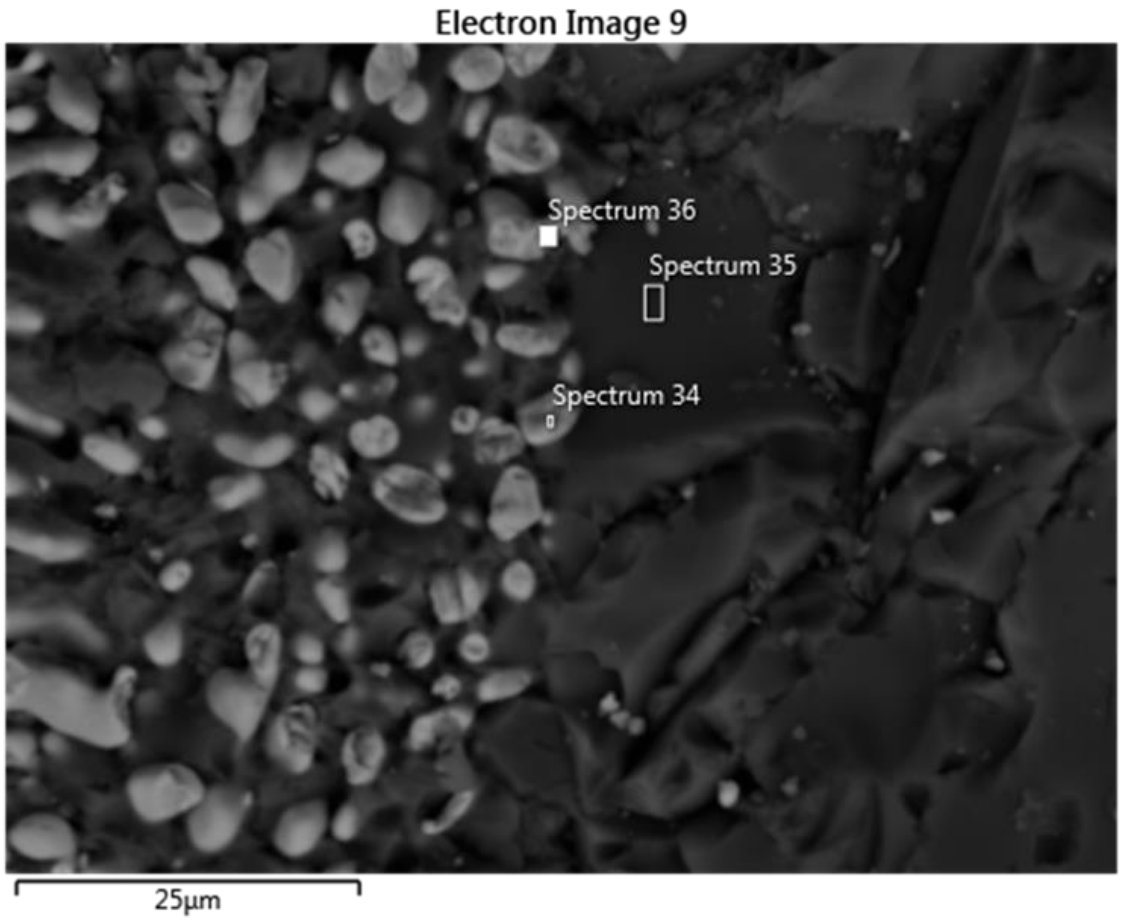

Figure 7-9: Soda lime Silicate – AZS-T1 interface showing grains of Zr1-xSnxO2 in chemical equilibrium with the glass.

In table 7-1, it is shown that about 1.1 wt. % of zirconia from the $Zr_{1-x}Sn_xO_2$ solid solution is dissolved from the refractory in the glass at the interface that makes up the boundary layer. No SnO_2 or Sn4+ ions were detected by SEM EDX quantification method to be present in the glass or at the interface. In contrast, from table 7-1, there is much dissolution of the zirconia grain from the AZS-01 refractory at equilibrium with SLS glass at the interface, presenting dissolution of about 4.9 wt. % into the SLS glass at the interface.

This shows and or validates the effect of reduced solubility potential in SLS glass of SnO2 in AZS refractories and finger and static cup tests proves this from the reduced flux line corrosion as shown in figure 7-8.

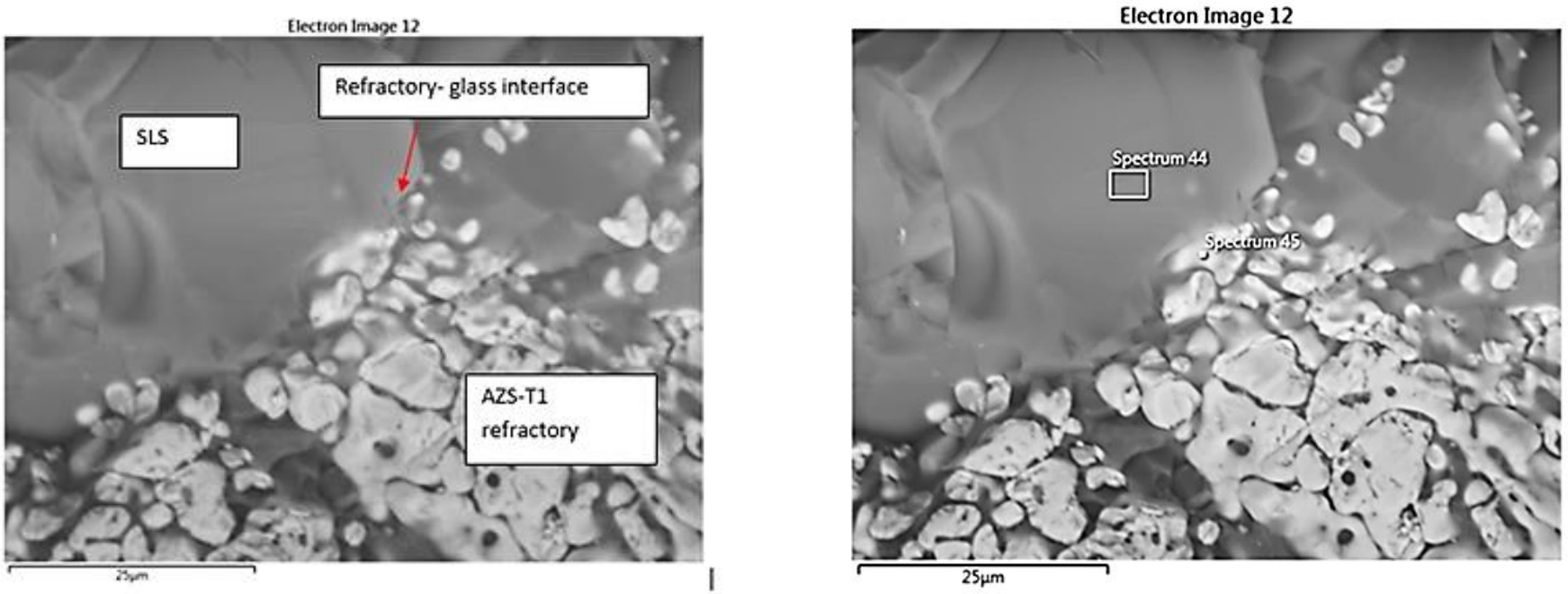

Figure 7-10: Soda lime Silicate – AZS-T1 interface showing grains of $Zr_{1-x}Sn_xO_2$ in chemical equilibrium with the glass.

7.5.3 Service Life of the AZS refractories

The "Before and After" material loss method was used to evaluate the corrosion indexes of the finger samples under dynamic conditions to estimate the length of forehearth service life of the developed refractories in reference to the standard PSR-315 widely used as a forehearth feeder refractory. The average service life of PSR-315 in industry at flow rates of 188 mm min^{-1} (~ 1.5rpm) is about 4 – 6 months depending on the glass throughput [14]. The diameters of the melt line regions of the test samples before and after the corrosion tests were measured and the materials loss calculated. The relative corrosion rate of the PSR-315 commercial refractory was taken as the reference with corrosion index = 1 (100%). The corrosion index for a test specimen sample for AZS-01, AZS-T1 and AZS-T2 was then identified according to the equation:

$$Corrosion\ index\ for\ test\ sample = \frac{[\pi\left(\frac{D_i}{2}\right)^2 \Delta l - \left(\frac{D_r}{2}\right)^2 \Delta l]_A}{[\pi\left(\frac{D_i}{2}\right)^2 \Delta l - \left(\frac{D_r}{2}\right)^2 \Delta l]_R}$$

$$= \frac{(D_i - D_r)_A^2}{(D_i - D_r)_R^2} \quad \ldots\ldots\ldots\ldots\ldots\ldots\ldots\ldots (34)$$

Where; D_i and D_r are the initial and remaining diameter of the test piece, respectively. Δl is the length of the specimen. ***A*** and ***R*** are the test piece and reference (PSR-315) piece, respectively. The fingers samples of the reference refractories PSR-315, PSR-333 and the developed AZS composition of interest refractories AZS-01 and AZS-T1; after dynamic corrosion are presented in figures 7-11 to 7-13.

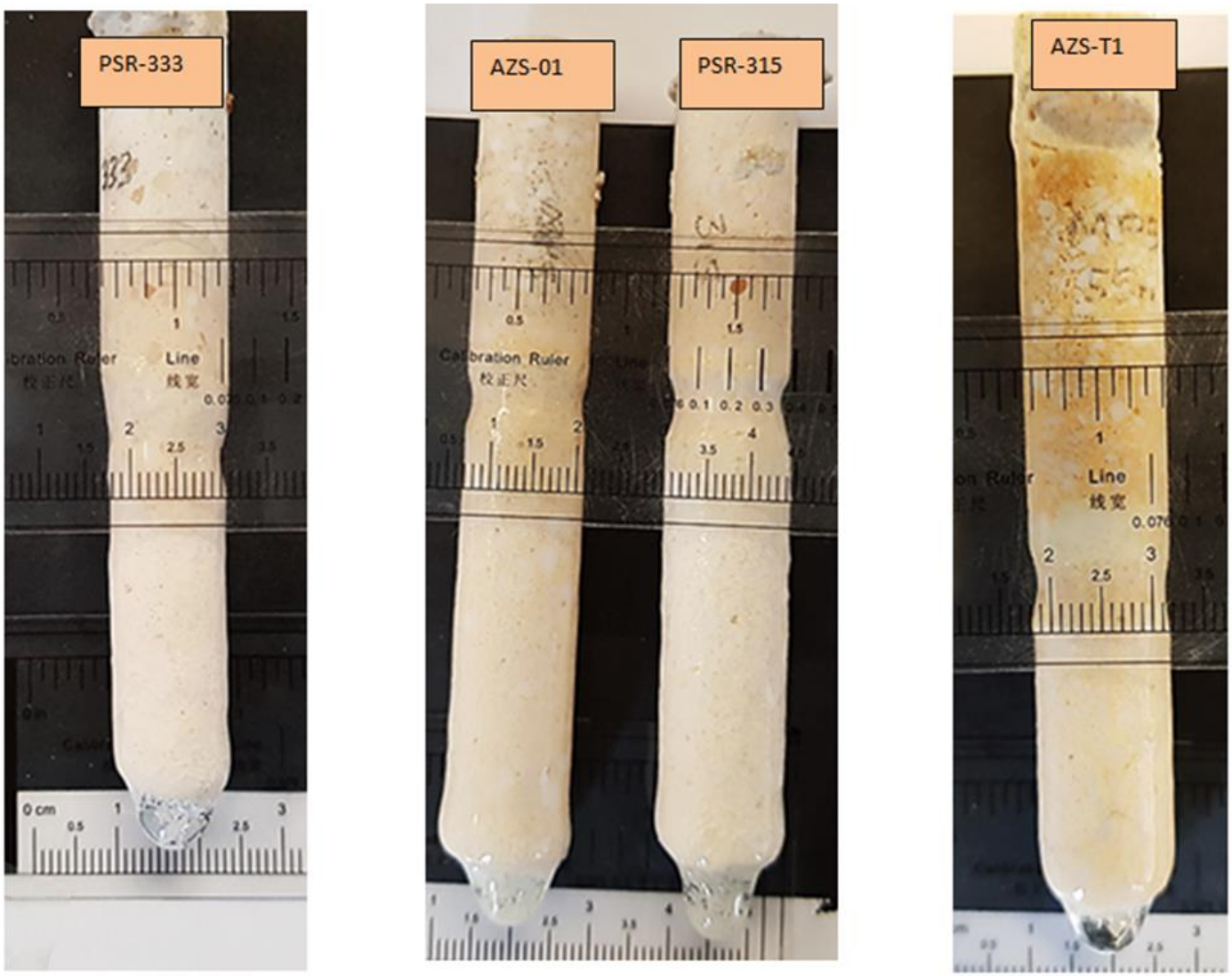

Figure 7-11: "After test" Finger corrosion samples of (a) PSR-315; (b) PSR-333; AZS-01 and (c) AZS-T1 after dynamic corrosion tests at 1370 for 72hr at 1.5rpm

Figure 7-12: Finger corrosion samples of (a) PSR-315; (b) PSR-333; AZS-01 and (c) AZS-T1 after dynamic corrosion tests at 1370 for 72hr at 3.5rpm

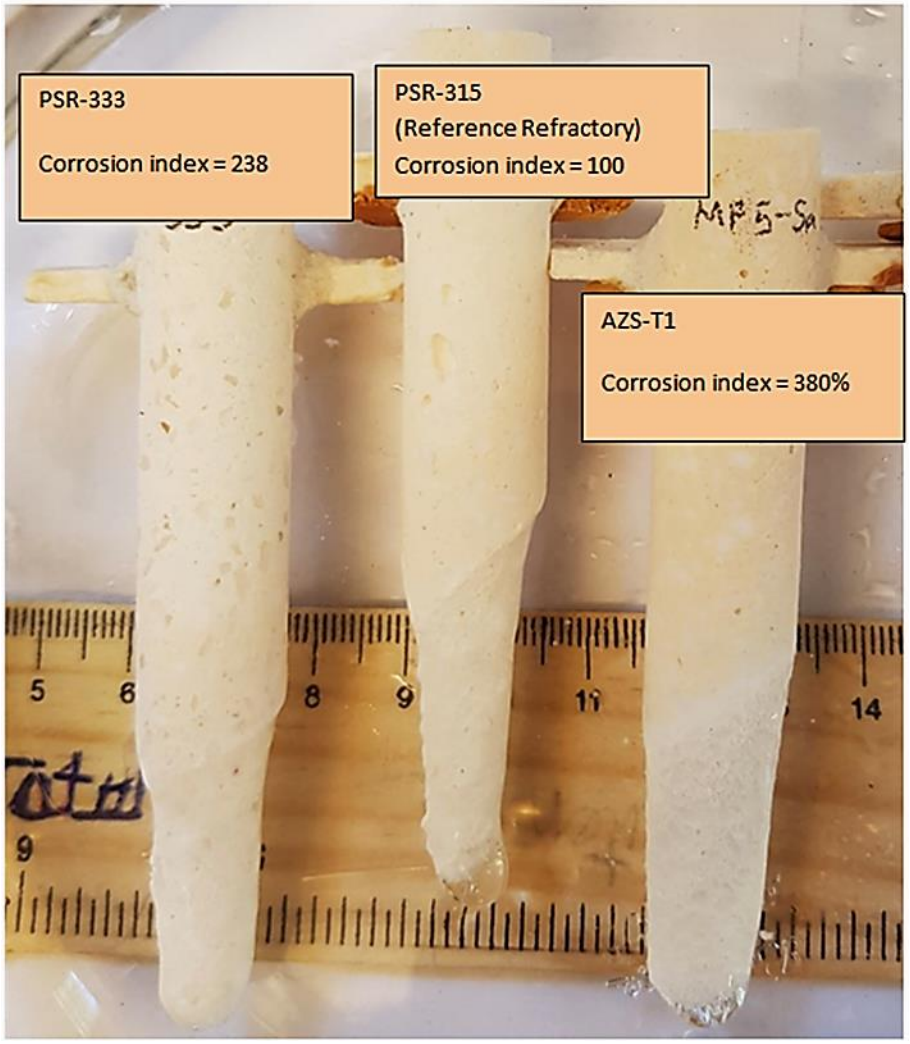

Figure 7-13:Finger corrosion samples of (a) PSR-315; (b) PSR-333; AZS-01 and (c) AZS-T1 after dynamic corrosion tests at 1370 for 72hr at 5.5rpm

Table 7-2 shows the calculated corrosion index of PSR -315, PSR-333, AZS-01 and AZS-T1 from dynamic glass corrosion tests in SLS glass. The higher the corrosion index of the refractory, the more corrosion resistant it is to the glass tested [14,51,65]. From the table it can be seen that at industrial glass flow rate of 187.5 mm/min (1.5rpm), AZS-01 presents improved corrosion resistance in SLS glass with expected increase in service life of about 30% from that provided currently by PSR-315. With an increased glass flow rates of about 437.5mm/min as from huge glass pull rates/ throughput; the service life of AZS-01 is improved from that of PSR-315 by about nearly twice the service life of PSR-315. This can be due to the interlocked zirconia grains at the glass refractory interface presented in section 7.3 from the optimised AZS-01 microstructure that prevents erosion of the refractory grains and reduces the corrosion rate of the refectory as compared with PSR-315.

Table 7-2: Calculated corrosion index of AZS-01, AZS-T1 and the standard PSR-Ltd refractories, from dynamic glass corrosion tests in Soda Lime Silica (SLS) glass melt.

Sample	Corrosion index of Refractories under SLS Glass Flow (mm/min)			
	0	187.5 (1.5rpm)	437.5 (3.5rpm)	687.5 (5.5rpm)
PSR 315	100.0	100.0	100.0	100.0
PSR 333	120.9	100.6	254.5	238.1
AZS-01	151.7	129.8	284	
AZS-T1	216.4	157.7	350.7	380.0

AZS-T1 shows enhanced corrosion resistant behaviour in SLS glass from the finger corrosion test samples under different flow rates, as shown in figures 7-11 to 7-13. This is further highlighted in the corrosion index of AZS-T1 for all SLS glass flow rates of 158%, 350% and 380% than PSR-315.

8 Conclusions

From the experimental studies and analytical work that was conducted in this research the following conclusions are summarised below.

- In the preliminary studies, developing AZS formulations with self-flow properties with the use of the Dinger and Funk model for particle packing, a distribution modulus (q-value) of 0.23 was identified to provide packed fractions of the formulations that give self-flow properties as suspensions.

- It was shown that an increase in zircon additions to the AZS-01, AZS-02 and AZS-03 compositions, sintered at 1500C did not translate into increased densification and improved physical properties. However, with the addition of SnO_2 as a sintering aid for zircon additions above 35 wt. %; there was an increase in the densification of the refractory bodies and improved physical and thermo-mechanical properties of the AZS refractories.

- The research results have shown and proved successfully the use of SnO_2 as sintering additive to develop and evolve reinforced alumina and mullite refractory composites AZS-T1 and AZS-T2 of the Alumina-Zirconia-Mullite system, from reaction sintering of Alumina and zircon starting mixtures having higher zircon content. The research objective of synthesising dense refractory bodies with relatively low apparent porosities (< 10%) were achieved by sintering the SnO_2 doped compositions above 1500 °C to 1550 °C. The presence of a liquid phase enhanced densification and mullitisation of the refractories and SnO_2 has a considerable influence in the enhancement of the kinetics of dissociation of zircon and subsequent reaction sintering of alumina and zircon.

- Three types of mullite crystals, namely primary mullite (MI); secondary mullite (MII) and acicular tertiary mullite MIII, based on the morphology and aspect ratios, were evolved to form zirconia reinforced network of the matrix microstructure. The MII and MIII mullite crystals evolved in regions of

aluminosilicate amorphous phases from the decomposed zircon grains and were shown to widely contribute to the hot flexural strength values of the refractories from the thermos-mechanical property tests conducted. The RUL results showed that the SnO_2 doped AZS refractories AZS-T1 and AZS-T2 have reduced upper service temperature. However, although, SnO_2 as a sintering aid does have an effect on the hot properties of the AZS refractories, the effects are not as significant as those imparted by TiO_2 which were reported to be reduced by up to 25%.

- Addition of SnO_2 as a sintering aid was shown to have the effect of lowering the monoclinic – tetragonal phase transformation temperature. The shift in the allotropic monoclinic-tetragonal phase change temperature range from 1080 °C – 1180 °C to 910 °C – 980 °C has wider technological benefits for forehearth and feeder expandable products that experience service temperatures in the range of 1100 – 1260 °C.

9 Future Work.

From the present work various research activities are recommended for further study on the development and synthesis of dense sintered refractories containing low apparent porosities and with improved glass contact corrosion resistance properties for the glass industries.

- The utilisation of the DigiPac particle packing software in tandem with the particle packing models of Andreaasen and Dinger and Funk utilised in this research can be made more use in determining optimised packed fractions of the formulations that represent the actual packing of refractory mixtures as a function of PSD and shape. A large set of DigiPac simulation runs on the AZS-01 formulation needs to be conducted to further optimise the packing fractions of the mixture and provide adequate statistical data for validation with the experimental work.

- In this study, the thermal shock properties of the developed compositions were evaluated qualitatively through thermal shock cycling test. Modulus of Rapture tests on the thermal shocked samples can be used to evaluate and quantify and grade the thermal shock resistance of the developed refractories.
- Addition of SnO_2 can be increased from the 5 wt% used in this study to investigate its effect on microstructural evolution as well the refractoriness under load (RUL) and Hot Modulus of Rupture (HMOR).

- Dynamic Corrosion tests to evaluate the corrosion resistance of the developed SnO_2 doped AZS refractories from this research against Chrome based refractories used in the glass industries can be conducted to determine whether SnO_2 doped AZS compositions are suitable and sustainable replacements for Chrome refractories currently being used in glass melting applications.

- The chemical compatibility of SnO_2 doped AZS composition developed in this study, can be evaluated as a function of both the temperatures and glass flow rates within the range 1370 °C– 1550 °C that represent regions of the glass furnace where chrome based refractories are utilised

10 References

1. D.A. Brosnan, Corrosion of refractories C.A. Schacht (Ed.), Refractories Handbook (2004), pp. 39–77
2. ASTM C71-12(2018), Standard Terminology Relating to Refractories, ASTM International, West Conshohocken, PA, 2018, www.astm.org
3. Lee, W. E. and Moore, R. E. Evolution of in Situ Refractories in the 20th Century. Journal of the American Ceramic Society, 81 (1998), pp1385-1410.
4. Da Luz et al. Mullite-based refractory castable engineering for the petrochemical industry. Ceramics International., 39 (2013). pp. 9063-9070.
5. Kingery, W. D.; Bowen, H. K. & Uhlmann, D.R. (1976). Introduction to ceramics (2nd Edition), John Wiley & Sons, Inc., ISBN 0-471-47860-1, United States of America
6. P. A. Bingham, A. J. Connelly, N. C. Hyatt and R. J. Hand,. Corrosion of glass contact refractories for the vitrification of radioactive wastes: a review. International Materials Reviews vol 56(4) pp 225-242 (2011).
7. Dyban', Y.P. and É.K. Keler, *Correlation between the slag resistance and other properties of semiacid ladle brick.* Refractories, 1973. **14**(9): p. 577-580.
8. Kasimagwa, I., V. Brabie, and P.G. Jönsson, *Slag corrosion of MgO–C refractories during secondary steel refining.* Ironmaking & Steelmaking, 2014. **41**(2): p. 121-131.
9. L.J. Manfredo, R.N. MacNally, J Mater Sci 19 (1984) 1272
10. Valle, M., Gandolfi, S., Dondi, M. and Fabbri, B., Effectiveness of various zirconium compounds in the body to improve the alkaline attack resistance of ceramic rollers. In Fourth Euro-Ceramics, vol. 13, (1995), pp. 131–136.
11. Byckov E,V, Refractories and Industrial Ceramics, 1999, Volume 40, Number 1-2, pp70
12. Varshneya, A.K. (2008) Fundamentals of Inorganic Glasses. Society of Glass. Technology, (2006), J. Mater. Chem. 111, 455-462.
13. Shelby, J.E., Introduction to Glass Science & Technology. 2nd ed. Vol. 2nd. 2005, Cambridge: Royal Society of Chemistry

14. O. V. Mazurin, M. V. Strel'tsina, T. P. Shvaiko-Schvaikovskaya,and A. O. Mazurina, "Investigation of the properties of glasses and melts from the end of the 20th century to the present day," Fiz. Khim. Stekla, 28(5), 385 – 400 (2002).
15. D.E. Parkinson, Feeder and forehearth refractories, Glass Technology 29 (5) (1988) 173–176
16. C. Aksel, F.L. Riley, F. Konieczny. The corrosion resistance of alumina–mullite–zircon refractories in molten glass. Key Eng. Mater., 264–268 (2004), pp. 1803-1806
17. Corinne Claireaux, Marie-Hélène Chopinet, Ekaterina Burov, Emmanuelle Gouillart, Mathieu Roskosz,et al. Atomic mobility in calcium and sodium aluminosilicate melts at 1200°C.Geochimicaet Cosmochimica Acta, Elsevier, 2016, 192, pp.235-247
18. Samaddar et al B.N. Samaddar, W.D. Kingery, A.R. Cooper, Dissolution in ceramic systems-11: Dissolution of alumina, mullite, anorthite, and silica in a calcium–aluminium–silicate slag.
19. O. N. Popov, "Kinetics of the reaction of fusion-cast refractories with industrial glass melts," in: Research on Refractories for Glass-Melting Furnaces [in Russian], Izd. GIS, Moscow (1984), pp.
20. King, B.W. and A.I. Andrews, Solubility of Zirconia In Soda-Borosilicate Glasses*. Journal of the American Ceramic Society, 1941. 24(11): p. 367-372.
21. C. Gogtasa, H.F. Lopeza, K. Sobolev Role of cement content on the properties of self-flowing Al2O3 refractory castables
22. Yuan, Q., Tan, J. And Jin, Z. Preparation and Properties of Zirconia-Toughened Mullite Ceramics. Journal of the American Ceramic Society, 69, (1986), pp. 265-267.
23. Valle, M., Gandolfi, S., Dondi, M. and Fabbri, B., Effectiveness of various zirconium compounds in the body to improve the alkaline attack resistance of ceramic rollers. In Fourth Euro-Ceramics, vol. 13, (1995), pp. 131–136.
24. Y. Hemberger et al. / Journal of the European Ceramic Society 32 (2012) 2859–2866
25. Oki K, Sugie M, Kurihara K, Aiba Y, Maeda T. Study of corrosion and penetration of zirconia refractories by molten steel and slag I. Taikabutsu Overseas (1983);3:3–11
26. Strakhov VI, Zhukovskaya AE. Slag-resistant products made from stabilized ZrO_2. Refractories and Industrial Ceramics 1979; 20:184–8.

27. Krämer S, Yang J, Levi CG, Johnson CA. Thermochemical interaction of thermal barrier coatings with molten CaO–MgO–Al_2O_3–SiO_2 (CMAS) deposits. Journal of the American Ceramic Society 2006; 89:3167–75.
28. Wellman R, Whitman G, Nicholls JR. CMAS corrosion of EB PVD TBCs: identifying the minimum level to initiate damage. International Journal of Refractory Metals and Hard Materials 2010; 28:124–32.
29. A. I. Andrews and R. W. Gates, "Solubility of ZrO_2 Opacifier in Enamel Glasses," Jour. Amer. Ceram. Soc., 23 [lo] 288-90 (1940).
30. Burnham, C. W., The Crystal Structure of Mullite, Carnegie Inst. Washington Yearb., 63, 1964, pp. 223-227.
31. Aksay, I. A., Dabbs, D. M. and Sarikaya, M.,Mullite for Structural, Electronic, and Optical Applications, J. Am. Ceram. Soc., 74 [10], 1991, pp. 2343-2358
32. D. Urffer, "The Use of Zircon in Refractories for Glass Making," Ind. Miner. (London), 344, 49– 53 (1996).
33. J. d'Ans and J. Loffler, "Studies on System NaDSi02- Zr02," 2. Anorg. allgem.Chem., 191 1-35 (1930); Cerum. Abs. 9 [ll] 985 (1930); see also J. Loffler, reference 45.8 H. Arnold
34. Mereno R., J.S Moya, J. Requena, Slip casting of zircon by using an organic surfactant, Ceram. Int. 17 (1991) 37 – 40.
35. Garrido, L.B. & Aglietti, E.F.. (2001). Effect of rheological properties of zircon-alumina suspensions on density of green casts. Materials Research. 4. 10.1590
36. Chaouki Sadik, Iz-Eddine El Amrani, Abderrahman Albizane, Recent advances in silica-alumina refractory: A review, Journal of Asian Ceramic Societies, 2:2, (2014), pp. 83-96,
37. H. Schneider, J. Schreuer, B. Hildmann, Structure and properties of mullite—A review, Journal of the European Ceramic Society, 28:2, (2008), pp. 329-344,
38. Zanelli C et al, J. Eur. Ceram. Soc., 30 (2010), pp. 29–35
39. Koyama, T et al. Microstructure and mechanical properties of mullite/zirconia composites prepared from alumina and zircon under various firing conditions, J. Eur. Ceram. Soc. 16 (2) (1996) 231–237

40. M. Hosseinzadeh, M. Akbari and F. Bashiri, "The effect of fused and sintered mullite on properties of ceramic heat shield in V94.2 gas turbines," 2015 30th International Power System Conference (PSC), Tehran, 2015, pp. 371-373.
41. T. Ebadzadeh. Reaction sintering of multicomponent mixtures for producing ceramics containing zirconia. J. Eur. Ceram. Soc., 20, (2000), pp. 725-729
42. Claussen, N. And Jahn, J. Mechanical Properties of Sintered, In-Situ Reacted Mullite-Zirconia Composites. Journal of the American Ceramic Society, 63, (1980), pp. 228-229.
43. Lee, WE & Iqbal, Yaseen. Influence of Mixing on Mullite Formation in Porcelain. Journal of the European Ceramic Society. 21, (2001). pp. 2583-2586.
44. Lee, W.E & Iqbal, Yaseen & Souza, Guilherme & McConvile, Caspar & Tarvornpanich, Tarnkamol. (2006). Mullite Formation & Characterization in Vitreous Ceramics.
45. Iqbal, Y. and Lee, W. E. Microstructural Evolution in Triaxial Porcelain. Journal of the American Ceramic Society, 83, (2000), pp. 3121-3127.
46. François Guillard, Alexandre Allemand, Jean-Daniel Lulewicz, Jean Galy, Densification of SiC by SPS-effects of time, temperature and pressure, Journal of the European Ceramic Society,Volume 27, Issue 7, 2007, Pages 2725-2728,
47. Kuxmann, U. and Dobner, R., 1980. Investigations on the Tin--Tin (IV) Oxide System in the Temperature Range of the Miscibility Gap. Metall, 34(9), pp.821-827.
48. Yin Tiantian, 2017. Coupled Thermodynamic Modelling and Experimental Study of SnO2-SnO-CaO-SiO2 system: Thesis. Department of Mining and Materials Engineering McGill University, Montreal, Canada.
49. Drábek, M. and Stemprok, M., 1974. The system Sn-S-O and its geological application. Neues Jahrbuch für Mineralogie Abhandlungen, 122, pp.90-118.
50. V. Barczak, R. Insley J. Am. Ceram. Soc., 45 (1962); pp144–144 Al2O3-SnO2 phase studies
51. P. Kumar, M. Nath, A. Ghosh, H.S. Tripathi, Thermo-mechanical properties of mullite—zirconia composites: Effect of CaO, Transactions of Nonferrous Metals Society of China, 26:9, (2016), pp. 2397-2403,

52. H S Tripathi, G Banerjee. Synthesis and mechanical properties of mullite from beach sand sillimanite: Effect of TiO_2. Journal of the European Ceramic Society, 18, (1998), pp. 2081-2087

53. M F Melo, M O Figueiredo. Behaviour of titanium in mullite– zirconia composites. Materials Science and Engineering A, 109 (1989), pp. 61-68

54. T. Ebadzadeh, E. Ghasemi, Effect of TiO_2 addition on the stability of t-ZrO_2 in mullite–ZrO_2 composites prepared from various starting materials, Journal of Ceramics International, 28:4, (2002), pp. 447-450,

55. Maitra, S Pal, S Nath, A Panday, R Lodha. Role of MgO and Cr_2O_3 additives on the properties of zirconia–mullite composites Journal of Ceramics International, 28 (2002), pp. 819-826

56. P Pena et al. Effect of magnesia addition on the reaction sintering of zirconia/alumina mixtures to produce zirconia toughened mullite. Journal of Materials Science Letters, 2 (1983), pp. 772-774

57. P Kumar, M Nath, A Ghosh, H S Tripathi. Enhancement of thermal shock resistance of reaction sintered mullite–zirconia composites in the presence of lanthanum oxide. Materials Characterization, 101 (2015), pp. 34-39

58. .F. Shackelford, W. Alexander, J.S. Park, CRC Materials Science and Engineering Handbook, CRC Press, Boca Raton, FL, 1994

59. Gaillard-Allemand et al. Experimental study of the SnO_2-ZrO_2 phase diagram. Journal of the European Ceramic Society. 22. (2002).

60. Jun Ma, Yuexiang Zhu, Jiying Wei, Xiaohai Cai, Youchang Xie, Lean NOx reduction over $Sn_{1-x}Zr_xO_2$ solid solutions, Studies in Surface Science and Catalysis, Elsevier, Vol. 130, (2000), pp. 617-622,

61. L.B. Kong, T.S. Zhang, J. Ma, F. Boey. Some main group oxides on mullite phase formation and microstructure evolution, Journal of Alloys and Compounds, Vol. 359, Issues 1–2, (2003), pp. 292-299.

62. A.P. Silva, D.G. Pinto, A.M. Segadães, T.C. Devezas, Designing particle sizing and packing for flowability and sintered mechanical strength, Journal of the European Ceramic Society 30 (2010) 2955–2962
63. Myhre B. Particle size distribution and its relevance in refractory castables. In proceedings of the 2nd India International Refractory Congress, New Delhi, (1996)
64. S.M. Jang, H.M. Cho, K.T. Kim., Alumina-mullite-zirconia composites. Part II, microstructural development and toughening, .J. Mater. Sci., 32 (1997), pp. 503–511
65. Cooper, A.R., Jr.; Kingery, W.D. Dissolution in ceramic systems: I, Molecular diffusion, natural convection, and forced convection studies of sapphire dissolution in calcium aluminum silicate. J. Am. Ceram. Soc. 1964, 47 (1), 37–3.
66. Kingery, W.D. Dissolution in ceramic systems: III, Boundary layer concentration gradients. J. Am. Ceram. Soc. 1965, 48 (2), 88–95.
67. McCauley R.A.M. Corrosion of Ceramic AND Composite Materials. MARCEL DEKKER, INC. New York. 2004.
68. Kato and Araki J NON-CRYST SOLIDS, vol. 80, no. 1-3, pp. 681-687, 1986
69. Pavlik, R. S., Holland, H. J. and Payzant, E. A. Thermal Decomposition of Zircon Refractories. Journal of the American Ceramic Society, 84: (2001), pp 2930-2936.
70. Baudin et al, Journal of the European Ceramic Society. 31 (2011) 697-703
71. P. Kumar, M. Nath, A. Ghosh, H.S. Tripathi, Thermo-mechanical properties of mullite—zirconia composites: Effect of CaO, Transactions of Nonferrous Metals Society of China, 26:9, (2016), pp. 2397-2403
72. B. H. Bieler, Am. Ceram. Soc. Bull. 61, 7 (1982) 74
73. Baspinar, M. Serhat & Kara, Ferhat. (2009). Optimization of the Corrosion Behavior of Mullite Refractories against Alkali Vapor Vvia ZrSiO4 Addition to the Binder Phase. Ceramics - Silikaty.
74. Dunkl, M.: Corrosion tests – a very important investigation method for the selection of refractories for glass tanks. Glastechn. Ber. 67 (1994) [12] 325–334
75. M., D., Boundary Layers Refractory/Glass melt and Glass Defects. Advanced Materials Research, 2008. 39 - 40: p. 601 - 606.

76. Pavlovskii, V.K. and Y.S. Sobolev, Refractory-oxide corrosion resistance in molten high-lead silicate glasses. Glass and Ceramics, 1991. 48(6): p. 233-23
77. Yurkov, A., Refractories and Carbon Cathode Materials for Aluminum Reduction Cells, in Refractories for Aluminum: Electrolysis and the Cast House. 2017, Springer International Publishing: Cham. p. 75-22
78. Wanibe Y., Tsuchida H., Fujisawa T., And Sakao H. Paper presented at 101st ISIJ meeting, Tokyo, Japan, April 1981.
79. Jansson, S., Brabie, V., And Bohlin, L. Corrosion mechanism and kinetic behaviour of refectory materials in contact. With CaO-Al2O3-MgO-SiO2. VII International Conference on Molten Slags Fluxes and Salts, The South African Institute of Mining and Metallurgy, 2004.
80. Makri H, H. Belhouchet, M. Hamidouche and G. Fantozzi. Journal of The Australian Ceramic Society Volume 51[1], 2015, 60 – 72
81. Cooper, A.R. The use of phase diagrams in dissolution studies. In Refractory Materials; Alper,
82. A.M., Ed.; Academic Press: New York, 1970; Vol. 6-III, 237–250.
83. ASTM C230 / C230M-03, Standard Specification for Flow Table for Use in Tests of Hydraulic Cement, ASTM International, West Conshohocken, PA, (2003), www.astm.org
84. ASTM C830-00(2016), Standard Test Methods for Apparent Porosity, Liquid Absorption, Apparent Specific Gravity, and Bulk Density of Refractory Shapes by Vacuum Pressure, ASTM International, West Conshohocken, PA, (2016), www.astm.org
85. ASTM C133-97(2015), Standard Test Methods for Cold Crushing Strength and Modulus of Rupture of Refractories, ASTM International, West Conshohocken, PA, (2015), www.astm.org
86. ASTM C24-09(2018), Standard Test Method for Pyrometric Cone Equivalent (PCE) of Fireclay and High-Alumina Refractory Materials, ASTM International, West Conshohocken, PA, 2018, www.astm.org
87. ASTM C583-15, Standard Test Method for Modulus of Rupture of Refractory Materials at Elevated Temperatures, ASTM International, West Conshohocken, PA, 2015Linear thermal expansion

88. M. Conconi, N. Rendtorff and E. Aglietti, "Evaluation of Non Crystalline Phase in AZS Refractories by XRD Methods," New Journal of Glass and Ceramics, Vol. 1 No. 2, 2011, pp. 28-33.
89. A. G. De La Torre, S. Bruque and M. A. G. Aranda, "Rietveld Quantitative Amorphous Content Analysis," Journal of Applied Crystallography, Vol. 34, 2001, pp. 196-202
90. A. Le Bail, "Modelling the Silica Glass Structure by the Rietveld Method," Journal of Non-Crystalline Solids, Vol. 183, No. 1-2, 1995, pp. 39-42.
91. C. R. Ward and D. French, "Determination of Glass Content and Estimation of Glass Composition in Fly Ash Using Quantitative X-Ray Diffractometry," Fuel, Vol. 85, 2006, pp. 2268–2277
92. C. Aksel. Mechanical properties and thermal shock behaviour of alumina–mullite–zirconia and alumina–mullite refractory materials by slip casting Ceram. Int., 29 (2003), pp. 311-316
93. Mori T et al, .Reactivity of high-purity ZrSiO4 sintered bodies for alkaline glass melts J. Ceram. Soc. Jpn, 100 (3) (1992), pp. 250–258
94. Jun Ma, Yuexiang Zhu, Jiying Wei, Xiaohai Cai, Youchang Xie, Lean NOx reduction over $Sn_{1-x}Zr_xO_2$ solid solutions, Studies in Surface Science and Catalysis, Elsevier, Vol. 130, (2000), pp. 617-622,
95. Manfredo, L. J. and McNally, R. N. Solubility of Refractory Oxides in Soda Lime Glass. Journal of the American Ceramic Society, 67, (1984). pp.155-158.
96. Toperesu M.P., W Kusepile, G Kale, J Daji and D Parkinson. Hot Corrosion Behaviour of Sintered AZS Refractories in Special (Type 1, Class A) Glass Melt with Increasing Soda Content. Submitted to Journal of European Society, 2018, (In press).
97. Harini Sosiati Sudarminto, Kan Sakamoto , Yoshihiro Tsuchiuchi & Masayasu Sugisaki) Segregation of Tin Oxide in Oxide Layer of Zircaloy-type Alloys, Journal of Nuclear Science and Technology, 39:2, (2002). pp. 150-155
98. German, Randall & Suri, Pavan & Park, Seong Jin. Review: Liquid Phase Sintering. Journal of Materials Science. 44, (2008). pp. 1-39
99. L. Kozma, W. Huppmann, L. Bartha & P. Mezei. Initiation of Directional Grain Growth during Liquid-Phase Sintering of Tungsten and Nickel, Journal of Powder Metallurgy, 24:1, (1981). pp 7-11

100. Courtney T.H. Journal of Metallurgical and Materials Transactions A: 15: 6, (1984). pp 1065–1074

101. Khandelwal S K and Cook R L. Effect of alumina additions on crystalline constituents and fired properties of electrical porcelain. Am. Ceram. Soc. Bull., 49, (1970). pp. 522-526 W.E. Lee, R.E. Moore, Evolution of in situ refractories in the 20th century, Journal of the American Ceramic Society 81 (1998) 1385–1410.

102. Byckov E,V, Refractories and Industrial Ceramics, 1999, Volume 40, Number 1-2, pp70

103. P. A. Bingham, A. J. Connelly, N. C. Hyatt and R. J. Hand,. Corrosion of glass contact refractories for the vitrification of radioactive wastes: a review. International Materials Reviews vol 56(4) pp 225-242 (2011).

104. Kingery, W. D.; Bowen, H. K. & Uhlmann, D.R. (1976). Introduction to ceramics (2nd Edition), John Wiley & Sons, Inc., ISBN 0-471-47860-1, United States of America.

105. O. V. Mazurin, M. V. Strel'tsina, T. P. Shvaiko-Schvaikovskaya,and A. O. Mazurina, "Investigation of the properties of glasses and melts from the end of the 20th century to the present day," Fiz. Khim. Stekla, 28(5), 385 – 400 (2002).

106. Jacobson N. S., Lee K. N., Yoshio J Am. Ceram. Soc. 79, 2161 (1996)

107. Hrma, P., Dissolution of a solid body governed by surface free convection. Chemical Engineering Science, 1970. **25**(11): p. 1679-1688.

108. Takahashi J., Kawai Y Shi,mada S J. Am. Ceram Soc 22 1959 (2002)

109. J.F. Shackelford, W. Alexander, J.S. Park, CRC Materials Science and Engineering Handbook, CRC Press, Boca Raton, FL, 1994.

110. Rendtorff N, E. Aglietti / Materials Science and Engineering A 527 (2010) 3840–3847

111. F.E, W., Predictions of Refractory Corrosion Rate form Glass Viscosity and Composition. UNITCR'89 Proceedings, 1987. McCauley R.A.M. Corrosion of Ceramic & Composite Materials. MARCEL DEKKER, INC. New York. 2004.

112. Jansson, S., Brabie, V., And Bohlin, L. Corrosion mechanism and kinetic behaviour of refectory materials in contact. With CaO-Al2O3-MgO-SiO2. VII International Conference on Molten Slags Fluxes and Salts, the South African Institute of Mining and Metallurgy, 2004.

113. Makri H, H. Belhouchet, M. Hamidouche and G. Fantozzi. Journal of The Australian Ceramic Society Volume 51[1], 2015, 60 – 72

114. Trier, W. *Glass Furnaces: Design, Construction, and Operation*. in *Society of Glass Technology*. 1987. Sheffield, UK: Society of Glass Technology

Appendix A: Slip preparation and slip test raw data.

Table 0-1: Deflocculation test data used to determine the best dispersant and optimum concentration for the production of AZS-01 slip.

Deflocculation Evaluation Test					
Spindle No.	3				
No. of Revs:	5	(30s)			
Spindle speed:	10rpm				
Beaker/Container used:	250ml beaker container				
Date:	03/02/2017				
Sample		AZS-01 (MP05)	AZS-01 (MP05)	AZS-01 (MP05)	AZS-01 (MP05)
wt.% solid loading		78.4	78.4	93	93
vol. % solid loading					
Dispersant		***Darvan 7***	***Dispex A40***	***Darvan 7***	***Dispex A40***
Volume	Concentration	Dynamic Viscosity (cP)			
ml	ml/kg	cP	cP	cP	cP
0	0	100000	1360	100000	100000
0.1	0.25	11840	1280	1120	960
0.2	0.5	2880	240	80	560
0.3	0.75	2960	1680	40	1360
0.4	1	4080	240	80	2160
0.5	1.25	9200	320	160	2560
0.6	1.5	528	240	80	3040
0.7	1.75		160	80	3840
0.8	2		160	160	5200
0.9	2.25			160	
1	2.5			230	

Appendix B: Physico-Thermo-mechanical Test Results

❖ Refractoriness:

PHYSICAL TESTING REPORT

LUCIDEON
insight creating advantage

Parkinson Spencer Refractories Ltd
Holmfield
Halifax
West Yorkshire
HX3 6SX

FAO: Dr. Jafar Daji
Report of Tests on: Zirconia Based Refractory
Your Reference: MP5-5Sn
Lucideon Reference: (172703)-19836
Date Reported: 03-Jul-2017 **Order Number:** TP Allowance
Date Logged: 19-Jun-2017 **Date(s) of Test(s):** 24-Jun-2017 **to** 03-Jul-2017

Determination of Refractoriness (PCE)
ASTM C24-09(13) Using Orton Pyrometric Reference Cones

Mr Simon Hall
Manager

This report is issued in accordance with the Conditions of Business of Lucideon Limited and relates only to the sample(s) tested. No responsibility is taken for the accuracy of the sampling unless this is done under our own supervision. This report shall not be reproduced in part without the written approval of Lucideon Limited, nor used in any way as to lead to misrepresentation of the results or their implications.

Lucideon is the trading name of Lucideon Limited. Registered in England No. 1960455.

Lucideon Limited
Queens Road, Penkhull
Stoke-on-Trent
Staffordshire ST4 7LQ

T +44 (0)1782 764428
enquiries@lucideon.com
www.lucideon.com

Test Results:

Cone: 32.5 - 33
Temperature: 1724 - 1743 °C

End of Test Report

PHYSICAL TESTING REPORT

LUCIDEON
insight creating advantage

Parkinson Spencer Refractories Ltd
Holmfield
Halifax
West Yorkshire
HX3 6SX

FAO: Dr. Jafar Daji

Report of Tests on:	Zirconia Based Refractory		
Your Reference:	MP12-5Sn		
Lucideon Reference:	(172703)-19835		
Date Reported:	03-Jul-2017	**Order Number:**	TP Allowance
Date Logged:	19-Jun-2017	**Date(s) of Test(s):**	24-Jun-2017 **to** 03-Jul-2017

Determination of Refractoriness (PCE)
ASTM C24-09(13) Using Orton Pyrometric Reference Cones

Test Results:

Cone: 32.5 - 33
Temperature: 1724 - 1743 °C

End of Test Report

Mr Simon Hall
Manager

This report is issued in accordance with the Conditions of Business of Lucideon Limited and relates only to the sample(s) tested. No responsibility is taken for the accuracy of the sampling unless this is done under our own supervision. This report shall not be reproduced in part without the written approval of Lucideon Limited, nor used in any way as to lead to misrepresentation of the results or their implications.

Lucideon is the trading name of Lucideon Limited. Registered in England No. 1960455.

Lucideon Limited
Queens Road, Penkhull
Stoke-on-Trent
Staffordshire ST4 7LQ

T +44 (0)1782 764428
enquiries@lucideon.com
www.lucideon.com

PHYSICAL TESTING REPORT

LUCIDEON
insight creating advantage

UKAS TESTING
0013

Parkinson Spencer Refractories Ltd
Holmfield
Halifax
West Yorkshire
HX3 6SX

FAO: Dr. Jafar Daji

Report of Tests on: Alumina-Zirconia-Silica (AZS) material
Your Reference: SAMPLE C - MP5-Optimised
Lucideon Reference: (181083)-8814
Date Reported: 12-Mar-2018 **Order Number:** Service Allowance
Date Logged: 26-Feb-2018 **Date(s) of Test(s):** 05-Mar-2018 **to** 12-Mar-2018

Determination of Cold Compressive Strength of Dense Shaped Refractory Products
BS EN 993-5: 2000

	Cold Compressive Strength
No.	**MPa**
1	199.0
2	198.0
3	153.0
4	188.0
5	210.0
Mean	190.0

Shape of Test Specimens: Cylinder
Size of Test Specimens: 50x50 mm
Standard Deviation: 21.9

All specimens should be loaded in the same direction of pressing during original manufacture, however, the direction of pressing and location from sample were not known.

Opinions and interpretations expressed herein are outside the scope of UKAS Accreditation.

End of Test Report

Miss Zoe Kinally
Manager

This report is issued in accordance with the Conditions of Business of Lucideon Limited and relates only to the sample(s) tested. No responsibility is taken for the accuracy of the sampling unless this is done under our own supervision. This report shall not be reproduced in part without the written approval of Lucideon Limited, nor used in any way as to lead to misrepresentation of the results or their implications.

Lucideon is the trading name of Lucideon Limited. Registered in England No. 1960455.

Lucideon Limited
Queens Road, Penkhull
Stoke-on-Trent
Staffordshire ST4 7LQ

T +44 (0)1782 764428
enquiries@lucideon.com
www.lucideon.com

PHYSICAL TESTING REPORT

LUCIDEON
insight creating advantage

UKAS TESTING
0013

Parkinson Spencer Refractories Ltd
Holmfield
Halifax
West Yorkshire
HX3 6SX

FAO: Dr. Jafar Daji

Report of Tests on: Alumina-Zirconia-Silica (AZS) material

Your Reference: SAMPLE A - MP5-5Sn (1500C)

Lucideon Reference: (181083)-8811

Date Reported: 12-Mar-2018 **Order Number:** Service Allowance

Date Logged: 26-Feb-2018 **Date(s) of Test(s):** 05-Mar-2018 **to** 12-Mar-2018

Determination of Cold Compressive Strength of Dense Shaped Refractory Products

BS EN 993-5: 2000

	Cold Compressive Strength
No.	**MPa**
1	150.0
2	138.0
3	145.0
4	163.0
5	138.0
Mean	147.0

Shape of Test Specimens: Cylinder

Size of Test Specimens: 50x50 mm

Standard Deviation: 10.4

All specimens should be loaded in the same direction of pressing during original manufacture, however, the direction of pressing and location from sample were not known.

Opinions and interpretations expressed herein are outside the scope of UKAS Accreditation.

End of Test Report

Miss Zoe Kinally
Manager

This report is issued in accordance with the Conditions of Business of Lucideon Limited and relates only to the sample(s) tested. No responsibility is taken for the accuracy of the sampling unless this is done under our own supervision. This report shall not be reproduced in part without the written approval of Lucideon Limited, nor used in any way as to lead to misrepresentation of the results or their implications.

Lucideon is the trading name of Lucideon Limited. Registered in England No. 1960455.

Lucideon Limited
Queens Road, Penkhull
Stoke-on-Trent
Staffordshire ST4 7LQ

T +44 (0)1782 764428
enquiries@lucideon.com
www.lucideon.com

PHYSICAL TESTING REPORT

LUCIDEON
insight creating advantage

UKAS TESTING
0013

Parkinson Spencer Refractories Ltd
Holmfield
Halifax
West Yorkshire
HX3 6SX

FAO: Dr. Jafar Daji

Report of Tests on: Alumina-Zirconia-Silica (AZS) material
Your Reference: SAMPLE B - MP12-5Sn (1550C)
Lucideon Reference: (181083)-8813
Date Reported: 09-Mar-2018 **Order Number:** Service Allowance
Date Logged: 26-Feb-2018 **Date(s) of Test(s):** 06-Mar-2018 **to** 08-Mar-2018

Modulus of Rupture & Modulus of Elasticity by 3 Point Loading
R102 Method 2

	Sample Reference	Width	Depth	Failure Load	Modulus of Rupture	Modulus of Elasticity
No.		mm	mm	N	MPa	GPa
1	1	24.350	15.600	903.16	18.34	14.75
2	2	24.290	15.620	799.14	16.22	14.98

Heating Rate: 3000 °C/h
Test Temperature: 1300 °C
Soak Time: 20 min
Steadying Load: 5 N
Test Span: 80 mm
Crosshead Speed: 0.50 mm/min

The specimen was placed in a furnace in three point flexure. If necessary a small load was placed on the specimen to steady the set up during heating.The specimen was heated to the test temperature and allowed to soak for the indicated time before being loaded to failure. The modulus of elasticity was calculated between 25% and 75% of the modulus of rupture.

Opinions and interpretations expressed herein are outside the scope of UKAS Accreditation.

Mrs Sharon Mansfield
Manager

This report is issued in accordance with the Conditions of Business of Lucideon Limited and relates only to the sample(s) tested. No responsibility is taken for the accuracy of the sampling unless this is done under our own supervision. This report shall not be reproduced in part without the written approval of Lucideon Limited, nor used in any way as to lead to misrepresentation of the results or their implications.

Lucideon is the trading name of Lucideon Limited. Registered in England No. 1960455.

Lucideon Limited
Queens Road, Penkhull
Stoke-on-Trent
Staffordshire ST4 7LQ

T +44 (0)1782 764428
enquiries@lucideon.com
www.lucideon.com

Lucideon Reference: (181083)-8813
Customer Reference: SAMPLE B – MP12-5Sn (1550C)
Description: Alumina-Zirconia-Silica (AZS) material

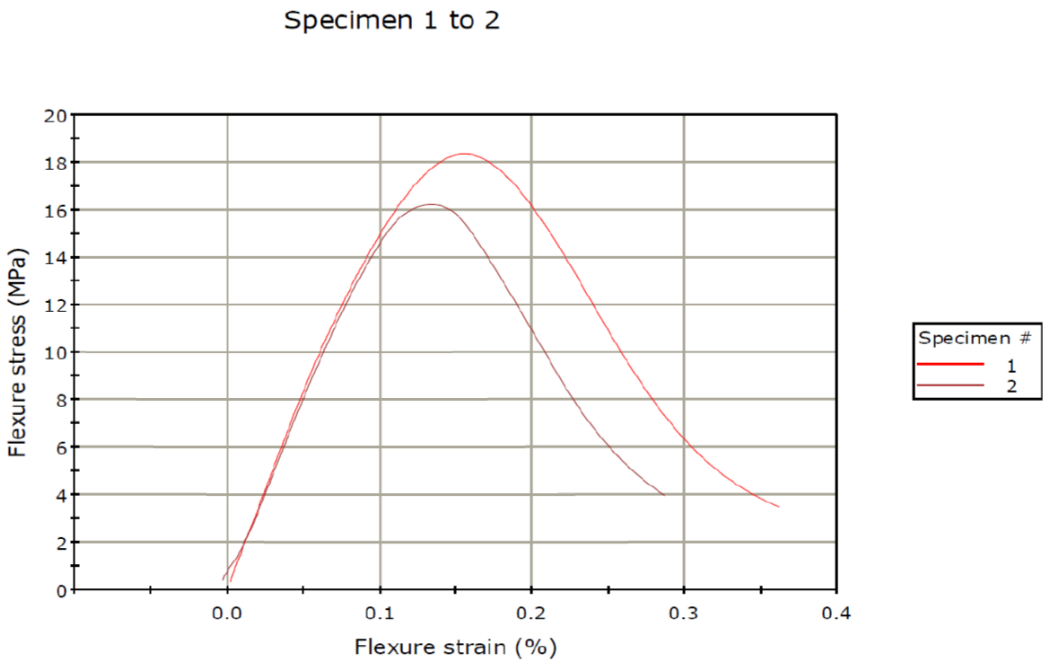

END OF TEST REPORT

PHYSICAL TESTING REPORT

LUCIDEON
insight creating advantage

UKAS TESTING
0013

Parkinson Spencer Refractories Ltd
Holmfield
Halifax
West Yorkshire
HX3 6SX

FAO: Dr. Jafar Daji

Report of Tests on: Alumina-Zirconia-Silica (AZS) material
Your Reference: SAMPLE A - MP5-5Sn (1500C)
Lucideon Reference: (181083)-8812
Date Reported: 07-Mar-2018 **Order Number:** Service Allowance
Date Logged: 26-Feb-2018 **Date(s) of Test(s):** 05-Mar-2018 **to** 06-Mar-2018

Modulus of Rupture & Modulus of Elasticity by 3 Point Loading
R102 Method 2

	Width	Depth	Failure Load	Modulus of Rupture	Modulus of Elasticity
No.	mm	mm	N	MPa	GPa
1	24.650	15.500	1040.11	21.13	17.67
2	24.740	15.550	968.34	19.48	21.22

Heating Rate: 50 °C/h
Test Temperature: 1300 °C
Soak Time: 20 min
Steadying Load: 5 N
Test Span: 80 mm
Crosshead Speed: 0.50 mm/min

The specimen was placed in a furnace in three point flexure. If necessary a small load was placed on the specimen to steady the set up during heating.The specimen was heated to the test temperature and allowed to soak for the indicated time before being loaded to failure. The modulus of elasticity was calculated between 25% and 75% of the modulus of rupture.

Opinions and interpretations expressed herein are outside the scope of UKAS Accreditation.

Mrs Sharon Mansfield
Manager

This report is issued in accordance with the Conditions of Business of Lucideon Limited and relates only to the sample(s) tested. No responsibility is taken for the accuracy of the sampling unless this is done under our own supervision. This report shall not be reproduced in part without the written approval of Lucideon Limited, nor used in any way as to lead to misrepresentation of the results or their implications.

Lucideon is the trading name of Lucideon Limited. Registered in England No. 1960455.

Lucideon Limited
Queens Road, Penkhull
Stoke-on-Trent
Staffordshire ST4 7LQ

T +44 (0)1782 764428
enquiries@lucideon.com
www.lucideon.com

Lucideon Reference: (181083)-8812
Customer Reference: SAMPLE A – MP5-5Sn (1500C)
Description: Alumina-Zirconia-Silica (AZS) material

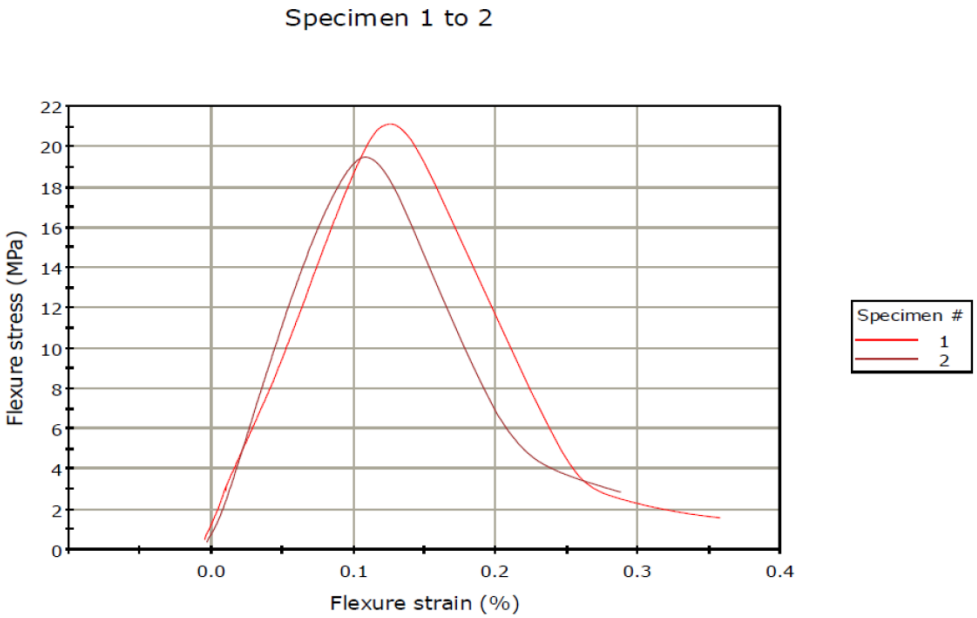

All volumes were reconstructed in *float* data type.

- Sample 0.5-1mm_Alumina 3D volume file size: ~48 GB

Voxel size: 2 um; whole volume reconstructed

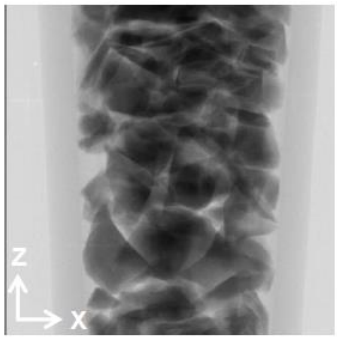

2D projection

- Sample 0-0.3mm_Alumina 3D volume file size: ~24 GB

Voxel size: 2 um; volume reconstructed measurements in voxels indicated in image below on right hand side (corresponding to bottom half of the sample).

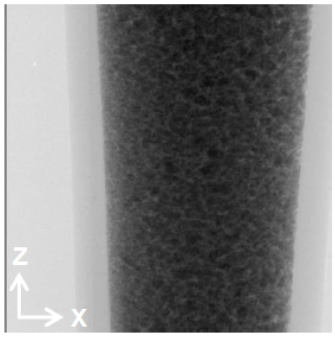

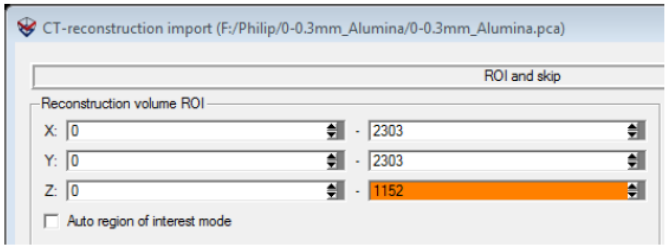

- Sample 0-0.5mm_Alumina 3D volume file size: ~24 GB

Voxel size: 2 um; volume reconstructed measurements in voxels indicated in image below on right hand side (corresponding to bottom half of the sample).

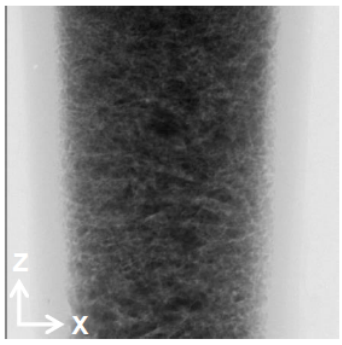

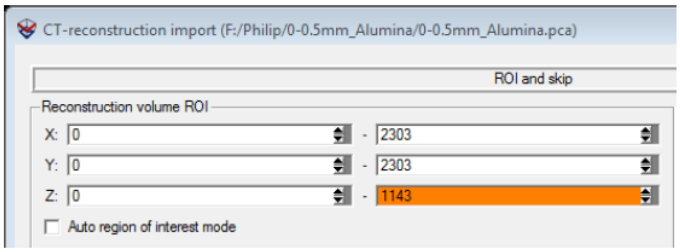

- Sample 1-2mm_Alumina 3D volume file size: ~29 GB

Voxel size: 3 um; volume reconstructed measurements in voxels indicated in image below on right hand side.

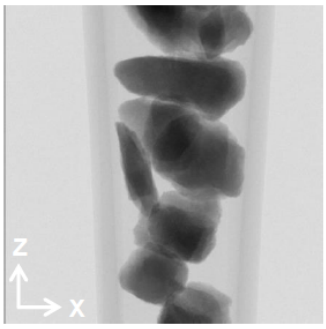

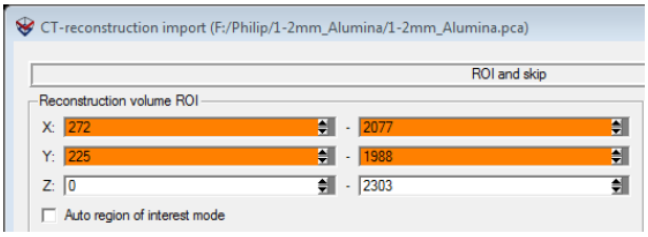

- Sample Zirco sand 3D volume file size: ~24 GB

Voxel size: 2 um; volume reconstructed measurements in voxels indicated in image below on right hand side (corresponding to bottom half of the sample).